Vascular Smooth Muscle Cell PIEZO-1 in Abdominal Aortic Aneurysm Formation

Mohammed Abdul Waduud

201192781

Submitted in accordance with the requirements for the degree of

Doctor of Philosophy

The University of Leeds, Leeds Institute for Cardiovascular and Metabolic Medicine

Leeds Vascular Institute, Leeds Teaching Hospitals NHS Trust.

Funded by The British Heart Foundation

March 2023

Intellectual Property and Publication Statements

The candidate confirms that the work submitted is their own and that appropriate accreditation credit has been given where reference has been made to the work of others.

Acknowledgements

I want to thank my supervisors; Dr Marc Bailey, Professor David Beech and Professor Julian Scott for their guidance, advice and support they have provided over the past few years. Without their academic, clinical and personal mentorship neither my fellowship or the pursuit of this degree would have been possible. I would like to thank the British Heart Foundation for funding this work and the National Institute for Health Research for funding the preliminary work required to secure my fellowship.

My exposure to the laboratory working environment made me feel like a “fish out of water”. Without the support from the members of the Bailey/Beech laboratory groups, none of this work would have been possible. I want to thank Marc Bailey, Karen Hemmings and Jason Scragg for teaching me how to successfully perform cell culture, cell counting, plating for experimentation and incucyte imaging. I want to thank Alan Burnett and Hannah Gaunt for teaching me how to conduct calcium imaging using the Flexstation 3. Lucinda Craggs, for teaching me how to isolate genomic material, design primers and conduct real-time PCR experiments. I would also like to thank Gregory Parsonage, Marjolaine Debant, Laeticia Lichtenstein, and Fiona Bartolli for helping me on countless occasions to source the correct reagents and experimental apparatus for the laboratory experiments conducted. Importantly, I want to thank all the patients who donated tissue to the Leeds Aneurysm Development Study (LEADS) and Ageing Aorta Tissue bank.

Furthermore, before starting this work I had never handled a mouse or any animal, for that matter. The animal work described was conducted with the help of the staff at core biomedical services, namely, Melanie Reay and Simon Futers. I want to thank Marc Bailey for teaching me how to perform murine ultrasound imaging and aneurysm induction surgery. I would also like to thank Naima Endesh for performing the wire myography experiments. Without question I have developed an understanding and respect for the vital work scientists do every day in laboratories all over the world to help humanity.

I would like to thank Michael Drozd who is a fellow clinician and has been a supportive friend working in the LICAMM. Finally and most importantly, I want to thank my family who have supported and have had confidence in me throughout this extremely challenging journey, which was complicated by the COVID-19 pandemic. The well wishes, prayers, and words of lost loved ones will always resonate in my heart. The arrival of my daughter in 2021 has also given me a new purpose in life for which I am grateful.

"No one who achieves success does so without acknowledging the help of others. The wise and confident acknowledge this help with gratitude."

Alfred North Whitehead, 1861-1947

Abstract

Background

An Abdominal Aortic Aneurysm (AAA) is a potentially life-threatening condition with no current disease-specific pharmacological therapies targeting aneurysm growth. Aortic vascular smooth muscle cells (VSMCs) maintain aortic vascular tone, due to their mature contractile differentiated phenotype. However, they can phenotypically switch to a de-differentiated cells which has shown to play a role in the aneurysmal disease process. PIEZO-1 is a calcium-permeable shear stress sensor previously shown to contribute to hypertension-induced wall remodelling and has recently AAA disease. Despite this, evidence potentially linking PIEZO-1 to AAA pathophysiological processes remains limited.

Methods

The hypothesis that activation of the PIEZO-1 mechanosensor in aortic VSMCs by stressors drives vascular remodelling (i.e. cell proliferation and stiffness) was assessed using in-vitro and in-vivo models. Non-diseased aortic VSMCs were exposed to constant oscillatory shear force, uni-axial stretch and high and low matrix stiffnesses. Additionally, cells were physiologically stressed by undergoing multiple cell passages, treated with the PIEZO-1 agonist Yoda-1 and cultured in serum-deprived media. Calcium imaging, using Yoda-1 to quantify PIEZO-1-dependent intracellular calcium entry, was performed. Cell behaviour was characterised using proliferation and migration assays. C57BL6/J [wild-type] and PIEZO-1 smMHCCre-ER(T2) [transgenic] male mice underwent aneurysm induction surgery to assess for changes in PIEZO expression. Serial ultrasound imaging was performed to quantify the anatomical changes. Quantitatively PCR was used to assess the expression of PIEZO mechanosensors, krüppel-like transcription factor 2 (KLF-2), krüppel-like transcription factor 4 (KLF-4) and transglutaminase 2 (TG2).

Results

PIEZO-1 was expressed in both non-diseased VSMCs as well as VSMCs

obtained from aneurysmal tissue. PIEZO-1 mRNA was shown to be elevated in aortic VSMCs following treatment with the PIEZO-1 agonist Yoda-1, the application of constant oscillatory shear stress, and cell culture with serum-deprived media. Proliferation was significantly slower following prolonged stimulation with PIEZO-1. Although there was no physiological evidence linking vessel distensibility or matrix stiffness to PIEZO-1, there is a suggestion that PIEZO-1 influences the mRNA expression of TG2. Functional knockdown of PIEZO-1 in VASCs could not be reliably achieved. Furthermore, the knockdown of VSMC PIEZO-1 in transgenic was inconclusive. Never the less the was a significant increase in both PIEZO mechanosensors at day 7 following surgery in C57BL6/J mice, however only PIEZO-2 remained significantly elevated at day 14.

Conclusions

In this thesis, VSMC PIEZO mechanosensors were shown to be able to detect and adapt to common mechanical stimuli and stressors likely to be experienced in the AAA microenvironment. The role of PIEZO-1 in aneurysmal disease may be one that is transient and potentially of limited clinical significance. However, further investigation is required to confirm the findings of this thesis and interrogate the role of PIEZO-2.

Funding and Outputs

The content of this thesis was possible due to the financial support from the following sources:

- **British Heart Foundation**. Clinical Research Training Fellowship. MA Waduud, DJA Scott, K Porter, DJ Beech, MA Bailey. Mechanosensor ion interaction in Abdominal Aortic Aneurysm. FS/18/30/33647. £247,655.
- **National Institute for Health Research**. Research Bursary. MA Waduud. Funded travel and course fee to attend the Royal Society of Biology Home Office Animal Licence training. £955.
- **Leeds Institute for Cardiovascular and Metabolic Medicine.** James Ellis Award. MA Waduud. Funding was secured to learn and develop murine operating skills. £5000. Unable to use due to the pandemic.

The following presentations were delivered in relation to the contents of this thesis:

- **Poster presentation**: Mechanosensor ion channel interaction in Abdominal Aortic Aneurysm. MA Waduud, L Craggs, K Hemmings, P Kandavelu, DJA Scott, K Porter, D Beech, MA Bailey. LICAMM Research Retreat 2018, Ullswater, UK. Local Meeting.
- **Poster presentation**: Mechanosensor ion channel interaction in Abdominal Aortic Aneurysm. MA Waduud, L Craggs, K Hemmings, P Kandavelu, DJA Scott, K Porter, D Beech, MA Bailey. Yorkshire and the Humber Academic Presentation Day 2018, York, UK. Regional Meeting.
- **Oral presentation**: Mechanosensor ion channel interaction in Abdominal Aortic Aneurysm. MA Waduud, L Craggs, K Hemmings, P Kandavelu, DJA Scott, K Porter, D Beech, MA Bailey. West Yorkshire Academic Surgeons Evening, Leeds, UK. Regional Meeting.

- **Oral presentation**: Validation of 3D ultrasonography: a pre-clinical study. MA Waduud. FujiFilm Visualsonic, UK Cardio User Meeting 2021, Online, UK. National Meeting.

The following paper has been published aspects of the work described in this thesis:

- Waduud MA, Kandavelu P, Reay M, Paradine K, Scott DJ, Bailey MA. High-Frequency Three-Dimensional Lumen Volume Ultrasound Is a Sensitive Method to Detect Early Aneurysmal Change in Elastase-Induced Murine Abdominal Aortic Aneurysm. Aorta. 2021 Dec;9(06):215-20.

Table of Contents

List of Tables

List of Figures

List of Abbreviations

Abdominal Aortic Aneurysm	(AAA)
Angiotensin-II	(Ang-II)
Area Under the Curve	(AUC)
Base pair	(bp)
Beats per minute	(bpm)
Beta-Actin	(BA)
Beta-2 Microglobin	(B2M)
British Heart Foundation	(BHF)
Calcium Chloride	($CaCl_2$)
Cardiovascular disease	(CVD)
Centimetres	(cm)
Complementary DNA	(cDNA)
Chronic Obstructive Pulmonary Disease	(COPD)
Computer Tomography	(CT)
Crossing Point	(CP)
Cyclophilin B	(CycB)
Data-Driven Expression-Prioritization Integration for Complex Traits	(DEPICT)
David Beech	(DB)
Dimethyl sulfoxide	(DMSO)
Dutch Randomised Endovascular Aneurysm Management	(DREAM)
Dulbecco's Modified Eagle's Medium	(DMEM)
Endothelial Cell	(EC)
Electrocardiogram	(ECG)

Epithelial Na^+ Channel	(ENaC)
Extra-Cellular Matrix	(ECM)
Electrocardiogram-gated Kilohertz Visualisation	(EKV)
European Society of Vascular Surgery	(ESVS)
Endovascular Aneurysm Repair	(EVAR)
Fetal Bovine Serum	(FBS)
Foetal Calf Serum	(FCS)
Finite Element Analysis	(FEA)
Genome-Wide Associate Study	(GWAS)
Glyceraldehyde 3-phosphate dehydrogenase	(GAPDH)
Gram	(g)
Haematoxylin and Eosin	(H&E)
half maximal Effective Concentration	(EC_{50})
Hypoxanthine-guanine Phosphoribosyl transferase	(HPRT)
Human Aortic Smooth Muscle Cells	(HAoSMC)
Integrated Research Application System	(IRAS)
Inositol triPhosphate Receptors	(IP3Rs)
Ionotropic Purinergic	(P2X)
Joint Photographic Experts Group	(JPEG)
Krüppel-Like Factor 2	(KLF2)
Krüppel-Like Factor 4	(KLF4)
Leeds Aneurysm Development Study	(LEADS)
Left Atrium	(LA)
Left Ventricle	(LV)
Limits of agreement	(LOA)
Litres per minute	(L/min)
Marc Bailey	(MB)

Maximum anterior-posterior diameter	(APd_{max})
Millilitres	(ml)
Millilitres per minute	(ml/min)
Millimetres	(mm)
Millimetres-cubed	(mm^3)
Millinewton	(mN)
Milli-seconds	(ms)
Micromolar	(µM)
Megapascal Pressure unit	(MPa^{-1})
Messenger RNA	(mRNA)
National AAA Surveillance Programme	(NAAASP)
Native Aortic Vascular Smooth Muscle Cell	(NAVSMC)
National Health Service	(NHS)
National Institute for Health and Care Excellence	(NICE)
National Institute for Health	(NIH)
National Institute for Health Research	(NIHR)
NICE guideline	(NG)
Observer 1	(O1)
Observer 2	(O2)
one-way ANalysis Of Variance	(ANOVA)
Open Aneurysm Repair	(OAR)
Open Versus Endovascular Repair	(OVER)
Oscillatory Force	(OF)
Paraformaldehyde	(PFA)
Penicillin/Streptomycin	(P/S)
Pearsons' correlation	(r)
PIEZO-1	(P1)

PIEZO-2	(P2)
Phosphate Buffered Solution	(PBS)
Polymerase Chain Reaction	(PCR)
Porcine Pancreatic Elastase	(PPE)
Peak Wall Strength	(PWS)
Quantitative PCR	(qPCR)
Randomised Control Trials	(RCTs)
Rat and mouse Maintenance No.1	(RM1)
Red Florescent Probe	(RFP)
Reverse Transcriptase	(RT)
Ribonucleic Acid	(RNA)
Right Atrium	(RA)
Right Ventricle	(RV)
Ryanodine Receptors	(RyR)
Saphenous Vein	(SV)
Sarcoplasmic Reticulum	(SR)
Scrambled	(scrm)
Schedule 1	(Sch1)
Short interfering RNA	(siRNA)
siRNA scrambled	(siScrm)
siRNA PIEZO-1	(siP1)
Single Nucleotide Polymorphisms	(SNPs)
Smooth Muscle Cells	(SMC)
Smooth Muscle Alpha-Actin	(α-SMA)
Smooth Muscle Heavy Chain	(SM-MHC)
Smooth Muscle 22α	(SM22α)
smMHCCre-ER(T2) PIEZO-$1^{+/+}$	($P1^{+/+}$)

smMHCCre-ER(T2) PIEZO-1$^{+/-}$	($P1^{+/-}$)
smMHCCre-ER(T2) PIEZO-1$^{-/-}$	($P1^{-/-}$)
Standard Buffer Solution	(SBS)
Standard error of the mean	(SEM)
Stromal Interaction Molecule-1	(STIM1)
Stromal Interaction Molecule-2	(STIM2)
Surgeon 1	(S1)
Surgeon 2	(S2)
Three-dimensional	(3D)
Three-dimensional lumen volume	(3DVL)
Threshold Cycle	(Ct)
Transient Receptor Potential Channel	(TRPC)
Transglutaminase 2	(TG2)
Tris-acetate-EDTA	(TAE)
Ultrasound scan	(USS)
United Kingdom	(UK)
United State of America	(USA)
Vascular Smooth Muscle Cell	(VSMC)
Voltage-Dependent Calcium Channels	(VDCC)
Wild-type	(WT)
World Health Organisation	(WHO)
75cm cell culture flasks	(T75)

Chapter 1: Introduction

This thesis focusses on the mechanosensor PIEZO-1 in vascular smooth muscle cells (VSMCs) in an attempt to further understand its role in the Abdominal Aortic Aneurysm (AAA) disease. This may facilitate future more in-depth interrogation of mechanistic intra-cellular signalling pathways involved in the complex pathophysiology processes with the intention of identifying a potential pharmacological therapeutic target.

This chapter will give an overview of established anatomical and physiological principles in relation to the arterial system, specifically the aorta. It then focuses on; AAA disease, VSMC physiology and pathological remodelling, aortic mechanics, mechanotransduction and the PIEZO mechanosensors. Finally, this chapter introduces the pertinent AAA mouse models utilised in this thesis.

1.1. The Arterial System and Aorta

1.1.1. Overview of the Arterial System

The arterial system consists of all the vessels which carry blood out from the right and left ventricles of the heart to the peripheral capillary beds (Figure 1a). The main purpose of the arterial system is to facilitate the transportation of; oxygen-rich blood, nutrients and hormones to the tissues. The two main circuits in which blood is carried include the pulmonary and systemic circulations (Figure 1b). The largest artery in the human body is the aorta which carries oxygenated blood throughout the body followed by the pulmonary trunk which carries deoxygenated blood to the lungs.

The arterial wall consists of three distinct layers. The tunica intima, which is the inner most layer and contains the endothelium and basement membrane, the tunica media, which is the middle layer and contains vascular smooth muscle cells (VSMCs) and the elastic lamina; and the tunica externa, which is

the outer most layer containing collagenous fibres, fibroblasts, vasa vasorum (in larger vessels) and nerve fibres (Figure 1c). The intima provides a smooth continuous surface for blood to glide over, ensuring blood reaches where it is required. Any disruption to this layer may initiate pathological processes such as thrombosis and atherosclerosis (Smith et al., 2015). The tunica media provides the strength required to withstand luminal pressures and determines the internal diameter through vasoconstriction and vasodilation determined by various stimuli. The tunica externa provides the structural shape to the vessels (Tucker et al., 2017). The structural composition of the arterial wall may change with age and to compensate for physiological and pathological processes as described in section 1.1.3.

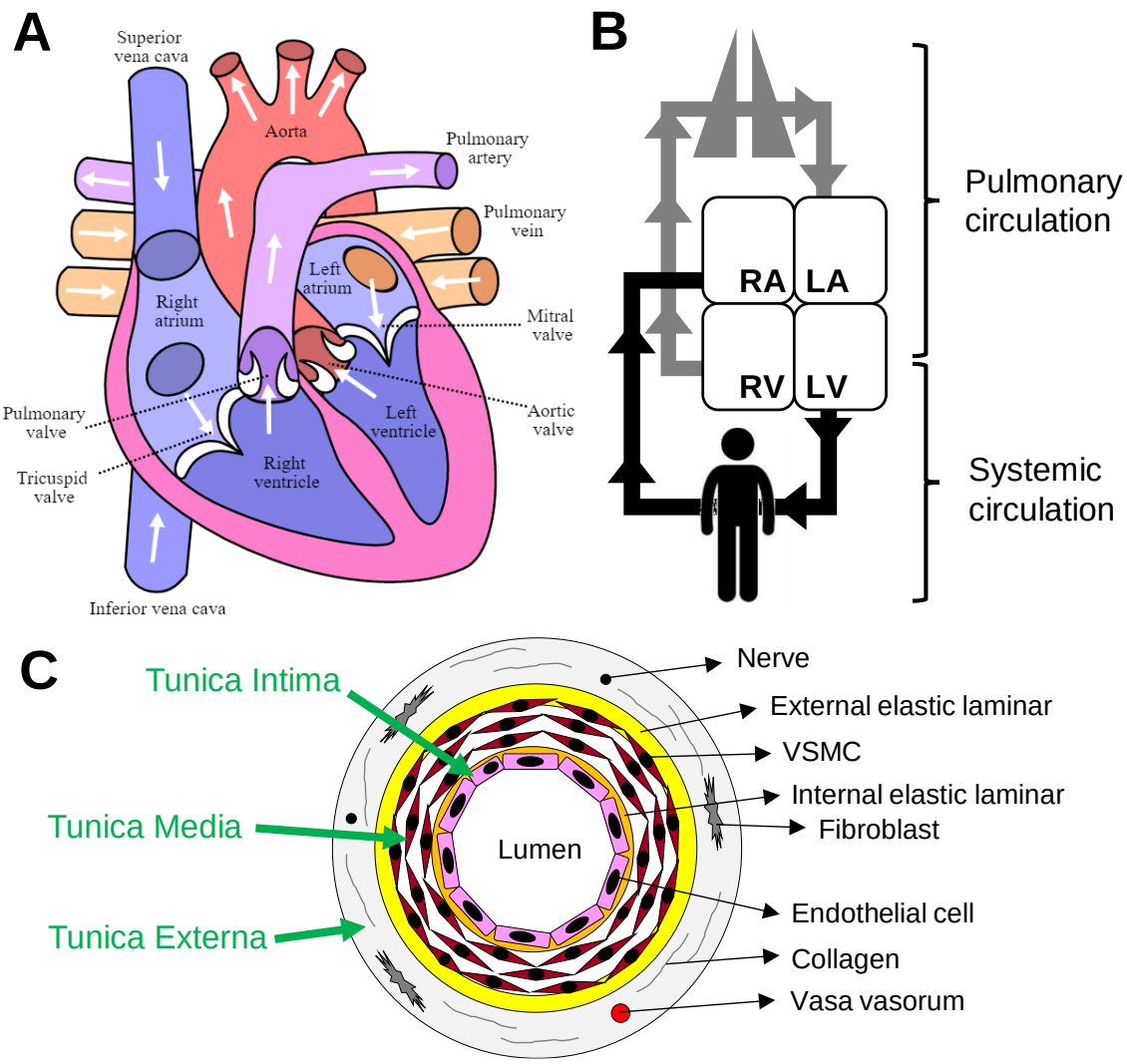

Figure 1. Anatomy and physiology of the arterial system.

A; Diagram of the heart illustrating the chambers of the heart and blood vessels entering and leaving the heart. Copied from google images under creative common licences. Arrows denote direct of blood flow. B; Illustration of the arterial circuits. RA = Right Atrium. LA = Left Atrium. RV = Right Ventricle. LV = Left Ventricle. Arrows denote direction of blood flow. C; illustration of the layers of the arterial wall.

1.1.2. The Aorta and Aortic Physiology

The aorta begins at the left ventricle and descends through the thoracic and abdominal cavities. Despite being one continuous structure the aorta is subdivided into the ascending aorta, aortic arch, descending aorta, thoracic aorta and the abdominal aorta based on the surrounding anatomical

boundaries (Figure 2). The abdominal aorta spans from the diaphragm to the aortic bifurcation, and is a retroperitoneal structure enclosed by the parietal peritoneum anteriorly and the bony spine posteriorly. The aorta subsequently divides into smaller arteries (i.e. iliac arteries), arterioles and finally into capillaries, which importantly supply tissue beds. Blood within the arteries travels in a pulse wave under pressure, with the greatest recoil at the aortic arch, which dissipates as blood travels down the arterial tree. The mean arterial blood pressure is typically around 80-90 mmHg whereas the mean venous pressure may vary between 8 and 10 mmHg (Opie and Paterson, 2004). The mechanical composition of the aortic wall therefore changes throughout its course to accommodate and adequately dissipate blood throughout the body.

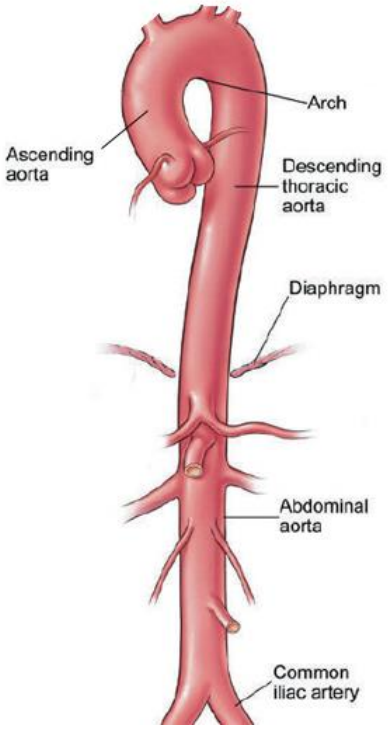

Figure 2. Schematic of the infra-renal aorta located between the diaphragm to the iliac bifurcation.

Adapted from clevelandclinic.org.

The aorta has a greater proportion of elastin and collagen in the proximal ascending aorta compared to the distal abdominal aorta (Humphrey et al.,

2015). In contrast, there is a greater proportion of vascular smooth muscle in the distal abdominal aorta compared to the proximal aorta (Humphrey et al., 2015). Therefore, genetic aneurysms involving connective tissue (i.e. Marfan's and Ehlers-Danlos syndrome), contractile proteins and aortic dissections often occur in the proximal aorta, whereas degenerative diseases such as AAA and aorto-occlusive diseases tend to affect the distal aorta (Milewicz et al., 2017). VSMCs in the tunica media are aligned circumferentially and their contractile phenotype allows them to determine vascular tone hence regulate pulse pressure and blood flow. Several mechanisms exist which determine vascular tone. These include receptors/sensors that can detect; myogenic pressure, neural, hormonal and metabolic stimulation (Folkow, 1964). Regardless of the origin of the stimulant, they ultimately activate intra-cellular calcium entry and contraction or relaxation of VSMCs.

1.1.3. Age-related Changes in Arteries

As the human body ages, natural physiological changes occur in these arteries. The arterial wall has decreased collagen, elastin undergo fragmentation, and calcium deposition is commonly evident (Butlin and Avolio, 2015). These changes may increase vessel diameter, increase wall rigidity and thickness, and decrease wall elasticity, ultimately impairing the function of the vessel (Thijssen et al., 2016). Clinically, age-related increases in blood pressure is often evident in the elderly. Furthermore, homeostatic adaptation of vascular receptors in response to the blood pressure may recalibrate, making it more difficult for the body to maintain a constant blood pressure. It is well established that in geriatric medicine, patients are prone to suffer from orthostatic hypotension. Baroreceptors fail to respond to predictable momentary physiological decreases in peripheral resistance that occurs when standing from a lying or seated position. This results in a significant decrease in cerebral blood flow, which manifests as the patient collapses (Lipsitz, 1989). Furthermore, thickening of the basement membrane of the capillary wall may affect the delivery of the nutrients and oxygen vitally required by tissues. The health-related sequelae of pathophysiological vessel calcification is further

evident by the high prevalence of peripheral arterial disease and aortic stenosis seen in this population. The relationship between advancing age and the development of atherosclerotic and thrombotic diseases is one that is well established, which is exacerbated by the presence of co-morbidities (Crow, 1996).

1.1.4. Vascular Disease

Cardiovascular disease is the leading cause of death worldwide, with 9 million deaths attributed to heart disease in 2019 (WHO, 2019). The British Heart Foundation (BHF) estimates that one in four people in the United Kingdom (UK) will die of cardiovascular disease (BHF factsheet January 2022). Conservative estimates of the prevalence of cardiovascular disease in the UK are around 4% (Bhatnagar et al., 2016). Approximately 7.6 million people in the UK are affected. The prevalence of cardiovascular disease has been stable throughout the past two decades, however, mortality associated with cardiovascular disease has more than halved (Bhatnagar et al., 2016). Despite this reduction in mortality, there have been increased hospitalisations, increased cardiovascular interventions and increased dependence on cardioprotective medications (Bhatnagar et al., 2016), placing an ever-growing burden on the healthcare system.

Vascular disease is a global term used to describe a spectrum of diseases affecting vessels within the body. They are predominantly either congenital or acquired. In the latter, the underlying pathologies may be broadly categorised into atherosclerotic, thrombotic and aneurysmal. The acquired pathologies are similar in that there is a maladaptive cellular response by the body to environmental factors, which damage the vessels.

1.2. Abdominal Aortic Aneurysm

1.2.1. Defining an Abdominal Aortic Aneurysm

An aortic aneurysm refers to an abnormal dilatation of a segment of artery greater than its normal maximal diameter. It may be further classified based on its anatomical location, underlying aetiology, or pathophysiology. The majority (approximately 80%) of aortic aneurysms occur in the infra-renal abdominal aorta (Figure 2), however the disease can occur anywhere from the aortic root to bifurcation (Jongkind et al., 2010). An Abdominal Aortic Aneurysm (AAA) is a focal dilatation of the abdominal aorta greater than 3 centimetres in maximal diameter (Moll et al., 2011a) or greater than 1.5 times its “normal” diameter (Johnston et al., 1991). The former definition however may not be applicable to women whom on average have smaller diameter arteries than men (Rogers et al., 2013). Structurally, a true aneurysm involves all three layers of the wall. Morphologically, an aneurysm may be fusiform (involving the whole circumference) or saccular (involving part of the circumference). Regardless of the imaging modality used, an aneurysm should be measured on a transverse cross-section of maximal distention. Measurements can be based on the inner-to-inner, leading edge-to-leading edge, or outer-to-outer boundaries and may vary from institution to institution (Johnston et al., 1991).

1.2.2. Risk Factors and Epidemiology

An AAA is a complex multi-factorial disease. It is most common among men aged above 65 years. A lower prevalence of AAA in women may be explained by sex hormone related protection, equivalent to that seen in other cardiovascular diseases (Villard and Hultgren, 2018). Smoking and a positive family history are well-established important risk factors and are associated with a higher rate of aneurysm growth (De Ceniga et al., 2006; Sweeting, M. et al., 2012b). It is estimated that 10-20% of patients with an AAA have a family history of an AAA (Sakalihasan et al., 2005; Kuivaniemi et al., 2015). This is further supported by the largest AAA genome-wide associate study (GWAS) study, which identified 9 AAA genetic risk loci (Jones et al., 2017).

Other risk factors include cardiovascular disease, hyperlipidaemia, hypertension and chronic obstructive pulmonary disease (COPD) (Lederle, F.A. et al., 2003b; Kent et al., 2010; Hernesniemi et al., 2015; Tang et al., 2016). However, in contrast to other cardiovascular diseases, a lower prevalence of diabetes mellitus is observed in patients with an AAA compared to the general population (Lederle, F., 2012) (Salata et al., 2018; Shantikumar et al., 2010). Furthermore, the rate of growth of an AAA is slower in patients with diabetes, raising the possibility that metformin may play a role in inhibiting AAA growth (Sweeting, M. et al., 2012a; Golledge et al., 2017).

Worldwide, the prevalence and incidence of AAAs have been declining over the past decade. This has been attributed to the global decline in smoking (Sampson et al., 2014). However, the prevalence of AAAs varies among ethnic groups, sex and ages. However, the true prevalence of AAAs cannot be established due to the asymptomatic nature of the disease, the reliance on imaging modalities for diagnosis and specialist post-mortem assessment when indicated (Sampson et al., 2014). Screening is offered only in a handful of countries (i.e. UK, Sweden, Italy, USA, Australia) and the socioeconomic limitations of others result in a bias representation. It is important to acknowledge that healthcare inequalities may be exacerbated by screening programmes as it is often the educated and well informed in society who are likely to appreciate the importance of such tests especially due to the asymptomatic nature of the disease. Nevertheless, it is estimated that 1.34% of men over 65 years have an AAA in the UK (Jacomelli et al., 2016) and approximately 6,000 deaths every year are attributed to the disease (www.vascularsociety.org).

1.2.3. Clinical Presentation and Natural History

Most patients with an unruptured AAA are asymptomatic and therefore undiagnosed. An AAA is often an incidental finding on imaging performed for an alternative indication or picked up through a formal AAA screening

programme. However, patients may report a constant abdominal ache, back pain, or even notice a pulsatile swelling near their umbilicus. If undetected, with time, the arterial wall weakens and may no longer be able to withstand the luminal forces required to maintain blood flow, resulting in the rupture of the vessel. The ruptured aneurysm may lead to the sudden-onset of severe abdominal or back pain. Ruptures may be contained within the retroperitoneal space or extend into the intra-peritoneal compartment, resulting in haemorrhagic shock. A ruptured AAA is a life-threatening surgical emergency with out of hospital mortality more than 80% and in-hospital mortality more than 40% if treated (Investigators, 2014; Filardo et al., 2015). If left untreated it results in almost 100% mortality (Moll et al., 2011b).

In the UK men at the age of 65 years are invited for a routine aortic ultrasound scan (USS) as part of a National Health Service (NHS) screening programme (Scott and Group, 2002; Jacomelli et al., 2016). If an AAA is identified on screening the patient is then enrolled onto the national AAA surveillance programme (NAAASP). If the AAA is detected incidentally (e.g. in a woman or a man who was not screened) then the patient is enrolled in the local hospital based surveillance programme under the care of vascular surgery. Similarly patients who had AAA diagnosed prior to the rollout of the NAAASP (i.e. 2013), remain in the local hospital surveillance programme. The scan intervals for the NAAASP and the local hospital surveillance programmes are identical in the UK.

As the probability of rupture increases with the size of the aneurysm or following a period of rapid aneurysm growth, for example greater than 0.5 cm per year (Lederle, F.A. et al., 2002). The RESCAN study meta-analysis assessed aneurysm growth and rupture risks in small AAAs (3.0 to 5.4 cm) (RESCAN Collaborators et al., 2013). For every 0.5 cm increase in the aortic diameter the annual growth rate increased by 0.59 mm per year and rupture risk increased by 1.91. Therefore, the current UK NICE Guidance (NG156) recommend surgical intervention if the rate exceeds 1 cm per year.

1.2.4. AAA Pathophysiology

Uncertainty exists behind the exact triggers underlying the histopathological processes observed in AAA disease. Understanding of the disease process has been largely attained through histological analysis of resected tissue obtained during open surgical repair of large aneurysms. Chronic aortic wall inflammation from immune cell infiltration and oxidative stress, thinning of the tunica media through destruction of the elastin and loss of VSMCs by apoptosis (so-called “medial degeneration”), and degradation of the extracellular matrix through proteolytic fragmentation have all been proposed to play important roles (Sakalihasan et al., 2005). It is likely that there is a complex interaction between these processes, which makes it challenging to identify an all-encompassing pharmacological target. However, it is evident that the concomitant loss in the integrity of the tunica media and tunica externa is thought to result in the development and progression of an AAA.

Meta-analysis of six GWAS data sets have identified nine AAA risk loci (Jones et al., 2017). The functional relationship of these genes were subsequently assessed using Data-Driven Expression-Prioritization Integration for Complex Traits (DEPICT), which evaluates how hundreds of nominally significant single-nucleotide-polymorphisms (SNPs) converge to known pathways linked to biological processes. One of these gene sets, MP:0005595, has been shown to be linked to abnormal vascular smooth muscle physiology. Interestingly, none of these loci were associated with thoracic aneurysms or dissections, which may suggest the embryological origin or the location of the VSMCs may play a role in explaining the underlying pathological processes as described below.

1.2.5. Current Surgical Management Strategies

1.2.5.1. Pre-Intervention Considerations

Although the size of the AAA is initially detected on ultrasound imaging, patients often undergo further detailed imaging, such as computerized tomography or magnetic resonance imaging of the entire aorta, to

characterise the morphology of the aneurysm and surrounding structures to help plan the most suitable intervention. Fitness for open surgery is also assessed through cardio-pulmonary exercise testing and review by an anaesthetist where appropriate. Patients are then discussed by a multi-disciplinary team including, surgeons, interventionalists, anaesthetists, nurses, and radiologists. The risks and benefits of interventional strategies suitable are then discussed with the patients to achieve a fully informed holistic patient-centred decision.

In the UK, surgical treatment is considered once the AAA reaches 5.5 cm in diameter. This threshold is somewhat arbitrary and was adopted following the results of the UK Small Aneurysm trial (The UK Small Aneurysm Trial Participants, 1998). This landmark study investigated the early surgical intervention of an AAA on diagnosis (between 4.0 to 5.5cm) compared to surgical intervention of an AAA at 5.5 cm. The rationale for selecting 5.5 cm as the cut-off is unclear. However, recently analysis of the National Health Service AAA Screen Programme showed no evidence that this threshold should be changed as small aneurysms measuring between 3.0-4.4cm had an annual rupture risk of 0.03% compared with large aneurysms measuring between 5.0-5.4 cm that had a rupture risk of 0.40% (Oliver-Williams et al., 2019). Nevertheless, the UK Small Aneurysm trial importantly showed there to be no survival advantage in patients undergoing early surgical invention, which was associated with higher post-operative mortality when compared to the general population (Powell, J., 2007).

1.2.5.2. EVAR and OAR

The two dominant surgical strategies in the management of an AAA include endovascular aneurysm repair (EVAR) and open aneurysm repair (OAR), Figure 3. The first successful OAR repair was performed by Dr Charles Dubost in 1951 in Paris (France) and the first successful EVAR was performed by Dr Juan Parodi in 1990 in Buenos Aires (Argentina) almost four decades later (Thompson, J.E., 1998; Coselli and Green, 2013). These two strategies were compared in the EVAR 1 trial conducted in the UK (Greenhalgh, 2004). In this

landmark study, EVAR was associated with reduced 30-day mortality due to lower post-operative mortality compared to OAR. However, this benefit was lost by 4-6 years post-procedure, and beyond 8 years OAR was associated with significantly lower mortality due to the absence of sac rupture and lower incidence of cancer (Patel, R. et al., 2016). Similarly, the Dutch Randomised Endovascular Aneurysm Management (DREAM) trial revealed initial survival advantage with EVAR which was lost on long-term follow-up at 6 and 12 years (Prinssen et al., 2004; De Bruin et al., 2010; van Schaik et al., 2017). Secondary intervention rates, however, were significantly higher in the EVAR group (van Schaik et al., 2017). Furthermore, the Open Versus Endovascular Repair (OVER) study in the United States of America supported these findings by also demonstrating early survival advantage with EVAR compared to OAR which was lost by 3 years with no long-term difference in mortality at 14 years (Lederle, F.A. et al., 2009; Lederle, F.A. et al., 2012; Lederle, F.A. et al., 2019). However, similar to the DREAM trial, patients in the EVAR group had significantly higher secondary interventions (Lederle, F.A. et al., 2019). Other contemporary studies have also reported the incidence of secondary re-intervention to be as high as 9-25% (Nordon et al., 2010; Patel, R. et al., 2016). The EVAR-2 trail was another landmark study conducted in the UK comparing the long-term outcomes of patients who were ineligible for OAR following EVAR and no intervention (EVAR Trial Investigators, 2010). It demonstrated EVAR to be associated with a significantly lower aneurysm-related mortality however there were no significant differences in overall all-cause mortality (Sweeting, M.J. et al., 2017).

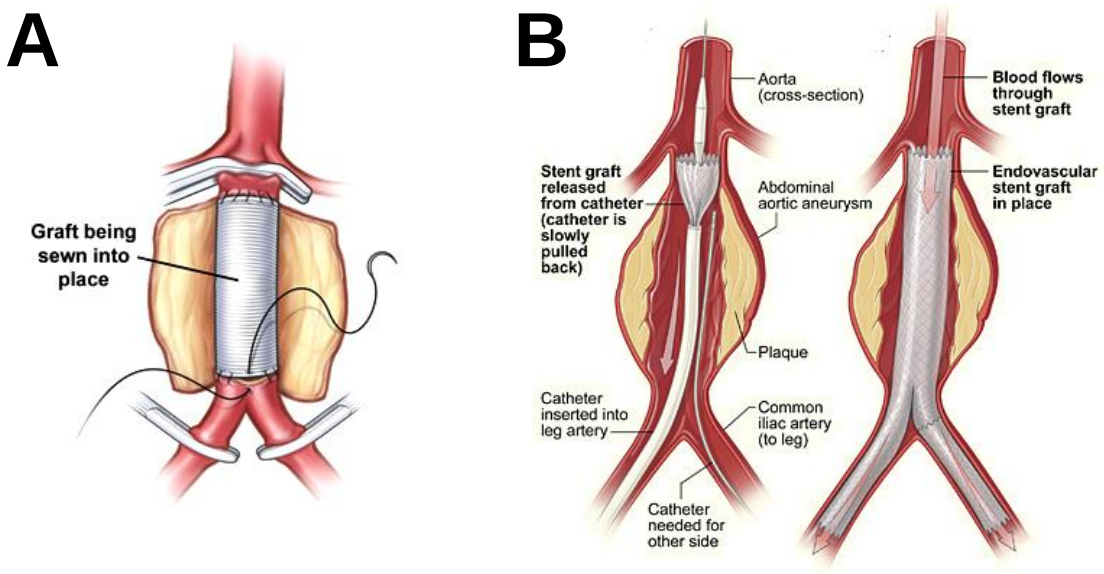

Figure 3. Illustration of surgical interventions for an AAA.

A; Open Aortic Repair. Performed by opening the abdominal cavity and exposing the abdominal aorta, allowing the aneurysm sac to be clamped above and below the iliac arteries, facilitating the disease sac to be opened and artery bridged with a synthetic material. B; EndoVascular Aneurysm Repair. Performed by percutaneously inserting two guidewires into the iliac arteries, allowing a catheter with a stent to be inserted to cover the aneurysmal portion.

Images were adapted from the Society of Vascular Surgery website (https://vascular.org).

1.2.5.3. Controversy in Surgical Management

In the UK, the role of EVAR has become a topic of much debate among vascular surgeons and interventionalists, with the initial National Institute for Health and Care Excellence (NICE) AAA guidelines (NG156) 2018 draft proposal recommending clinicians not to offer EVAR in patients suitable for OAR. EVAR was shown not to be cost effective and associated with a risk of late rupture compared to OAR. Furthermore, it was suggested that patients not suitable for OAR due to co-morbidities or the perceived anaesthetic risks should also not be offered EVAR. However, in 2020, the final published version of NG156 had made a complete u-turn with the recommendations in

relation to EVAR. Initial recommendations were changed to accept EVAR as a suitable option in patients with a hostile abdomen or co-morbidities that would make OAR technically challenging. Furthermore, patients were to be given the choice in the method of intervention they would prefer following careful discussion of the risks and benefits. The expert committee assembled to develop this guideline released a statement distancing themselves from the guidelines as the revised contents were not discussed with themselves. Suggestions have been made that NICE, which is presumed to be impartial, evidence led and transparent, has been pressured by certain stakeholders (i.e. device manufacturers) to ignore their own cost-effective analysis and expert census (Hinchliffe and Earnshaw, 2020).

1.2.6. Current Pharmacological Therapies

Once an AAA has formed, the progression of the disease is heterogeneous and cannot be accurately predicted (Bailey et al., 2013; Thompson, A. et al., 2010). Aneurysms less than 5.5 cm in diameter have a relatively low risk of rupture and large randomised controlled trials have reported no survival advantages with elective surgery in this cohort (The UK Small Aneurysm Trial Participants, 1998; Merali and Anand, 2002; Lederle, F.A. et al., 2003a).

Current NICE (NG156) and ESVS guidelines both echo the absence of any disease specific pharmacological therapies along with the absence of any robust evidence in supporting secondary prevention strategies utilised in cardiac disease. However, the NICE guidelines do recommend pharmacological interventions to manage hypertension and smoking cessation counselling is appropriate. Furthermore, the ESVS guidelines recommend the use of antiplatelet and lipid lowering therapy due to the survival benefits demonstrated from the retrospective analysis of large databases (Bahia et al., 2016; Salata et al., 2018). However, the use of these therapies remains a topic of debate due to the absence of data from prospective randomised controlled trials. The National Institute for Health and Care Research has recently awarded a grant worth approximately £1 million to Mr Athanasios Saratzis for the “cardiovascular risk reduction in the NHS

AAA screening programme: a co-developed cardiovascular prevention intervention" study (CRISP study, NIHR 300059) aimed at identifying secondary prevention measures to help prevent secondary cardiovascular incidents observed in the patient population with AAA. Furthermore, drugs targeting histopathological pathways described above (i.e. transmural inflammation, elastin degradation etc.) have failed to translate to viable medical options (Sillesen et al., 2015; Meijer et al., 2013).

1.2.7. The Unmet Need

Patients with an AAA are often in their seventh decade of life with multiple co-morbidities (Powell, J.T. et al., 2017). Invasive intervention carries a significant morbidity and mortality risk in this patient population (Kazmers et al., 1998). At present, no comprehensive data exist with regards to the number of patients turned down for the intervention. The results of the EVAR-2 trial show, of the patients who were randomised to no surgical intervention, only 34% of patients were alive after four years (Greenhalgh et al., 2005). Even with successful EVAR, patients did not gain any survival advantages as death resulted from non-aneurysm related causes, such as cardiovascular events, sepsis, or cancer. Therefore, surgical intervention seem to only change the mode of death without extending the life span of this group of patients. Furthermore, surgical repair has a negative impact on midterm quality of life (Coughlin et al., 2013). Consequently, there has been a recent shift in the management of AAA advocating conservative treatment strategies in this high-risk population (AAA NICE Guidelines, 2018).

However, to date there are no pharmacological therapies specifically stop or slow the progression of an AAA (Sweeting, M. et al., 2012b; Lederle, F.A., 2013). Therefore once an AAA is identified, patients are placed onto a surveillance programme and aneurysm growth is monitored. The identification of novel pathophysiological targets may facilitate the development of new therapeutic drugs, which is of high priority in the field of vascular surgery. To achieve this, a greater understanding of the key pathophysiological triggers involved in early aneurysmal development and progression is required. As it

is impossible to histologically study the disease as it progresses in humans, animal models may be the best option to gain a useful insight into these early changes.

1.3. Aortic Vascular Smooth Muscle Cells

1.3.1. Embryological Origin of Aortic VSMCs

Despite being part of one continuous structure, aneurysmal disease observed in the thoracic aorta is pathophysiologically different from that observed in the abdominal aorta. The differences in pathological presentations may be attributable to the embryological origins of VSMCs. In the aortic wall, VSMCs have different embryonic origins depending on the region in which they are situated. For example, VSMCs in the aortic arch arise from the neural crest, VSMCs in the thoracic aorta arise from somites and those in the abdominal aorta arise from the splanchnic mesoderm (Kuivaniemi et al., 2015). This results in the VSMCs having different physiological characteristics. VSMCs found in the abdominal aorta are primitive and have not been replaced in a second wave of SMC migration from the neural crest like those of the thoracic aorta which are suited to adaptive remodelling (Tromp et al., 2010). Furthermore, VSMCs in the thoracic aorta lay down more elastic lamellae during development and growth and can therefore withstand higher pulse pressures and ejection volumes encountered. The differences in regional VSMC characteristics can be further demonstrated by their responses to the same chemicals. For example, homocysteine plays a well-established role in atherosclerotic disease and elastolysis, which can stimulate neo-intimal proliferation and synthetic activity in thoracic VSMCs which is not seen in abdominal VSMCs (Dalton et al., 1997). Differences are also evident when infusing angiotensin II in apolipoprotein E knockout mice where vascular remodelling and atherosclerosis are seen in the thoracic aorta and not the abdominal aorta. The differences in characteristics of VSMCs in the abdominal aorta may explain the low prevalence of aorto-occlusive disease in the general population compared to AAA disease.

1.3.2. VSMCs Characteristics and Remodelling

VSMCs in the abdominal aorta are located in the tunica media and are arranged in a circumferential layer and bulk of the vessel wall. In healthy adults, VSMCs are mature (i.e. highly differentiated), quiescent, non-proliferative, non-migratory and have a low synthetic ability. They are referred to as having a contractile phenotype. They are morphologically fusiform with a large central nucleus with an abundance of contractile proteins (Figure 4). Components of the contractile apparatus include smooth muscle alpha-actin (α-SMA), smooth muscle heavy chain (SM-MHC) and smooth muscle 22α (SM22α), which may be used as markers of mature differentiated VSMCs (Gomez and Owens, 2012; Wang, J. et al., 2006), Figure 5. However, these markers may be also be expressed transiently in cell types during physiological remodelling or disease states (Owens et al., 2004). Unlike striated muscle, vascular smooth muscle cells have end-to-end junctions to provide a large surface area to facilitate mechanical tight junctions and electrical coupling. They are innervated primarily by the sympathetic nerve system that initiate vasoconstriction or vasodilation. However, VSMCs may contract and relax independently to accommodate changes in intra-luminal mechanical pressure and respond to endogenous stimuli to ensure nutrients are adequately transported to capillary beds. Irrespective of the trigger, it is the membrane potential of VSMCs that is the key regulator of vascular tone and therefore regulates circulatory flow and pressure.

In angiogenesis, after the initial endothelial tube formation, mesenchymal cells are recruited which later differentiate into VSMCs. This requires the careful interactions between endothelial and mural cells through cell signalling. During the formation of arteries, the phenotype of VSMCs is synthetic and only later switches to contractile. This is an important transition in angiogenesis as it is during the synthetic state that the ECM proteins (including elastin) and intracellular sarcoplasm are formed that are later maintained during the contractile state (Owens, 1996; Stegemann et al., 2005). This results in mature arteries having the ability to recoil and regulate vessel tone. The initial synthetic phenotype is thought to be driven by the high pressures present

within arteries. This is not the case in veins.

Arterial VSMCs are phenotypically plastic. They may be switched out of the contractile phenotype to the synthetic phenotype by a variety of stimuli, such as abnormal mechanical forces, changes to the extracellular matrix, inflammation and growth factors (Raines, 2004). This switch in phenotype causes the arterial wall to change morphologically in response to stressors through remodelling of the extra-cellular matrix, inflammation and VSMC proliferation. Importantly, mechanical stimuli can not only cause pathological changes in VSMCs but also reset normal homeostatic functions resulting in remodelling and dysfunction. For example, sustained hypertension leads to arterial wall thickening and stiffness (Kaess et al., 2012; Korneva and Humphrey, 2019). Furthermore, when using vein grafts as conduits in arterial bypass surgery, the vein is subjected to the high arterial pressures of the systemic circulation. This may result in VSMC proliferation, graft stenosis limiting flow and eventual failure due to thrombosis (Fitzgibbon et al., 1996). Therefore, mechanical forces is an essential component in maintaining of vessel structure and function.

Under certain pathological conditions VSMCs may undergo phenotypic modulation. This process describes de-differentiation of the VSMC back to a synthetic phenotype that existed during vascular patterning in vasculogenesis (Bacakova et al., 2018). This is characterised by the loss of contractile filaments and associated apparatus in favour of organelles associated with proteosynthesis (Figure 4). VSMCs of the synthetic phenotype may proliferate and migrate. This is evident in the atherosclerotic plaque formation (Owens, 1995; Bennett et al., 2016)**.** VSMCs have also been shown to become senescent and even apoptose in aortic aneurysmal disease contributing to the disease process (Bennett et al., 2016). This is supported by recent observations from a Meta-Genome Wide Association Study on AAAs, analysing bioinformatics pathways, which has identified there to be abnormal activation of VSMC physiological pathways, i.e. MP:0005595 and GO:0000989 (Jones et al., 2017). Phenotypic switching may occur early in the

pathophysiological processes of AAA development, however, the exact mechanistic role of VSMCs in AAA formation remains unclear.

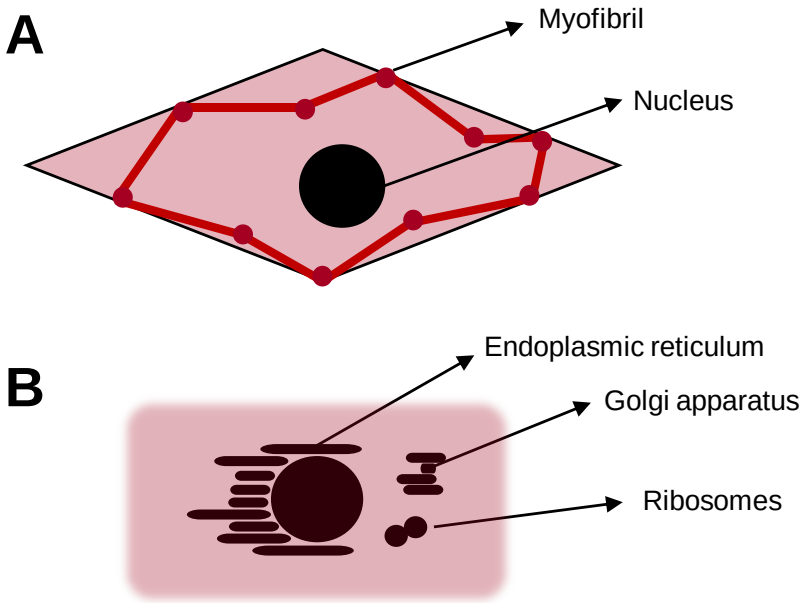

Figure 4. Illustration of VSMC phenotypes. [A] contractile phenotype and [B] synthetic phenotype.

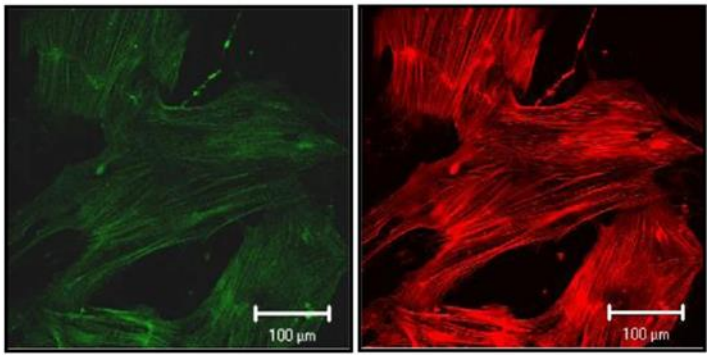

Figure 5. Immunocytochemical staining of AAA VSMCs with α-SMA (left, green) and SM-MHC (red, right).

Adapted from (Riches et al., 2013).

1.3.3. VSMC and Downstream Pathways

VSMC proliferation and migration into the intima, from tunica media, in the development of atherosclerotic plaques is well established (Rudijanto, 2007; Ross and Glomset, 1973). However, over the past decade it has been demonstrated that VSMCs may also migrate and proliferate into the adventitia, in response to mechanical stress, due to the dynamic cell populations it hosts; i.e., leucocytes, microvessel, adipocytes, and vascular progenitor cells (Passman et al., 2008; Psaltis et al., 2012). There is a growing body of evidence describing the role of dysfunctional mechanosensing and the intermediary pathways, involving transforming growth factor–β (TGF–β) and platelet-derived growth factor (PDGF), in AAA development and growth (Humphrey et al., 2014; Humphrey et al., 2015). Furthermore, there is evidence that mechanosensor stimulation may activate downstream pathways involved in cell proliferation and stiffness, such as: Krüppel-Like transcription Factors 2 and 4 [KLF-2, KLF-4] and Transglutaminase 2 [TG2] (Retailleau et al., 2015; Choi et al., 2017). In addition to the scientific rationale for selecting these three genes, they were also selected based on expertise and resources available within the research group.

PDGF is a growth factor with 4 different isomers of which PDGF-B and its receptor have been described to play an instrumental role in blood vessel formation and shown to be highly expressed in vascular endothelium and VSMCs (Hellström et al., 1999). Furthermore, many studies have demonstrated its association with pathological processes of vascular disease and is thought to be critical in driving VSMC de-differentiation and phenotypic modulation (Raines, 2004). TGF–β on the other hand is a multifunctional cytokine thought to be a driver of VSMC differentiation and protective against vascular remodelling (Owens et al., 1988; Majesky et al., 1991). The TGF–β receptor, once activated, results in the transcription of target genes involved in cell differentiation and proliferation (Massagué, 2012).

1.3.3.1. Krüppel-Like transcription Factor 2

Krüppel-Like transcription Factor 2 (KLF-2) is a member of the zinc finger protein which is involved in the development vessels, through the activation of cellular migration and proliferation. It plays a similar role in the other cell types, including endothelial cells, lymphocytes, monocytes and adipocytes. KLF-2 expression is typically triggered by laminar flow over the normal endothelium. Several studies have demonstrated that KLF-2 is critical in blood vessel wall integrity (Kuo et al., 1997; Lee, J.S. et al., 2006). The absence of KLF-2 in-utero results in the failure of vascular maturation due to the absence of mural cells migrating around endothelial cells (Wu, Jinghai et al., 2008). Therefore, it is strongly suggested that KLF-2 is implicated in vascular remodelling (Moehle and Owens, 2009).

1.3.3.2. Krüppel-Like transcription Factor 4

Krüppel-Like transcription Factor 4 (KLF-4), another member of the zinc finger protein family, is also involved in cell proliferation, differentiation and apoptosis of cells. It has been shown to be upregulated in humans during AAA formation and has been localised to VSMCs (Salmon et al., 2013). Furthermore, KLF-4 is one of the main factors in inducing pluripotent stem cells (Takahashi et al., 2007; Takahashi and Yamanaka, 2006). It has been shown that KLF-4 regulates the generation and maintenance of AdvSca1 progenitor cells which have been shown to self-renew and differentiate into VSMCs (Passman et al., 2008). Global conditional KLF-4 knockout in mice demonstrate a delay in phenotypic switching of VSMCs after endothelial injury (Yoshida et al., 2008). Furthermore, the deletion of KLF-4 prevents the formation of aortic aneurysms in knockout mice (Salmon et al., 2013).

1.3.3.3. Transglutaminase 2

Transglutaminase 2 (TG2) is a calcium-dependent enzyme shown to contribute to mechanical stability of the vessel wall (Iismaa et al., 2009). It plays a physiological role in age-related vascular stiffness (Armstrong Filho et al., 2018). However, it has been shown to be involved in resistance

remodelling induced by chronic vasoconstriction secondary to hypertension, a key risk factor in the development of an AAA (Bakker et al., 2005; Retailleau et al., 2015). TG2 also plays an important role in hypoxia-induced VSMC remodelling observed in pulmonary hypertension (Penumatsa et al., 2014). In AAA disease, TG2 expression has been shown to be increased when infra-renal aortic aneurysm is induced in rats (Munezane et al., 2010). However, in TG2 knockout mice, it results in the exacerbation of AAA formation in the $CaCl_2$ model (Griffin et al., 2021).

1.3.4. Smooth Muscle Cell Contraction and Cellular Calcium Entry

Smooth muscle can perform tonic phasic contractions in response to stimuli. The absence of striations is what differentiate smooth muscle cells from cardiac and skeletal muscle. Myosin and actin are the two main contractile proteins that generate the contractile force. Smooth muscles lack voluntary control. Contractions are initiated by autonomic nerve stimulation, membrane receptors, or through direct activation of stretch dependent ion channels resulting in a change in the membrane potential. Intra-cellular calcium is the primary mediator of the smooth muscle contraction. The interaction of calcium with calmodulin to stimulate myosin light chain phosphorylation and subsequent actin-myosin cross-bridge formation and generation of mechanical force (Webb, 2003). Smooth muscle relaxation is initiated through the removal of the calcium from the cytosol and stimulation of myosin phosphatase.

There are two mechanisms by which calcium enters the cytosol. Calcium either enters from the extracellular space or is released from intra-cellular stores. Plasma membrane changes, which mediate calcium influx predominantly include voltage-dependent calcium channels (VDCC) and non-selective cation channels, such as transient receptor potential (TRP) and ionotropic purinergic (P2X) receptors (Hill-Eubanks et al., 2011). The sarcoplasmic reticulum (SR) represents the largest store of intracellular calcium, which may be released upon stimulation through ryanodine receptors (RyR) and inositol triphosphate receptors (IP3Rs) (Hill-Eubanks et al., 2011).

1.4. Aortic Mechanics and AAA disease

The arterial pulse generates both radial force due to cyclic stretching caused by blood volume, and shear stress due to blood flowing tangential to the intima. Radial force is transmitted through all constituent layers of the vessel wall, including the VSMCs. Shear stress, on the other hand mainly interacts with endothelial cells (ECs). In diseases such as aneurysmal disease, the endothelium may be damaged and disrupted resulting in the exposure of VSMCs. This may result in the application of shear stress directly onto VSMCs (Sheinberg et al., 2019; Franck et al., 2013). The mechanisms by which these mechanical stimuli affect VSMC function, including mechanical-induced biochemical signalling pathways, are unclear.

Evidence implicating the role of mechanical forces in aneurysm development goes back as far as 1968 (Nakata et al., 1968). Humphrey et al. comprehensively described several biomechanical factors to be at play in explaining the development of aneurysms, including abnormal haemodynamic intra-luminal forces, high aortic wall stress and disrupted the perivascular tissue (Humphrey and Holzapfel, 2012). It is well established that the arterial pulse pressure increases as the blood passes from the heart and down the aorta (McDonald, 1968). This results in a high wall stress within the abdominal aorta, compared to the aortic arch, resulting in an increased propensity to develop an aneurysm (Khosla et al., 2014). Furthermore, the infra-renal aorta can experience oscillatory wall stress due to the aorta narrowing conically prior to bifurcating into the iliac arteries, which is also thought to increase susceptibility to AAA development (Amirbekian et al., 2009). The aorta is also thinner posteriorly due to support provided by the spine. Therefore pulsatile wall strain is higher on the anterior aspect. These factors may explain the antero-lateral morphological presentation of most AAA (Goergen et al., 2007). Furthermore, the asymmetric bulging of the arterial wall, like that observed in early aneurysmal disease, can exacerbate wall stress (Doyle et al., 2009; Rodríguez et al., 2008). As the aneurysm morphologically develops/progresses there is also a disruption to the normal laminar flow of blood to one of turbulence. This change shear force to oscillating shear stress

(Boussel et al., 2008; Sughimoto et al., 2016). Additionally, ex-vivo biaxial biomechanical assessment of AAA tissue harvested at the time of open surgery has demonstrated increased arterial stiffness in the aneurysm wall result in disruption of the natural dynamic phenotype of the abdominal aorta (Pancheri et al., 2017; O'Leary et al., 2014). However, Sonesson et al. reported no differences in wall stiffness (pulsatile diameter change) in patients who rupture compared to those which did not (Sonesson et al., 1999). Low shear stress has also been shown to be associated with AAA expansion and rupture or repair (Bappoo et al., 2022). It has been demonstrated in autopsy studies that 10-24% of all ruptured AAA have a diameter less than 5.5cm, and some larger AAAs may never rupture (Nicholls et al., 1998). Therefore, the maximal diameter criterion may not be useful in some circumstances. However, aortic measurements from autopsy studies must be interpreted with caution as the aorta is often distorted due to the absence of luminal blood and the constriction and hardening of tissue.

An AAA may rupture with the intraluminal pressure is higher than the strength of the aortic wall. The term "finite element analysis" (FEA) is used to mathematically describe the likely mechanical behaviour in situations where it cannot be tested experimentally. Computerized tomography (CT) data may be utilised to determine likely variations in peak wall strength (PWS), determined through FEA, which has been demonstrated to be a better predictor of AAA rupture (Fillinger et al., 2002; Venkatasubramaniam et al., 2004; Fillinger et al., 2003). Despite this, it has failed to translate into routine clinical use to the demands of image processing, 3D rendering, mathematical calculations, which make it complex and time consuming.

1.5. Mechanotransduction

Mechanosensing is the cellular ability to detect mechanical stimuli in the surrounding microenvironment. It is not limited to forces, but also includes stress and strain (Chen et al., 2017). Receptor mediated mechanosensing is

a complex multistep process that initiates from the cell surface or adjacent cells and then converted to intracellular biochemical signals and pathways. The ability to perform this function is key for cell survival as it allows the cell to adapt to changes in the microenvironment through (de) differentiation, proliferation, or apoptosis. Ultimately, the tissues morphology and function may be altered through chronic stimulation. Examples of cellular mechanosensing and remodelling include; bone remodelling in response to mechanical strain, or skeletal muscle growth in response to lifting weights or the alignment of endothelial cells toward shear stress.

Vascular mechanosensors are specialised protein complexes, which can detect, process and react to changes in mechanical forces within the vasculature to regulate vascular tone and maintain adequate circulation (Fang et al., 2019). Vascular mechanotransduction describes the process by which mechanical stimuli within vessels are converted to vessel contraction. VSMCs can sense mechanical stimuli via cell membrane-ECM interactions, ion channels, membrane receptors, and transmembrane proteins. These can all play a role in mechanical transduction and trigger downstream pathways and changes in gene expression and protein synthesis (Anwar et al., 2012; Ye et al., 2014). Mechanosensitive ion channels in VSMCs are typically cation channels which are activated by mechanical stress resulting in the generation of excitatory electric signals, hence converting the mechanical stimulus into a chemical signal. Examples of mechanosensitive ion channels include PIEZO, TRP, K2P and ENaC channels. Mechanical stimulation may also mediate and co-ordinate change in integrins, connexin, cytoskeleton proteins and nuclear structures to achieve mechanotransduction. Despite the growing body of evidence, describing the role of mechanosensors in relation to vascular endothelial cells (EC), their role in VSMC pathophysiology remains poorly understood (Yamaguchi, 2004; Retailleau et al., 2015; Zaragoza et al., 2012).

1.6. Piezo and Other Mechanosensors

1.6.1. PIEZO Mechanosensors

The Piezo mechanosensors are relatively recent discovery shown to play a crucial role in the development and preservation of good cardiovascular health (Beech and Kalli, 2019). The name Piezo originates from the Greek word “piezi”, which translates to “pressure”. PIEZO-1, also known as FAM38A, and PIEZO-2, also known as FAM38B, are tri-bladed propeller-like transmembrane structures, Figure 6 (Zhao et al., 2018; Saotome et al., 2018; Wang, L. et al., 2019). When a force is applied the Piezo channels are reversibly flattened, allowing the detection of mechanical stimuli (Wu, Jason et al., 2017). They are calcium permeable non-selective cation ion channels which are non-specifically inhibited by gadolinium (Coste et al., 2010). Both PIEZO-1 and PIEZO-2 have been shown to be activated with the following: increase in fluid flow, the application of membrane tension or pressure and increased stiffness (Coste et al., 2010; Murthy et al., 2017; Wu, Jason et al., 2017).

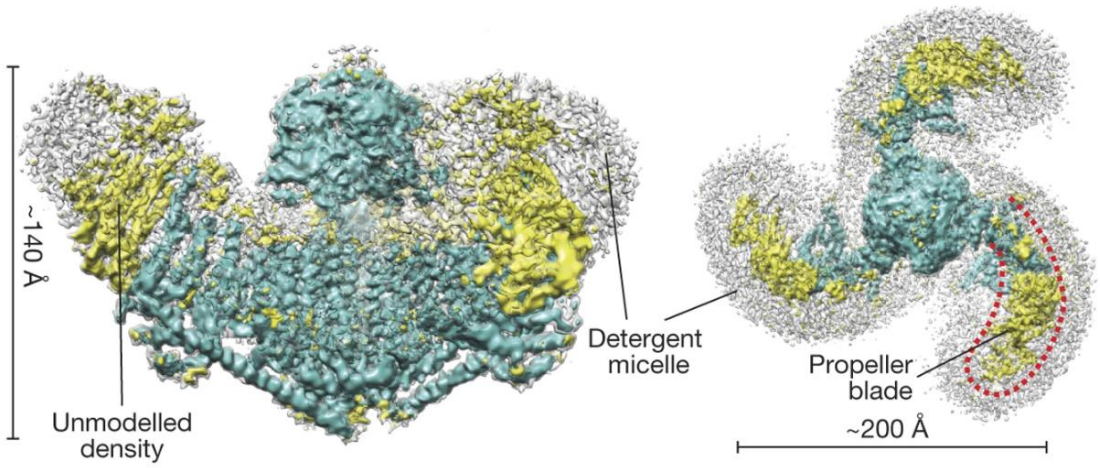

Figure 6. PIEZO-1 cryo electromagnetic map refined with C3 symmetry imposed illustrating propeller like structure. A; side view and B; ariel view.

Adapted from (Saotome et al., 2018).

Researchers at the University of Leeds Institute for Cardiovascular and

Metabolic Medicine, led by Professor David Beech, have been instrumental in demonstrating that PIEZO-1 plays a fundamental role in cardiovascular biology (Li et al., 2014) and homeostasis (Rode et al., 2017). Global knockout of the of the gene has been shown to be lethal in embryonic mice due to failed vessel maturation due to the inability to supply nutrients (i.e. oxygen and glucose) and remove waste products, resulting in organ failure (Li et al., 2014). It is thought that the flow of blood against endothelial cells is sensed by PIEZO-1 and somehow translated to vascular remodelling (Lucitti et al., 2007). PIEZO-1 has been demonstrated to be potentially clinically relevant in an array of pathological conditions, including; wound closure (Kang et al., 2019), limb ischaemia (Kang et al., 2019), hypertension and hypertensive arterial remodelling (Wang, S. et al., 2016; Retailleau et al., 2015), platelet activation (Ilkan et al., 2017), varicose vein disease (Shadrina et al., 2019; Fukaya et al., 2018) and lymphedema (Nonomura et al., 2018; Choi et al., 2019).

PIEZO-2, on the other hand has been shown to be associated with sensory neurobiology (Woo et al., 2014). However synergistic relationship, has been described with the suggestion that the Piezo sensors may act as backup for one another and share a function (Lee, W. et al., 2014). Therefore, it is important to consider that the disruption of either one of these channels in experimental models may not result in any significant differences in PIEZO activity. It senses aortic baroreceptor pressure in conjunction with PIEZO-1 (Zeng et al., 2018) to regulate angiogenesis like activity in tumours (Yang et al., 2016). Therefore, the relevance of PIEZO-2 in the cardiovascular system may increase with further research.

PIEZO-1 is expressed in both ECs and VSMCs and activated by shear stress and stretching of the cell membrane (Douguet et al., 2019) and is required to regulate vascular tone (Wang, S. et al., 2016). It is highly expressed in VSMCs of small arteries, which regulate peripheral resistance (Douguet et al., 2019). When luminal shear stress is high, EC PIEZO-1 can activate voltage-gated Ca^{2+} channels in adjacent VSMCs, causing vasoconstriction and eventually hypertension-induced arterial remodelling (Rode et al., 2017; Beech, 2018).

Furthermore, the direct stimulation of PIEZO-1 channels in VSMCs may also increase vessel diameter and wall thickness, which is absent when PIEZO-1 is knocked out (Douguet et al., 2019). Piezo also controls KLF-2 activity (Duchemin et al., 2019). The activation of VSMC PIEZO-1 increases intracellular calcium, which stimulates transglutaminase II activity, which is involved in cytoskeletal and ECM remodelling (Retailleau et al., 2015).

The study of mechanosensors is difficult in cells isolated from an intact vessel as it is not possible to recapitulate the *in vivo* environment. Many mechanosensors are studied *in vitro* with the aid of a chemical which can be demonstrated to specifically activate the mechanosensor in question. Yoda-1, or 2-[5-[[(2,6-dichlorophenyl)methyl]thio]-1,3,4-thiadiazol-2-yl]-pyrazine, is a synthetic irreversible agonist of the PIEZO-1 channel named after the famous Star Wars character, Yoda, who has telekentic powers (Syeda et al., 2015). It can selectively activate human and mouse PIEZO-1 in the absence of mechanical force, by stabilising the open PIEZO-1 conformation, without influencing PIEZO-2 (Lacroix et al., 2018; Evans et al., 2018). To identify the mechanistic activation of Yoda-1, an antagonist of Yoda-1, named Dooku1, has been recently described (Evans et al., 2018). This too was fittingly named after the the Star Wards Sith Lord Count Dooku a one-time disciple turned enemy of Master Yoda. Furthermore, there is an established antagonist of PIEZO-1 called GsMTx4 (Gnanasambandam et al., 2017).

1.6.2. Other Mechanosensors

Transcient Receptor Potential (TRP) receptors are a family of channel proteins comprising of seven subclasses. They are present in VSMCs and are important mechanosensors which regulate vasoconstriction (Earley and Brayden, 2015). Changes in luminal pressure can cause a myogenic response in vascular smooth muscle through the gradual depolarisation of VSMCs, leading to the opening of non-selective stretch-activated cations channels, such as the TRP channels, on the cell membrane as well as store-operated calcium (Brayden et al., 2008; Sharif-Naeini et al., 2009). Prolonged membrane stretch can lead to increased intracellular calcium and sodium and

pathologically active TRP channels leading to VSMC dysfunction (Martín-Bórnez et al., 2020). The knockout of TRP channels has also been demonstrated to reduce vasoconstriction, hypertension and subsequent pathological remodelling (Bulley et al., 2018; Dietrich et al., 2005; Nemeth et al., 2020). Vasodilation may be indirectly achieved by TRP channels through the activation of Ca^{2+}-dependent K^+-Ca^{2+} channels and the release of endothelial nitric oxide (Goldenberg et al., 2015).

Two-Pore-Domain Potassium Channels is a type of cellular potassium protein family with six isoforms and is important in smooth muscle myogenic circulatory regulation (Mathie and Veale, 2007; Gurney and Manoury, 2009). They may be activated through membrane stretch (i.e. in hypertension) resulting in vasoconstriction. They can sense different degrees of mechanical force, with stronger forces more likely to open channels (Ma et al., 2013; Brohawn, 2015). The negative resting potential of VSMCs is low; therefore, they are extremely sensitive to changes in K^+ (Salomonsson et al., 2017). Furthermore, they are independent of intra-cellular Ca^{2+} (Patel, A.J. et al., 1998). Reduced expression of certain two-pore-domain potassium channels in VSMCs has been shown to affect cell proliferation and migration (Burg et al., 2008).

The Epithelial Sodium Channel (ENaC) are a family of voltage-insensitive sodium-selective protein channels important in mechanotransduction (Drummond et al., 2008). It plays an important role in the regulation of blood pressure, as genetic mutations resulting in the loss of function in ENaC can result in monogenic hypertension (Mutchler et al., 2021; Schild, 1996). Furthermore, ENaC may promote cell differentiation in response to mechanical strain (Nam et al., 2020). Changes in extracellular sodium may alter VSMC mechanosensory sensitivity therefore impact myogenic responses.

1.7. Murine Circulation and Models of Aortic Disease

1.7.1. The Murine Arterial Circulation

Mouse models remain the dominant experimental technique in gaining mechanistic insights into AAA development, due to their small size, relative cost and well-established genetics. The C57BL6/JBL/6 black mouse strain is the most commonly used mouse in laboratory science. The murine infra-renal aortic anatomy is representative of the human anatomy, Figure 7. However, no mouse model fully mimics the human cardiovascular system, therefore, results should be interpreted with caution. Furthermore, in murine models assessments of blood pressure, the pathological impact of stressors and the impact of genetic knockout are evaluated is often evaluated in the caudal artery, which is absent in humans.

The most obvious difference between the two species is their size. The average adult male in the UK weighs approximately 83.6 kg (www.ons.gov.uk), compared with a 12-week-old male mouse that weighs 28.9 g (The Jackson Laboratory, strain datasheet). With mice weighing less than 0.0005% of their human counterparts, this has important relative circulatory implications. Furthermore, the cardiac output of a human is 5L/min compared to 15ml/min in mice (Doevendans et al., 1998). The average human heart rate is also much lower at 60bpm compared with 600bpm in mice (Papadimitriou et al., 2008) and the number of cardiac cycles over a lifetime is higher in humans than in mice (2.2×10^9 vs 6.3×10^8) (Greenwald, 2007). Furthermore, in contrast to the human aorta, mice aorta has very few VSMCs, therefore prone to dissection and rupture. Finally, the average life expectancy in the UK is 81.2 years (www.ons.gov.uk), compared with 28 months, for a wild-type mouse.

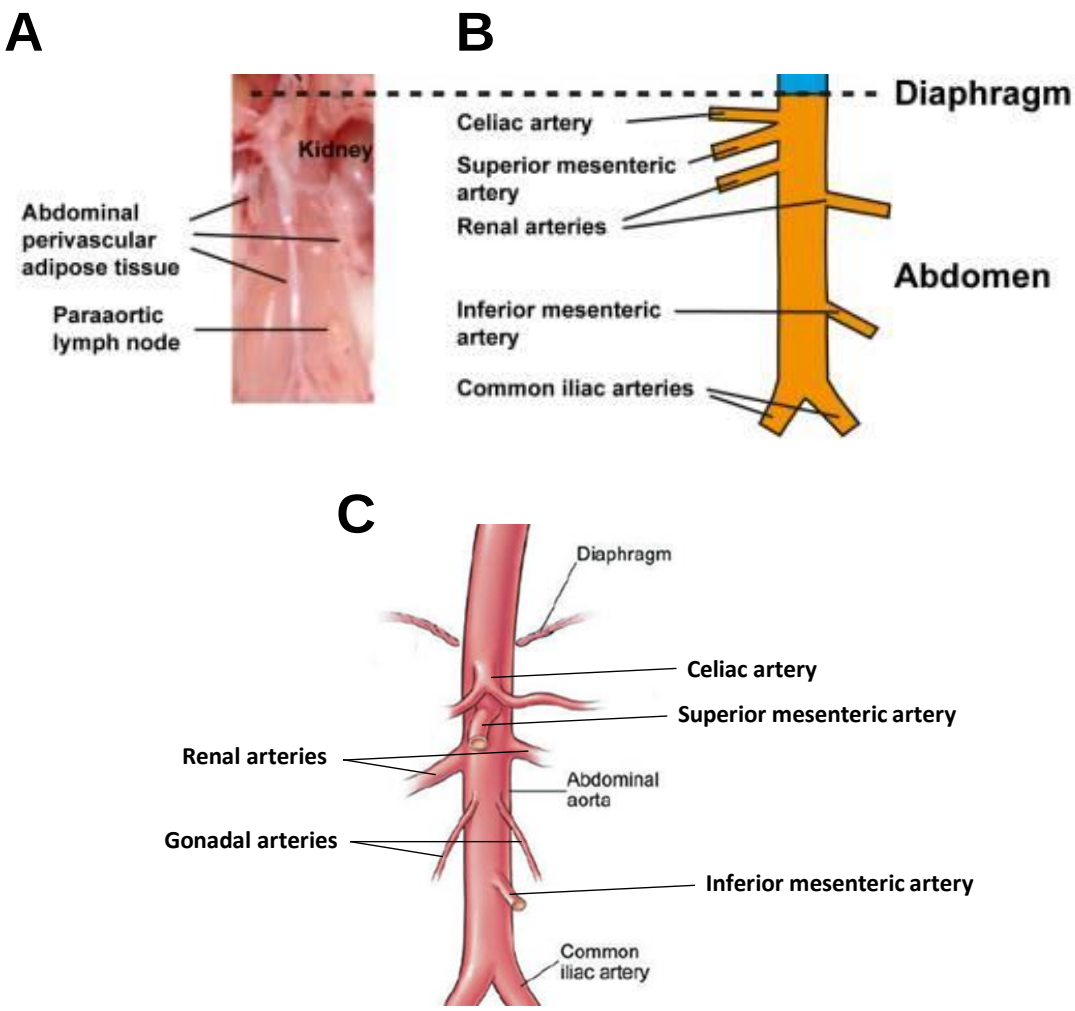

Figure 7. Illustrations comparing mouse and human abdominal aorta.

A; in-situ photo of a mice abdominal aorta (Mohanta et al., 2016). B; schematic representation of abdominal aorta with major branches (Mohanta et al., 2016). C; Schematic of the human abdominal aorta. Adapted from clevelandclinic.org.

1.7.2. Murine AAA models

An AAA may be surgically induced in mice with reagents used to trigger pathological processes resulting in aortic dilatation. Several mouse models which have been previously described over the past two decades include; angiotensin-II (Ang-II), calcium chloride ($CaCl_2$), and elastase infusion (Daugherty and Cassis, 2004). No one model completely mimics the AAA disease process with the advantages and disadvantages briefly discussed below. Multiple models are often utilised to validate observed trends.

1.7.2.1. Angiotensin-II model

The angiotensin-II model is the most widely utilised AAA mice model, and was described by Saraff and colleagues in 2003 (Saraff et al., 2003). Hyperlipidaemic male mice ($ApoE^{-/-}$) are infused with AngII for a 28 day period through an osmotic mini pump inserted under the skin. AngII is thought to cause microdissections in the aorta, which leads to an intramural haematoma in the media. This is thought to drive the inflammation and development of the aneurysm. However, mice may experience an early aortic rupture due to the microdissection propagating into a large lethal dissection. Therefore, it is deemed mainly as a model for dissecting aneurysms. Importantly, this technique translates to an 80% incidence of an AAA, and aneurysms continue to progress even after AngII infusion has ceased (Xie et al., 2012). Unsurprisingly, in this model, mice are susceptible to developing thoracic aneurysm, dissections and rupture. Interestingly, only 25% of mice develop an AAA is utilised in wild-type mice C57BL6/J background). However, the technical simplicity of implanting pumps into mice makes it a commonly used model in preclinical AAA research.

1.7.2.2. Porcine Pancreatic Elastase model

The elastase perfusion model is the second most commonly utilised, which was first described by Anidjar and colleagues in 1990 (Anidjar et al., 1990). The abdominal aorta is surgically isolated, temporarily ligated at the superior and inferior boundaries and elastase perfused throughout the aortic segment. An aneurysm subsequently develops over a two-week period. Elastase causes aortic elastic fibres to split and triggers an inflammatory response. This method is technically challenging and has high variability in AAA formation so is used by only a few groups worldwide. However, it has the advantage that it may be utilised in any genetically modified mouse. A simplified modified method, involving the localised extra-luminal peri-aortic application of elastase, has also been shown to produce similar results, Figure 8 (Bhamidipati et al., 2012). Further adaptations involving iliac impingement surgery help to mimic human AAA physiology have also been recently

described (Busch et al., 2018). Furthermore, the addition of 3-aminopropionitrile fumarate salt (BAPN) to the drinking water may be used to prevent elastin healing, and may be used in chronic models of AAA (Lu, G. et al., 2017).

1.7.2.3. Calcium Chloride model

The calcium chloride model, similar to the modified (peri-aortic) elastase model, involves the localised application of calcium chloride. This AAA murine model was first described by Chiou and colleagues in 2001 after realising that $CaCl_2$ can induce carotid aneurysm in rabbits (Chiou et al., 2001). $CaCl_2$ is thought to induce an inflammatory reaction in the aortic wall via the infiltration of neutrophils, lymphocytes, monocytes and multinucleated giant cells. This induces fibromuscular hyperplasia and disruption of the elastin network, resulting in the disorganisation of tunica media, which consequently leads to the formation of an aneurysm. However, AAA develop over a period of 4-6 weeks. Similar to the peri-adventitial elastase model, it requires technical expertise, and is feasible in any genetically-modified mice.

1.7.2.4. Low-density lipoprotein Receptor-related Protein (LRP1) model

The LRP1 model relies on a disruption aortic elastin and PDGFR driven VSMC cell proliferation. It was first described by Boucher and colleagues who achieved VSMC specific LRP1 knockdown by breeding Sm22Cre transgenic mice with LRP^{flox} mice (Boucher et al., 2003). They observed the thickening and distension of the aortic wall resulting in spontaneous aneurysm formation. However this model, unlike those described above, have pronounced atherosclerosis in the aorta therefore is often a model utilised to study atherosclerosis. Never the less the role of LRP-1 in AAA disease is supported by the Genome wide association study by Bown and colleagues (Bown et al., 2011).

1.7.2.5. Accuracy of Modelling of Human AAA

In mouse models, the AAA develops within 2 to 6 weeks which is much faster

than that seen in humans. Furthermore, it is important to acknowledge that none of the models reproduce all the pathological processes described in human AAAs (Busch et al., 2021). For example, in the AngII model, intraluminal thrombus and calcification are often absent. Similarly, in the PPE and $CaCl_2$ models, aortic dissection, and intramural haemorrhage are absent. However, the infiltration of inflammatory cells in to the aortic wall and the reactive VSMC physiology seen in mouse models are similar to that suspected to occur in humans. Therefore, more than one model is often used in in-vivo studies for validation. Furthermore, in both the PPE and $CaCl_2$ models, the aneurysm growth tends to plateau, unlike the AngII model. Therefore, the findings should be interpreted with caution when extrapolating inferences.

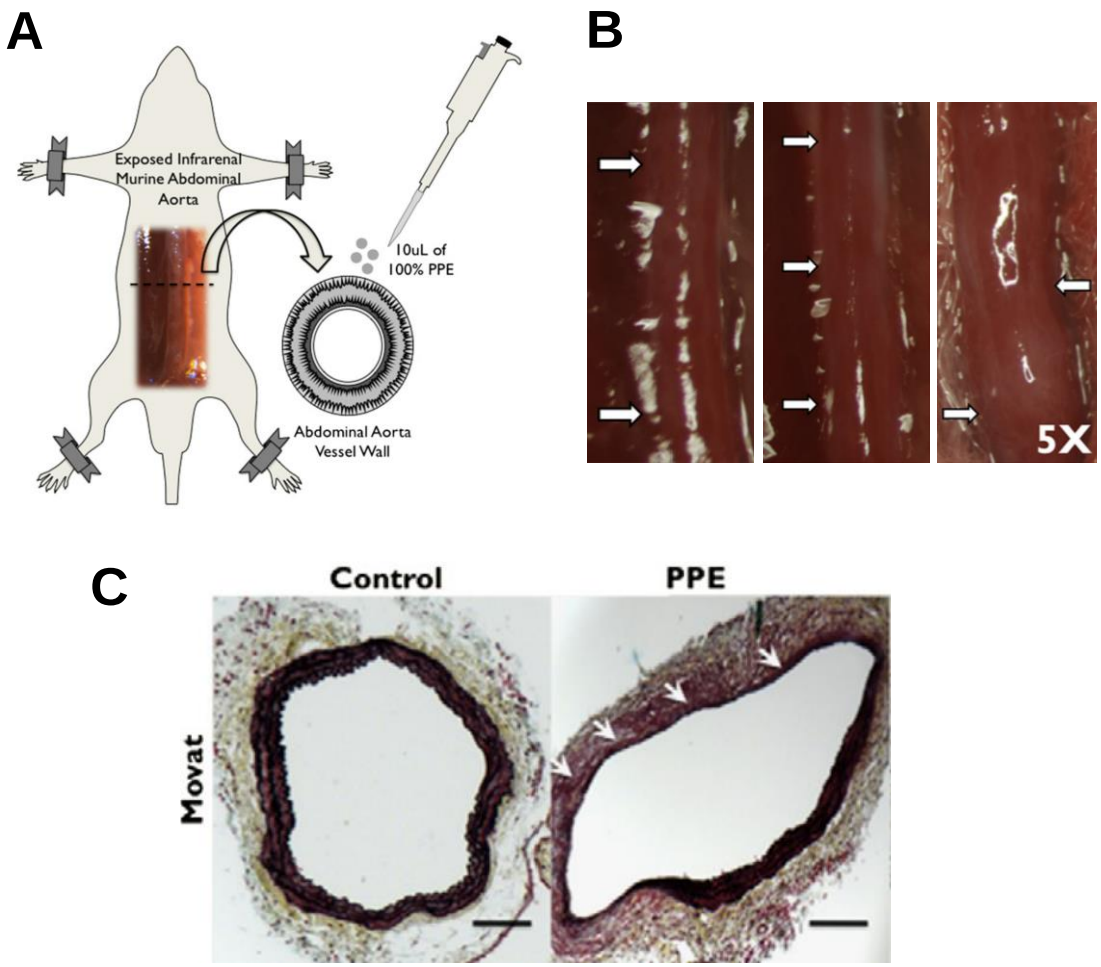

Figure 8. Example of the per-aortic elastase mouse model.

A; The infra-renal abdominal aorta dissected for the application and 10µL of 100% porcine pancreatic elastase (PPE) applied. B; left- microscopic image

(x5) of the abdominal aorta following dissection, middle- microscopic image (x5) of the abdominal aorta after 5 minute of elastase application showing wall thinning, right- photo of the abdominal aorta at 14 days following PPE application. C; Movat staining (x10) showing elastin and smooth muscle layer(s) with PPE application (solid white arrows).

Adapted from (Bhamidipati et al., 2012).

1.7.3. VSMC PIEZO-1 Knockout Mice

Retailleau and colleagues were the first to confirm the presence of PIEZO-1 in VSMCs in the arteries of mice and identify its important role in hypertensive vascular remodelling (Retailleau et al., 2015). LacZ staining was used to demonstrate the presence of PIEZO-1 in VSMC in the caudal artery of $PIEZO^{LacZ/+}$ mice compared with $PIEZO\text{-}1^{+/+}$ mice (Figure 9A). Furthermore, they also demonstrated PIEZO-1 mRNA knockdown without any compensatory increase in PIEZO-2 mRNA expression in sm22Cre $PIEZO\text{-}1^{+/+}$ mice compared with sm22Cre $PIEZO\text{-}1^{-/-}$ mice (Retailleau et al., 2015). This was also supported by the absence of functional activation of PIEZO-1 channels in response to maintained pressure in myocytes isolated from the caudal artery of sm22Cre $PIEZO\text{-}1^{-/-}$ mice compared with sm22Cre $PIEZO\text{-}1^{+/+}$ mice (Figure 9B). Finally they demonstrated PIEZO-1 dependent VSMC remodelling, in response to hypertension, in sm22Cre $PIEZO\text{-}1^{+/+}$ mice compared with sm22Cre $PIEZO\text{-}1^{-/-}$ mice (Figure 9C).

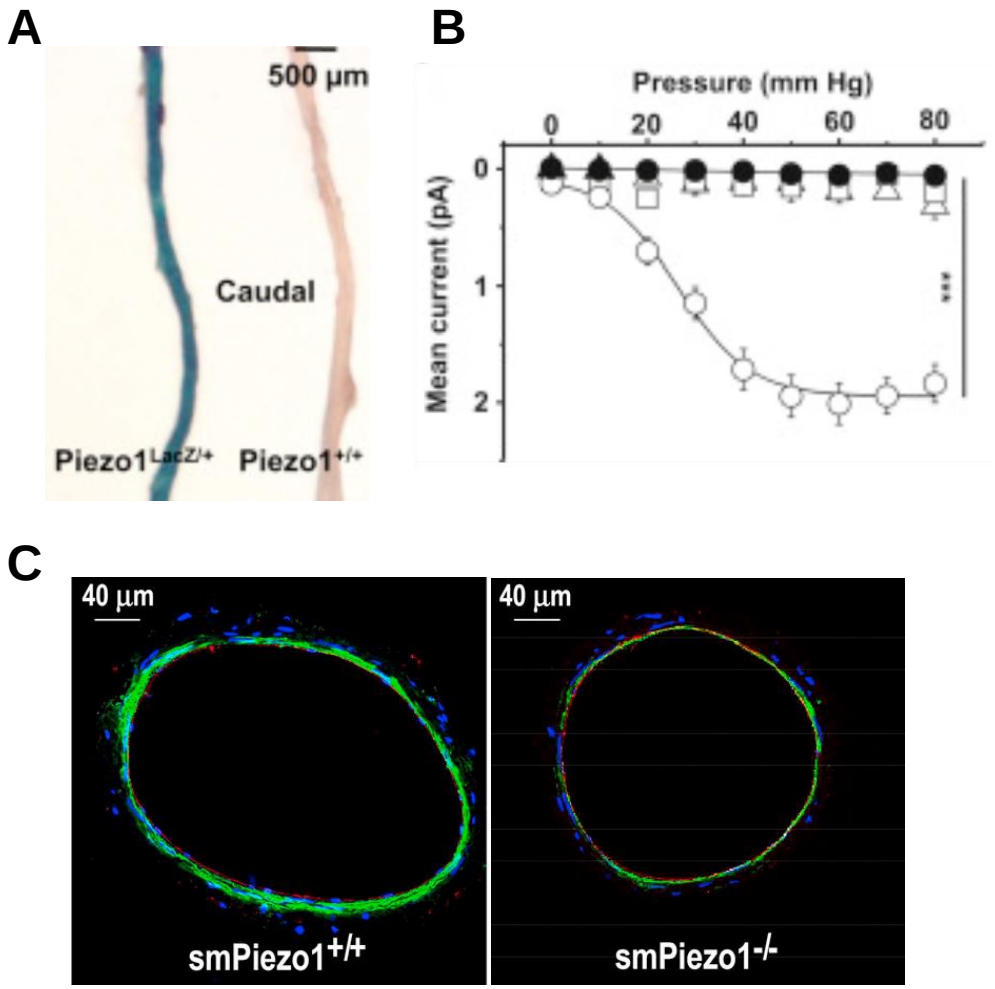

Figure 9. Illustrates expression of PIEZO-1 in arterial VSMCs.

A; LacZ staining of PIEZO-1 in the caudal artery from; PIEZO $^{LacZ/+}$ mice (left) and PIEZO-$1^{+/+}$ mice (right). B- Mean stretch activated channel amplitude in sm22Cre PIEZO-$1^{+/+}$ (white circles) and sm22Cre PIEZO-$1^{-/-}$ (black circles) in myocytes from the caudal artery. C- Caudal artery remodelling (VSMCs [green], EC [red] and adventitia [blue]) with hypertension in sm22Cre PIEZO-$1^{+/+}$ (left) and sm22Cre PIEZO-$1^{-/-}$ (right).

Adapted from (Retailleau et al., 2015).

1.8. Novel Hypothesis

The novel hypothesis of this thesis is that mechanical force (i.e. axial stretch and oscillatory shear force) and vessel stiffness, sensed by the VSMC PIEZO-1 channel, are important in AAA development inducing VSMC remodelling through KLF-2, KLF4 and TG2-mediated pathways (Figure 10).

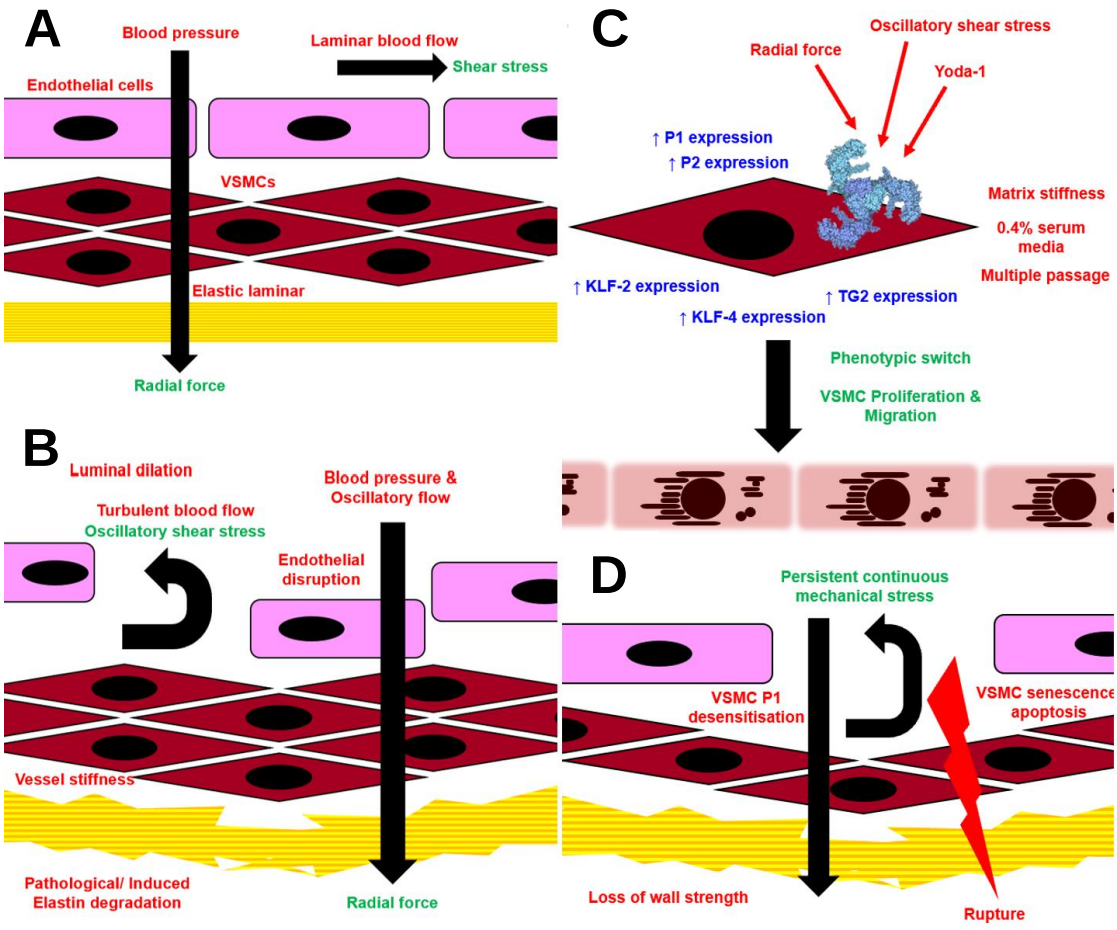

Figure 10. Schematic representation of the thesis hypothesis.

A; simplified pictorial representation of cellular components of the abdominal aortic wall. B; simplified pictorial representation of hypothesised early pathophysiological stressors and changes resulting in AAA formation. C; pictorial representation of hypothesised VSMC stressors precipitating remodelling. D; pictorial representation of hypothesised end-stage AAA disease.

1.9. Aims of the Thesis

The overall aim of this thesis is to evaluate the role of the PIEZO-1 mechanosensor in VSMCs in response to stressors likely to be encountered in the AAA microenvironment and in murine AAA models.

The aims of the in vitro experiments in this thesis were to:

- Establish the presence of PIEZO-1 and PIEZO-2 in non-diseased human aortic VSMCs and human AAA VSMCs, and compare the functional activity of the PIEZO-1 mechanosensor between these cell types.
- Evaluate the effects (i.e. gene expression and PIEZO-1 dependent calcium movement) of mechanical stressors (i.e. constant axial force, constant oscillatory shear flow and matrix stiffness), constant chemical activation of PIEZO-1 (i.e. Yoda-1) and environmental stressors (i.e. serum starvation and multiple passage) on non-diseased VSMCs in relation to the PIEZO mechanosensors and KLF-2, KLF-4 and TG2.

The aims of the in-vivo experiments performed in this thesis were to:

- Validate high-resolution ultrasound techniques used to analyse the abdominal aorta of AAA mice models.
- Compare the gene expression of the PIEZO mechanosensors and proliferative markers in sham and AAA aortae of C57BL6/J mice.
- Investigate the effect of VSMC PIEZO-1 knockout in transgenic mice by comparing aortic morphology, vessel distensibility and vessel contractility following sham and AAA induction surgery.
- Evaluate the effect of PIEZO-1 modulation in relation to VSMC proliferation and cell stiffness.

Chapter 2: Materials and Methods

2.1. In-Vitro Experimental Methods

2.1.1. Experimental Cells

2.1.1.1. Normal Aortic VSMCs (NAVSMCs)

Primary non-diseased Human Aortic Smooth Muscle Cells (HAoSMC) and recommended growth media, VascuLife SMC Medium- Complete Kit, were purchased from the commercial supplier CellSystems® (Troisforf, Germany). The exact location within the aorta the cells were retrieved from was unknown to the supplier. Cells were received in a vial containing 0.5 million cells cryopreserved in liquid nitrogen. These were thawed and plated as per manufactures guidelines with the use of their proprietary cell media. The exact constituents of these media were not disclosed, however the manufacturers reported that they contained supplements, no antimicrobials, and growth factors, which guaranteed a successful cell colony expansion. HAoSMC was utilised from the third passage onwards to allow for the adequate expansion of the colony so that it may be utilised to replicate. These cells were immunohistochemically stained for α-SMA to confirm that the cells being cultured were likely to be VSMCs. The term; Normal Aortic Vascular Smooth Muscle Cells (NAVSMCs) has been used throughout this thesis to describe HAoSMC.

2.1.1.2. Abdominal Aortic Aneurysm VSMCs (AAAVSMCs)

Primary human Abdominal Aortic Aneurysm Vascular Smooth Muscle Cells (AAAVSMCs) were obtained from the Leeds Aneurysm Development Study and Ageing Aorta Tissue bank (Ethical approval, Ref: 03/142). The tissue from the anterior aneurysmal abdominal aortic wall was retrieved from patients undergoing elective OAR at the Leeds Vascular Institute (Leeds Teaching Hospital NHS Trust, Leeds, UK). VSMCs were isolated from aneurysmal tissue using an explant technique, previously described (Porter et al., 2002), cultured and cryopreserved in liquid nitrogen. Vials containing AAASMCs

were; retrieved from the tissue bank, thawed, cultured and the colony expanded. AAAVSMCs were cultured in standard culture media described in section 2.1.2.2. Cells within the tissue bank have been previously been shown to be VSMCs by staining for α-SMA and SMMHC (Riches et al., 2013). Similar to the NAVSMCs, AAAVSMCs were utilised for experimentation at either a maximal passage 3 or 4 unless otherwise stated. These cells were very slow to grow and sensitive to any disruption to the culture environment which made it very challenging to work with these cells.

2.1.1.3. Saphenous Veins VSMCs (SVVSMCs)

Primary long saphenous veins VSMCs (SVVSMCs) were also used from the Institute tissue bank to learn and optimise experimental protocols before the utilisation of NAVSMCs and AAAVSMCs. Briefly, surplus graft tissue of patients undergoing elective coronary artery bypass surgery at the Yorkshire Heart Centre was taken at the time of surgery (Ethical approval, Ref 01/040). SVVSMCs were isolated using the same explant method as AAAVSMCs (Porter et al., 2002). They were cultured and the colonies expanded identically to NAVSMCs and AAAVSMCs. Similarly, SVVSMCs were cultured in standard culture media described in section 2.1.2.2.

2.1.1.4. Mouse Cardiac Fibroblasts

Cardiac fibroblasts were isolated in order to demonstrate the efficacy of the Cre system in the transgenic mice. The hearts from three male transgenic mice (smMHCCre-ER(T2) PIEZO-$1^{+/+}$ [wild-type], smMHCCre-ER(T2) PIEZO-$1^{+/-}$ [heterozygote] and smMHCCre-ER(T2) PIEZO-$1^{-/-}$ [homozygote]), which were not injected with tamoxifen, were harvested under terminal anaesthesia at 12 weeks. The hearts were washed with Dulbecco's Phosphate Buffered Saline [PBS] (Sigma-Aldrich, Germany) three times to remove any blood clot. PBS contained 2.67mM KCl, 137.93mM NaCl, 1.47mM KH2PO4 and 8.06mM Na2HPO4.7H_2O titrated to pH7.4. The heart was then stored in a Dulbecco's Modified Eagle's Medium [DMEM] (Thermo Fisher Scientific, UK) supplemented with 10% Foetal Calf Serum [FCS] (Sigma-Aldrich, USA) and 1% penicillin/streptomycin [P/S] plus fungizone.

To isolate cardiac fibroblasts, the hearts were subsequently homogenised in a 10 cm sterile Petri dish with a scalpel and transferred to a sterile 5ml bijou. The homogenate was treated with collagenase and the supernatant was collected in a 15ml sterile falcon tube (Thermo Fisher Scientific, UK). DMEM with 0.5mg/ml Bovine Serum Albumin [BSA] (Sigma-Aldrich, USA) with 1% P/S plus fungizone was added to the isolated supernatant and gently mixed. The solution was subsequently spun in a centrifuge to allow the cells to collect as a pellet. Cells were subsequently resuspended in DMEM with 10% FCS and 1% P/S and cultured in 12-well plates for experimentation.

2.1.2. Cell Culture

2.1.2.1. Cell Culture Equipment

Cell culture was performed in a Class II Biological Safety Cabinet with downward laminar air flow in a designated room within the Leeds Institute for Cardiovascular and Metabolic Medicine (University of Leeds, UK). All cell work was undertaken utilising aseptic technique. Primary human cell and primary mouse cell cultures were performed in separate rooms. All cells were stored in humidified incubators (Sanyo, Japan) at 37^{o}C with 5% CO_2.

Cells were routinely cultured in 75 cm cell culture flasks [T75] (Sigma-Aldrich, USA). An electronic pipette using 5 ml, 10 ml and 25 ml polystyrene serological pipettes (Corning, Thermo Fisher Scientific, UK). Smaller volume media and solutions were handled using a sterile Pipetman Classic (P2-P5000, Gilson, USA) and sterile filter tips (Starlabs, Germany). Falcon tubes (Thermo Fisher Scientific, UK) were utilised for transiently holding liquids.

2.1.2.2. Culture Media

Cells were cultured in DMEM (Thermo Fisher Scientific, UK) supplemented with 10% fetal bovine serum [FBS] (Sigma-Aldrich, USA) and 1% Penicillin/Streptomycin (Sigma-Aldrich, USA), unless otherwise stated. This

will be referred to as the “standard culture media” throughout this thesis. Cells were serum starved in DMEM (Thermo Fisher Scientific, UK) with minimal serum, 0.4% FBS (Sigma-Aldrich, USA) and 0.1% P/S (Sigma-Aldrich, USA).

2.1.2.3. Cell Colony Expansion

The flasks were split once they reached 70-80% confluence, which was estimated by eye on light microscopy. To passage cells, the monolayer of cells was initially washed with PBS warmed to room temperature, to remove growth media. Two milliliters of 0.25% trypsin at room temperature was then applied and the flask was incubated for 2 minutes. The flask was subsequently inspected under light microscopy to assess the successful detachment of cells. Gentle agitation with the palm of the hand was applied, to encourage cell detachment. Once majority or all the cells were detached, 8 ml of fresh growth media was added to the flask and the bottom of the flask was washed with the media to encourage any further detachment of cells. The resulting 10 ml of liquid was then transferred into a 15ml falcon tube, then spun down at 1500 rpm for 5 minutes to constitute a pellet of cells. The supernatant liquid was then discarded and 1 ml of fresh media added. The pellet was then agitated to encourage the cells to redisperse into the media. The cells were split into a maximum of four T75 flasks. Fresh media was then added, depending on the number of flasks the cells were being split too. Each flask required a minimum of 2-ml of media containing cells to ensure successful coverage of the base of the flask and encourage cell reattachment. Flasks were assessed in 24 hours to assess cell reattachment and for a media change. Each T75 flask had a total of 4 ml of standard culture media. They were subsequently reassessed every 72 hours to monitor cell replication and growth. Nutrients in the media were also replenished with half media changes. For example, 2-ml of media were withdrawn and discarded and replaced with 2 ml of fresh standard culture media.

2.1.3. Generic In-Vitro Experimental Procedures

2.1.3.1. Cell counting

Manual cell counting was performed before plating for the experiments, using 0.4% trypan blue (Sigma-Aldrich, USA) and a haemocytometer (Louis and Siegel, 2011). Cells were detached from the donor vessel using 0.25% trypsin, as described above, and re-suspended in 1ml of standard culture media. Ten microlitres of 0.4% trypan blue was mixed with 10µl of media containing cells before being loaded onto the haemocytometer. Viable cells were counted from a single square using a cell counter. The count was repeated on a second square and the cell counts were averaged. This allowed for the cell count per ml to be calculated and the sample appropriately diluted to achieve the desired loading density per well.

2.1.3.2. Experimental plating

The number of cells in each flask was manually counted, as described in section 2.1.3.1, before seeding to experimental wells. The number of cells required in each well varied depending on experimental plate size, cell type being utilised and the experimental time frame. The cell counts for the experiments described below were optimised through trial and error. After the experimental cells were seeded, a 48 hour recovery period was allowed. All wells in the experimental plate were subsequently serum starved (described in section 2.1.2.2.) for 48 hours before experimentation. Following this, the media was changed to the standard culture media with any required reagents added. When reagents were added, every 48 hours a full media change of each experimental well was also performed to ensure a consistent level of nutrients and reagents in the culture media. Where no reagents were added half-media changes were performed to minimise disruption to the culture environment. In all experiments, 3 separate identical plates (i.e. biological replicates) were set-up, at different times, with a minimum of two replicate wells (i.e. technical replicates) for each experimental condition, to ensure results were both reproducible and reliable. Six well plates had a minimum of 2-ml of media per well and 96 well plates had a minimum of 100µL of media per well.

2.1.3.3. Cell microscopy

Visualisation of cells in culture bottles and experimental plates was routinely performed using a light microscope to assess cell viability and confluence. Microscopic imaging for demonstrative purposes and quantitative analysis were performed using the IncuCyte FLR (Essen Bioscience, UK) time lapse fluorescent microscope. It was housed within a standard 5% CO_2 tissue culture incubator, which allowed for real-time imaging without altering the surrounding climate of the cells. High-resolution images at a times 150 magnification were captured, which were downloaded as Joint Photographic Experts Group (JPEG) files. Furthermore, the fluorescent settings facilitated imaging of Live-Dead assays, transfection assays and proliferation assays. The automated image capture feature allowed for sequential time-dependent imaging to be performed for the migration and proliferation assays, so that cell behaviour could be studied.

2.1.4. Image Analysis with ImageJ

ImageJ (National Institutes of Health, USA) is an open source software which was exclusively utilised to analyse JPEG images taken by the IncuCyte FLR (Essen Bioscience, UK). Macros were developed to analyse imaging performed for this thesis, as the laboratory was closed in some capacity for approximately a year during the second year of when bulk of the experiments and concomitant analysis were planned.

2.1.4.1. Automated Cell Counting

The automated macro developed to count cells using ImageJ (National Institutes of Health, USA) is illustrated in Figure 11. Within this, all images were converted to an 8-bit monotone format to simplify image processing. It was subjectively apparent that the cells, especially the nuclei, had a higher density than their background (Figure 11A). Images were transformed to a black and white images through thresholding, based on pixel density. This delineated likely cellular tissue (black) from the surrounding media (white),

Figure 11B) The number of cells were subsequently counted based on the clustering of pixels that was likely to represent an individual cell (Figure 11C). This method was an adaptation of a previously described method by Grishagin et al (Grishagin, 2015).

This method was validated by selecting 20 random IncuCyte FLR images taken of NAVSMCs. Subjectively images were a mixture of those perceived to have a high cell count and images perceived to have a low cell count (Figure 12). The number of cells in each image were manually counted on ImageJ (National Institutes of Health, USA) using the counter and compared to the cell count derived automatically by the macro. The macro was found to capture a lower cell count compared to the manual count, therefore, underestimating the true number of cells. However, this trend was consistent and both the manual cell count and the automated macro cell count were highly correlated. Furthermore, the macro had perfect reproducibility at 100%. The cell count from experimental plates could not be checked against a haemocytometer count as RNA from the samples were often required.

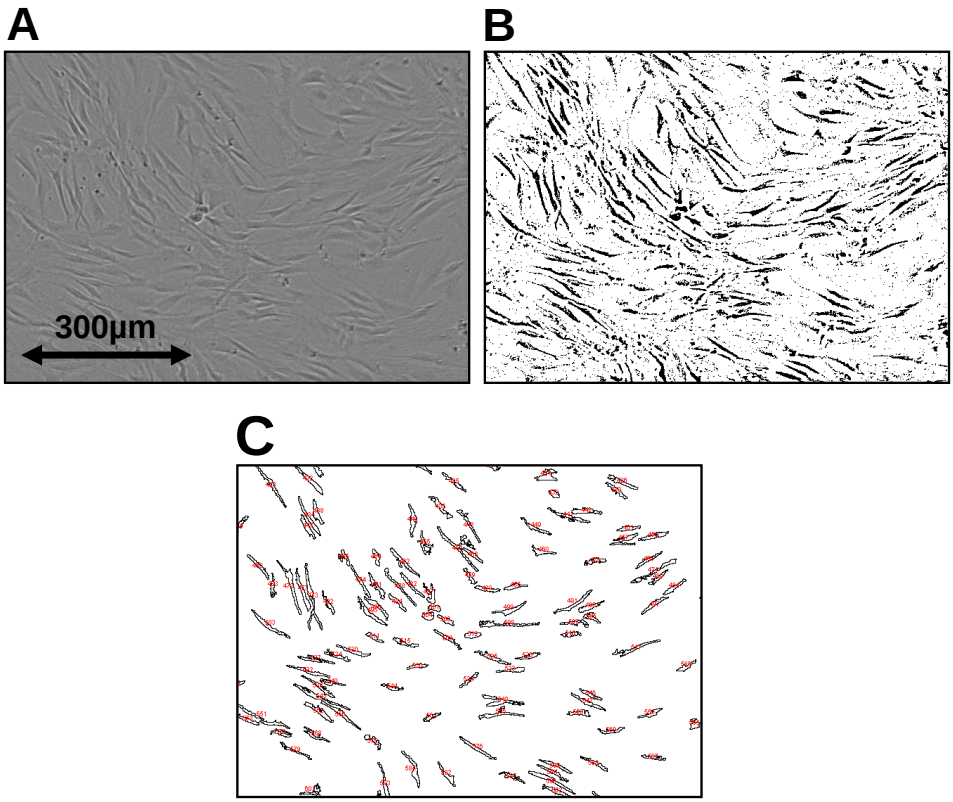

Figure 11. ImageJ automated cell count.

A; unprocessed image of NAVSMCs. B; post-threshold image of NAVSMCs. C; automated cell count following clustering of pixels. Cell count = 356. Red double ended arrow indicates scale of images.

2.1.4.2. Automated Measurement of Cell Confluence

Cell confluence was also assessed using a macro developed on ImageJ (National Institutes of Health, USA). Similar to the method of cell counting, images were converted to an 8-bit format and binary thresholding was undertaken to delineate the cellular tissue. The ratio of areas of increased density (black) compared to the background (white) gave an automated, reproducible and quantifiable indication of cell confluence. Importantly, this allowed cell confluence to be compared between wells, as consistent cell confluence was important in the calcium imaging experiments. This technique was calibrated against manual assessment of cell confluence so that the image pixilation could be translated to cell confluence. The built-in confluence algorithm on the IncuCyte count not be used as analysis had to be performed on the equipment that was not assessable during laboratory closures and restrictions during the COVID-19 pandemic.

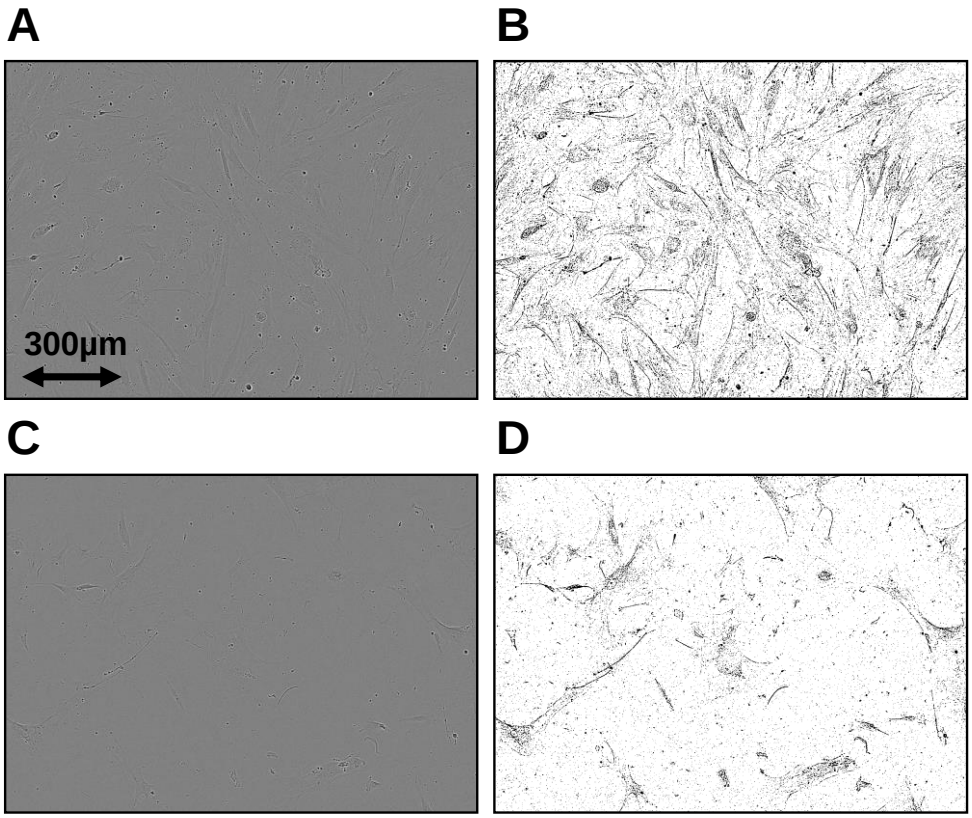

Figure 12. Representative examples of assessment of cell confluence in a 96 well plate.

A; IncuCyte image of confluent cells in a well. B; Post-processing imaging showing 12.4% pixilation. C; IncuCyte image of sparsely distributed cells in a well. D; Post-processing imaging showing 3.5% pixilation.

2.1.5. Migration, Proliferation and Live-Dead Assays

2.1.5.1. Migration Assay

Migration assays were performed in 96 well Image Lock plates (Essen Bioscience, UK). These plates have a laser cut reference line which allowed imaging to be performed in exactly the same location. Each experimental plate was prepared with 7,000 NAVSMCs per well. Once a confluent monolayer of cells had formed, a scratch line (rectangular area) parallel to the reference line was made using a 96 well WoundMaker™ (Essen Bioscience, UK). The wells were subsequently washed three times with PBS to wash away any debris before applying the media, which was adjusted based on the four experimental treatments. Cells were treated with either; the standard culture

media with the addition of Dimethyl sulfoxide (DMSO) [control], Yoda-1 3µM, or Yoda-1 10µM. Yoda-1 was dissolved in DMSO, therefore, the DMSO concentration was kept consistent in these three experimental conditions. An additional control condition involved the use of the 0.4% FBS (serum starvation media). A full media change was performed on day 2 to replenish the reagents.

A baseline image of each well was taken pre-scratch (straight out the culture incubator) and post-scratch (after a period of 30 minutes in the IncuCyte FLR allowing the plate to re-climatise). Images were then taken every 24 hours, up to 96 hours. Quantification of cell migration into the scratched surface, containing no cells, at fixed time points allowed for assessing the behavioural effects of the different stressors. Images were downloaded as JPEG files and migration was quantified using a macro developed in ImageJ (National Institutes of Health, USA), Figure 13. Again, this macro was developed due to restrictions in laboratory access during the COVID-19 pandemic. In brief, images were converted to an 8-bit format, binary threshold was performed based on pixel density to delineate the probable cellular tissue from the background, pixels were clustered/amalgamated based on pixel size and proximity to one another. This helped delineate the scratched surface (with no cells) and cells, Figure 13.

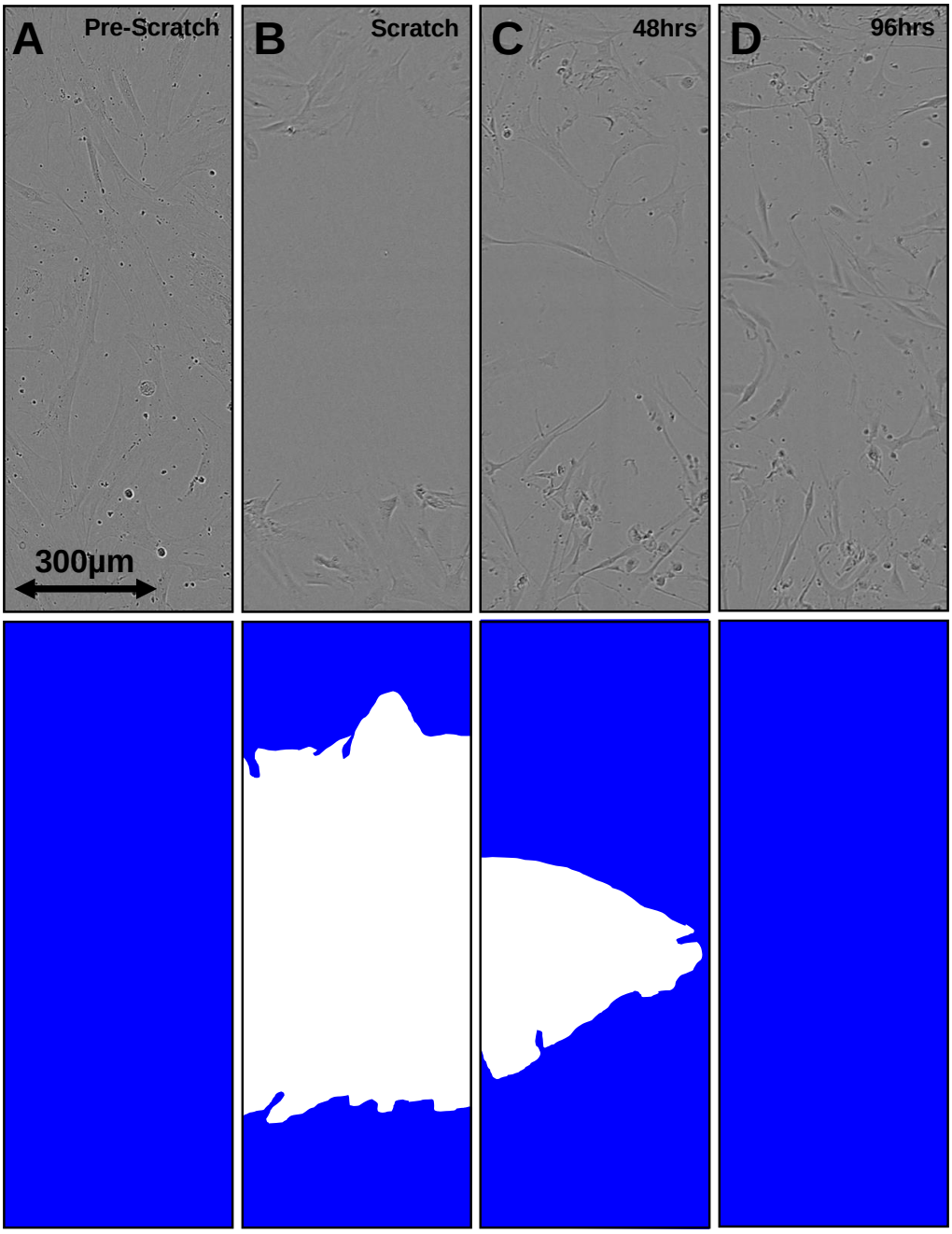

Figure 13. Sequential IncuCyte imaging (top) and ImageJ automated analysis (bottom) of untreated NAVSMC migration.

Representative IncuCyte image and ImageJ analysis of: A; pre-scratch. B; post-scratch. C; 48 hours post-scratch. D; 96 hours post-scratch. White = scratched area. Blue = area populated with cells.

2.1.5.2. Proliferation Assay

Assessment of cell proliferation in response to different stimuli was performed using an end-point fluorescent counting assay and a fluorescent nuclear stain Vybrant DyeCycle Green® (Invitrogen, Thermo Fisher Scientific, UK). It was utilised at a final concentration of 1 µM. NAVSMCs were seeded in clear plastic 96 well plates (Corning, Thermo Fisher Scientific, UK) at a density of 5,000 cells per well. This ensured a sparse distribution of cells and allowed adequate space for cells to proliferate over a 96-hour timeframe, without the well becoming oversaturated with cells and prematurely becoming senescent. Similar to the migration assay, cells were treated with media containing 0.4% FBS or the standard culture media with DMSO, Yoda-1 3µM, or Yoda-1 10µM. A full media change was performed on day 2 to replenish reagents.

The assay was performed and images were captured with the IncuCyte FLR pre-treatment and every 24 hours up to 96 hours. All images were downloaded as JPEG images and NAVSMCs were counted using an automated macro also developed in ImageJ (National Institutes of Health, USA), Figure 14. In brief, colour threshold of images was undertaken to delineate the fluorescent green within the images (Figure 14B). Areas identified were subsequently counted at a set particle size to derive a cell count (Figure 14C).

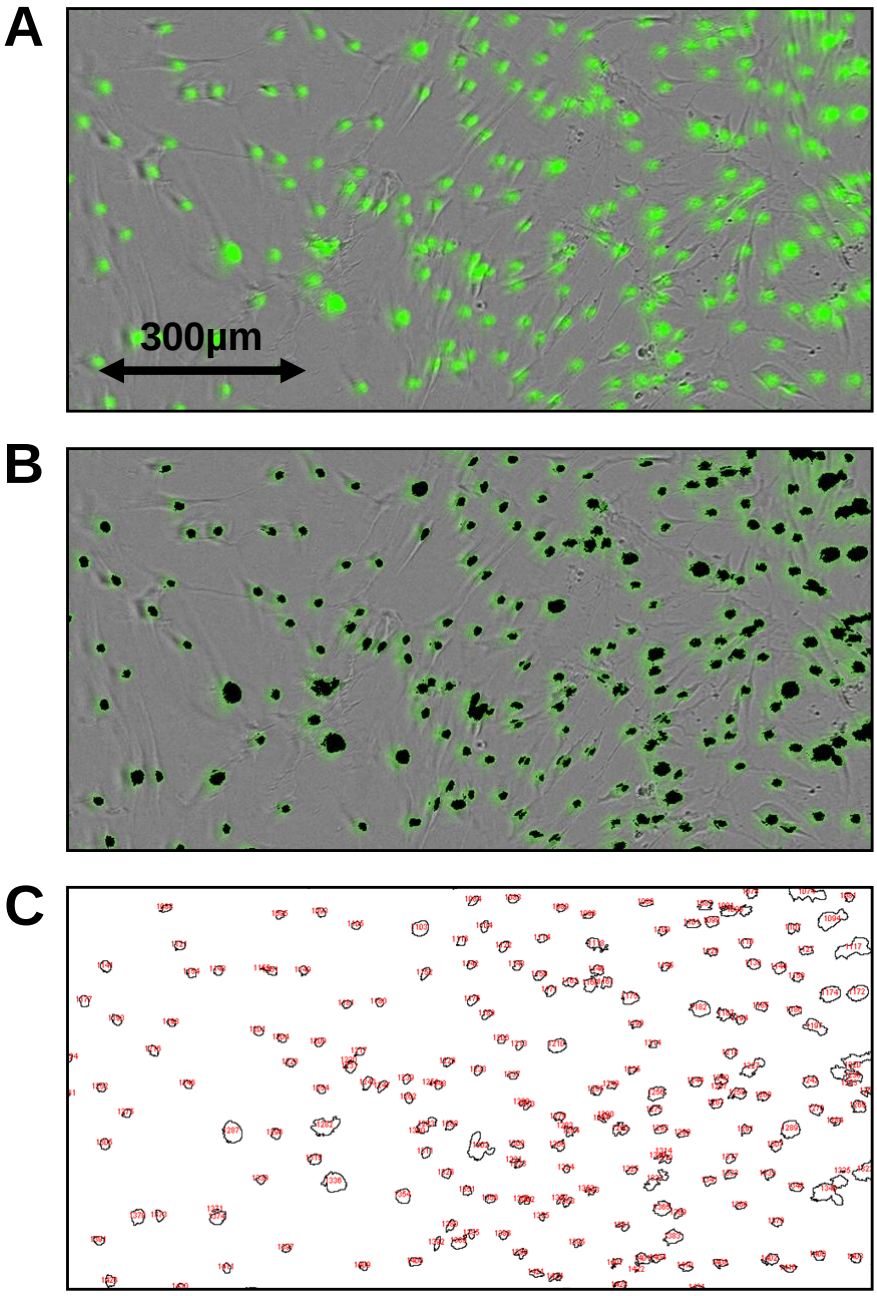

Figure 14. IncuCyte imaging of proliferation Assay and ImageJ automated analysis of untreated NAVSMCs.

Representative example of: A; fluorescent nuclear stain image. B; Colour threshold of fluorescent green nuclei stain. C; NAVSMC count.

2.1.5.3. Live-Dead Assay

Live-dead assays, with the LIVE/DEAD® viability and cytotoxicity kit (Thermo Fisher Scientific, UK) were performed to determine the viability of the VSMCs after the application of the various experimental conditions described. In brief, culture medium was removed, cells were washed with PBS and then incubated in 2µM Calcein AM [green fluorescents] and 4µM Ethidium homodimer 1 [red fluorescents] for 30minutes before imaging with green and red wavelengths in the IncuCyte FLR was performed. This assay simultaneously stained live cells with Calcein [green fluorescents] and dead cells with Ethidium [red fluorescents]. Global cell death was subsequently induced using Blasticidin (Thermo Fisher Scientific, UK), which was applied for 1 hour. Blasticidin is a potent translational inhibitor causing rapid cell death in both prokaryotic and eukaryotic cells. Plates were then re-imaged to confirm the assay had worked.

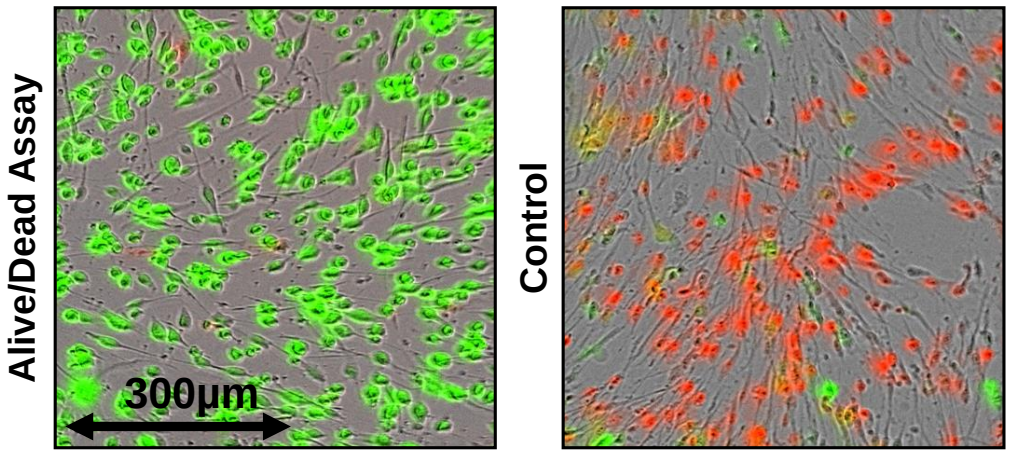

Figure 15. Live/Dead Assay (left) of untreated NAVSMCs and control assay (right) after treatment with blasticidin.

Green = live cells. Red = dead cells.

Similar to the migration and proliferation assays, images were downloaded as JPEG files. An automated ImageJ macro was developed to colour threshold and delineate the green and red fluorescence, allowing the quantification of the number of live and dead cells.

2.1.6. Intracellular Calcium Imaging

Cells were seeded onto a standard 96 well black-walled clear bottom cell culture plates (Corning, Thermo Fisher Scientific, UK) at a density of 10,000 cells/well with standard culture media and were given 48 hours to recover before imaging. The Flexstation III bench top fluorometer (Molecular Devices, Thermo Fisher Scientific, UK) was used to record intracellular calcium entry (Figure 16). It operated at room temperature and allowed fluid transfer from a 96 well compound plate during a live recording, using individual pipette tips.

Figure 16. Photograph of the Flexstation III.

Taken from www.moleculardevices.com. The device has 3 draws as illustrated containing; top- pipette tips for chemical transfers, middle- compound plate and bottom- experimental plate.

The experimental plate, containing the cells, required careful preparation before imaging. In brief, the culture media was removed. Fifty microlitres of 2µM Fura-2 acetoxymethyl ester [Fura-2 AM] (Molecular Probes, Invitrogen, Thermo Fisher Scientific, UK) in standard buffer solution 1.5 [SBS 1.5] (NaCl

135mM, KCl 5mM, MgCl2 1.2mM, Glucose 8mM, HEPES 10mM, $CaCl_2$ 1.5mM, pH7.4, 290mosmol) with 0.01% pluronic acid was added to each well. Fura-2 AM is a membrane permeable ratiometric intracellular calcium indicator. It was prepared in DMSO (vehicle) and stored at -20^{o}C in the dark, at a concentration of 1mM. Pleuronic acid, a non-ionic surfactant, was added with Fura-2 AM to enhance dispersion. The plate was then incubated for 1 hour in the dark at 37^{o}C. The cells were then washed once with SBS 1.5 and then incubated with SBS 1.5 containing DMSO (vehicle) for a further 30 minutes at room temperature.

Yoda-1 was loaded onto the compound plate at 8 different concentrations (DMSO [vehicle], 0.3μM, 0.6μM, 1.3μM, 2.5μM, 5μM, 10μM and 20μM). Calcium signals of cells treated with only vehicle (i.e. DMSO) were used as controls. The calcium movement at each concentration was averaged and a dose-response curve was calculated by fitting the data on a modified Hill equation, to derive the EC50. The presence of a Yoda-1 response in cells would also confirm the presence of PIEZO-1 membrane channels in the cell type tested.

Signals were recorded every 5 seconds for a minimum of 180 seconds. The solution from the compound plate was added at 60 seconds. Fura-2 AM can be excited with a light wavelength of 340nm and 380nm, resulting in the emission of light at a wavelength of 510nm. The ratio of the 2 excitatory wavelengths (i.e. 340nm/380nm) was proportional to the intracellular calcium concentration. Results were analysed based on the mean ± standard error of the mean (SEM) at each time point in quadruplicate. The peak ΔF340/380 in each experimental condition was also assessed. The SOFTMax® Pro software v4.3.1 (Molecular Devices, Thermo Fisher Scientific, UK) was used for data collection that allowed data to be downloaded as .txt files to be processed using Microsoft Excel (Microsoft, USA).

2.1.7. Genomic Analysis

2.1.7.1. Ribonucleic Acid (RNA) Isolation

High-quality RNA extraction forms the foundation of PCR experiments. Before RNA isolation, all laboratory equipment was cleaned using 70% ethanol, followed by RNaseZap (Sigma-Aldrich, USA). Furthermore, cells were washed with PBS to remove any remaining media. During RNA isolation, all samples were kept on ice and at the end stored at -80^{o}C.

RNA isolation using the TRIreagent method was performed by lysing the cells with TRIreagent, centrifuging at 10,000*g* at 4°C to remove high molecular weight genomic DNA, then using bromochloropropane (Sigma-Aldrich, USA) and glycogen (as an RNA carrier to aid detection of the pellet) (Sigma-Aldrich, USA). The clear layer containing the RNA was transferred to a fresh centrifuge tube, and the RNA was precipitated using isopropanol (Sigma-Aldrich, USA) . The pellet was washed in 75% ethanol then air-dried and re-suspended in 10µl of nuclease-free water. It was then treated with DNase using the TURBO DNA-free kit (Ambion, Invitrogen, UK) for 1 hours at 37^{o}C followed by enzyme inactivation. The supernatant containing the RNA was subsequently pipetted into a fresh Eppendorf. RNeasy Plus RNA isolation was performed according to the manufacturer's instructions. Briefly, cells were homogenised in "Buffer RLT" and the cell lysate was transferred to a gDNA eliminator spin column placed inside a 2 ml collection tube. Samples were centrifuged for 30 seconds at <8000g. The supernatant was mixed with an equal volume of 70% ethanol and then transferred to a "QIAquick" column and sequentially washed with "Buffer RW1" and "Buffer RPE", before being eluted from the column in a volume of elution buffer.

With both methods, the RNA isolated was evaluated using the NanoDrop 2000 spectrophotometer (Thermo Fisher Scientific, UK), which allowed the assessment of RNA quality (260/A280 ratio) and concentration (ng/L) (Desjardins and Conklin, 2010). The NanoDrop was calibrated with 1µl of PCR

grade water, followed by readings of each sample in turn. After each result the NanoDrop pedestal were cleaned and dried. Samples with a 260/A280 ratio of ~2.0 were considered pure as described in the manufacturers guidelines.

2.1.7.2. Validation of RNA Isolation

To determine the optimal method of RNA isolation in NAVSMCs, the quality and quantity of RNA with both the TRI-reagent (Sigma-Aldrich, USA) method and RNeasy Plus Mini Kit (QIAGEN, England) were compared. RNA was isolated using the TRI-reagent method and RNeasy Plus Mini Kit from 6 and 4 samples of untreated NAVSMCs, respectively. The RNA quality was significantly higher ($p=0.005$) using the RNeasy Plus Mini Kit (2.03 ±0.00) compared to the TRI-reagent method (1.96 ±0.01). The RNA concentration was however significantly higher ($p=0.01$) using the TRI-reagent method (751.8ng/L ±46.9) compared to the RNeasy Plus Mini Kit (147.5ng/L ±2.1). RNA isolation using the TRI-reagent method was found to yield an acceptable RNA quality (i.e. 260/280 ratio above 1.8) at higher concentrations. Therefore, RNA was harvested using the TRI-reagent method throughout this thesis, unless otherwise stated, as a greater quantity of cDNA at a standardised concentration could be produced for replicate PCR experiments.

The TRI-reagent method was therefore solely used to harvest RNA from NAVSMCs (N=8) and AAAVSMCs (N=4) to compare the differences in the RNA quality and concentration. The RNA from NAVSMCs were on average of greater quality (difference 0.13 ±0.02, $p<0.0001$) and concentration (difference 746.9ng/L ±172.8, $p=0.002$) compared to RNA from AAAVSMCs. In NAVSMCs, the mean RNA quality was 1.95 ±0.01 and concentration of 917.4ng/L ±118.7. In contrast, AAAVSMCs had a mean RNA quality of 1.82 ±0.01 and a concentration of 170.5ng/L ±25.0. These are indicative of the slow growing poorly differentiated senescent nature of AAAVSMCs evident on cell culture.

2.1.7.3. Reverse Transcriptase Step

Complementary DNA (cDNA) was synthesised from RNA extracted using the high-capacity RNA-to-cDNA kit (Life Technologies, Thermo Fisher Scientific, UK) in accordance to the guidance provided by the manufacturer. In summary, 20µl solutions were prepared consisting of; 10µl 2x RT Buffer, up to 9µl of RNA (at a concentration of 1µg/1000ng) and PCR grade water, and either 1µl of 20x RT enzyme mix for (RT+ samples) or PCR grade water (RT- controls). Control samples were used to monitor for genomic DNA contamination. Thermal cycling of the solution was performed for 60 minutes at 37ºC, 5 minutes at 95ºC and then held at 4ºC. Samples were subsequently stored at -20ºC.

2.1.7.4. Quantitative Polymerase Chain Reaction (qPCR)

Real time quantitative PCR (qPCR) was used to evaluate the mRNA expression of PIEZO-1, PIEZO-2, KLF2, KLF4 and TG2 in VSMCs. RNA-sequencing data illustrating the expression of these genes of interest in human vascular tissue is signposted in Appendix A. PCR was performed using the Lightcycler ® 480 system (Roche Molecular Systems, UK) and SYBR Green molecular probes (Invitrogen, FisherScientific, UK). The following protocol was utilised; pre-incubation at 95ºC for 10 minutes; amplification for 40 cycles at 95ºC for 10 seconds and 55ºC for 1 minute; melt curve at 95% for 5 seconds, 65ºC for 1 minute, 97ºC extension; and cooling at 40ºC for 20 seconds. The reaction threshold cycle (Ct) and melt curve were determined using the Lightcycler analysis software v3.5 (Roche Molecular Systems, UK).

Primers were obtained from the master stocks of the laboratories (LICAMM, University of Leeds, UK) led by Dr Marc Bailey (MB) and Professor David Beech (DB). An aliquot of 100 µM master stocks was diluted with PCR grade water to form a 20µM sample. Sequences of human and mouse primers used for qPCR are described in Table 1 and Table 2, respectively, and have been previously validated by members of the laboratory teams, therefore,

sequencing of the PCR products was not performed. New stock samples were ordered if there was doubt over potential contamination or the age of the primer. Certain primers were ordered from the commercial supplier Biorad as described in Table 1 and Table 2.

Experimental plates (384 well) contained a final reaction volume of 10µl per well loaded in triplicates. Reaction volumes included; SYBR green reaction mix (5µl), PCR grade DNA free water (3.5µl), forward (0.5µl) and reverse (0.5µl) target gene probes, and 1µl of the experimental reagent (i.e. RT+ cDNA [test], RT- sample [control], or H_2O [control]). Individual Ct and melting temperatures were manually checked in triplicates. Wells with 2 melting points, or a difference in melting point of greater than a 2^{o}C compared to other wells, or those with a crossing point (CP) greater than 40 cycles, were excluded. RT positive and RT negative experiments alongside melt curve analysis indicated the reliability of results. Furthermore, PCR plates were ran on 3 separate dates to ensure the accuracy of results.

Standard efficiency curves for primers were performed to identify the most suitable concentration of cDNA to be utilised in reactions. cDNA prepared from AAAVSMCs were used as they were theoretically likely to yield the poorest quality samples, therefore, it was important to determine the efficiency to ensure results were reliable. The stock cDNA sample (1:1) was diluted 1:2, 1:4, 1:10, 1:100 and 1:1000 using PCR grade water. Efficiency was calculated automatically by the software by plotting Ct values against the log dilution.

Table 1. Human forward and reverse primer sequences and anticipated amplicon sizes.

*For: Forward primer sequence, Rev: Reverse primer sequence.

Gene	Primer sequence 5’ → 3’	Size (bp)	Reference / Source
Housekeeper /Control genes			
GAPDH	For: AGATCATCAGCAATGCCTCC Rev: CATGAGTCCTCCCACGATAC	Unknown	Drewlo et al., 2012 / DB
BA	For: TCGAGCAAGAGATGGC Rev: TGAAGGTAGTTTCGTGGATG	200	MB
18S	For: CGATTGGATGGTTTAGTGAGG Rev: AGTTCGACCGTCTTCTCAGC	Unknown	MB
B2M	For: GGCTATCCAGCGTACTCCAAA Rev: CGGCAGGCATACTCATCTTTTT	Unknown	Drewlo et al., 2012 / DB
HPRT	For: TGACACTGGCAAAACAATGCA Rev: GGTCCTTTTCACCAGCAAGCT	Unknown	Drewlo et al., 2012 / DB
CycB	For: AGATGAAGATGTAGGCCGGG Rev: GATGCTCTTTCCTCCTGTGC	196	MB
Genes of interest			
PIEZO-1	For: AGATCTCGCACTCCAT Rev: GGACTCGTGAGAAGGAG	182	(Ge et al., 2015 / DB
PIEZO-	For: TTTCCTTCCTGTTGCTGCAC	160	DB

2	Rev: CTGATCCCATTGCCAGCATC		
KLF2	For: ACCTACACCAAGAGTTCGCA Rev: CGTGTGCTTTCGGTAGTGG	138	MB
KLF4	For: CCCATCTTTCTCCACGTTCG Rev: AAGTCGCTTCATGTGGGAGA	112	MB
TGM2	For: AACTACAACTCGGCCCATGA Rev: TACGTCCCTTCGCTCTTCTC	209	MB

Table 2. Mouse forward and reverse primer sequences and anticipated amplicon sizes.

*For: Forward primer sequence, Rev: Reverse primer sequence.

Gene	Primer sequence 5’ → 3’	Size (bp)	Reference / Source
Housekeeper genes			
GAPDH	For: TGAAGCAGGCATCTGAGGG Rev: CGAAGGTGGAAGAGTGGGAG	102	MB
BA	For: CACTATTGGCAACGAGC Rev: CGGATGTCAACGTCAC	126	MB
18S	For: GATGCTCTTAGCTGAGTGT Rev: GCTCTGGTCCGTCTTG	233	MB
B2M	Not disclosed	Unknown	BIORAD
HPRT	Not disclosed	Unknown	BIORAD
Genes of interest			
PIEZO-1	For: TGAGCCCTTCCCCAACAATAC Rev: TGCAGGTGGTTCTGGATATAG	142	DB
PIEZO-2	For: AATCAAACCAACATTCCCCTTCA Rev: CAGGTAGACGAGCAAAGGAGA	Unknown	DB
KLF2	For: GCCACACATACTTGCAGCTA Rev: GTCTGTGACCTGTGTGCTTT	185	MB
KLF4	For: TCACAAGTCCCCTCTCTCCA Rev: AAGTGTGGGTGGCTGTTCTT	121	MB
TG2	Not disclosed	Unknown	BIORAD

2.1.7.5. PCR Primer Efficiencies and Housekeeper Gene Selection

The identification of a housekeeper gene that has a similar expression in different tissue samples being compared was fundamental for standardised comparative analysis of other genes of interest on qPCR. For these experiments cDNA from untreated NAVSMCs and AAAVSMCs from 3 biologicals replicates were used. GAPDH was the most commonly used housekeeper in our group, and was compared to Glyceraldehyde 3-phosphate dehydrogenase (GAPDH), Beta-Actin (BA), 18S, Beta-2 microglobin (B2M) and Hypoxanthine-guanine phosphoribosyltransferase (HPRT). The gene sequences of these are described in Table 1. Standard curves for PIEZO-1, PIEZO-2 and CycB (positive control in transfection studies reported below) were also carried out so that an appropriate concentration of cDNA was identified to ensure that the crossing points of key genes would be captured by the proposed PCR protocol and comparable to the housekeeper gene.

The efficiency and regression co-efficient for; GAPDH, BA, 18S, B2M and HPRT housekeeper primers are summarised in Table 3. Similarly, the efficiencies and regression co-efficient for PIEZO-1, PIEZO-2 and CycB are summarised in Table 4. The efficiency for GAPDH and B2M was most similar between NAVSMCs and AAAVSMCs. Furthermore, GAPDH had a similar efficiency to PIEZO-1 and CycB therefore, was selected as the primary housekeeper gene. The standard curves for GAPDH, PIEZO-1 and PIEZO-2 from NAVSMCs and AAAVSMCs are illustrated in Figure 17. Primer efficiencies identified were used for the interpretation of experimental results for a more accurate representation of relative expression of each gene. GAPDH was consistently utilised for all qPCR experiments, to allow standardised comparative analysis between different cell types and animal models.

Table 3. Efficiencies and regression co-efficient for housekeeper primers on RNA from NAVSMCs and AAAVSMCs.

	NAVSMCs		AAAVSMCs	
	Efficiency (%)	Regression co-efficient	Efficiency (%)	Regression co-efficient
GAPDH	77.2	-4.0	78.8	-4.3
BA	72.6	-4.2	66.0	-4.5
18S	72.5	-4.2	51.5	-5.5
B2M	74.4	-4.1	79.4	-3.9
HPRT	80.8	-3.9	70.3	-4.3

*N/n = 3/12.

Table 4. Efficiencies and regression co-efficient for primers of genes of interest for NAVSMCs and AAAVSMCs samples.

	NAVSMCs		AAAVSMCs	
	Efficiency (%)	Regression co-efficient	Efficiency (%)	Regression co-efficient
PIEZO-1	75.6	-4.1	75.3	-4.1
PIEZO-2	93.3	-3.5	128.1	-2.8
CycB	74.4	-4.1	78.3	-4.0

*N/n = 3/12.

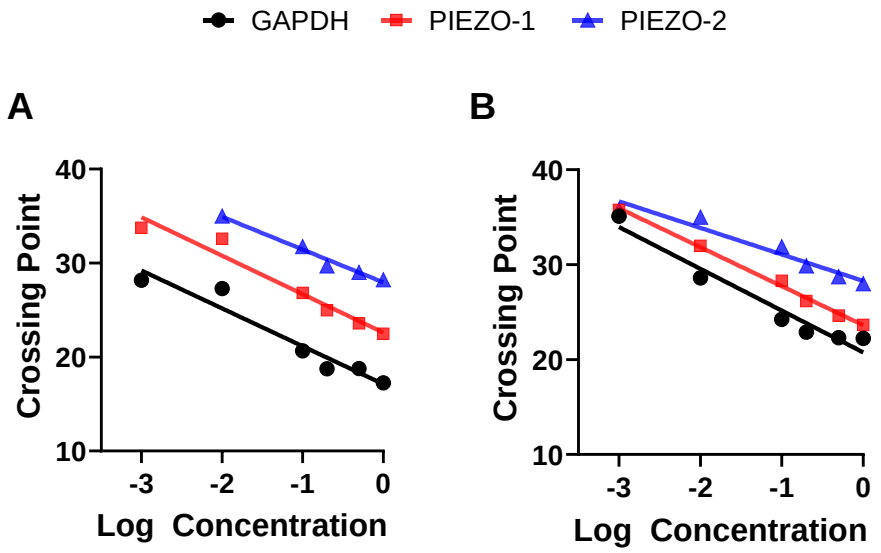

Figure 17. PCR standard curves for GAPDH, PIEZO-1 and PIEZO-2 primers in NAVSMCS (A) and AAAVSMCs (B).

GAPDH= close circle, PIEZO-1= closed square, PIEZO-2= closed triabgle.

2.1.7.4. Gel electrophoresis

PCR plates were centrifuged and products were mixed with a loading dye (Sigma-Aldrich, USA). The products were run on a 2% agarose gel made up of 1x Tris-acetate-EDTA (TAE) buffer with SYBR Safe DNA dye (Invitrogen, Thermo Fisher Scientific, UK) as another control measure. RT+ reactions were evaluated for the presence of a single product at the anticipated size. RT- reactions and H_2O reactions were also run as controls. A 90 volt current was run through the gel to separate product(s). A parallel 100 base pair (bp) ladder (Sigma-Aldrich, USA) was performed so that product sizes could be estimated.

2.1.8. Application of Mechanical Stressors to NAVSMCs

2.1.8.1. Uni-Axial Stretch

NAVSMCs were cultured in specialised stretchable 10cm^2 cell chambers (Strexcell, USA, Figure 18). Constant uni-axial stretch was applied at either 0% (control) or +20% (maximum possible). The chambers (STB-100-10 stretch unit, Strexcell, USA) were made of silicone and coated with a 0.1%

bovine gelatin (Sigma-Aldrich, USA) to facilitate cell attachment. NAVSMC were counted and seeded into each chamber at a density of 60,000 cells per chamber with standard culture media. Cells were initially cultured in the silicone chamber (Figure 18, A) until a confluent monolayer of cells had formed. The chamber was subsequently serum starved for 48 hours and then mounted onto the stretching apparatus (Figure 18, B). At this point, either no stretch or a constant +20% stretch was applied. Each experiment was performed in isolation as a single stretching apparatus was available. Each experiment was performed on 3 separate occasions. Cells were visualised every 24 hours under light microscopy to ensure that the cells remained attached to the floor of the chamber. RNA was isolated at 96 hours for PCR. It was not feasible to take images on the IncuCyte FLR, therefore, live-dead assays were not possible. Furthermore, it was impossible to successfully trypsinize and isolate cells to seed onto 96 well plates as agitation to the silicone chamber through washing with PBS and media caused the entire sheet of cells to detach, recoil and cells to die.

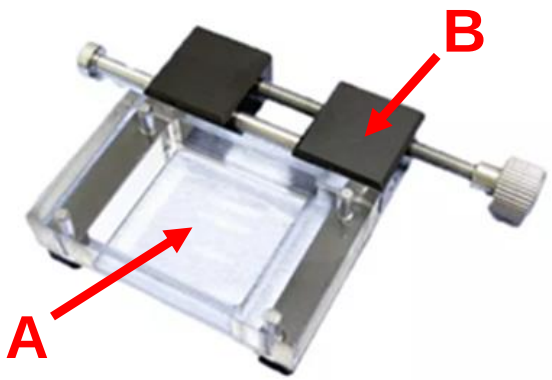

Figure 18. Picture of Strexcell chamber (A) and stretch apparatus (B).

2.1.8.2. Oscillatory Shear Stress

Constant oscillatory shear stress was applied using an orbital shaker (Corning, FisherScientific, UK) placed within an incubator (Sanyo, Japan). NAVSMCs were seeded into the wells of two 6 well plates with a seeding density of 60,000 cells per well and were prepared using the standard method described above (see section 2.1.3.2 Experimental Plating). Each well contained a 2ml of standard culture media. The experimental plate was then placed onto an orbital shaker and another placed beside it for 96 hours. The orbital shaker was set to 25 oscillations per minute and was constantly in this setting for the entire duration of the experiment, only being stopped momentarily when performing microscopy or a media change. The NAVSMCs were observed every 24 hours and a half media change (1ml) was performed after 48 hours to ensure adequate nutrients.

At 96 hours IncuCyte imaging of both plates was performed. Then, two wells per plate were utilised for a Live/Dead assay, 2 wells for RNA extraction and the final 2 wells were trypsinized and the cells were seeded onto a 96 well plate for calcium imaging. The preparation of cells for calcium imaging differed from that previous described, as NAVSMCs were loaded at 12,000 cells per well with the standard culture medium as they were only left for 24 hours before calcium imaging with Yoda-1. Results obtained for NAVSMCs, which underwent oscillatory shear stress were compared to those that did not experience oscillatory shear stress in paired experiments in the same incubator. This was repeated on three separate occasions as biological replicates.

2.1.8.3. Matrix Stiffness

NAVSMCs were cultured on specialised 6 well plates (CytoSoft Imaging, CellSystems, Germany) with stiffened cell culture matrices at a stiffness of either 0.2kPa (control) and 64kPa (highest available from manufacturer). Cells were seeded into all 6 wells of two separate 6 well plates (i.e. one with a 0.2kPa matrix and the other with a 64kPa matrix) at a density of 60,000 cells per well with standard culture media and then observed for 96 hours. Similar

to the plates utilised for oscillatory shear stress; 2 wells were for a Live/Dead assay, 2 wells were for RNA extraction and 2 wells had the cells trypsinized and seeded onto a standard 96 well tissue culture plate (Corning, Thermo Fisher Scientific, UK) for calcium imaging with Yoda-1. Plates with different stiffness matrices were cultured simultaneously side by side. The results obtained for NAVSMCs cultures on 0.2kPa and 64kPa plates were subsequently compared. Again, this was repeated on three separate occasions as biological replicates.

2.1.8.4. Yoda-1 mediated PIEZO-1 Activation

Yoda-1 was used to chemically activate PIEZO-1 in NAVSMCs to assess the effect on cell survival, migration and proliferation as well as gene expression of the PIEZO mechanosensors and KLF-2, KLF-4 and TG-2. All plates were prepared using the standard method described above (see 2.1.3.2 Experimental plating). Wells were either treated with 10µM of Yoda-1 or DMSO (vehicle/ control). In all experimental conditions the cells were treated for a period of 96 hours, with a complete media change being performed after 48 hours to ensure the concentrations of test regents remained constant throughout the experiment.

NAVSMCs were seeded into 4 wells of a 6-well plate (Corning, Thermo Fisher Scientific, UK) at a density of 60,000 per well. After 96 hours of treatment cell survival was assessed using a Live-Dead assay and RNA was harvested to evaluate gene expression. NAVSMCs were also seeded onto a 96-well Image Lock plate (Essen Bioscience, UK) at a density of 7,000 cells/well for a migration assay and a clear 96-well tissue culture plate (Corning, Thermo Fisher Scientific, UK) at a density of 5,000 cells/well for a proliferation assay. Serial imaging with the IncuCyte FLR was performed every 24 hours.

2.1.9. Application of Physiological Stressors

2.1.9.1. Prolonged Serum Starvation

NAVSMCs were serum starved for 96 hours to evaluate the effects of a hostile microenvironment. Cells were seeded into a standard 6-well cell culture plate at a density of 60,000 cells/well. Plates were prepared using the standard method described above (see section 2.1.3.2 Experimental plating). Wells were treated in parallel with either media containing 0.4% FBS or 10% FBS (control) for 96 hours, with a complete media change being performed at 48 hours. Following this period, a Live/Dead assay was performed to assess cell viability, RNA was harvested to evaluate any changes in gene expression and cells were trypsinized and seeded onto a 96-well plate for calcium imaging with Yoda-1.

2.1.9.2. Multiple Cell Passage and Physiological Aging

NAVSMCs were repeatedly passaged in T25 flasks to physiologically exhaust the cells. NAVSMCs were assumed to have been received at passage 1. Flasks were split when they had reached approximately 70% confluence on light microscopy. Flasks were seeded with different densities of cells, as those seeded with higher cell densities were likely to become confluent quicker than flasks seeded with lower cell densities. This method of cell seeding was adopted to ensure flasks with cells at differing passages were simultaneously available for calcium imaging with Yoda-1 and for comparison of RNA expression of genes of interest.

2.1.10. VSMC Transfection and PIEZO-1 Knockdown

2.1.10.1. Lipofectamine versus Accell Transfection

Short-interfering RNA (siRNA) was used to transfect cells to investigate the feasibility of PIEZO-1 knockdown in VSMC. Methods of cells transfection were optimised on SVVSMCs. Two different siRNA transfection techniques were investigated; Lipofectamine (Invitrogen, Thermo Fisher Scientific, UK) and Accell (Horizon Inspired Cell Solutions, Dharmacon, UK). These two methods

were attempted as AAAVSMCs have been shown to be difficult to transfect by our laboratory. SVVSMCs were seeded into standard 6-well cell culture plates (Corning, Thermo Fisher Scientific, UK) at a density of 60,000 cells/well and cultured until more than 70% confluent. Cell confluence was estimated using a macro developed in ImageJ (National Institutes of Health, USA), see section 2.1.4.2. Transfection of SVVSMCs and PIEZO-1 knockdown was then evaluated with 50nM Lipofectamine, 100nM Lipofectamine and Accell (concentration fixed as per manufacturers specifications). RNA were harvested at 72 hours for PCR, by which point RNA knockdown should have occurred with both methods, according to the manufacturer guidance.

Lipofectamine, a commonly used transfection reagent within most laboratories, contains transfection payloads in liposomes which fuse with the cell membrane of the target cell. Lipofectamine, PIEZO-1 siRNA or scrambled (scrm) siRNA (see Table 5 for sequences) were added to Opti-MEM transfection media. This was added to an equal volume of 0.4% DMEM containing no antibiotics. Cells were washed with PBS prior to the addition of 500µL of transfection solution. Cells were treated for 5 hours after which point the reagents were replaced with the standard culture media. Accell, on the other hand, is a proprietary transfection reagent for difficult to transfect primary cells, which did not require any transfection reagent or viral vector for siRNA delivery systems to knockdown PIEZO-1. The mechanism of delivery was not disclosed by the manufacturer. To compare RNA knockdown of PIEZO-1, Accell scrm siRNA SMARTpool (negative control) and Accell PIEZO-1 siRNA SMARTpool were utilised. “SMARTpool” samples contained a mixture of 4 target sequences to maximise potential knockdown of the target gene. Target sequences utilised in Accell transfection are also described in Table 5.

The siRNA targets of scrm siRNA smart pool were screened against the exon coding for PIEZO-1 and PIEZO-2, and could not be identified on either sequences (Appendix B). The PIEZO-1 siRNA smart pool sequences were also screened against the exon coding for PIEZO-1, which were found to be well spread out across the PIEZO-1 mRNA sequence. Furthermore, the

targets were upstream of the primer sequences used to determine PIEZO-1 expression, therefore if knockdown had occurred it should be readily detectable by qPCR. None of the siRNA PIEZO-1 targets were identifiable on the PIEZO-2 mRNA sequence (Appendix B), therefore, any changes in PIEZO-2 expression observed with PIEZO-1 siRNA knockdown was likely to be independent of siRNA interference.

2.1.10.2. Accell PIEZO-1 Knockdown and Calcium Imaging

To maximise the likelihood of PIEZO-1 knockdown, the Accell transfection reagent was utilised as the method of choice for PIEZO-1 knockdown, to evaluate subsequent functional effects. NAVSMCs were seeded into; 96-well plates (Corning, Thermo Fisher Scientific, UK) at a density of 5,000 cells/well for calcium imaging with Yoda-1 stimulation, and a 6 well tissue culture plate (Corning, Thermo Fisher Scientific, UK) at a density of 60,000 cells/well to evaluate VSMC viability. VSMCs were transfected for 96 hours (i.e. single transfection) and 192 hours (i.e. double transfection) to maximise the likelihood of functional knockdown as protein knockdown should have occurred after 72 hours according to the manufacturer guidelines. Live-dead assays were performed to ensure the results obtained from calcium imaging and PCR were a reflection of successful VSMC transfection and not the physiological effects of cell death.

To further validate this method of transfection additional conditions were included: mock transfection (buffer), Cyclophilin B-red florescent probe (RFP) siRNA (positive control), scrm siRNA SMARTpool and PIEZO-1 siRNA SMARTpool. The efficacy of Accell transfection delivery was evaluated using IncuCyte FLR quantification of RFP labelled cyclophilin B siRNA and the efficiency of RNA knockdown was confirmed with qPCR. A Live-Dead assay (LIVE/DEAD® Viability/Cytotoxicity Kit, Eugene, USA) of the cells was also performed, as described in section 2.1.5.3., on VSMCs cultured in a 6-well plate.

Table 5. siRNA transfection sequences.

*Seq = sequence.

Delivery method	Name	Target gene	siRNA sequences	Manufacturer
Lipofectamine	siRNA.85	PIEZO-1	GCAAGUUCGUGCGCGGAUU AAUCCGCGCACGAACUUGC	Sigma-Aldrich
Lipofectamine	siScrm	NA	UGGUUUACAUGUCGACUAA UGGUUUACAUGUUGUGUGA UGGUUUACAUGUUUUCUGA UGGUUUACAUGUUUUCCUA	Dharmacon
Accell	Red CycB siRNA	CycB	GCCTTAGCTACAGGAGAGA	Dharmacon
Accell	siScrm smart pool	NA	Seq 1: TGGTTTACATGTCGACTAA. Seq 2: TGGTTTACATGTTTTCTGA. Seq 3: TGGTTTACATGTTTTCCTA. Seq 4: TGGTTTACATGTTGTGTGA.	Dharmacon
Accell	siP1 smart pool	PIEZO-1	Seq 1: GCCCTGTGCATTGATTATC . Seq 2: TATGTTCGAGGAGCT. Seq 3: GCGTCATCATCGTGTGTAA. Seq 4: GCATCAGTCTACGTTTTAG.	Dharmacon

2.2. In-Vivo Experimental Methods

2.2.1. Experimental Animals

2.2.1.1. Animal Husbandry and Ethics

GM500 ventilated cages (Techniplast, Italy) were used to house all mice at 21^{o}C with a 12 hour light/dark cycle in 50-70% humidity in the University of Leeds Animal facility. Rat and mouse Maintenance No.1 (RM1) diet in 9.5 mm pellets (Special Diet Services, UK), and water pouches (Hydropac®, UK) were provided to all mice. A maximum of 5 mice were housed per cage. All experimental procedures involving mice in this thesis were conducted with the guidance outlined by the UK Home Office Animals (Scientific Procedures) Act 1986 under the project licence P606320FB (holders: Marc Bailey and David Beech, 2016-2021) and personal licence I80886334 (Mohammed Waduud, September 2018 onwards). All animals were observed for signs of ill-health and were terminated in the event of any suffering or distressed by approved Schedule 1 (Sch1) methods.

2.2.1.2. C57BL6/J Mice

Male C57BL6/J mice were purchased from Charles River (https://www.criver.com, UK). These were the primary strain of mice utilised throughout this thesis. Experimentation was started at 12 weeks of age. C57BL6/J mice were used for: validating imaging protocols; validating operator technique, assessing and comparing aortic size and stiffness between mice models; and evaluating mRNA expression of the PIEZO channels, KLF-2, KLF-4 and TG2 in mice models.

2.2.1.3. Transgenic PIEZO-1 Knockout Mice

Smooth muscle specific PIEZO-1 knockout mice were produced via crossing PIEZO-1$^{lox/lox}$ female mice (The Jackson Laboratory, USA) with a tamoxifen (TAM) inducible smMHCCre-ER(T2) male mice (The Jackson Laboratory, USA) (Wirth et al., 2008; Frutkin et al., 2007). An inducible Cre is therefore inserted into the Y chromosome and the male mice was then further bred to

yield; smMHCCre-ER(T2) PIEZO-1$^{-/-}$ (homozygote), smMHCCre-ER(T2) PIEZO-1$^{-/+}$ (heterozygote) and smMHCCre-ER(T2) PIEZO-1$^{+/+}$ (wild-type) male mice. Mice between the age of 10-11 weeks were injected with intraperitoneal TAM (50 mg/kg dissolved in peanut oil) everyday for 5 days, followed by a week of quarantine. Sham control mice were injected with an intraperitoneal injection containing only peanut oil. The infra-abdominal aorta from the transgenic mice were harvested at baseline (i.e. 12 weeks) to evaluate PIEZO-1 knockout on PCR. Experimentation with these transgenic mice, similar to the C57BL6/J mice, was carried out at 12 weeks.

Validation of PIEZO-1 knockout in the transgenic mice bred in-house was evaluated by isolating cardiac fibroblasts (described in section 2.1.1.4) from homozygote, heterozygote and wild-type mice who did not receive tamoxifen. Cardiac fibroblasts were cultured in standard 12-well cell culture plates to confluence. The culture media was removed and wells were washed with PBS before treatment with 150µl TAT-Cre (Sigma-Aldrich, USA) in 2.25ml of 10% FBS for 12 hours. Cells were trypsinized and plated for experimentation after a further 12 hours. PIEZO-1 knockout from cardiac fibroblasts was confirmed on qPCR and functional knockout was evaluated on calcium imaging with Yoda-1.

2.2.2. Animal Procedures

2.2.2.1. Peri-Adventitial PPE AAA model

Mice were subjected to peri-adventitial application of PPE to the abdominal aorta at 12 weeks of age to induce an infra-renal AAA (Bhamidipati et al., 2012). This procedure was performed using an aseptic technique in a custom built operating theatre containing a heated down-draft operating table and a wall mounted operating microscope (ZEISS OPMI Pico) with an attached camera, MEDALINK100 (Carl Zeiss, Germany). Inhaled isoflurane was administered using a recovery anaesthesia system (VetTech, UK) requiring oxygen. Mice were initially sedated in a chamber with an anaesthetic flow rate of 5 L/min and then transferred to a facemask to maintain sedation with a flow

rate of 1.5 to 2 L/min. Downward laminar air flow system AFA500 helped maintain a sterile field. The instruments utilised included; a stainless steel iris scissor (11.5 cm, straight), stainless steel iris forceps (10 cm, curved), Dumont fine forceps, tissue forceps, Alms retractor and a standard needle holder. All work surfaces were cleaned with 70% ethanol and instruments autoclaved before operating.

All mice were weighed and then secured in position using micropore tape. The anterior abdominal wall was; shaved with a handheld trimmer, de-epilated with Veet cream (Reckitt, UK) and finally cleaned with ethanol, followed by chlorhexidine 2% (Ecolab, UK). A subcutaneous bolus of 0.1ml of levobupivacaine 0.05% was then administered using a Terumo Luer slip syringe and 26G needle. A mid-line laparotomy was performed and the bowel contents was removed to the left of the abdomen using atraumatic sterile cotton buds. The bowel was wrapped in gauze and soaked in warmed PBS. The aorta was exposed using blunt dissection with cotton buds and 10µl PPE or PBS (for sham control) which was applied to the aorta for 5 minutes. The peritoneal cavity was then washed out three times with sterile PBS and the abdominal wall was closed in layers with Vicryl sutures (Ethicon, USA). The incision wound was then further reinforced with skin glue (3M Vetbond, USA). Mice were weighed at day 7 and 14 post-operatively to ensure they maintained a healthy weight. A weight loss of 15% resulted in the mice being terminated for welfare reasons.

The surgical technique was validated within the group by comparing the aortic measurements following sham and PPE surgery of the trainer (surgeon 1 [S1]) and the trainee (surgeon 2 [S2]) in an independent cohort of mice. The trainee was first deemed competent to perform the procedure safely. Surgeries were carried out independently by each surgeon on different days. USS imaging was performed on day 14 by a single operator blinded to the surgical model and surgeon who had performed the procedure. The 3DLV measurements of sham and PPE models were subsequently compared for each surgeon to evaluate if the aneurysm induction surgery had been successful. The 3DLV

measurements of mice who had undergone sham and PPE surgery were subsequently compared between surgeons to evaluate if any surgeon-dependent differences was evident.

2.2.2.3. Photography of the Aorta

Following successful blunt dissection and exposure of the infra-renal abdominal aorta, a macroscopic image at x12.5 magnification with the MEDALINK100 system (Carl Zeiss, Germany) was recorded for demonstrative purposes at baseline and before harvest. During photography, the aorta remained in situ under normal haemodynamic pressure, with blood still being pumped through.

2.2.2.4. Aorta Harvest and Preparation for RNA Extraction and Histology

Murine aortae were harvested, under terminal anaesthesia, for PCR and histological assessment at baseline, day 7 and 14 post-operatively. Aorta were prepared for RNA extraction by perfusing the left ventricle with 5mls of PBS and dissecting off the peri-vascular fat. The infra-renal aorta was resected and placed in a 2ml Eppendorf tube and immediately snap frozen in liquid nitrogen. The aorta was then homogenised in 1.5ml of TRIreagent, initially with a hand-held homogeniser and then with a TissueLyser (Qiagen, USA). A 4mm metal bead was added to the 2ml Eppendorf and the TissueLyser was set at 30 oscillations per second or 60 seconds. This cycle was repeated until the aorta had completely disintegrated. The sample was then stored at -80^{o}C. RNA was later extracted as described in section 2.1.7.1.

Histological samples were prepared by exsanguinating the mice via the inferior vena cava. Then, similar to the preparation of the aorta for RNA extraction the left ventricle was perfused with 5mls of PBS and fixed with 5mls of 4% Paraformaldehyde (PFA). The peri-vascular fat was cleaned and the aorta was dissected out. The aorta was then fixed in 4% PFA for a further 48 hours at 4^{o}C after which point they were transferred into 70% ethanol and stored at 4^{o}C until processing.

2.2.3. Ultrasound (USS) Imaging

2.2.3.1. Mice Ultrasound Imaging Protocol

USS imaging was performed pre-operatively, at days 7 and 14 post-operatively in sham and PPE-operated mice for comparative analysis throughout this thesis. Imaging of the infra-renal aorta was performed using the Vevo2100 high-frequency micro-ultrasound system (VisualSonics, Netherlands), which was equipped with; an automatic motor holding an MS-550D probe (40 MHz frequency), a temperature rectal probe and a heated platform. Electrodes allowed electrocardiogram (ECG) and respiratory gating. The abdomen of the mice was prepared in an identical manner to that before surgery (i.e. shaved and de-epilated). Mice were placed in a supine position on the heated platform, to maintain a core body temperature between 36-38^{o}C, under-recovery isofluorane anaesthesia. The transducer was applied to the abdomen on a layer of aquasonic gel (Parker Labs, Netherlands).

A single subjective transverse Electrocardiogram-gated Kilohertz Visualisation (EKV) image was recorded in the “B mode” at the largest visible section of the aorta for measurement of the maximum anterior-posterior diameter (APd_{max}, Figure 19). The inner-to-inner diameter was measured in VevoLab v1.7.0 (VisualSonics, Netherlands) in line with the current ultrasound measures used in the UK National AAA screening programme. Measurement of the APd_{max} was recorded in millimetres (mm). Sequential transverse imaging was then performed along a 12mm (157 frames at 0.076mm intervals) region of interest caudally from the left renal artery. Images were gated for respiration and triggered at 50ms after the R wave (this corresponded to peak dilation in the infra-renal aorta), therefore, factoring in physiological movement artefact. These images were used to calculate the three-dimensional lumen volume (3DLV, Figure 19) using semi-automated segmentation and a reconstruction tool available with the VevoLab v1.7.0 software (VisualSonics, Netherlands). Measurement of the 3DLV was made in millimetres-squared (mm^3). These two recordings were typically carried out minutes apart.

The EKV image also allowed for vessel distensibility to be calculated using an add-on software package, VevoVasc (VisualSonics, Netherlands). The lumen boundaries were marked manually, which allowed the software to track the pulsatile motion. Vessel distensibility was calculated based on changes in the aortic wall motion over the cardiac cycle and measurements were quantified in megapascal pressure unit (MPa^{-1}).

2.2.3.2. Validation of Observer Measurement

To assess the observer variability and reproducibility of measurements, APd_{max} and 3DLV measurements were carried out on post-operative imaging from an independent cohort of mice. Two independently trained observers (observer 1 [O1] and observer 2 [O2]) recorded measurements presented in a random order different to one another. They were blinded to the measurements of the other and blinded to the surgery performed on the animal (i.e. sham or PPE). These allowed the assessment of inter-observer variability. Both observers were doctoral students who were trained by an independent expert co-investigator with at least 5 years of experience in mice ultrasonography using the Vevo2100 high-frequency micro-ultrasound system (VisualSonics, Netherlands). O1 had a basic science background and O2 was a resident in vascular surgery with prior experience in USS. O2 measured the images twice (O2a and O2b) blinded to the results from his previous measurement to determine intra-observer variability. Observer variations in murine abdominal aortic measurements were presented as Bland-Altman plots with limits of agreement (LOA), Pearsons' correlation and regression analysis.

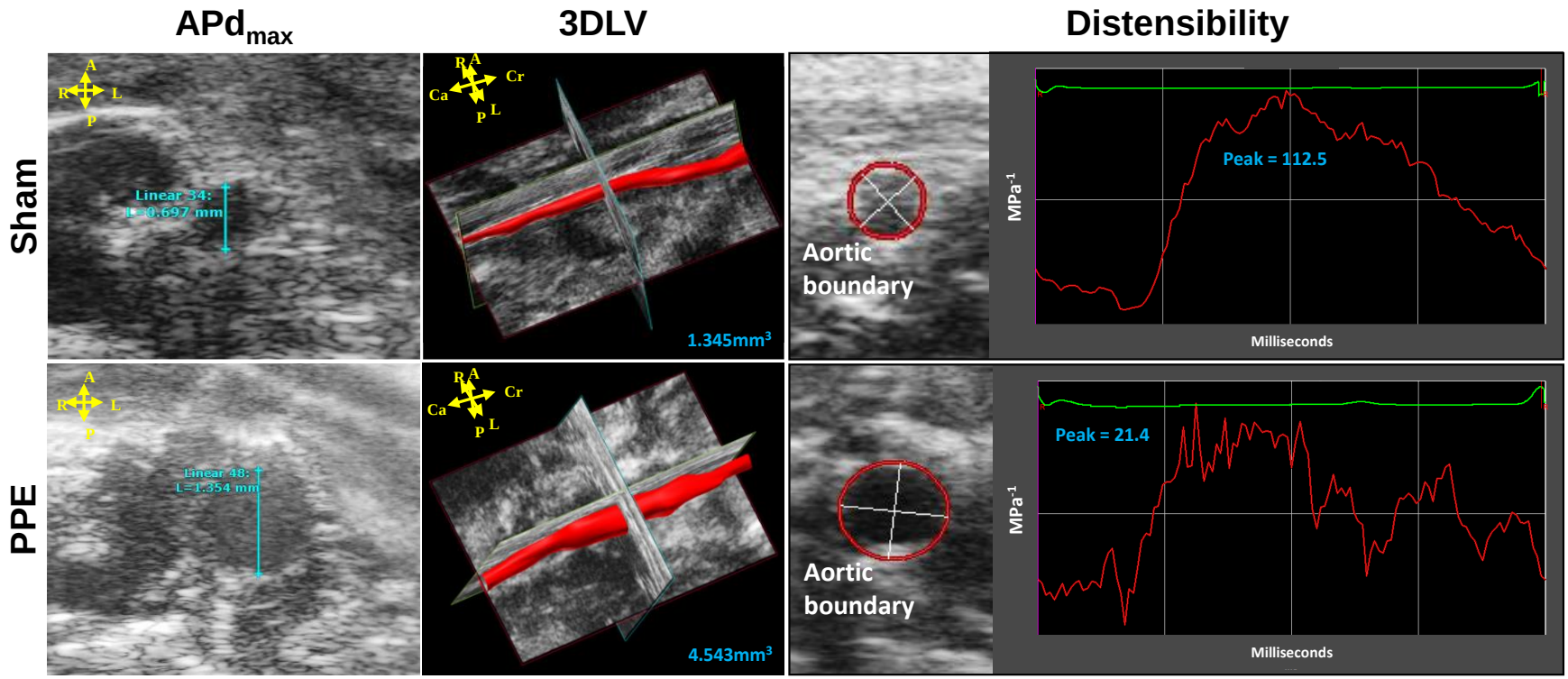

Figure 19. Representative ultrasound images of the APd$_{max}$, 3DLV and vessel distensibility of sham and PPE mice at day 14 obtained with the Vevo2100 ultrasound scanner.

A = anterior, P = posterior, R = right, L = left, Cr = cranial, Ca = caudal. The blue lines on the images on the left hand side indicate the inner-to-inner diameter. The red circle and corresponding red line indicates movement of the aortic wall. The green line on the images on the right hand side represent the cardiac cycle.

2.2.3.3. Relationships between APd_{max}, 3DLV and Aortic Distensibility

Mice abdominal aorta in both sham and PPE models were imaged pre-operatively and then every 3 to 5 days post-operatively for 14 days in an independent cohort of C57BL6/J mice. Single observer measurements were utilised as this reflected routine laboratory practise. At each time point, the APd_{max} and 3DLV measurements were recorded for the same mouse. This allowed direct paired comparison of APd_{max} and 3DLV measurement techniques. The percentage change between sequential measurements of the aorta following PPE surgery stratified using measurement technique allowed the identification of the most sensitive method to detect subtle morphological changes in the murine aorta. Comparison of aortic measurements in sham and PPE mice based on the imaging technique and time point helped confirm which technique was the most sensitive in detecting morphological differences. However, aortic distensibility was assessed on days 7 and 14 post-operatively. The relationship between; APd_{max} and 3DLV, MPa-1 and APd_{max}, and MPa-1 and 3DLV were assessed using Pearson's correlation and linear regression analysis. Finally, the relationship between PIEZO-1, PIEZO-2, KLF-2, KLF-4 and TG2 gene expression in relation to aortic size and distension was also evaluated using Pearson's correlation and linear regression analysis.

2.2.3. Wire Myography

Wire myography was conducted on the aorta from transgenic mice to evaluate any functional differences in vasomotor function in relation to PIEZO-1 knockout. These were performed by Naima Endesh (Post-doctoral Research Fellow, David Beech Laboratory Group, LICAMM) who has unique expertise in conducting these studies. The aorta of 2 male transgenic mice (smMHCCre-ER(T2) PIEZO-$1^{-/-}$ and smMHCCre-ER(T2) PIEZO-$1^{+/+}$) at 12-weeks gestation (following tamoxifen induction) were dissected and flushed through with PBS as described in section 2.2.2.4. These were mounted in parallel on to a four channel myograph under isometric techniques. Contraction (millinewton [mN]) of the aortic wall was recorded over time (seconds) in response to stimuli; potassium, phenylephrine, acetylcysteine, Yoda-1 and KC289 (a novel agonist of PIEZO-1 developed by the Beech group).

2.2.4. Histological Assessment

Histological assessment was performed to confirm the morphological findings on ultrasound and characterise the makeup of the aortic wall. It was performed at the Leeds Institute of Cancer and Digital Pathology Service. For histological stains, slides were de-waxed in xylene followed by rehydration in ethanol. Haematoxylin and Eosin (H&E) staining was performed to assess the gross architecture of the aorta and quantify luminal dimensions. Samples were stained in Mayer's Haematoxylin solution for 8 minutes and counterstained with eosin-phloxine for 30 seconds. Imaging of the slides was performed on Aperio® AT2 (Leica Biosystems) digital slide scanner at a magnification of x20 (maximum). Images were accessed remotely using the Aperio® Image Scope software (Leica Biosystems) from the secure Leeds Institute of Cancer and Pathology digital server. The luminal area of the aorta on the slides was manually traced on ImageJ (National Institutes of Health, USA) with the assessor blinded to the mice genotype or any surgery undertaken. The area (mm^2) was subsequently derived.

2.3. Data Management and Statistical Analysis

2.3.1. Data Handling

Data was collected on or converted to a Microsoft Excelsheet (Microsoft, USA). Images were captured as JPEG images. All data was stored on the secure University of Leeds server. Statistical analyses were performed predominantly using GraphPad Prism 9 (Dotmatics, USA). Analysis was also performed using Origin v8.6 (OriginLab, USA) and Minitab® (Minitab, USA).

2.3.2. Data Analysis

Data were checked for normality using the Shapiro-Wilk test, which determined whether parametric or non-parametric testing would be performed. In in vitro experiments, “N” represents the number of biological replicates and “n” represents the number of technical repeats. However, in in vivo experiments “N” represents the number of mice utilised. Parametric data were summarised as the mean ± the standard error of the mean (SEM) unless otherwise stated. Non-parametric data were summarised with the median and 95% confidence interval (95% CI) so the skewness of data could be presented. Similarly, scatter graphs comparing groups or data from different time points were summarised on the graph using lines representing the mean ±SEM. Comparisons between two groups were made using two-tailed t-tests (parametric) and the Mann-Whitney test (non-parametric). Paired-test were undertaken when the samples were related to one another. Multiple groups were compared using one-way analysis of variance (ANOVA) with Bonferroni correction. The area under the curve (AUC) was used to assess differences between groups over time. $P < 0.05$ was considered significant. * represents a p-value ≤ 0.05, ** represents a p-value ≤ 0.01 and *** represents a p-value ≤ 0.001.

2.3.3. Relative Abundance of Transcripts and Primer Efficiency

Crossing-point values were then averaged for each triplicate. Ct values were normalised to a reference gene (i.e. GAPDH) to obtain the delta Ct (ΔCt) value. Primer efficiency was calculated automatically by the Lightcycler analysis software v3.5 (Roche Molecular Systems, UK) and plotting Ct values against the log dilution. The Livak method was then used for relative quantification ([efficiency on standard curve] $^{-\Delta\Delta Ct}$).

2.3.4. Dose Response Curves

The dose-response curves were constructed for calcium imaging experiments within NAVSMCs and AAAVSMCs to determine the relationship between the maximal intra-cellular calcium entry (y-axis) and the concentration of Yoda-1 (log10[conc], x-axis). Origin Pro v8.6 was utilised to fit the scatterplot using the logistic fit Hill 1 equation [$y = START+(END-START) \times (k^n/(k^n+x^n))$] where the Michealis constant is k equivalent to the EC_{50}.

2.3.5. Sample Size and Power Calculations

Power calculations were not performed for in vitro experiments. Control and experimental groups were matched 1:1 for biological and technical replicates. This was demonstrated to be adequate in preliminary experiments and through expert consensus within the laboratory group.

Sample size calculations were performed for in vivo experiments and conducted in accordance with the 3Rs. Sample size calculations were performed using the online epidemiological sample size calculator (openepi.com). The primary “effect” was a change in the APd_{max} (mm) and 3DLV (mm^3) in PPE treated aorta compared to the sham control aorta. Variance in the APd_{max} and 3DLV between the two surgical groups was determined from a retrospective analysis of USS imaging of the aorta. In vivo experiments involving C57BL6/J mice were powered at 80% with alpha set at 0.05 and a minimum effect size of 25%. It was determined that 10 PPE mice

and 5 sham mice would be required, factoring in any potential post-operative loss. The sample size calculation for the transgenic mice was more challenging as the physiological impact of VSMC PIEZO-1 knockout had yet to be established. With the effect size reduced to 15%, it was calculated a minimum of 18 PPE mice and 6 shams would be required for these experiments.

Chapter 3: Cellular Analysis of AAA stressors

3.1. Confirmation of VSMCs

In vitro experiments in this thesis primarily used NAVSMCs. Therefore, it was pertinent to confirm these to be VSMCs. Immunohistochemical staining with α-SMA indicated that the cells were probably VSMCs (Figure 20). Similarly, AAAVSMCs from the Leeds Aneurysm Development Study (LEADS) and Ageing Aorta Tissue bank have been previously shown to be VSMCs on immunohistochemistry through the identification of α-SMA and SMMHC which were co-stained (Riches et al., 2013), Figure 5. Therefore, this was not repeated.

Different stressors mimicking pathophysiological aspects of the AAA microenvironment were tested on NAVSMCs. Any mechanistic changes in relation to PIEZO-1 were likely to have occurred early in the AAA disease process therefore utilising AAAVSMCs would have been futile. Furthermore, AAAVSMCs were senescent and resistant to normal physiological processes such as proliferation, therefore, it would not have been feasible to conduct the experiments outlined in a timely manner.

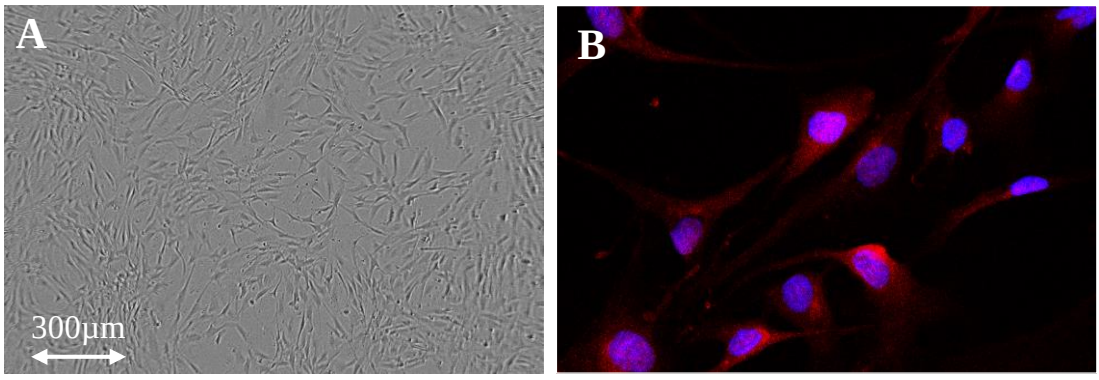

Figure 20. Representative Incucyte FLR image of NAVSMCs (A) and fluorescent immunohistochemical staining of α-SMA [red] (B).

*Immunohistochemistry image was produced by Dr Karen Hemmings (Post-Doctoral Fellow for the Dr Bailey Laboratory Group).

3.2. PIEZO, KLF-2, KLF-4 and TG2 Gene Expression in NAVSMCs and AAAVSMCs

Before applying different stressors, it was important to compare the baseline mRNA expression of PIEZO-1, PIEZO-2, KLF-2, KLF-4 and TG2 between NAVSMCS and AAAVSMCs, Figure 21. No significant differences in PIEZO-1 and KLF-4 mRNA were observed between NAVSMCs and AAAVSMCs, Figure 21. However, there was a trend towards a lower expression of both these genes in AAAVSMCs. Significantly higher expression of PIEZO-2 and KLF-2 mRNA was observed in AAAVSMCs compared to NAVSMCs ($p<0.0001$ and $p=0.004$, respectively). Furthermore, TG2 mRNA in AAAVSMCs was significantly lower compared to NAVSMCs ($p=0.023$). Reassuringly, single-product bands were observed in all samples, Figure 21.

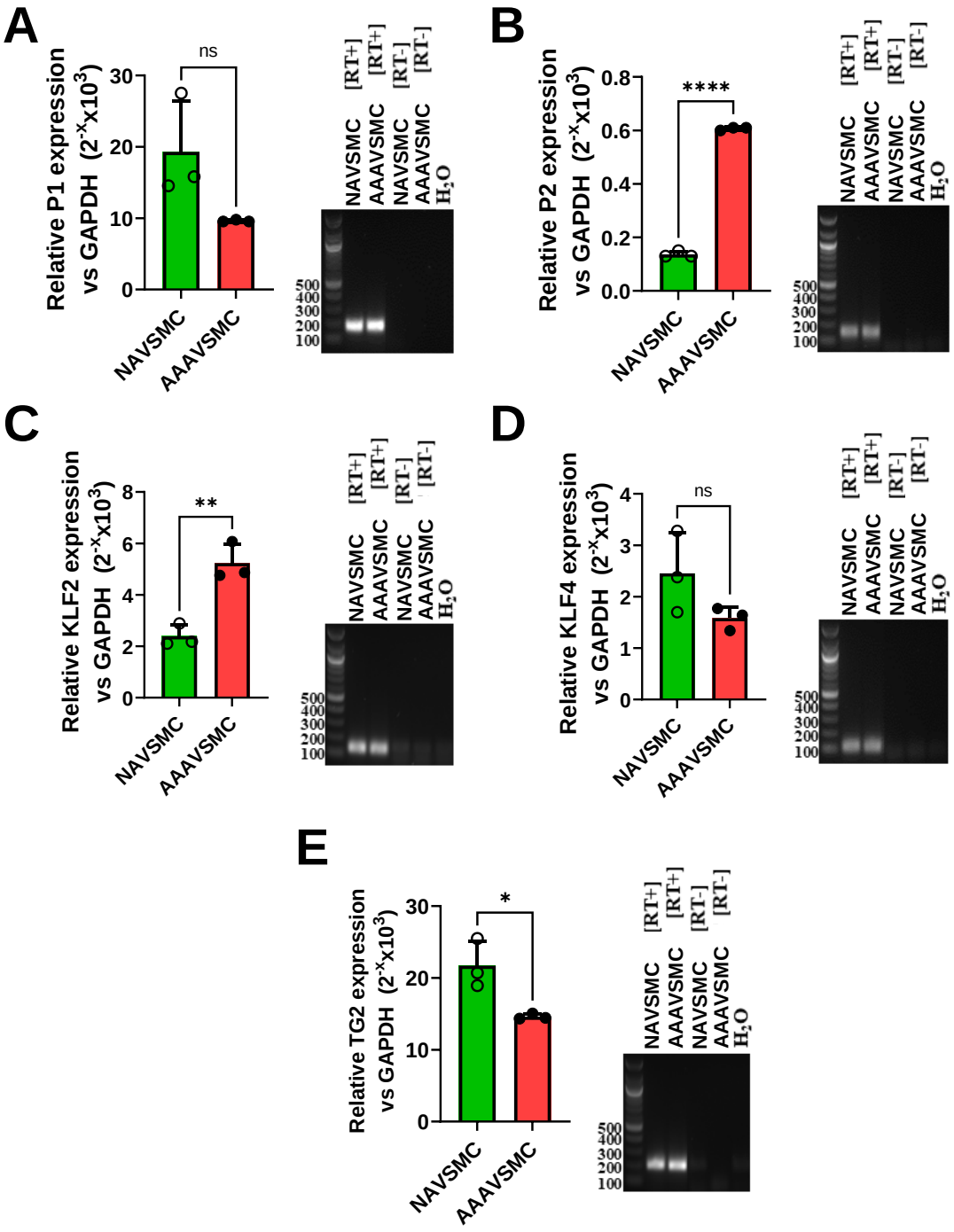

Figure 21. Relative gene expression and gel electrophoresis blots for PIEZO-1 (A) [182bp], PIEZO-2 (B) [160bp], KLF-2 (C) [138bp], KLF-4 (D) [112bp] and TG2 (E) [209bp] in NAVSMCs and AAAVSMCs at baseline (pre-experimentation).

NAVSMCs= green. AAAVSMCs= red. Error bars (black) represent mean ±SEM. *= $p<0.05$, **= $p<0.01$, ***= $p<0.001$, ns= no significant difference. bp=base pairs. N/n = 3/9.

3.3. Effects of Yoda-1 in VSMCs

3.3.1. Acute Activation of PIEZO-1 by Yoda-1 in VSMCs

Differences in PIEZO-1-dependent intra-cellular calcium entry were subsequently compared between NAVSMCs and AAAVSMCs. A potent and specific activator of the PIEZO-1 channel, Yoda-1, was used to study the downstream effects of PIEZO-1 activation. Yoda-1-induced intra-cellular calcium entry was evident in NAVSMCs (Figure 22A). Significantly higher intracellular calcium entry was observed when using Yoda-1 at 5μM and 10μM concentrations compared to the lower concentration of 2.5μM (Figure 22B and Figure 22C, $p<0.001$). No significant differences in PIEZO-1 calcium entry were observed between Yoda-1 used at 5μM and 10μM concentrations. The half maximal effective concentration (EC_{50}) of Yoda-1 in NAVSMCs was 2.65 ±0.17μM, Figure 22D. Yoda-1-induced calcium entry was also evident in AAAVSMCs (Figure 23A). However, there were no significant differences in intracellular calcium entry with increasing concentrations of Yoda-1 (Figure 23B and Figure 23C). The EC_{50} of Yoda-1 for AAAVSMCs was 2.2 ±0.72μM, Figure 23D.

No significant differences in Yoda-1 activated intracellular calcium entry in NAVSMCs and AAAVSMCs using 2.5μM Yoda-1 (closest concentration to EC_{50} of both cell types) were observed, Figure 24. However, greater variability in intracellular calcium entry in the AAAVSMCs was evident at all concentrations of Yoda-1. There were no noticeable differences in VSMC morphology on microscopy when comparing wells pre- and post- Yoda-1 calcium exposure (Figure 25). Yoda-1, at a 10μM concentration (maximum without causing compound precipitation), was utilised for all subsequent calcium imaging to maximise the probability of PIEZO-1 activation. This was to minimise any variability in calcium imaging, similar to that seen in AAAVSMCs, in NAVSMCs after being subjected to a period of stress.

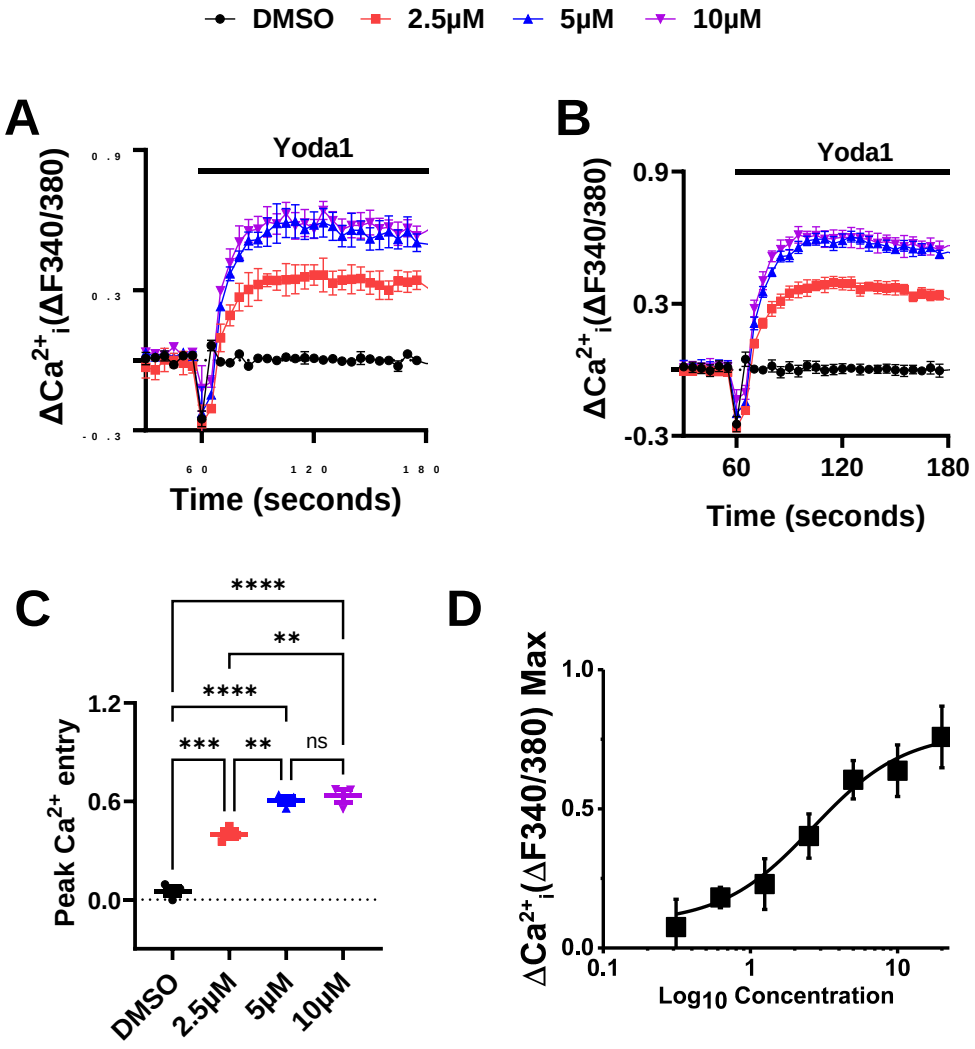

Figure 22. Yoda-1 calcium imaging of NAVSMCs.

A; representative example (N/n= 1/3) of Yoda-1 activated intra-cellular calcium entry into NAVSMCs over time with DMSO [vehicle] (black circle), 2.5µM Yoda-1 (red square), 5µM Yoda-1 (blue triangle) and 10µM Yoda-1 (purple inverted triangle). B; averaged (N/n= 3/9) Yoda-1 activated intra-cellular calcium entry into NAVSMCs over time with DMSO and different Yoda-1 concentrations. C; Averaged (N/n= 3/9) peak Yoda-1 activated calcium entry into NAVSMCs with DMSO and different Yoda-1 concentrations. D; EC50. Error bars represent mean ±SEM. **= p<0.01, ***= p<0.001, ***= p<0.001, ns= no significant differences.

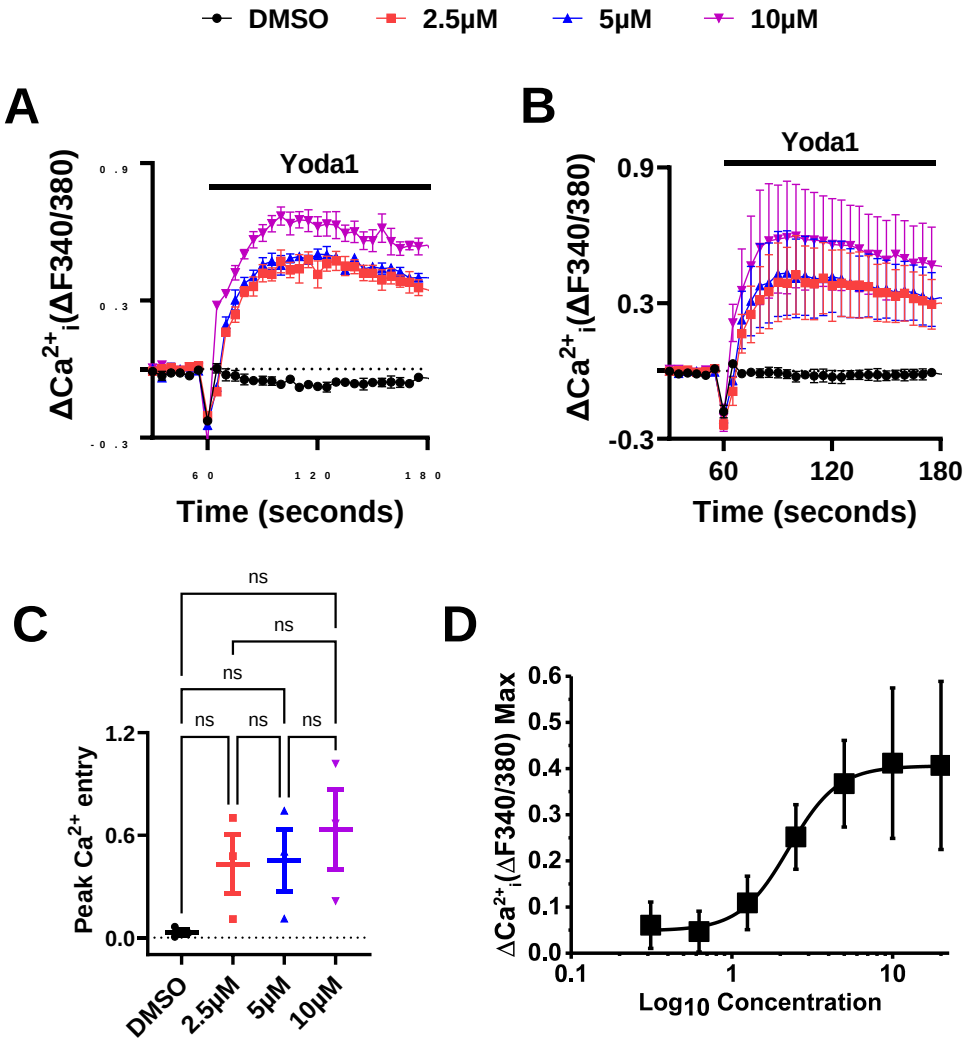

Figure 23. Yoda-1 calcium imaging of AAAVSMCs.

A; representative example (N/n= 1/3) of Yoda-1 activated intra-cellular calcium entry into AAAVSMCs over time with DMSO [vehicle] (black circle), 2.5μM Yoda-1 (red square), 5μM Yoda-1 (blue triangle) and 10μM Yoda-1 (purple inverted triangle). B; averaged (N/n= 3/9) Yoda-1 activated intra-cellular calcium entry into AAAVSMCs over time with DMSO and different Yoda-1 concentrations. C; Averaged (N/n= 3/9) peak Yoda-1 activated calcium entry into AAAVSMCs with DMSO and different Yoda-1 concentrations. D; EC50. Error bars represent mean ±SEM. ns= no significant differences.

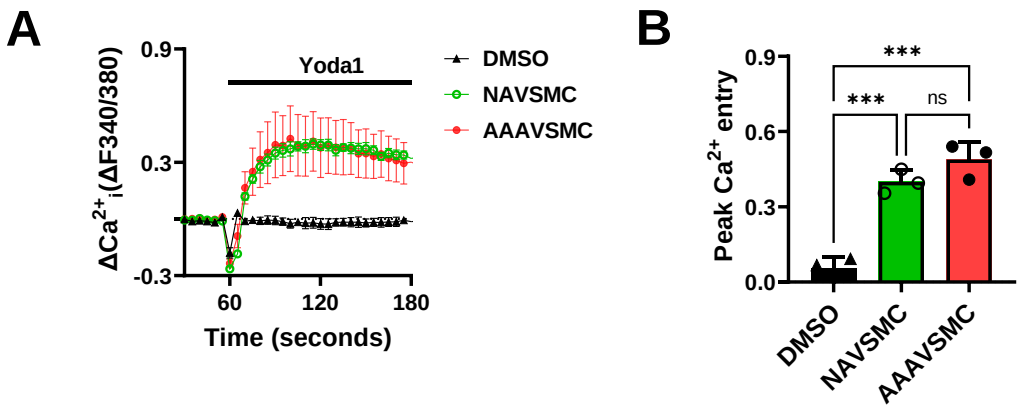

Figure 24. Comparison of Yoda-1 activated intra-cellular calcium entry into NAVSMCs and AAAVSMCs with 2.5µM Yoda-1.

A; Comparison of Yoda-1 activated calcium entry over time and B; Peak Yoda-1 activated calcium entry. NAVSMCs= green, AAAVSMCs= red. Error bars (black) represent mean ±SEM. ***= p<0.001, ns= no significant differences. N/n= 3/9.

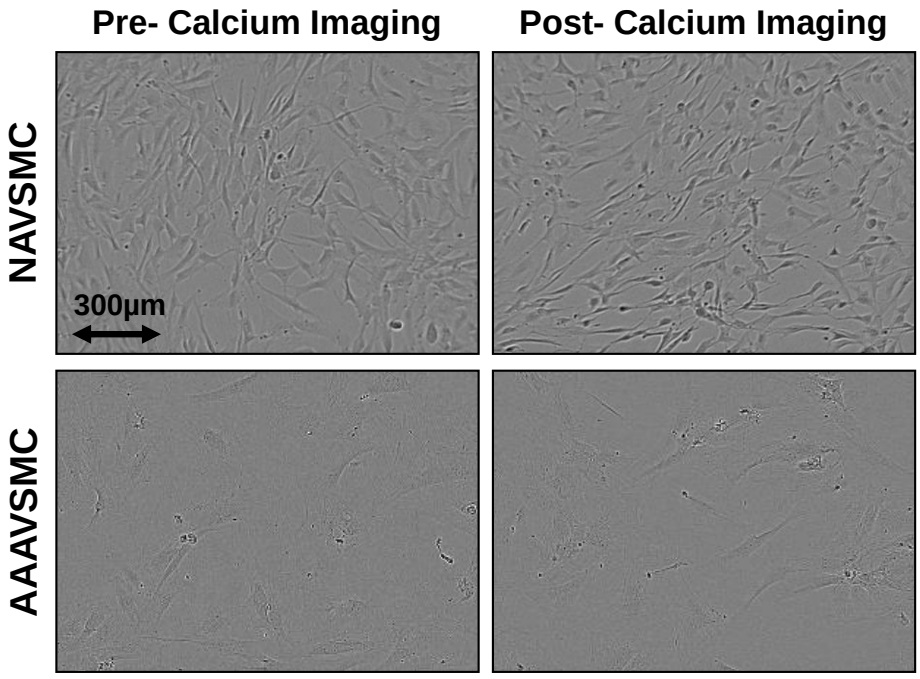

Figure 25. Phase contrast IncuCyte FLR images before (left) and after (right) 10µM Yoda-1 calcium imaging of NAVSMCs (top) and AAAVSMCs (bottom).

Scale on bottom right corner. N/n= 3/3.

3.3.2. Prolonged activation of PIEZO-1 by Yoda-1 in VSMCs

Yoda-1 was administered for 96 hours to assess the functional effects of prolonged activation of PIEZO-1. After 96 hours of treatment with 10μM DMSO (vehicle) or 10μM Yoda-1, there were no significant differences in the percentage of viable NAVSMCs (DMSO; 79.0 ±1.8% vs Yoda-1; 78.0 ±5.7%, p=0.87) or the Live/Dead ratio (DMSO; 12.8 ±5.2 vs Yoda-1; 12.9 ±9.5, p=0.99), Figure 26.

Overall, NAVSMCs treated with 10μM Yoda-1 for 96 hours showed a 1.8-fold increase in proliferation compared to vehicle-treated cells (AUC; DMSO 4232, 95% CI 3976 to 4489; Yoda-1 7792, 95% CI 7334 to 8249; p<0.001), Figure 27. There was no evidence of any significant difference in NAVSMC proliferation between the groups at 24 hours (mean cell count difference 29.6 ±75.0, p=0.71). Irrespective of the treatment group, NAVSMC proliferation had an upward trajectory. However, at 48 hours there was significantly higher cell proliferation in NAVSMCs treated with 10μM Yoda-1 (count difference 811.9 ±107.1, p=0.002). This trend persisted at 72 hours (count difference 2185 ±176.4, p<0.001) and 96 hours (count difference 1087 ±79.7, p<0.001), albeit less marked at 96 hours, Figure 27. There were no significant differences in NAVSMC migration in NAVSMCs treated with 10μM Yoda-1 for 96 hours compared to DMSO (vehicle control), Figure 28.

When NAVSMCs were treated with 10μM Yoda-1 for 96 hours, PIEZO-1 mRNA significantly increased (difference 8.1 ±2.2x10^3, p<0.001) while PIEZO-2 mRNA significantly decreased (difference -0.8 ±0.1x10^3, p<0.001), Figure 29. KLF-2 and KLF-4 mRNA also significantly increased in Yoda-1 treated cells (differences 0.9 ±0.1x10^3, p=0.002 and 4.9 ±0.2x10^3, p<0.001, respectively). However, TG2 mRNA significantly decreased (difference -45.1 ±8.7x10^3, p=0.007).

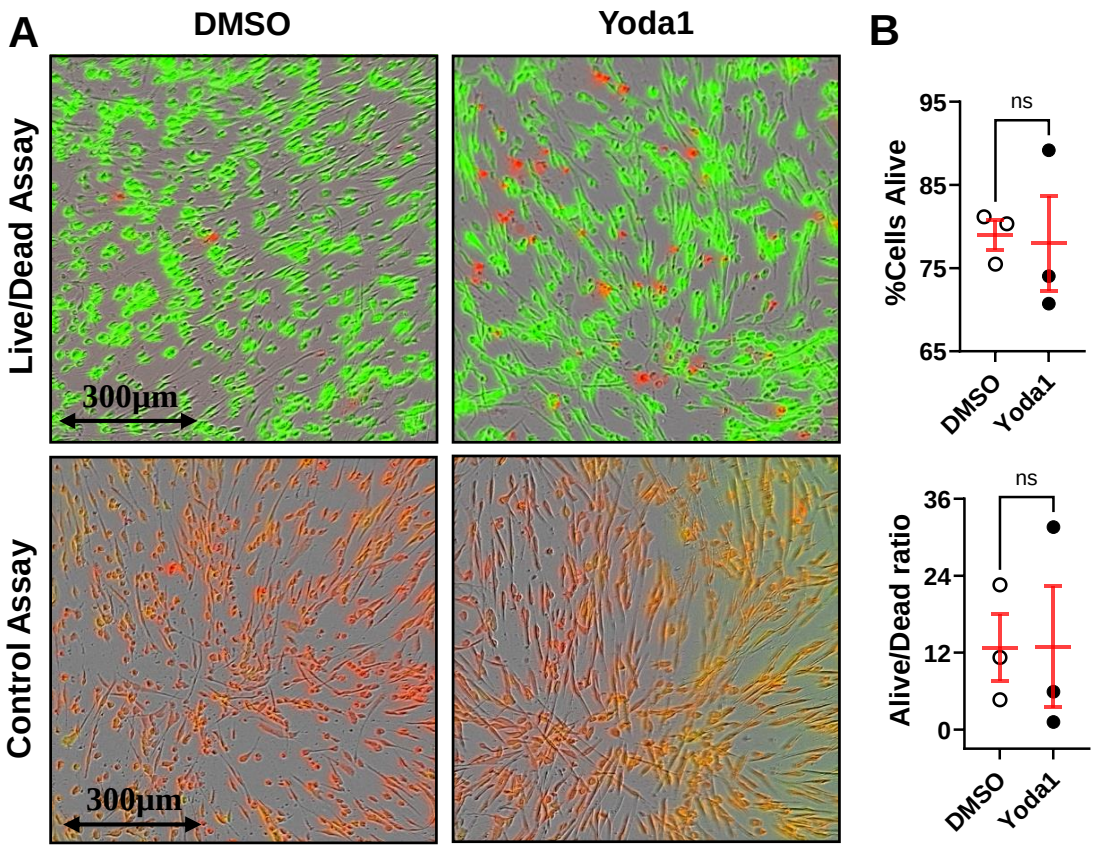

Figure 26. Representative IncuCyte FLR images of the Live/Dead assay (A) of NAVSMCs following treatment with 10µM DMSO (left) and 10µM Yoda-1 (right) for 96 hours with scatter graphs of analyses (B).

Control assay (bottom) after the application of Blasticidin. Green fluorescents= live cells, Red fluorescents= dead cells. DMSO= open circle. Yoda-1= closed circles. Error bars (red) represent mean ±SEM. ns= no significant differences. N/n= 3/3.

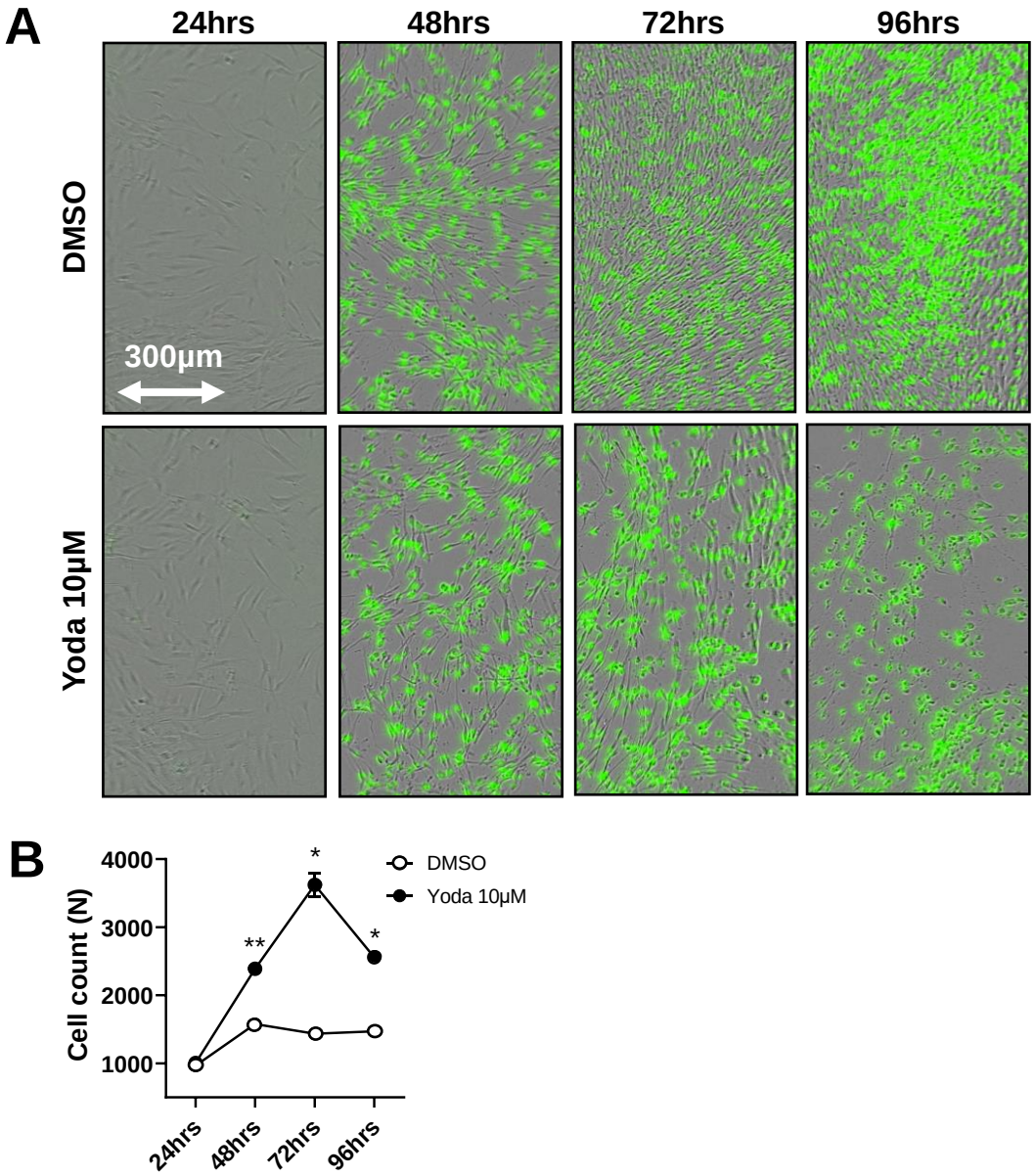

Figure 27. Representative sequential IncuCyte FLR images of the proliferation assay of NAVSMCs treated with 10μM DMSO (A; top) and 10μM Yoda-1 (A; bottom) for 96 hours alongside corresponding interval graph illustrating changes in cell count over time (B).

Green fluorescents delineates individual cells. Scale represented in bottom left corner. DMSO= open circle. Yoda-1= closed circle. Error bar (black) represents mean ±SEM cell count. *= $p<0.05$, **= $p<0.01$. N/n= 3/24.

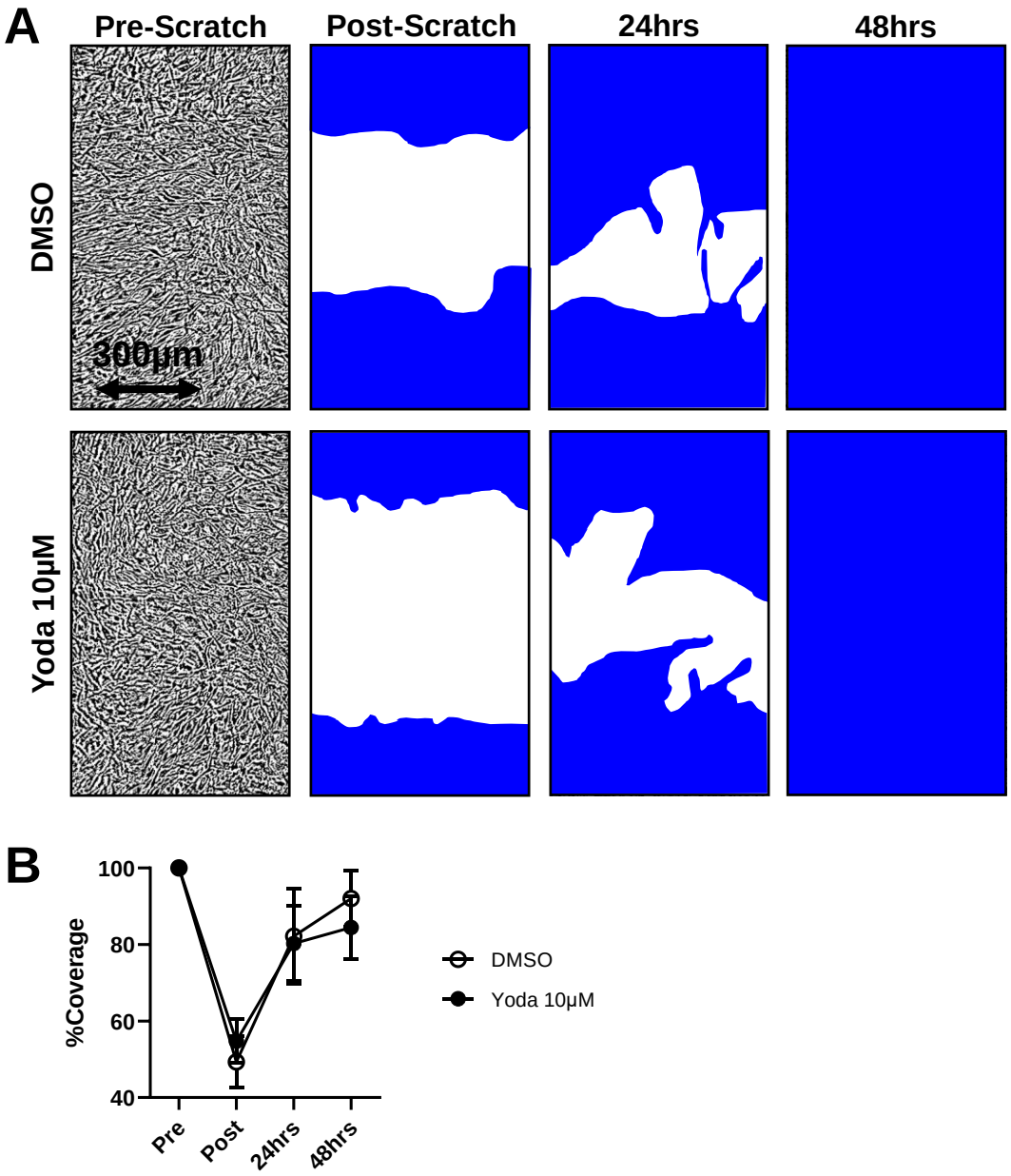

Figure 28. Representative sequential IncuCyte FLR images of the migration assay of NAVSMCs treated 10µM DMSO (A; top) and 10µM Yoda-1 (A; bottom) for 48 hours alongside interval line graph illustrating changes in scratch coverage over time (B).

Cell coverage= blue, Scratch wound= white. Scale represented in bottom left corner. DMSO= open circle, Yoda-1= closed circle. Error bars (black) represent mean ±SEM cell coverage. N/n= 3/24.

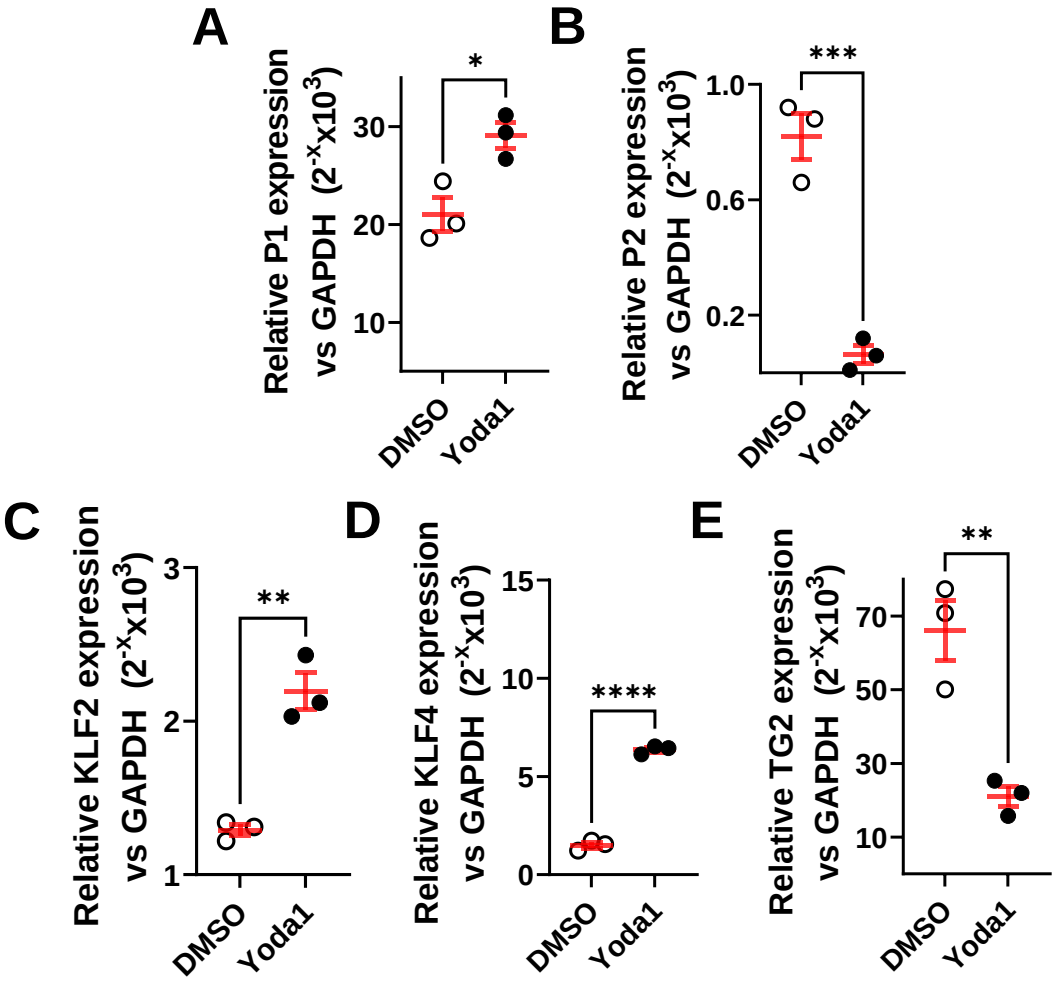

Figure 29. Relative gene expression of PIEZO-1 (A), PIEZO-2 (B), KLF-2 (C), KLF-4 (D) and TG2 (E) in NAVSMCs after 96 hours of treatment with 10μM Yoda-1 and DMSO (vehicle control).

DMSO= open circles, Yoda-1= closed circles. Error bars (red) represent mean ±SEM. *= p<0.05, **= p<0.01, ***= p<0.001. N/n= 3/3.

3.4. Effects of Mechanical Stress

3.4.1. Constant Axial Stretch

To facilitate the application of axial stretch, NAVSMCs were seeded into specialised stretch chambers. A mono-layer of cells remained attached to the floor of the chamber throughout the experiment. Constant stretch was applied for 96 hours while cell morphology remained unchanged on light microscopy. IncuCyte FLR Imaging of the chambers was not undertaken with the IncuCyte due to the size of the apparatus. No significant differences in PIEZO-1, PIEZO-2, KLF-2, KLF-4, or TG2 mRNA were observed between NAVSMCs treated with 0% and 20% axial stretch, Figure 30. One sample appeared to respond and two samples did not respond to the stretch applied in this experiment. Therefore there appears to be an obvious outlier and results require interpretation with caution. Single products were evident on gel electrophoresis on all RT+ samples, Figure 30.

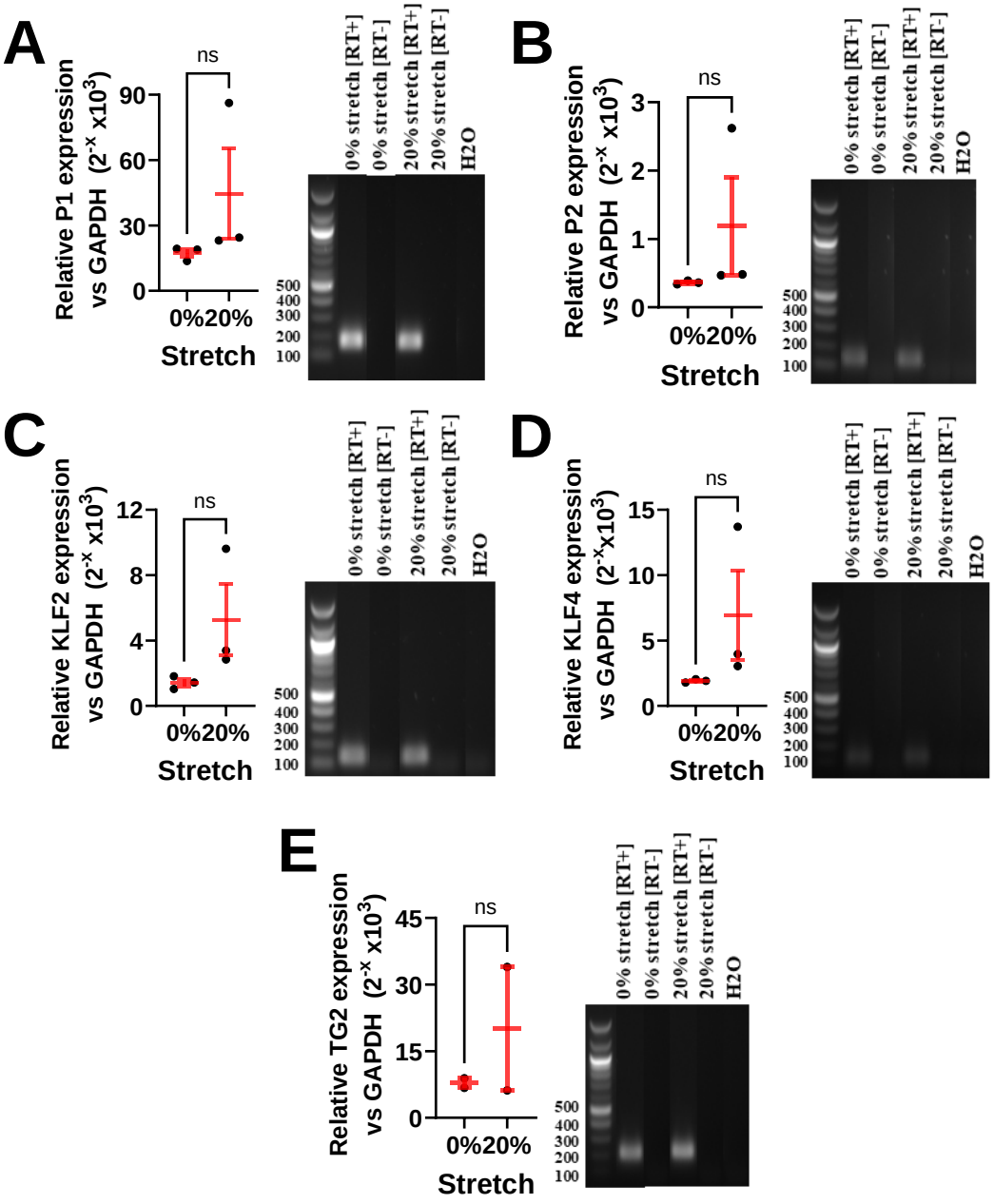

Figure 30. Relative gene expression and gel electrophoresis blots of PIEZO-1 (A) [182bp], PIEZO-2 (B) [160bp], KLF-2 (C) [138bp], KLF-4 (D) [112bp] and TG2 (E) [209bp] in NAVSMCs after 0% and 20% constant uni-axial stretch.

Error bars (red) represent mean ±SEM. ns= no significant differences. bp=base pairs. N/n= 3/3.

3.4.2. Oscillatory Shear Force

As no change in mRNA expression was observed after 96 hours of constant uni-axial stretch, a more physiological oscillatory shear force was used. There were no obvious morphological differences between NAVSMCs which were treated with 96 hours of; oscillatory force (OF) and no oscillatory force (No OF), Figure 31. Furthermore, there were no significant differences in the cell count (mean difference 29.0, 95% CI -128.9 to 186.9, p=0.22, N/n = 3/18 for each group), the percentage of live cells (mean difference -4.2%, 95% CI -27.9 to 19.57, p=0.17, N/n = 3/3 for each group) or the Live/Dead ratio (mean difference 0.2, 95% CI -3.5 to 3.9, p = 0.3242, N/n = 3/3 for each group) between NAVSMCs treated with OF and no OF.

Higher Yoda-1 mediated intracellular calcium entry was observed in NAVSMCs which had been exposed to OF for 96 hours (mean difference in peak calcium entry 0.52, 95% CI 0.05 to 0.99, p=0.038, N/n = 3/9 in each group), Figure 32A. Furthermore, there were significant increases in the gene expression of PIEZO-1 (p=0.005), PIEZO-2 (p=0.003) and TG2 (p=0.001). No significant differences in the expression of KLF-2 and KLF-4 were observed. However, there was a trend towards increased expression (Figure 32D and Figure 32E, respectively). There was no evidence of any contamination on gel electrophoresis (Figure 32B-F).

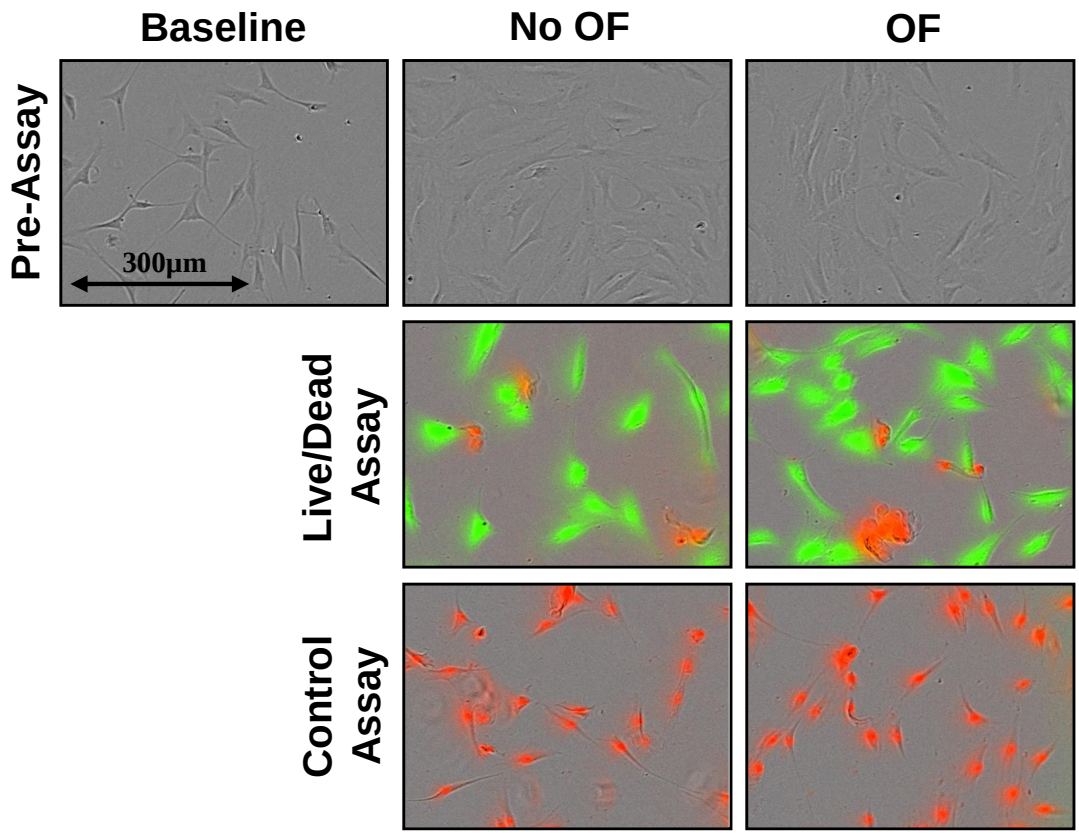

Figure 31. Representative IncuCyte FLR images of Live/Dead assay of NAVSMCs following the application of oscillatory force (OF) and no oscillatory force (No OF).

Example IncuCyte FLR images show NAVSMCs: prior to assay (baseline) [top left], after 96 hours of no oscillatory force (No OF) [top centre], after 96 hours with oscillatory force (OF) [top right], Live/Dead assay (live cells [green fluorescents] and dead cells [red fluorescents]) [middle], and control assay with cell death induced with Blasticidin [bottom]. Scale represented in bottom left corner. N/n= 3/6.

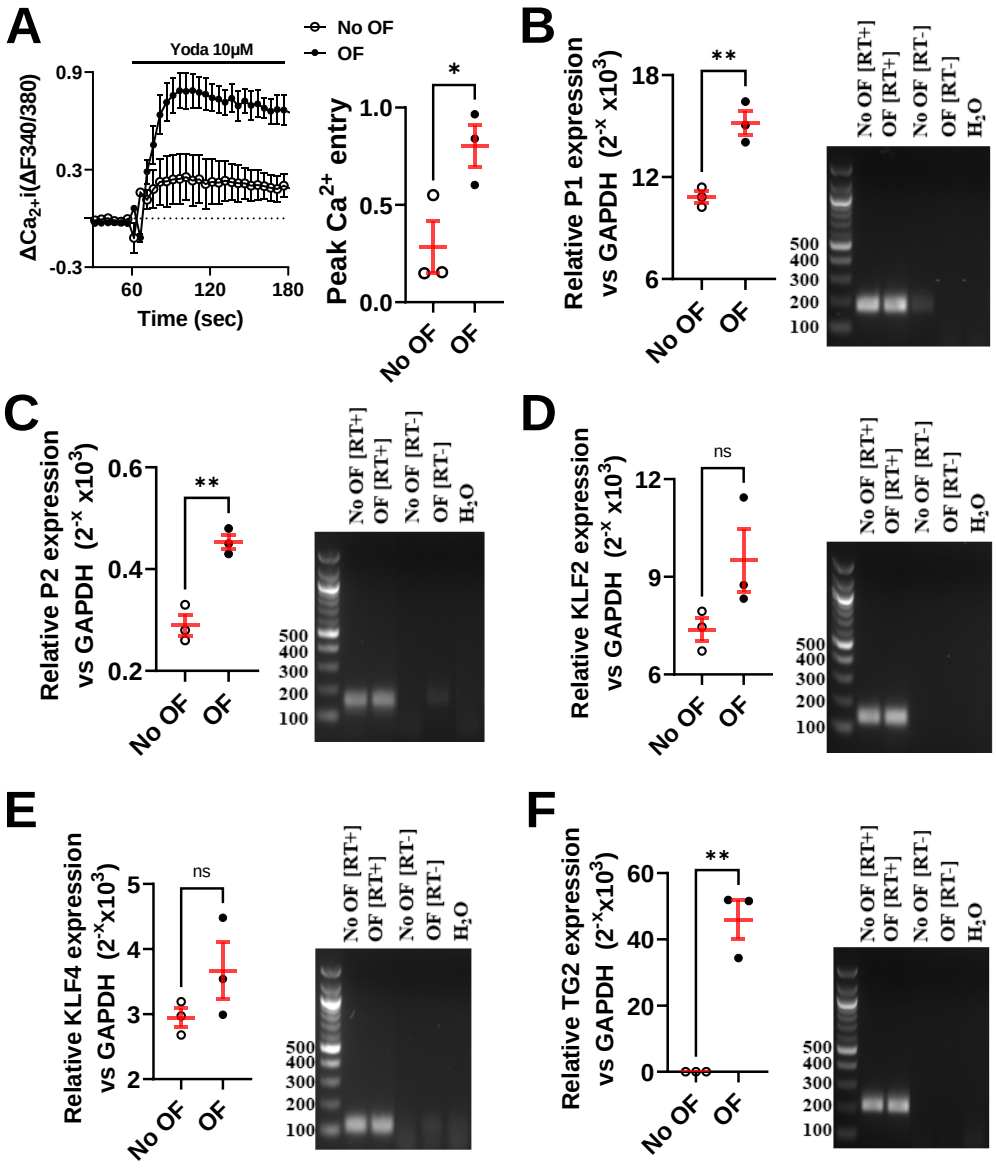

Figure 32. Yoda-1 stimulated calcium imaging, relative gene expression and gel electrophoresis blots of PIEZO-1, PIEZO-2, KLF-2, KLF-4 and TG2 in NAVSMC following oscillatory force (OF) and no oscillatory force (No OF).

A; averaged Yoda-1 activated calcium entry over time and peak Yoda-1 activated calcium entry into NAVSMCs after 96 hours of No OF (N/n= 3/9) and OF (N/n= 3/9). Relative (to GAPDH) gene expression and gel electrophoresis gel of PIEZO-1 (B) [182bp], PIEZO-2 (C) [160bp], KLF-2 (D) [138bp], KLF-4 (E) [112bp] and TG2 (F) [209bp] in NAVSMCs after 96 hours of No OF (N/n= 3/3) and OF (N/n= 3/3). No OF= open circles, OF= closed circles. Error bars (red) represent mean ±SEM. *= p<0.05, **= p<0.005, ns= no significant differences. bp= base pairs.

3.4.3. Changes in Matrix Stiffness

To simulate the wall stiffness observed in AAAs, NAVSMCs were cultured in a matrix with a low stiffness (0.2kPa [lowest available]) and high stiffness (64kPa [highest available]). There were no apparent morphological differences between NAVSMCs cultured on 0.2kPa and 64 kPa stiffness matrices for 96 hours. There were also no significant differences in the cell count (mean difference 8.1, 95% CI -17.4 to 33.5, p=0.43, N/n = 3/18 for each group). However, there was a significantly higher proportion of viable cells after being cultured on the 64kPa cell culture plate (mean difference 16.3, 95% CI 7.0 to 25.7, p=0.008, N/n = 3/3 in each group). The Live/Dead ratio had a non-significant trend of being higher in NAVSMCs cultured on 64kPa plates (mean difference 1.5, 95% CI -1.0 to 3.9, p=0.17, N/n = 3/3 for each group).

There were no significant differences observed in Yoda-1 stimulated intra-cellular calcium entry between NAVSMCs cultured on a 64kPa stiffness matrix compared to those on a 0.2kPa stiffness matrix (Figure 34). However, there is a trend towards a lower peak intra-cellular calcium entry with 64kPa (mean difference -0.23 ±0.09, p=0.054). There were no significant differences in the expression of PIEZO-1 or PIEZO-2 with the different matrix stiffness, Figure 34. RNA expression of KLF-4 was significantly higher with NAVSMC cultures at 64kPa (mean difference 0.85 ±0.25, p=0.015). There were no significant differences in the gene expression of KLF-2 or TG2, Figure 34. There was no evidence of any contamination on gel electrophoresis.

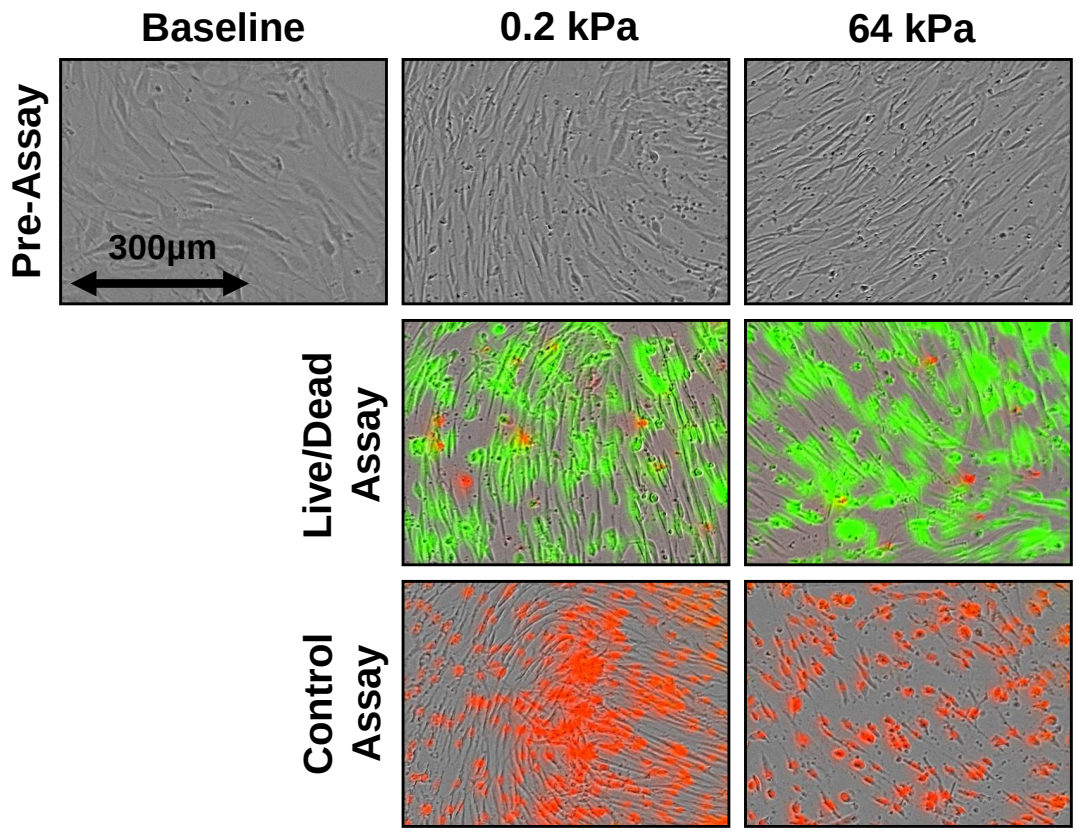

Figure 33. Representative IncuCyte FLR images of Live/Dead assay of NAVSMCs following culture in 0.2kPa and 64kPa matrix stiffnesses.

Example IncuCyte FLR images show NAVSMCs: prior to assay (baseline) [top left], after 96 hours of growth on a 0.2kPa stiffness matrix [centre], after 96 hours of growth on a 64kPa stiffness matrix [right], Live/Dead assay (live cells [green fluorescents] and dead cells [red fluorescents]) [middle], and control assay with cell death induced with Blasticidin [bottom]. Scale represented in bottom left corner. N/n= 3/6.

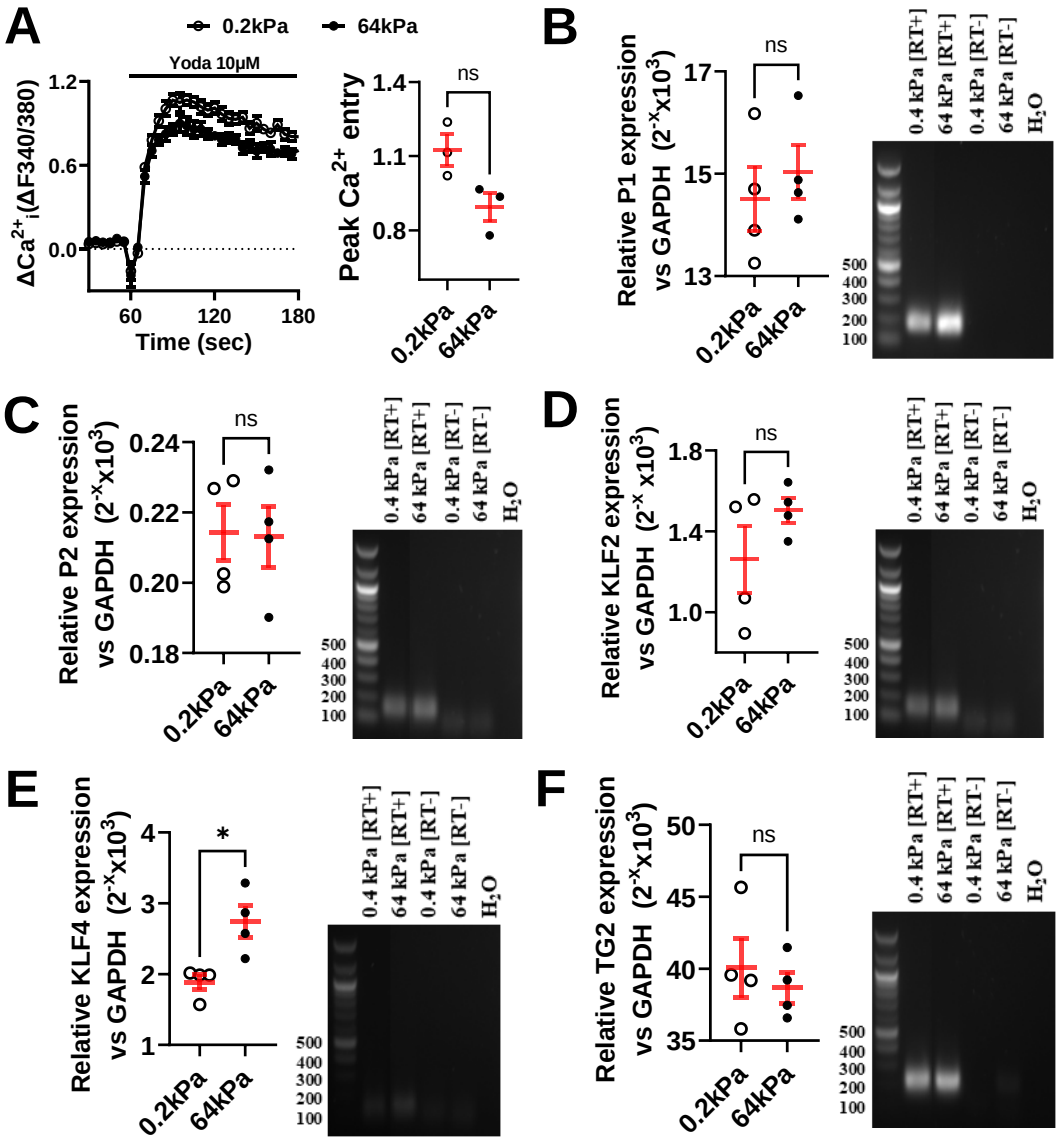

Figure 34. Yoda-1 stimulated calcium imaging, relative gene expression and gel electrophoresis blots for PIEZO-1, PIEZO-2, KLF-2, KLF-4 and TG2 in NAVSMCs following cell culture at 0.2kPa and 64kPa stiffnesses.

A; averaged Yoda-1 activated calcium entry over time and peak Yoda-1 activated calcium entry into NAVSMCs after 96 hours of culture on 0.2kPa (N/n= 3/9) and 64kPa (N/n= 3/9) matrix stiffness. Relative (to GAPDH) gene expression and gel electrophoresis gel of PIEZO-1 (B) [182bp], PIEZO-2 (C) [160bp], KLF-2 (D) [138bp], KLF-4 (E) [112bp] and TG2 (F) [209bp] in NAVSMCs after 96 hours of culture on 0.2kPa (N/n= 3/3) and 64kPa (N/n= 3/3) matrix stiffness. 0.2kPa= open circles, 64kPa= closed circles. Error bars (red) represent mean ±SEM. *= $p<0.05$, ns= no significant differences. bp= base pairs.

3.5. Effects of Environmental and Physiological Stress

3.5.1. Prolonged Culture in 0.4% FBS Culture Media

NAVSMCs were subsequently cultured in serum-deprived media (0.4% FBS) to mimic the senescent behaviour observed in AAAVSMCs. There were significantly fewer cells after 96 hours of cell culture in 0.4% FBS culture media compared to standard 10% FBS culture media (mean difference -90.33 ±19.68, p=0.010). Live/Dead assay did not show any significant differences, Figure 35. There were no significant differences in the percentage of viable cells (difference -14.3% ±10.4, p=0.24) and Live/Dead ratio (difference -2.0 ±1.5, p=0.25) between treatment groups after 96 hours.

There were no significant differences in Yoda-1 stimulated calcium entry in NAVSMCs treated with 10% FBS and 0.4% FBS, Figure 36. However, there was a trend towards increased peak Yoda-1 stimulated intracellular calcium entry in NAVSMCs cultured in 0.4% FBS (mean difference 0.2 ±0.1, p=0.077). There was significantly higher mRNA expression of PIEZO-1 and PIEZO-2 in NAVSMCs treated with 0.4% FBS (p=0.002 and p=0.001, respectively). No significant differences were apparent in the expression of KLF-2, KLF-4 or TG2, Figure 36.

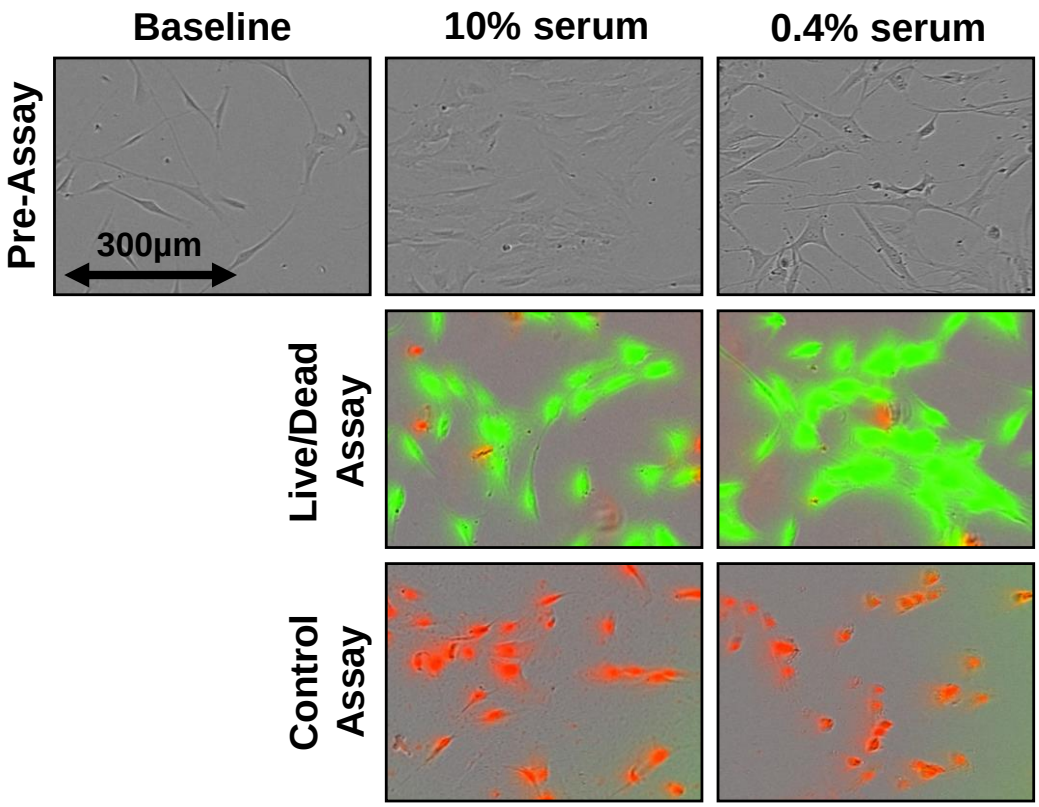

Figure 35. Representative IncuCyte FLR imaging and Live/Dead assay of NAVSMCs following culture in 0.4% FBS media and 10% FBS media.

Example IncuCyte FLR images show NAVSMCs: prior to assay (baseline) [top left], after 96 hours of growth in 10% FBS [centre], after 96 hours of growth in 0.4% FBS [right], Live/Dead assay (live cells [green fluorescents] and dead cells [red fluorescents]) [middle] , and control assay with cell death induced with Blasticidin [bottom]. Scale represented in bottom left corner. N/n= 3/6.

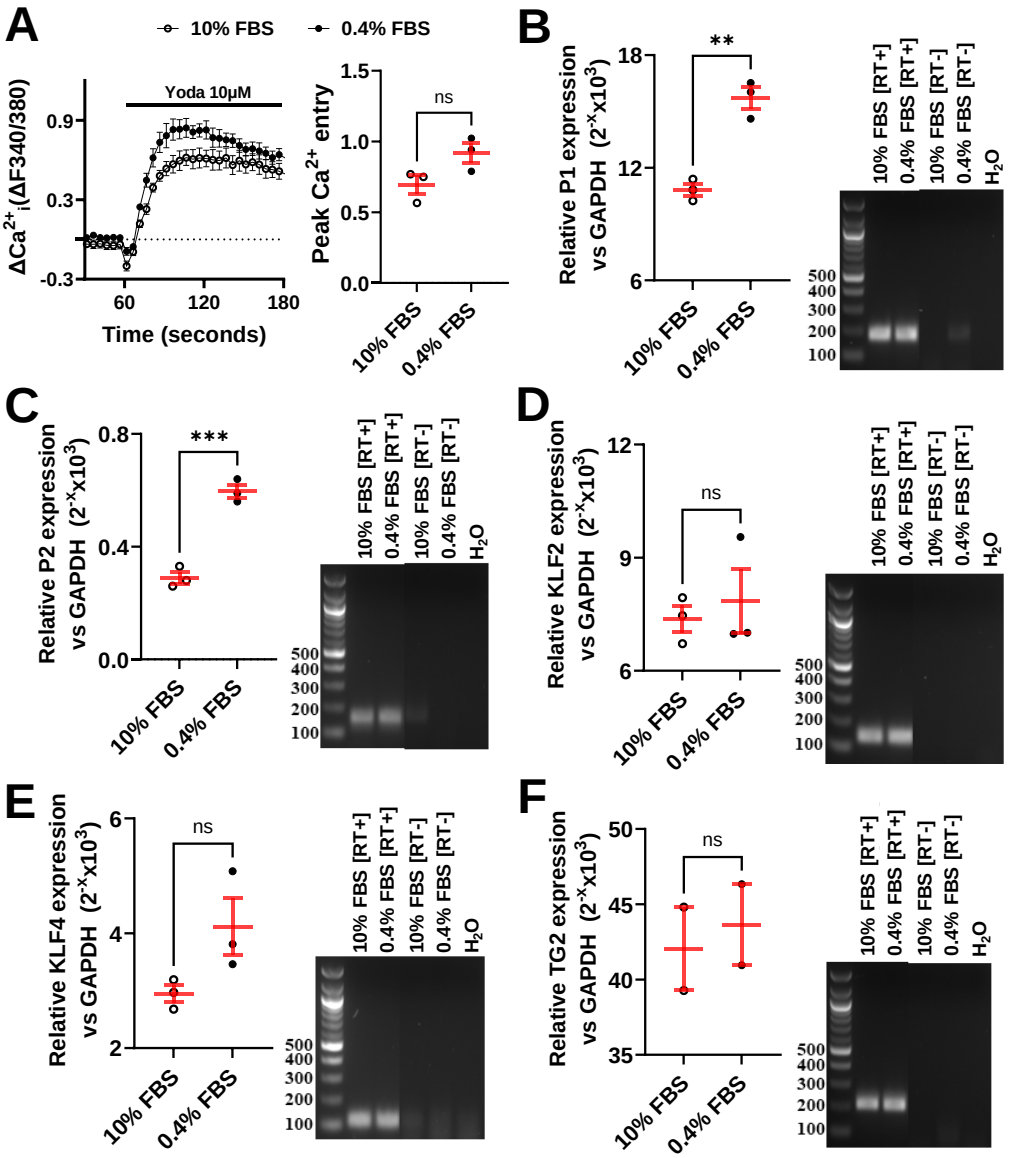

Figure 36. Yoda-1 stimulated calcium imaging, relative gene expression and gel electrophoresis blots of PIEZO-1, PIEZO-2, KLF-2, KLF-4 and TG2 in NAVSMC following cell culture with 0.4% FBS and 10% FBS.

A; averaged Yoda-1 activated calcium entry over time and peak Yoda-1 activated calcium entry into NAVSMCs after 96 hours of culture with 0.4% FBS (N/n= 3/9) and 10% FBS (N/n= 3/9) media. Relative (to GAPDH) gene expression and gel electrophoresis gel of PIEZO-1 (B) [182bp], PIEZO-2 (C) [160bp], KLF-2 (D) [138bp], KLF-4 (E) [112bp] and TG2 (F) [209bp] in NAVSMCs after 96 hours of culture with 0.4% FBS (N/n= 3/3) and 10% FBS (N/n= 3/3) media. 0.4% FBS= open circles, 10% FBS= closed circles. Error bars (red) represent mean ±SEM. ns= no significant differences, ** = p<0.01, ***=p<0.001. bp= base pair.

3.5.2. Multiple Cell Passage

NAVSMCs were cultured and proliferation was encouraged through multiple passages to physiologically exhaust cells. There were no obvious morphological differences in IncuCyte FLR imaging at passage 3 (P3), passage 4 (P4), passage 5 (P5) or passage 7 (P7), Figure 37. No significant differences in NAVSMC count were observed after 96 hours of cell culture (One-way ANOVA, p= 0.60). NAVSMC Yoda-1 mediated intra-cellular calcium entry was significantly higher at P3 and P4 compared to P5 and P7, Figure 38. No significant differences were observed when comparing the peak calcium entry into NAVSMCs at P3 (mean 0.59 ±0.04, N/n= 3/12) and P4 (mean 0.64 ±0.09, N/n= 3/12), p=0.90. Similarly, no significant difference in the peak calcium entry was observed in NAVSMCs at P5 (mean 0.15 ±0.03, N/n= 3/12) and P7 (mean 0.24 ±0.02, N/n= 3/12), p=0.63. No significant changes in PIEZO-1 or PIEZO-2 mRNA expression was seen, with increasing cell passage, Figure 39. However, there was a trend with a decline in KLF-4 and TG2 mRNA expression with increasing cell passage, Figure 39. No significant differences in the expression of KLF-2 was observed.

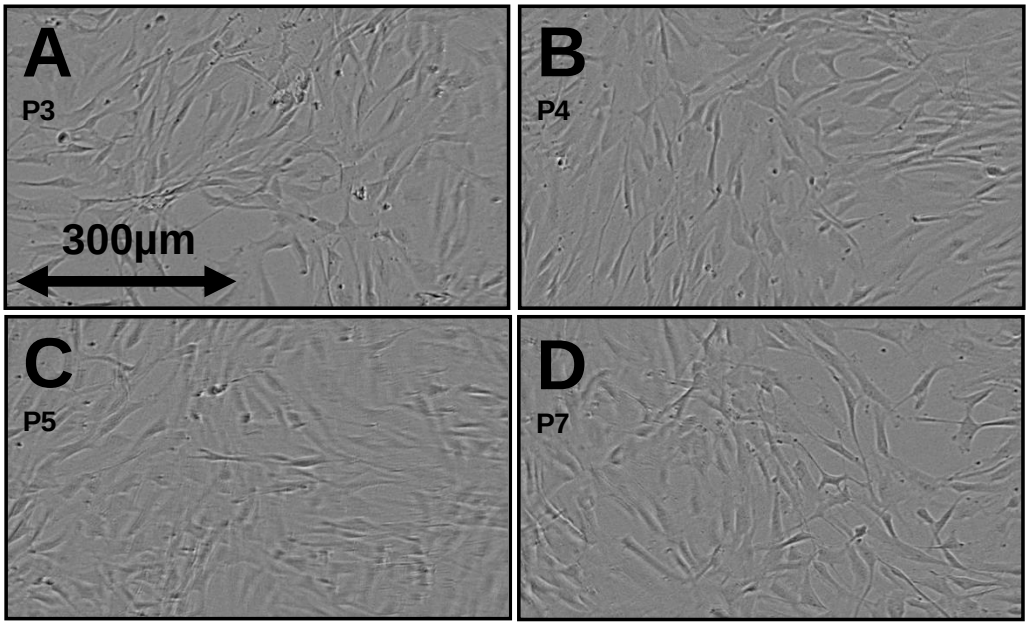

Figure 37. Phase contrast IncuCyte FLR images of NAVSMCs at P3 (A), P4 (B), P5 (C), and P7 (D).

Scale on bottom right corner. N/n= 1/3.

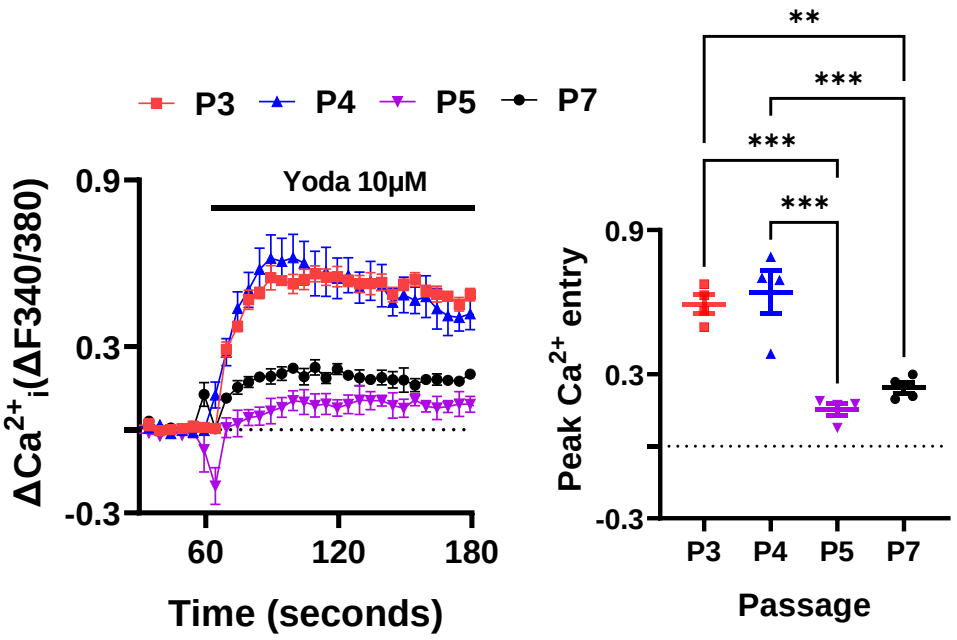

Figure 38. Comparison of Yoda-1 activated calcium entry over time (left) and peak Yoda-1 activated calcium entry (right) into NAVSMCs at each passage.

P3= red square, P4= blue triangle, P5= inverted triangle, P7= close circle. Error bars represent mean ±SEM. **= p<0.01, ***= p<0.001. N/n= 3/12.

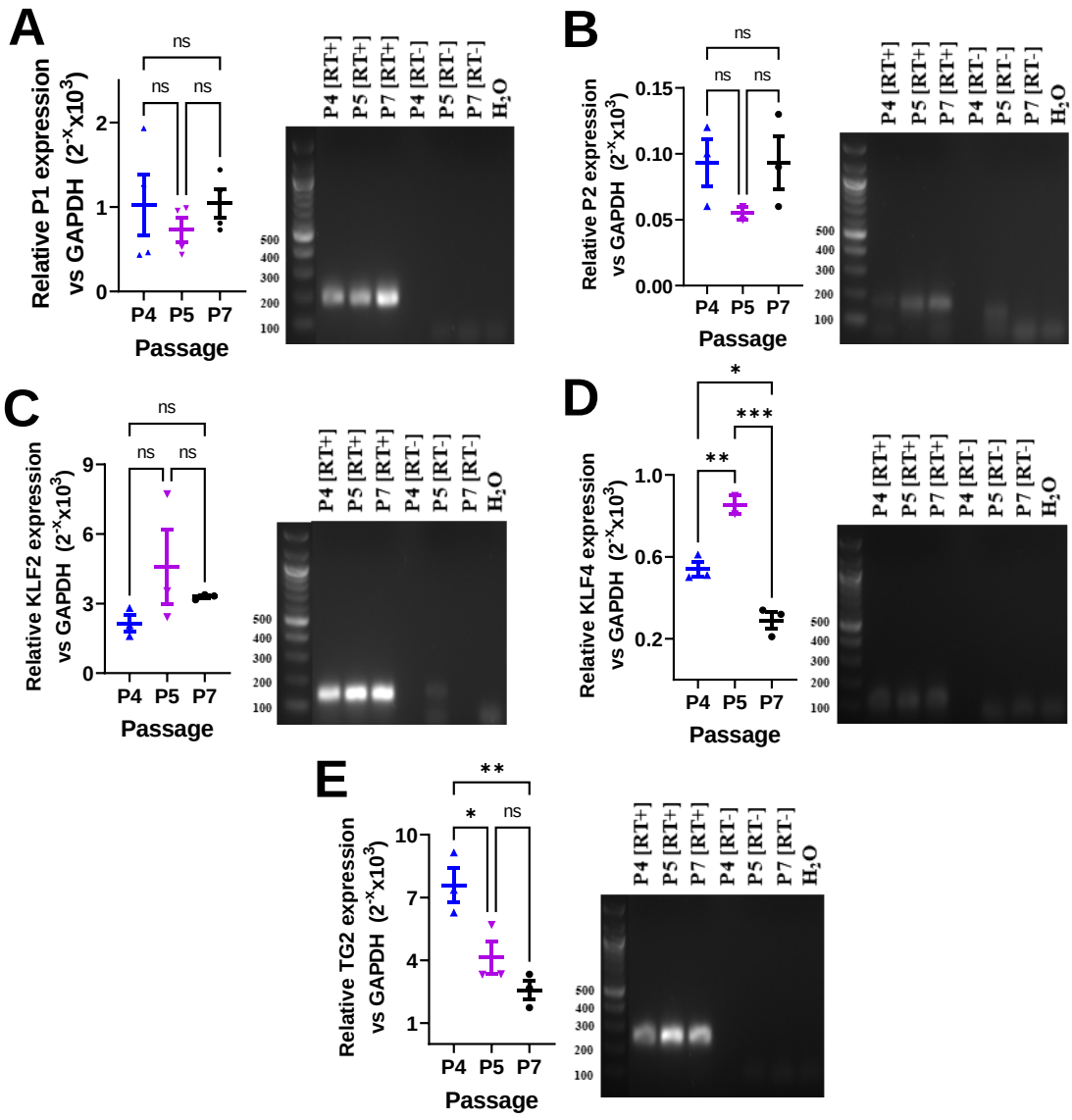

Figure 39. Relative gene expression and gel electrophoresis blots for PIEZO-1 (A) [182bp], PIEZO-2 (B) [160bp], KLF-2 (C) [138bp], KLF-4 (D) [112bp] and TG2 (E) [209bp] in NAVSMCs at P3, P4, P5 and P7.

P4= blue triangle, P5= inverted triangle, P7= close circle. Error bars represent mean ±SEM. ns= no significant differences, *= $p<0.05$, **= $p<0.01$, ***= $p<0.001$. bp=base pairs. N/n= 3/9.

3.6. Effects of PIEZO-1 Knockdown

3.6.1. Comparison of Methods of NAVSMC Transfection

The knockdown of PIEZO-1 from SVVSMCs was attempted, as a lower expression of PIEZO-1 was evident in AAAVSMCs. Successful knockdown of PIEZO-1 mRNA was achieved with all three transfection reagents (Lipofectamine 50nM, Lipofectamine 100nM and Accell smart-pool), Figure 40. There were no significant differences in PIEZO-1 mRNA expression following knockdown with Lipofectamine 50nM siP1, Lipofectamine 100nM siP1 and Accell smart-pool siP1 (Figure 40) indicating all 3 methods of transfection are acceptable methods in VSMCs. However, the Accell method was used to knockdown PIEZO-1 in NAVSMCs as our group has previously found it to be challenging to knockdown mRNA species in primary AAAVSMCs. Furthermore, the Accell system was marketed as being successful in achieving knockdown in difficult to transfect primary cells.

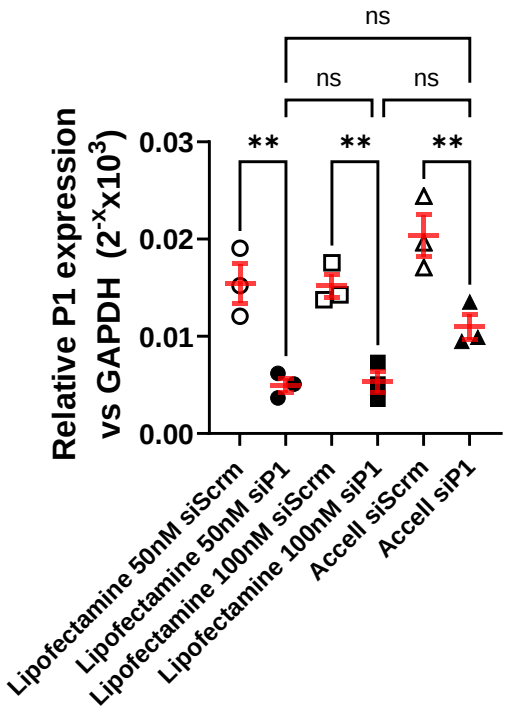

Figure 40. Comparison of PIEZO-1 mRNA expression following treatment with Lipofectamine 50nM (circle), Lipofectamine 100nM (square) and Accell (triangle).

siScrm= open shapes, siP1= closed shapes. Error bars (red) represents mean ±SEM. **= p<0.01, ns= not significant. N/n= 1/3

3.6.2. Accell siRNA NAVSMC Transfection

PIEZO-1 knockdown was then attempted in NAVSMCs so that experiments with the different stressors could be repeated and any changes in cell behaviour compared with those before knockdown. There were no evident morphological differences observed on IncuCyte FLR imaging after 96 hours and 192 hours of Accell transfection with buffer (mock control), red cyclophilin B (CycB) siRNA (positive control), smart-pool Scrm siRNA (negative control) and smart-pool PIEZO-1 siRNA, Figure 41. Furthermore, there were no significant differences in NAVSMC count before and after transfection with siScrm and siP1 in 96 hours (difference 1.4 ±0.8%, p=0.16). At 192 hours post-transfection, there was a higher reduction in NAVSMCs treated with siP1 compared to those treated with siScrm (difference -13.5 ±1.9%, p=0.002). A Live/Dead assay in 192 hours post-transfection showed significantly fewer NAVSMCs to be live with siP1 compared to siScrm (difference -7.1 ±2.5%, p=0.047), Figure 42. However, no significant differences were observed in the Live/Dead ratio (difference -12.0 ± 8.7, p=0.24).

The assessment of red fluorescence in NAVSMCs transfected with red fluorescent probe tagged CycB siRNA (Figure 41), suggested that the transfection efficiencies at 96 and 192 hours were 97.2% and 98.3%, respectively. Furthermore, CycB siRNA knockdown in PCR compared with siScrm was 91.2 ±0.3% (p=0.002) in 96 hours and 94.2 ±0.4% (p<0.001) in 192 hours. Similarly, siP1 knockdown on PCR compared to siScrm was 94.1 ±0.4% (p<0.001) in 96 hours and 96.0 ±0.5% (p<0.001) in 192 hours. However, the successful knockdown of PIEZO-1 in NAVSMCs did not translate into any functional differences in Yoda-1-mediated intracellular calcium entry with either single or double transfection, Figure 43. After 96 hours, when comparing RNA from NAVSMCs treated with siScrm and siP1, there were; no significant differences in PIEZO-2 expression (p=0.24), both KLF-2 and KLF-4 expression were significantly lower (p=0.047 and p=0.002, respectively) and TG2 expression was significantly higher (p=0.005), Figure 44. However, after 192 hours the expression of PIEZO-2 was also significantly higher in siP1-treated NAVSMCs (p=0.008) and trends observed with KLF-2,

KLF-4 and TG2 persisted, Figure 45.

Additional experiments planned, i.e. repetition of the cell proliferation and migration assays following siP1 knockdown, to evaluate any differences to those already conducted could not be performed due to the restrictions imposed on our laboratory due to the COVID-19 pandemic. However, PIEZO-1 knockout mice enabled further assessment of the morphological implications of PIEZO-1 knockout.

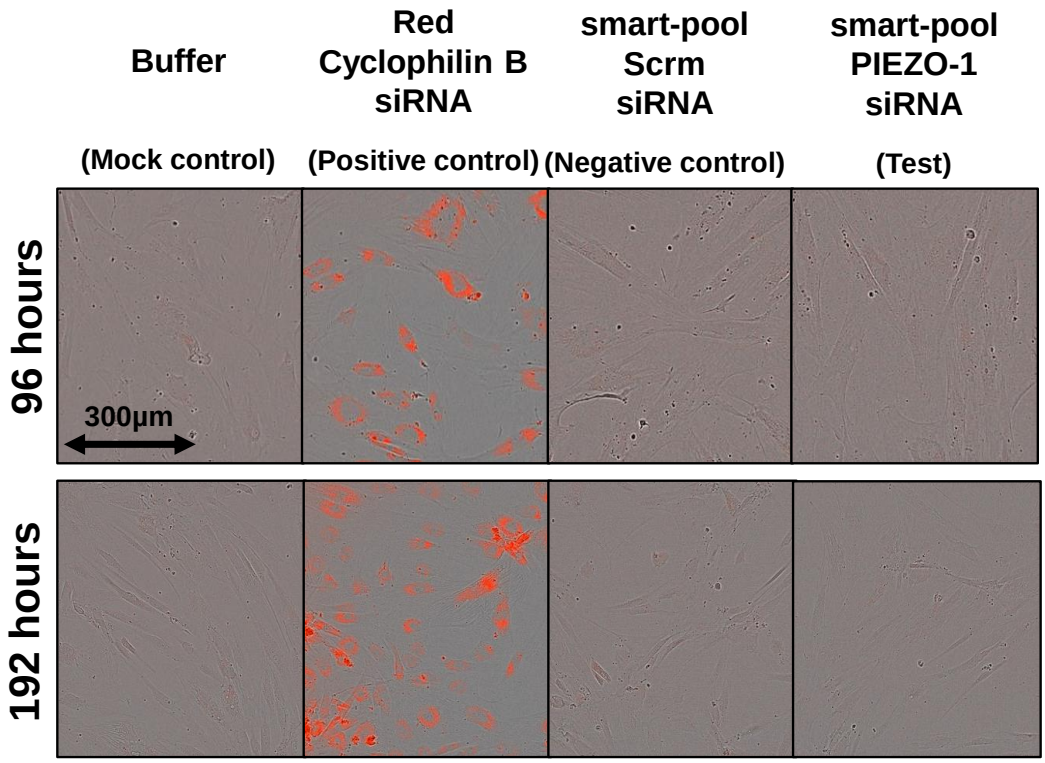

Figure 41. IncuCyte FLR images of NAVSMCs following Accell transfection using: buffer (mock control), red cyclophilin B siRNA (positive control), smart-pool Scrm siRNA (negative control) and smart-pool PIEZO-1 siRNA at 96 hours (top) and 192 hours (bottom).

Scale on bottom right corner. N/n= 3/9.

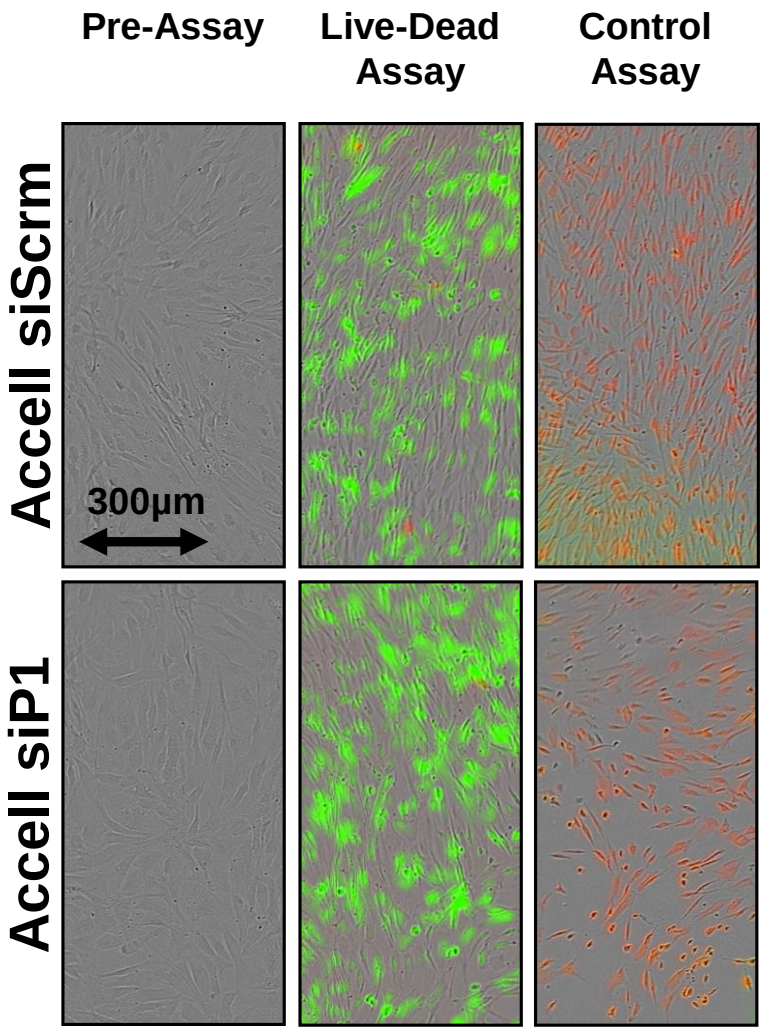

Figure 42. Representative IncuCyte images from Live/Dead assay of NAVSMCs at 192 hours following transfection with Accell Scrm smart-pool siRNA (top) and Accell PIEZO-1 smart-pool siRNA (bottom).

Example IncuCyte FLR images show NAVSMCs: prior to assay (baseline) [left], Live/Dead assay (live cells [green fluorescents] and dead cells [red fluorescents]) [centre] and control assay with cell death induced with Blasticidin [right]. Scale represented in bottom left corner. N/n = 3/3.

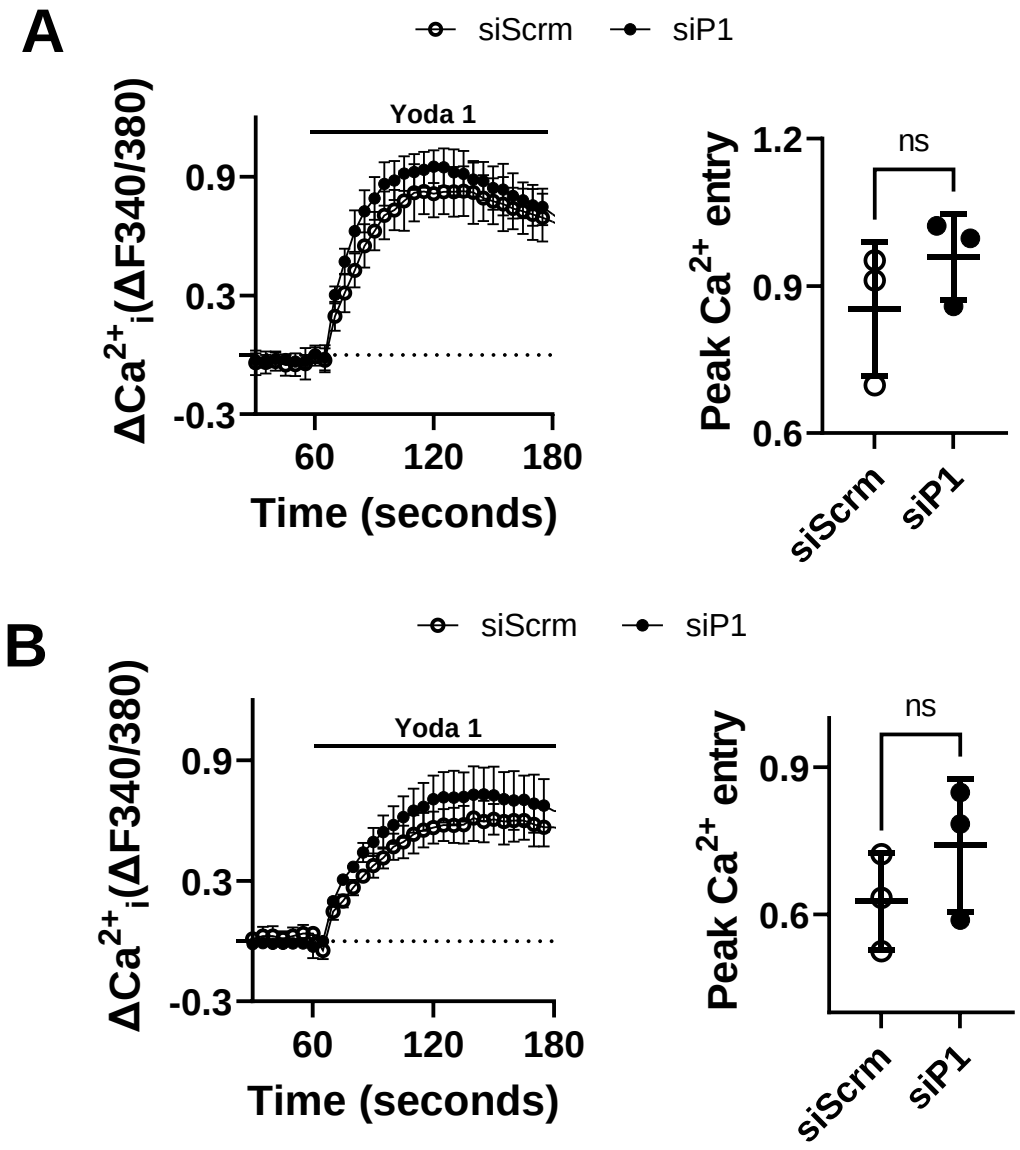

Figure 43. Comparison of Yoda-1 activated intracellular calcium entry over time (left) and peak calcium entry (right) into NAVSMCs after 96 hours (A, top) and 192 hours (B, bottom) of treatment with siScrm and siP1.

Open circles= siScrm, Close circles= siP1. Error bars (black) represent mean ±SEM. ns = no significant differences. N/n= 3/9.

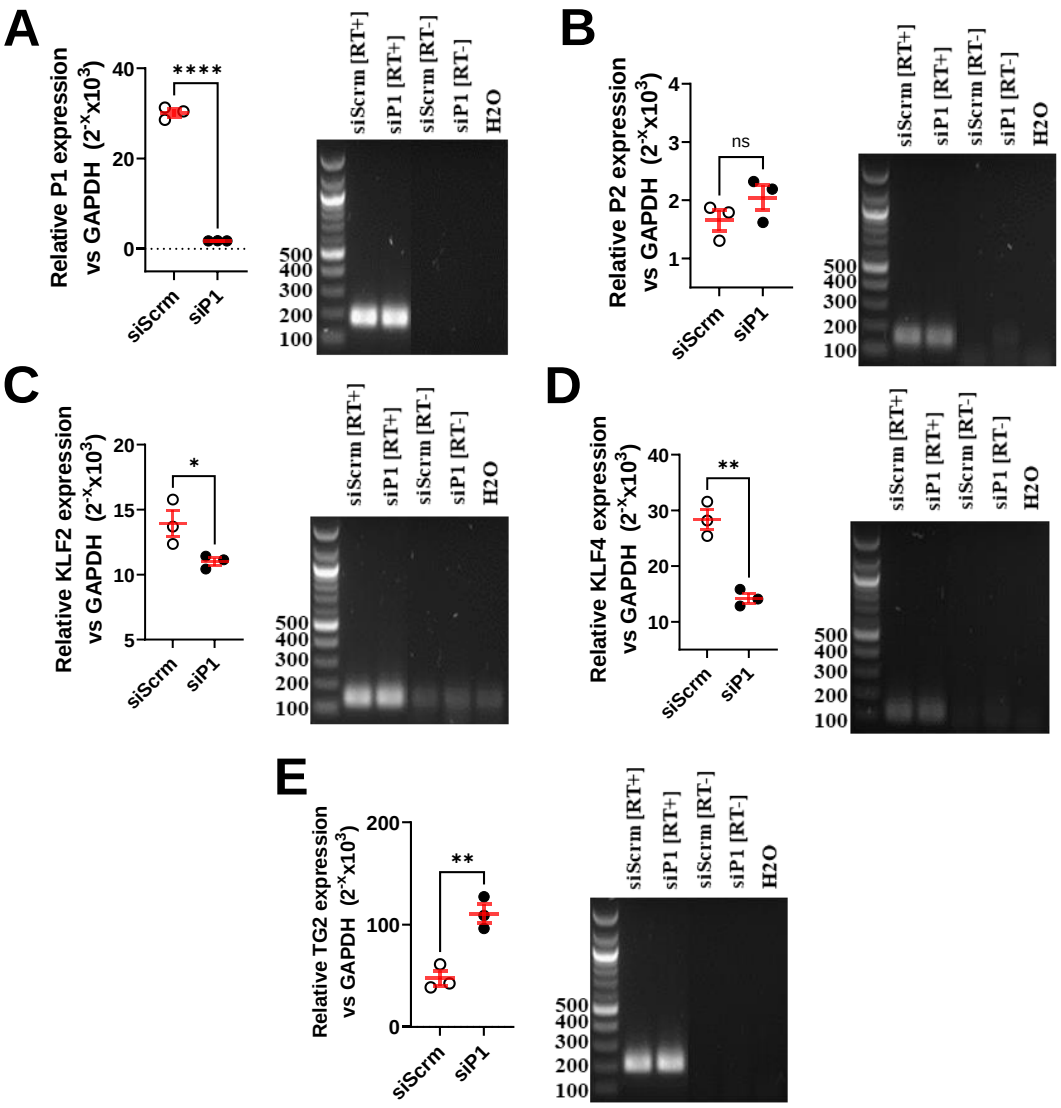

Figure 44. Relative gene expression and gel electrophoresis blots for PIEZO-1 (A) [182bp], PIEZO-2 (B) [160bp], KLF-2 (C) [138bp], KLF-4 (D) [112bp] and TG2 (E) [209bp] in NAVSMC after 96 hours of PIEZO-1 siRNA knockdown.

Open circles= siScrm, Close circles= siP1. Error bars (red) represent mean ±SEM. ns= no significant differences, *= p<0.05, ** = p<0.01, ***=p<0.001. bp=base pairs. N/n= 3/9.

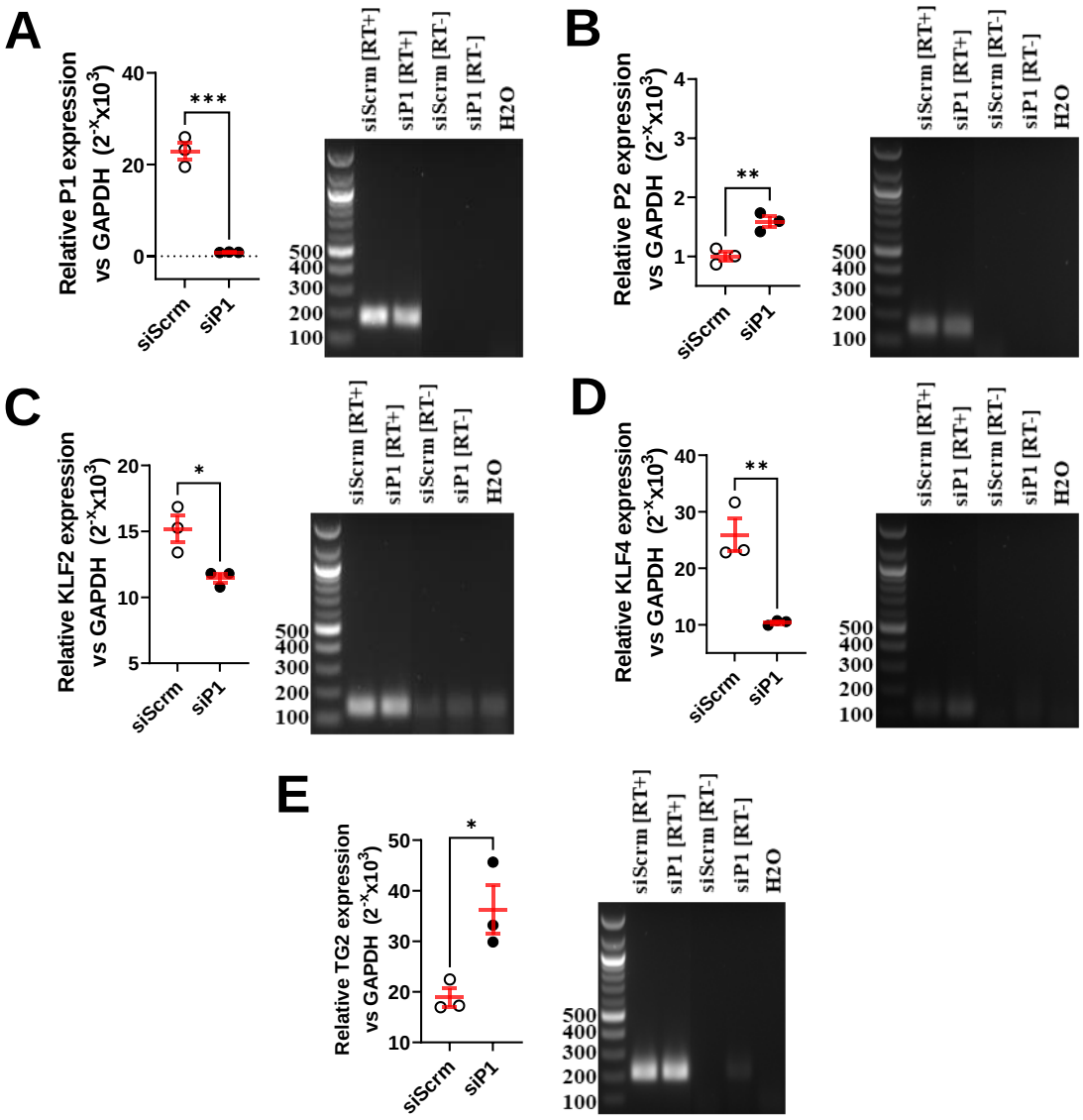

Figure 45. Relative gene expression and gel electrophoresis blots for PIEZO-1 (A) [182bp], PIEZO-2 (B) [160bp], KLF-2 (C) [138bp], KLF-4 (D) [112bp] and TG2 (E) [209bp] in NAVSMCs after 192 hours of PIEZO-1 siRNA knockdown.

Open circles= siScrm, Close circles= siP1. Error bars (red) represent mean ±SEM. ns= no significant differences, *= $p<0.05$, ** = $p<0.01$, ***=$p<0.001$. bp=base pairs. N/n= 3/9.

3.7. Summary of In-Vitro Experiments

There were no significant differences in the mRNA expression of PIEZO-1 between AAAVSMCs and NAVSMCs. However, PIEZO-2 mRNA expression was significantly higher in AAAVSMCs compared to NAVSMCs. The application of oscillatory shear stress to NAVSMCs resulted in significantly higher mRNA expression of PIEZO-1 and PIEZO-2. Furthermore, this translated to an increased intra-cellular PIEZO-1 mediated intra-cellular calcium entry. The application of static uni-axial force and culture on a high matrix stiffness did not influence the mRNA expression either PIEZO mechanosensor. However, serum deprived hostile culture environment resulted in increased mRNA expression of both PIEZO mechanosensors. However no significant differences in PIEZO-1 mediated intracellular calcium entry was evident. Cell fatigue through multiple passage did not impact PIEZO mRNA expression however reduced PIEZO-1 mediated intra-cellular calcium entry was evident in cells of higher passage. Prolonged activation of PIEZO-1 with Yoda-1 resulted in a reduction in PIEZO-2 mRNA expression. Conversely, knockout of PIEZO-1 resulted in an increase in the expression of PIEZO-2 mRNA. A full summary of the cell viability, mRNA expression of the PIEZO mechanosensory and downstream pathways, the results of calcium imaging and physiological assessment are detailed in Table 6. The findings of the *in-vitro* experiments demonstrated some associations between mechanical and physiological stressors pertinent in AAA disease which were further evaluated in-vivo.

Comparators	mRNA					Cell viability	Yoda-1 Calcium Entry	Proliferation	Migration
	PIEZO-1	PIEZO-2	KLF-2	KLF-4	TG2				
AAAVSMCs vs **NAVSMCs**	↔	↑	↑	↔	↓	NC	↔	NC	NC
DMSO vs **Yoda-1**	↑	↓	↑	↑	↓	↔	NA	↓	↔
0% vs 20% **uni-axial force**	↔	↔	↔	↔	↔	NC	NC	NC	NC
No OF vs **OF**	↑	↑	↔	↔	↑	↔	↑	NC	NC
0.2kPa vs **64kPa**	↔	↔	↔	↑	↔	↓	↔	NC	NC
10% FBS vs **0.4% FBS**	↑	↑	↔	↔	↔	↔	↔	NC	NC
Passage	↔	↔	↔	IC	↓	NC	↓	NC	NC
96 hour siScrm vs **siP1**	↓	↔	↓	↓	↑	NC	↔	NC	NC
192 hour siScrm vs **siP1**	↓	↑	↓	↓	↑	↔	↔	NC	NC

Table 6. Summary of differences observed in experiments of mRNA expression, cell viability, Yoda-1 stimulated intracellular calcium entry, cell proliferation and cell migration.

Comparators: Control vs Test condition (Bold). ↔= no significant differences. ↑= significantly higher in test. ↓= significantly lower in test. NC = not compared. IC= Inconclusive.

Chapter 4: PIEZO in Mouse AAA Models

4.1. Description and Validation of Experimental Mice

4.1.1. Baseline Characteristics of C57BL6/J Mice

Firstly, vascular phenotyping on C57BL6/J wild-type mice was carried out to establish baseline characteristics of mice following intervention and allow genetic manipulation to be compared. Baseline characteristics were assessed at 12 weeks. C57BL6/J mice were morphologically heterogeneous, as illustrated in Figure 46A. The mean weight of the mice was 27.2 ±0.3g, Figure 46B. The mice's aorta was cylindrical in structure, which tapered off to become conical before the iliac bifurcation, Figure 46C and F. The mean luminal area on histological cross-section was 0.33 ±0.029mm^2, Figure 46D. The aorta on in vivo ultrasound at baseline measured 0.66 ±0.02mm (APd_{max}) and 3.9 ±0.2mm^3 (3DLV), Figure 46E and Figure 46F. Distensibility at baseline was 90.7 ±5.1 MPa^{-1}, Figure 46G. PIEZO-1, PIEZO-2, KLF-2, KLF-4 and TG2 were detectable in the aortic tissue of the wild-type mice, Figure 46H.

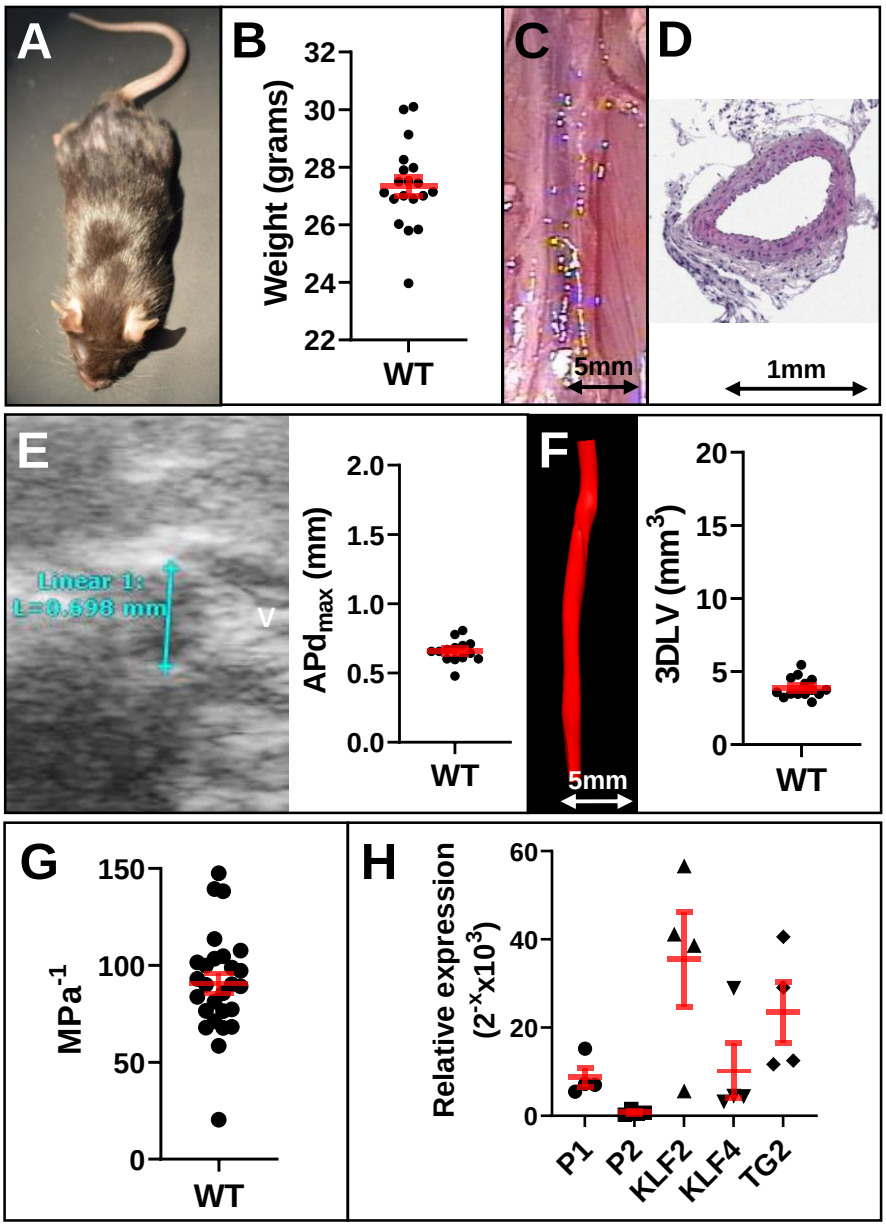

Figure 46. Baseline characteristics of C57BL6/J mice at 12 weeks (baseline).

A; Representative photo of an anaesthetised mouse. B; Scatterplot illustrating the baseline weight of mice (N=19). C; In-situ image of a murine abdominal aorta under physiological blood pressure. D; Representative histological cross-section of the aorta. E; Representative example and scatterplot of the APd_{max} (N=14). F; Representative example and scatterplot of the 3DLV (N=14). G; Representative example screenshot and scatterplot of distensibility (N=27). H; Relative (to GAPDH) expression of P1 (8.7 ±2.2x10^3), P2 (0.8 ±0.3x10^3), KLF2 (35.5 ±10.7x10^3), KLF4 (10.3 ±6.2x10^3) and TG2 (23.5 ±7.0x10^3) in mice aorta (N=4, error bars represent mean ±SEM).

4.1.2. Validation of PIEZO-1 Knockout in Transgenic Mice

The PIEZO-1 flox system was checked to ensure that the knockout system was functioning correctly. Cardiac fibroblasts were isolated from PIEZO-1 flox females ($P1^{+/+}$ [wild-type], $P1^{+/-}$ and $P1^{-/-}$ [knockout]) and exposed to ex-vivo TAT-Cre. As anticipated, there was a significant reduction in PIEZO-1 mRNA in $P1^{+/-}$TAT-Cre^{+} and $P1^{-/-}$TAT-Cre^{+} fibroblasts compared with the respective TAT-Cre negative controls and the wild-type ($P1^{+/+}$) cells (Figure 47A). Furthermore, the successful knockdown of PIEZO-1 was supported by Yoda-1-dependent calcium imaging of TAT-Cre^{+} cardiac fibroblasts from each genotype, Figure 47B. A significantly lower peak Yoda-1 stimulated intra-cellular calcium entry was observed in $P1^{-/-}$TAT-Cre^{+} cardiac fibroblasts compared to wild-type $P1^{+/+}$TAT-Cre^{+} ($p<0.001$) and heterozygote $P1^{+/-}$TAT-Cre^{+} ($p=0.003$) cells, Figure 47B.

Next the PIEZO-1 floxed mice were crossed with SMMHCCreER(T2) males to generate conditional, tamoxifen-inducible, VSMC PIEZO-1 knockout mice; smMHCCre-ER(T2) PIEZO-$1^{+/+}$ [$P1^{+/+}$], smMHCCre-ER(T2) PIEZO-$1^{-/+}$ [$P1^{-/+}$] and smMHCCre-ER(T2) PIEZO-$1^{-/-}$ [$P1^{-/-}$]. Mice were injected with tamoxifen between 9-10 weeks, and the aorta was harvested at 12 weeks. A significantly lower expression of PIEZO-1 mRNA was evident in $P1^{-/-}Tam^{+}$ aorta compared to $P1^{+/+}Tam^{+}$ aorta ($p=0.009$), Figure 47C.

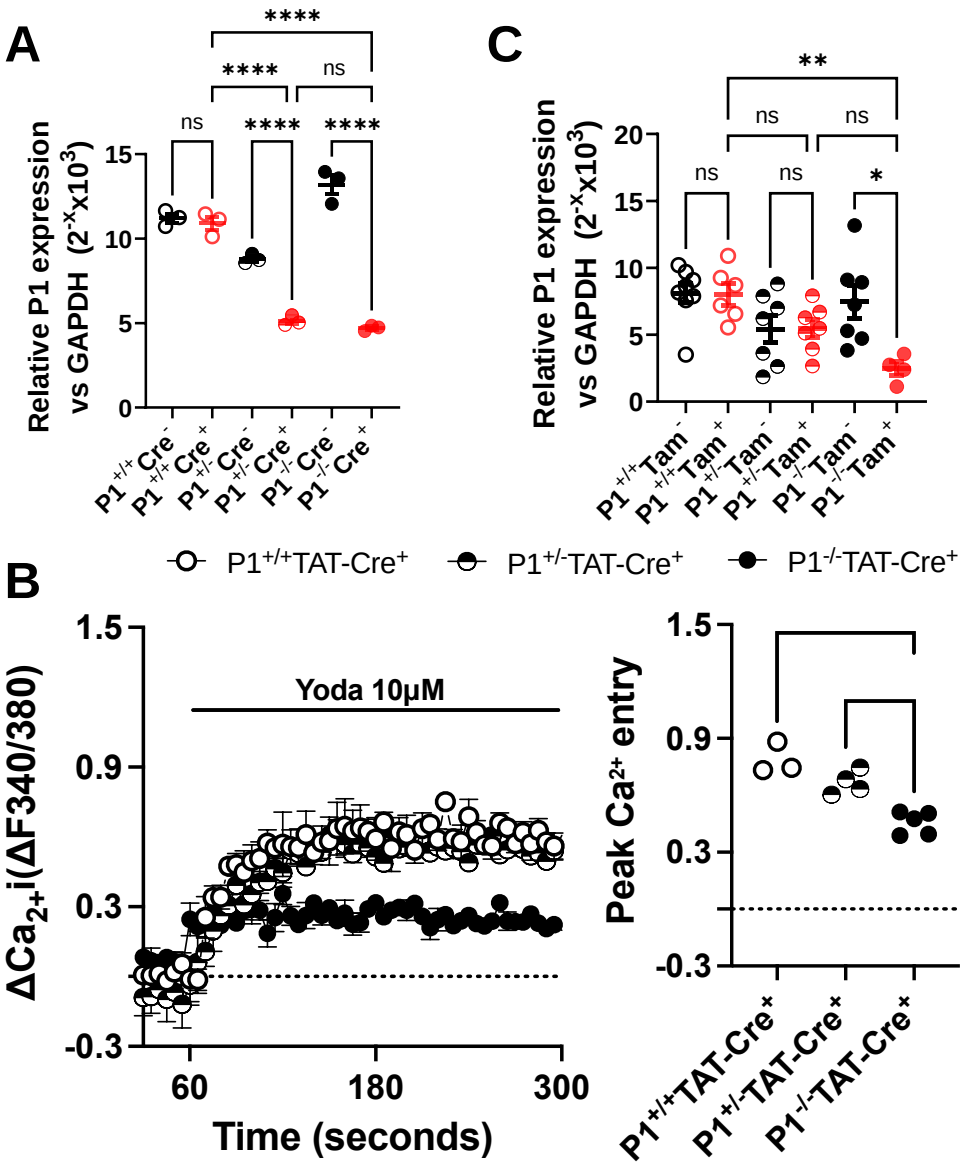

Figure 47. Validation of conditional VSMC PIEZO-1 knockdown in SM-MHC.CreER$_{T2}$; dSMC P1$^{+/+}$, dSMC P1$^{+/-}$ and dSMC P1$^{-/-}$ mice.

A; Relative (to GAPDH) gene expression of PIEZO-1 in cardiac fibroblasts from transgenic mice treated with no TAT-Cre [Cre^{-}] and TAT-Cre [Cre^{+}] (N/n=3/3). B- Yoda-1 activated intracellular calcium entry over time and peak calcium entry into cardiac fibroblasts from transgenic mice (N/n=3/9). C- Relative (to GAPDH) gene expression of PEIZO-1 in transgenic mice aorta following no tamoxifen [Tam^{-}] and tamoxifen [Tam^{+}] at 12-weeks gestation (N/n=3/9). P1$^{+/+}$= open circle, P1$^{+/+}$= half circle, P1$^{+/+}$= closed circle, Black= control, Red= Test. Error bars represent mean ±SEM. *=p<0.05, **=p<0.01, ***=p<0.001, ****=p<0.0001, ns = no significant differences.

4.1.3. Phenotyping of SMMHCCreERT2.Piezo1 Flox Mice

Phenotypic characteristics between the three genotypes were compared at baseline. There were no obvious morphological differences (Figure 48A, 48F, 48K) and no significant differences in mean weight were observed (one-way ANOVA, p=0.50, $P1^{+/+}$ 27.4 ±0.3g, N=20 ; $P1^{+/-}$ 26.9 ±0.3g, N=26; and $P1^{-/-}$ 27.2 ±0.3g, N=22). There were also no significant differences in the APd_{max} (one-way ANOVA, p=0.18) and 3DLV (one-way ANOVA, p=0.48) measurements between genotypes ($P1^{+/+}$ mean APd_{max} 0.66 ±0.01mm and mean 3DLV 3.55 ±0.12mm^3, N=20; $P1^{+/-}$ mean APd_{max} 0.63 ±0.01mm and mean 3DLV 3.33 ±0.13mm^3, N=22; $P1^{-/-}$ mean APd_{max} 0.63 ±0.02mm and mean 3DLV 3.46 ±0.13mm^3, N=22), Figure 48B, 48G, 48L and Figure 48C, 48H, 48M, respectively. Aortic distensibility was also comparable between genotypes (one-way ANOVA, p=0.82, $P1^{+/+}$ 95.5 ±5.2 MPa^{-1}, N=20; $P1^{+/-}$ 91.4 ±4.7 MPa^{-1}, N=22; and $P1^{-/-}$ 94.3 ±4.5 MPa^{-1}, N=22). Furthermore, no obvious morphological differences in aortic appearance was observed on microscopy (Figure 48D, 48I, 48N) and histology (Figure 48E, 48J, 48O). The sample sizes of microscopic images (N=3/3) and histological specimens (N=3/3) were too few for any meaningful mathematical comparisons.

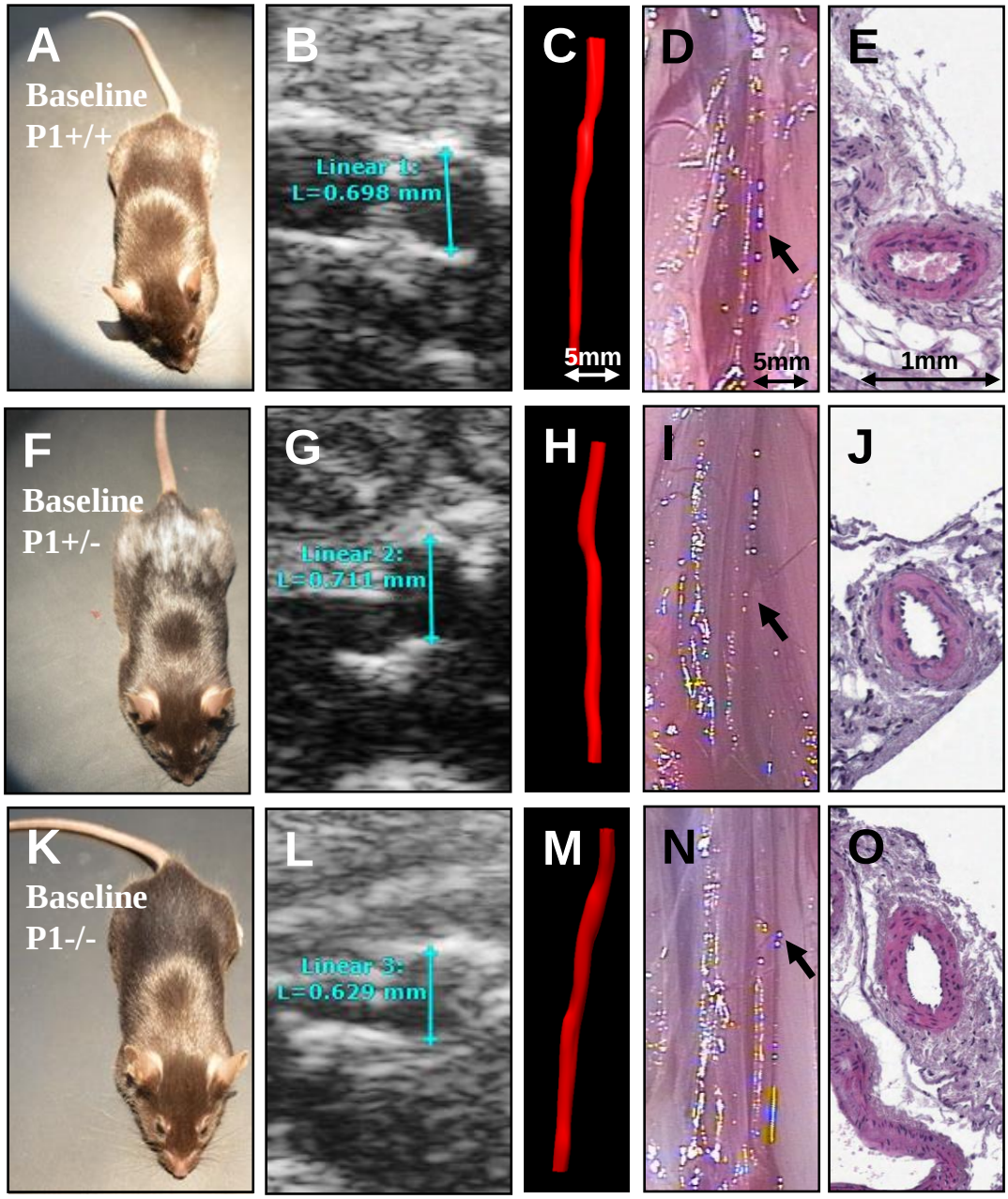

Figure 48. Phenotypic characteristics of SMMHCCreERT2.Piezo1 Flox Mice at 12 weeks (baseline).

Representative illustrations by genotype of: A, F, K; photo of an anaesthetised mice, B, G, L; representative examples of APd_{max} measurements, C, H, M; representative examples of 3DLV measurements, D, I, N; in-situ image of the murine abdominal aorta under physiological blood pressure, E, J, O; representative histological cross-sections of the aorta. smMHCCre-ER(T2) PIEZO-$1^{+/+}$= $P1^{+/+}$, smMHCCre-ER(T2) PIEZO-$1^{-/+}$= $P1^{-/+}$ and smMHCCre-ER(T2) PIEZO-$1^{-/-}$= $P1^{-/-}$. Arrow pointing to aorta.

4.2. Validation of Murine Imaging and Surgery

4.2.1. Reproducibility of Ultrasound Detection of Aortic Size

The two main measurement techniques (i.e. APd_{max} and 3DLV) were assessed for variability and reproducibility of measurements to ensure that these methods were reliable. An independent cohort of 10 mice was used (3 sham vs 7 PPE). In total, 12 ultrasound images from the sham group and 26 USS images from the PPE group were analysed. Both APd_{max} and 3DLV measurements were well-correlated between O1 and O2 (Figure 49A and Figure 49C). Both sets of measurements (APd_{max} and 3DLV) by O2 (O2a, O2b) were also well-correlated (Figure 49B and Figure 49D). There were no significant inter-observer (mean difference: -0.05, LOA: 0.14 to -0.24, p=0.10, Figure 49A) or intra-observer (mean difference -0.03mm, LOA 0.16 to -0.21, p=0.36, Figure 49B) differences in APd_{max} measurements. There were also no significant intra-observer differences in 3DLV measurements (mean difference -0.55, LOA 1.19 to -2.28, p=0.053). However, despite a strong positive correlation (r=0.98, p<0.001) there was a small but significant difference in the inter-observer variability in 3DLV measurements (mean difference -1.38, LOA 1.58 to -4.34, p=0.008).

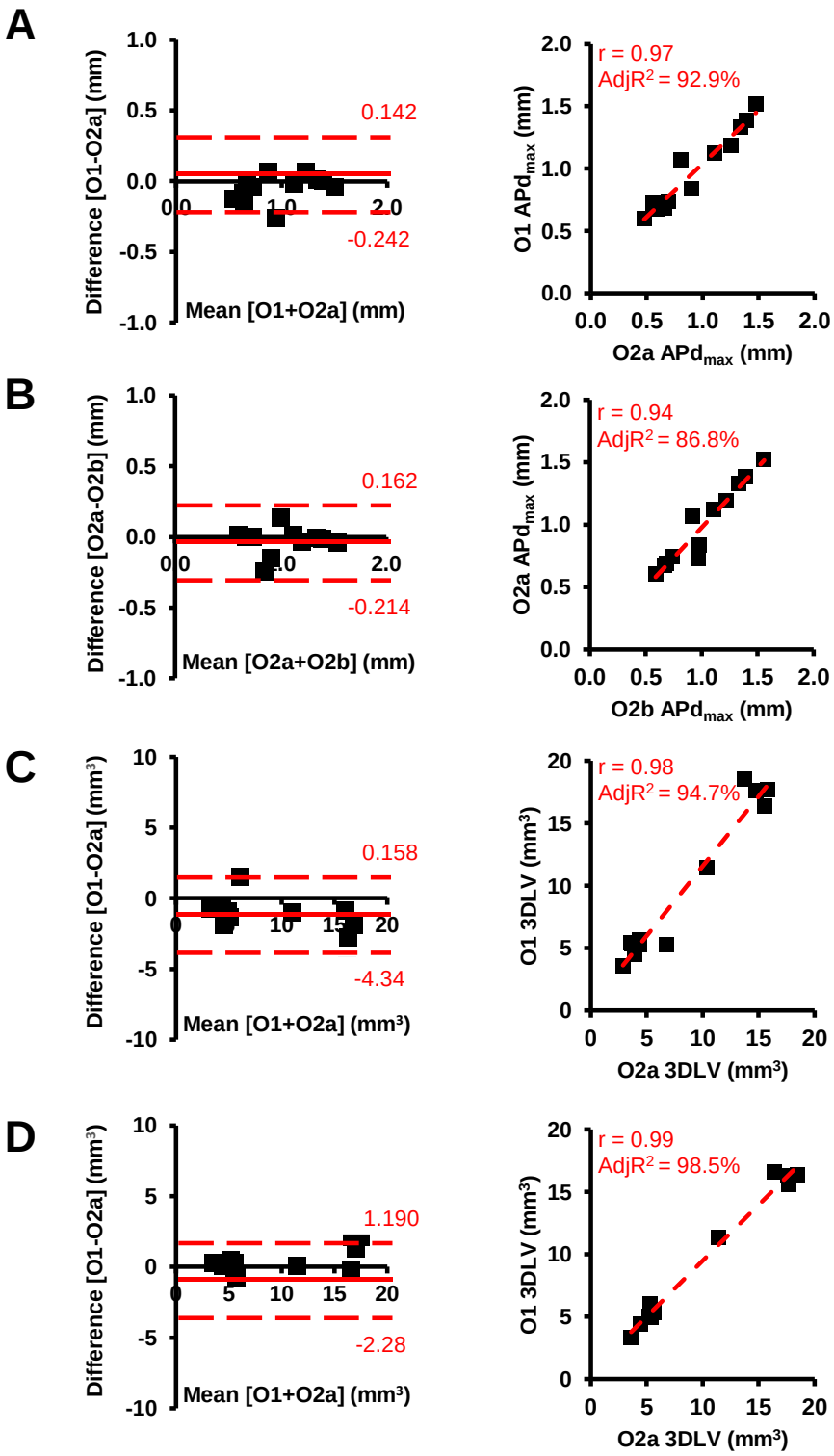

Figure 49. Bland-Altman plots and correlation analysis of USS measurement of mice aorta.

(A) Inter-observer variations in APd_{max} measurements, (B) Intra-observer variations in APd_{max} measurements, (C) Inter-observer variation in 3DLV measurements and (D) Intra-observer variation in 3DLV measurements. Adapted from Waduud et al., 2022.

4.2.2. Comparison of Aortic Measurements Techniques

The relationship between APd_{max} and 3DLV measurements was assessed to identify how accurately each could detect morphological changes in the aorta. Sequential ultrasound images from 14 mice (5 sham vs 9 PPE) were analysed. In total, APd_{max} and 3DLV measurements were obtained from 48 images. Both APd_{max} and 3DLV detected AAA at the standard time point of the model at 14 days post-operatively, at the pre-defined level of statistical significance (Figure 50A and 5B). Absolute mean differences between the sham and PPE AAA groups were 0.66 ±0.11mm for APd_{max} and 5.72 ±0.56mm^3 for 3DLV. However, the 3DLV technique identified a statistically significant aortic dilatation earlier than the APd_{max} method, 6 days versus 10 days, respectively (Figure 50C). Furthermore, the magnitude of lumen change detectable over the course of the 14-day experiment was approximately two-fold greater using 3DLV compared to APd_{max} (2.9 days vs. 6.6 days) as was the rate of growth (slope: 5.7 vs. 12.3, Figure 50C) . A significant positive correlation was evident between APd_{max} and 3DLV measurements ($r=0.70$, $p<0.001$) which remained evident in the aorta following PPE surgery ($r=0.83$, $p<0.001$), Figure 50D. There was increased variability in APd_{max} measurements following sham surgery, which was not evident on 3DLV measurements, therefore, no significant correlation between APd_{max} and 3DLV was evident (r0.24, $p=0.50$, Figure 50D).

Therefore, 3DLV was slightly more variable but more sensitive in the detection of aortic expansion. Both APd_{max} and 3DLV measurements were utilised for assessing mouse aorta throughout this thesis to increase the probability of capturing any relationships between AAA disease progression and parameters of interest.

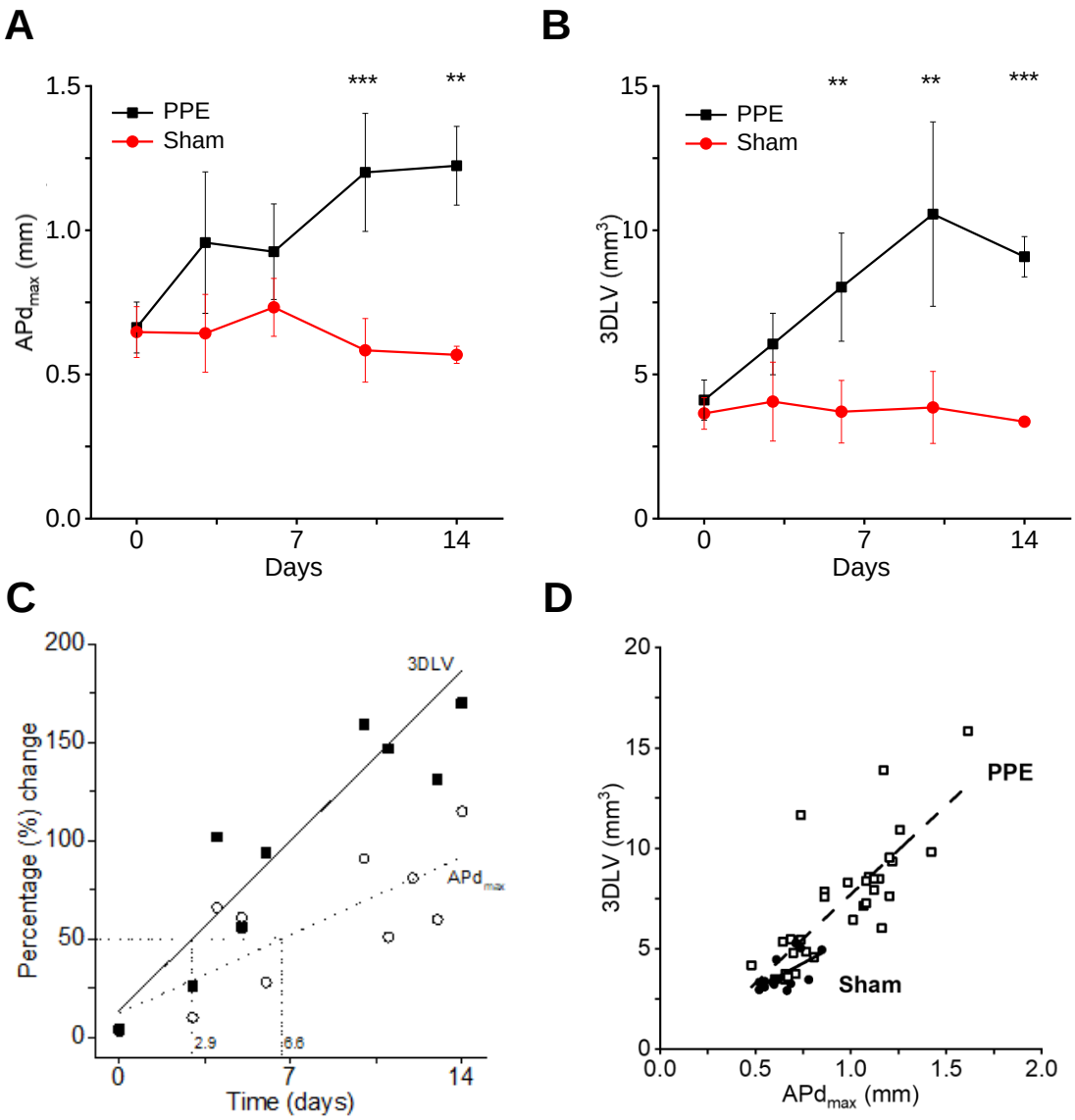

Figure 50. Changes in mice aortic size detected with APd_{max} and 3DLV measurement following sham and PPE surgery.

A; Changes in the APd_{max} following sham and PPE surgery. B; Changes in 3DLV following sham and PPE surgery. C; Scatterplot illustrating the percentage change in aortic size detected with time using the APd_{max} (open circles) and 3DLV (closed squares) measurement techniques. The time taken to detect a 50% increase in aortic size represented by dotted lines. D; Scatterplot illustrating the correlation between 3DLV and APd_{max} measurement in mice following sham and PPE surgery.

4.2.3. Validation of Surgical AAA Modelling

The post-operative outcomes, i.e., aortic morphometry was compared between the 2 independent surgeons (myself and my trainer), to ensure that mice were not inappropriately put through ineffective surgeries. AAA induction surgery was validated via comparison of aortic 3DLV measurements in a cohort of 12 mice (5 sham and 7 PPE) operated on by surgeon 1 (S1- expert trainer) and another independent cohort of 13 mice (4 sham and 9 PPE) operated on by surgeon 2 (S2- myself). Surgery performed by both surgeons resulted in the successful induction of an aneurysm (sham versus PPE; S1 mean difference -8.8 ±1.8mm^3, p=0.001 and S2 mean difference -6.8 ±1.9mm^3, p=0.008), Figure 51. There were no significant differences in 3DLV measurements of the sham models of each surgeon (mean difference 1.3 ±2.1mm^3, p=0.93). Furthermore, there were no significant differences in the 3DLV measurements of PPE models between surgeons (mean difference 3.3 ±1.6mm^3, p=0.18).

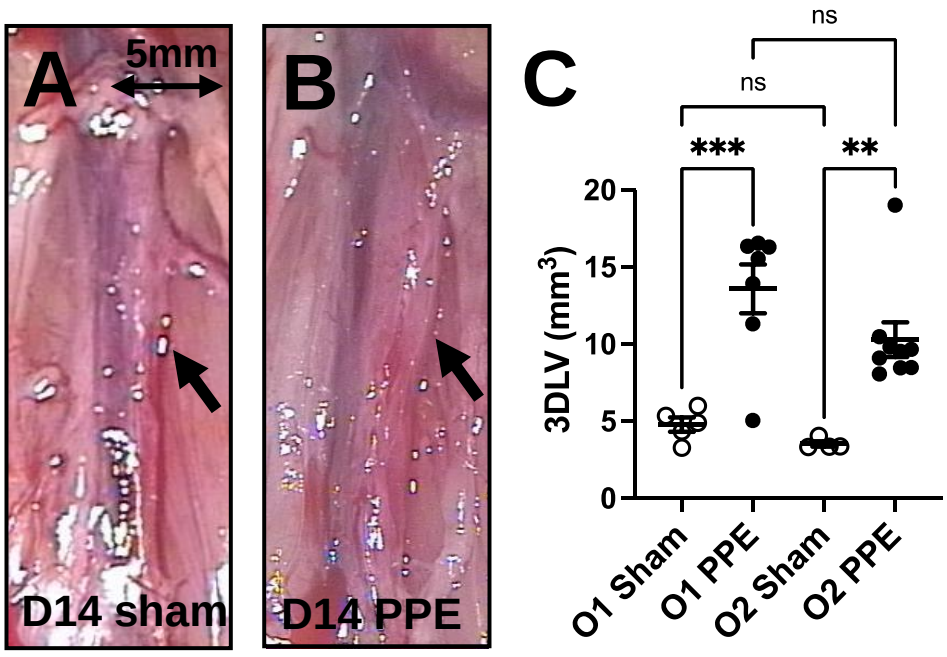

Figure 51. Representative in-situ image of a mice aorta under physiological blood pressure at 14 days after sham (A) and PPE (B) surgery performed by S1.

Arrow points to infra-abdominal aortic region.

4.3. Trends between PIEZO-1 and AAA in C57BL6/J Mice

4.3.1. Aortic Remodelling following Surgery in Wild-Type Mice

Aortic remodelling was characterised to ensure morphological differences were evident between the sham and PPE aorta prior to PIEZO-1 knockout. A total of 15 mice (5 sham and 10 PPE) were used. There were no significant differences in weight throughout the 14-day experimental period in both groups following surgery, Figure 52A. AAAs were evident in the PPE group from day 7 onwards using both measurement techniques, APd_{max} (Figure 52B) and 3DLV (Figure 52C). The mean difference between sham and PPE aorta on day 7 was 4.14 $\pm$0.67mm^3 ($p<0.001$) and on day 14 was 6.56 $\pm$0.75mm^3 ($p<0.001$). As anticipated, AAAs were significantly larger on day 14 compared to day 7 (mean difference 2.17 $\pm$0.86mm^3, $p=0.017$). The majority, 91.9% of mice in the PPE group developed an AAA (i.e. >50% increase in the 3DLV compared to baseline) on day 14. The mean percentage difference in aortic size on day 14 compared to pre-PPE measurements was 87.8 $\pm$13.9% ($p<0.001$). Standardisation of the aortic size to the weight did not influence the differences observed, Appendix C.

Aortic distensibility was significantly lower from day 7 in the PPE group, Figure 52D. There was a significant correlation between aortic size and distensibility following PPE surgery, Figure 53. Illustrations of the measurement of the APd_{max}, 3DLV and distensibility are shown in Figure 54.

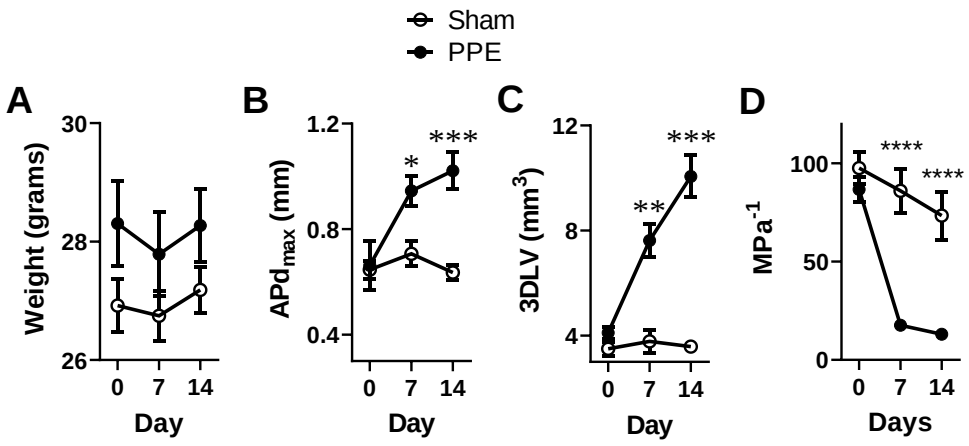

Figure 52. Trends in C57BL6/J wild-type mice weight (A), APd_{max} (B), 3DLV (C) and distensibility (D) following sham (open circles, N=5) and PPE (closed circles, N=10) surgery.

Error bar (black) represents mean ±SEM. *= p<0.05, **= p<0.01, ***= p<0.001, ****= p<0.0001.

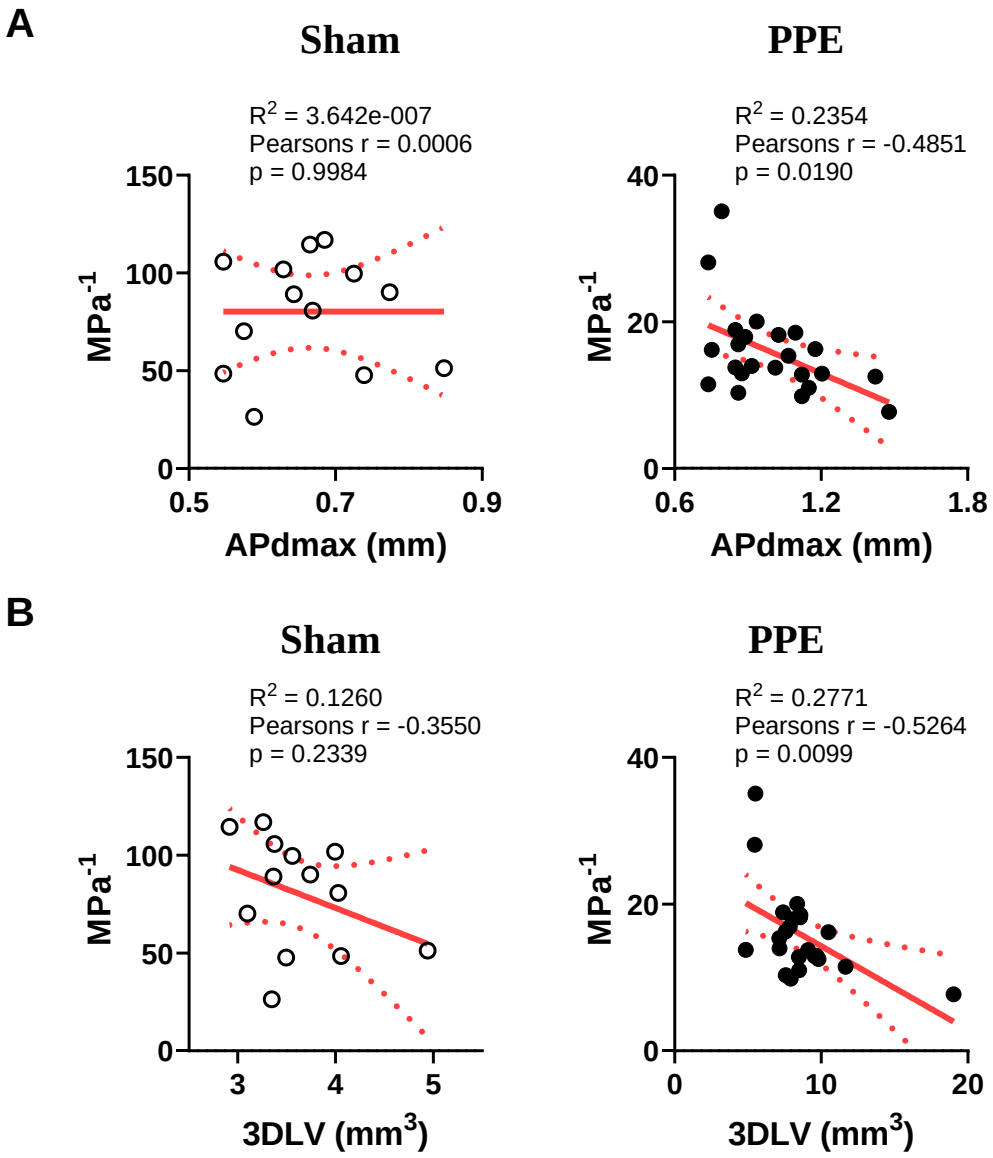

Figure 53. Assessment of correlation between the APd_{max} versus vessel distensibility (A) and 3DLV versus vessel distensibility (B) in C57BL6/J mice following sham (left, open circles) and PPE (right, closed circles) surgery.

Linear regression line= Red, 95% confidence interval of regression line= Red dotted line.

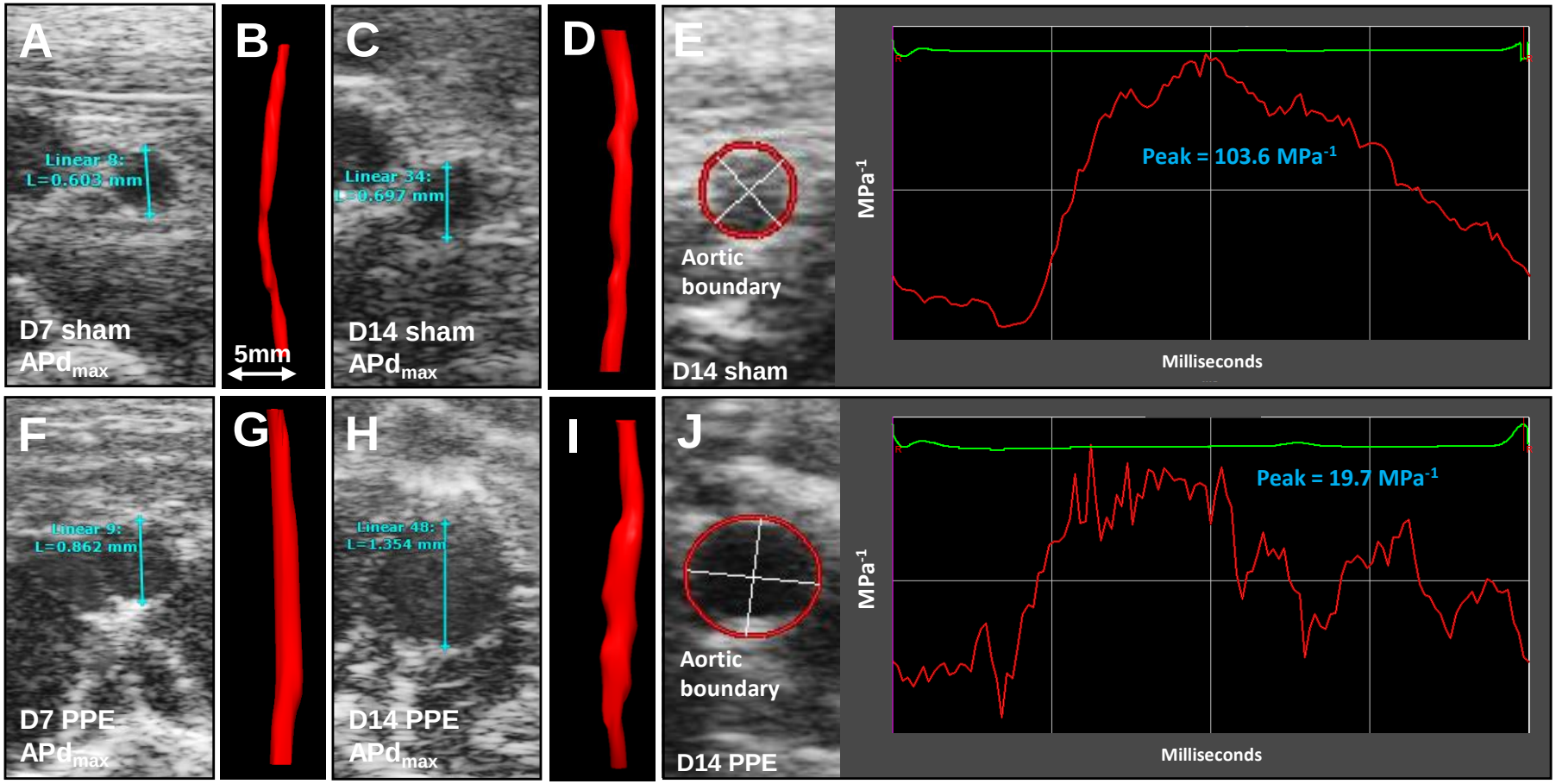

Figure 54. Representative example of the APd$_{max}$ (A, C, F, H), 3DLV (B, D, G, I) and distensibility (E and J) measurements at day 7 and 14 following sham (top) and PPE (bottom) surgery in C57BL6/J wild-type mice.

4.3.2. Associations between Aortic Morphology and PIEZO, KLF-2, KLF-4 and TG2 gene expression in Wild-Type Mice

PIEZO mechanosensor, KLF-2, KLF-4 and TG2 mRNA expression was assessed in mice aorta following sham and PPE surgery to identify any associations. At day 7, the relative expression of PIEZO-1 (p=0.008), PIEZO-2 (p=0.006), KLF-4 (p=0.010) and TG2 (p=0.011) were significantly higher in PPE group compared to the sham group, Figure 55. However, these differences were lost by day 14, except for PIEZO-2 mRNA expression (p=0.007), Figure 56. In contrast, KLF-2 was not significantly altered at day 7 (p=0.69) but had higher expression in the PPE group at day 14 (p=0.029).

There were no significant correlations between PIEZO-1 and the APd_{max} (p=0.11), 3DLV (p=0.42) or MPa-1 (p=0.78), Figure 57. However, there was a significant positive correlation between PIEZO-2 and APd_{max} (R2=0.2, Pearsons r=0.5, p=0.017). No significant correlations were observed between PIEZO-2 and 3DLV (p=0.14) or MPa-1 (p=0.11), Figure 57. Finally, there were no significant correlations between aneurysm size (both APd_{max} and 3DLV) and KLF-2, KLF4 or TG2 mRNA expression, Figure 57.

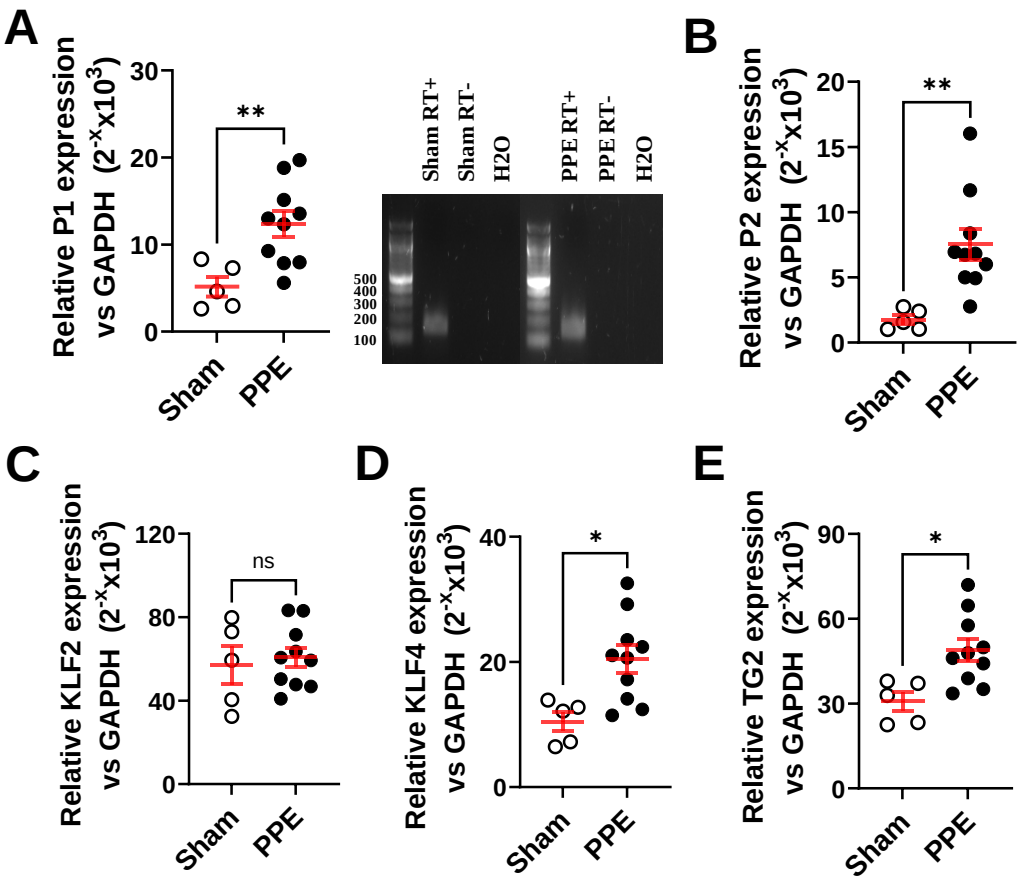

Figure 55. Relative (to GAPDH) mRNA expression of PIEZO-1 (A, with gel electrophoresis blot, 142bp), PIEZO-2 (B), KLF-2 (C), KLF-4 (D), TG2 (E) in the infra-renal aorta of C57BL6/J mice at day 7 following sham (N=5, open circles) and PPE (N=10, closed circles) surgery.

Error bars (red) represent mean ±SEM. *=p<0.05, **=p<0.01, ns = no significant differences. Bp= base pairs.

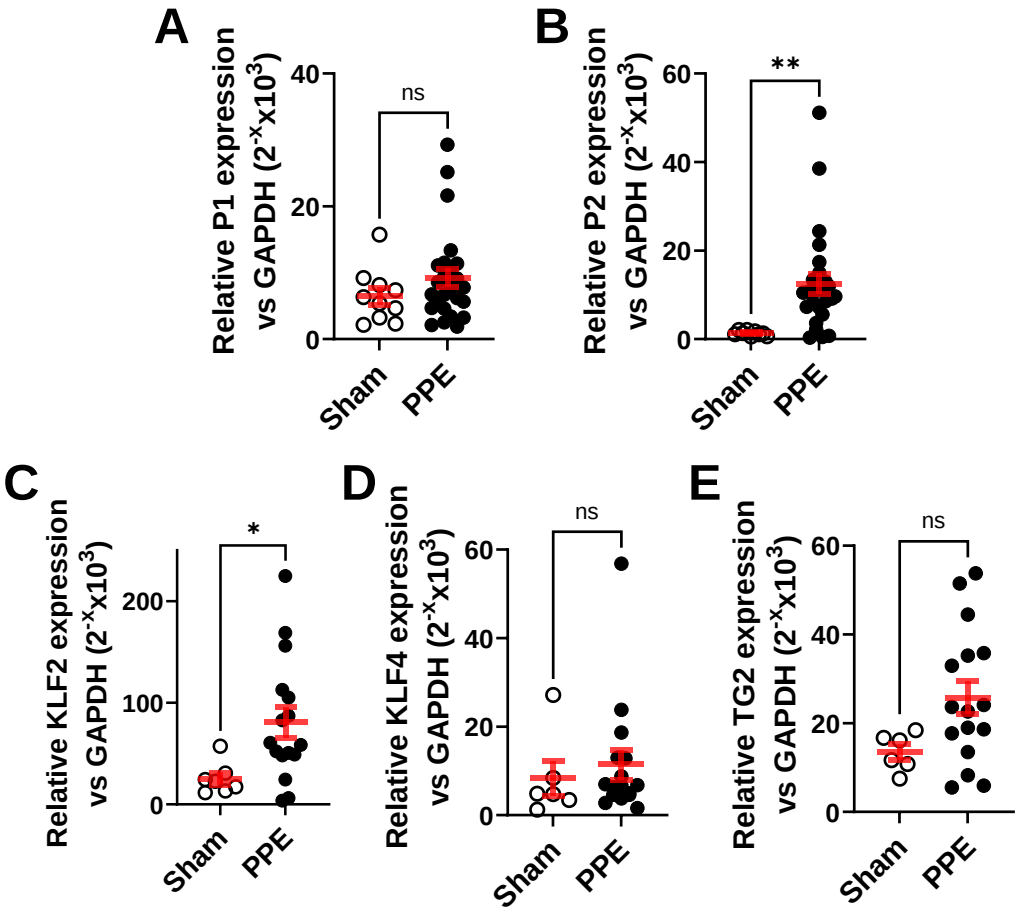

Figure 56. Relative (to GAPDH) mRNA expression of PIEZO-1 (A; sham, N=10 and PPE, N=25), PIEZO-2 (B; sham, N=9 and PPE, N=25), KLF-2 (C; sham, N=7 and PPE, N=16), KLF-4 (D; sham, N=6 and PPE, N=16), TG2 (E; sham, N=6 and PPE, N=16) in the infra-renal aorta of C57BL6/J mice at day 14 following surgery.

Sham= open circles, PPE= closed circles. Error bars (red) represent mean ±SEM. *=p<0.05, **=p<0.01, ns = no significant differences.

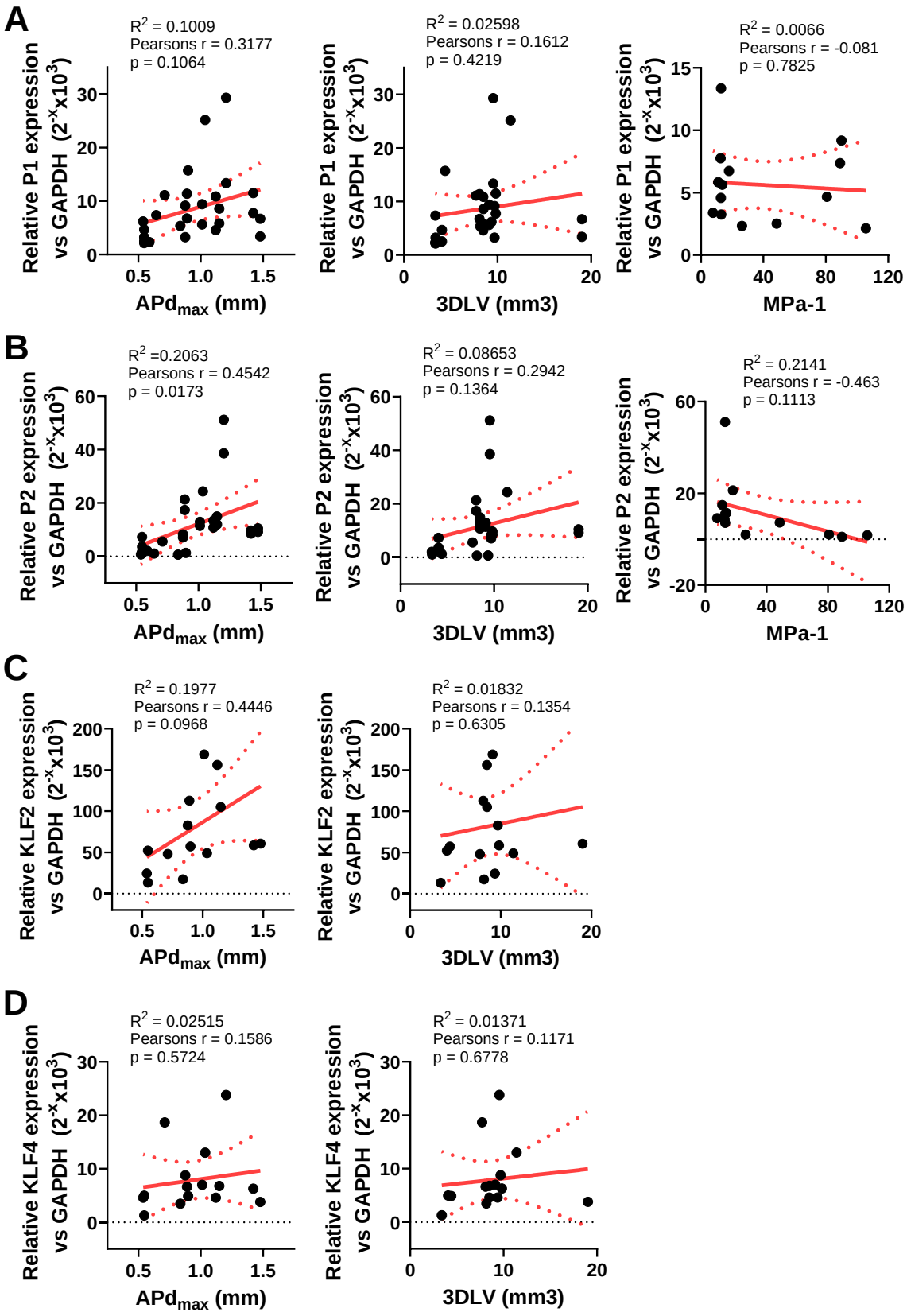
A
R2 = 0.1009
Pearsons r = 0.3177
p = 0.1064
Relative P1 expression vs GAPDH (2-^x x10^3)
APdmax (mm)
R2 = 0.02598
Pearsons r = 0.1612
p = 0.4219
3DLV (mm3)
R2 = 0.0066
Pearsons r = -0.081
p = 0.7825
MPa-1
B
R2 =0.2063
Pearsons r = 0.4542
p = 0.0173
Relative P2 expression vs GAPDH (2-^x x10^3)
APdmax (mm)
R2 = 0.08653
Pearsons r = 0.2942
p = 0.1364
3DLV (mm3)
R2 = 0.2141
Pearsons r = -0.463
p = 0.1113
MPa-1
C
R2 = 0.1977
Pearsons r = 0.4446
p = 0.0968
Relative KLF2 expression vs GAPDH (2-^x x10^3)
APdmax (mm)
R2 = 0.01832
Pearsons r = 0.1354
p = 0.6305
3DLV (mm3)
D
R2 = 0.02515
Pearsons r = 0.1586
p = 0.5724
Relative KLF4 expression vs GAPDH (2-^x x10^3)
APdmax (mm)
R2 = 0.01371
Pearsons r = 0.1171
p = 0.6778
3DLV (mm3)

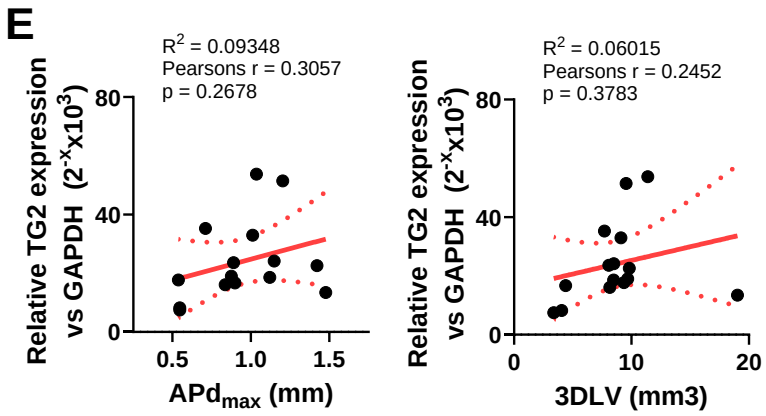

Figure 57. Regression and correlation analysis between PIEZO-1 (A), PIEZO-2 (B), KLF-2 (C), KLF-4 (D) and TG2 (E) mRNA expression and APd_{max} (left), 3DLV (middle) and vessel distensibility (right).

Linear regression line= solid red line, 95% confidence interval= dotted red line.

4.4. Trends between PIEZO, KLF-2, KLF-4, TG-2 and Aortic Morphology in Conditional PIEZO-1 VSMC Knockout Mice

4.4.1. Impact of VSMC PIEZO-1 Deletion on Aneurysm Formation and Progression

Morphological comparison of the mice aorta was made following surgery to assess for any relationship to VSMC PIEZO-1 conditional knockout. There were no significant differences in weight between the different genotypes following sham and PPE surgery, Figure 58A. Overall, 92.4% of all transgenic mice who underwent PPE surgery developed an AAA (50% increase in the 3DLV volume compared to baseline). There were no significant differences in the proportion of mice developing AAAs when stratified by genotype. The morphological appearance of aorta following PPE and sham surgery on sequential imaging and pre-harvest microscopy and histology are illustrated in Figure 59-Figure 61. Again, the number of microscopic images taken (N=3/3) and harvested for histology (N=3/3) was too few for any meaningful mathematical comparisons between genotypes.

The APd_{max} was significantly higher in $P1^{+/+}$ PPE mice compared to $P1^{+/+}$ sham mice (mean difference 0.44 ±0.14mm, p=0.034). No significant differences in the APd_{max} were observed following sham and PPE surgery in $P1^{+/-}$ and $P1^{-/-}$ mice, Figure 58B. There were no significant differences in APd_{max} measurements when comparing the PPE groups in each genotype (p=0.54).

The 3DLV was significantly higher in $P1^{+/+}$ PPE mice compared to $P1^{+/+}$ sham mice on day 7 (mean difference 4.57 ±1.34mm^3, p=0.019) and the size continued to increase until day 14 (mean difference 6.19 ±1.43mm^3, p=0.001). There were no significant differences in 3DLV measurements of $P1^{+/-}$ mice following sham and PPE surgery at either time point (Day 7, p=0.66 and Day 14, p=0.87), Figure 58C. However, similar to that observed in $P1^{+/+}$ mice, in $P1^{-/-}$ mice the 3DLV was significantly higher in the PPE group compared to the sham group on both day 7 (mean difference 3.71 ±1.12mm^3, p=0.024) and day 14 (mean difference 4.09 ±1.36mm^3, p=0.043). The rate of growth between days 7 and 14 appeared subjectively greater in the $P1^{+/+}$ mice however AUC analysis highlighted the rate of change to be non-significant (p=0.20). Comparison of 3DLVs of the PPE groups of all 3 genotypes highlighted that there were no significant differences in size (p=0.98).

Similar to that observed in C57BL6/J mice, aortic distensibility was significantly reduced following PPE surgery compared to sham surgery in all three genotypes, Figure 58D. There were also no significant differences in vessel distensibility between the three genotypes following PPE surgery (one-way ANOVA, p=0.94).

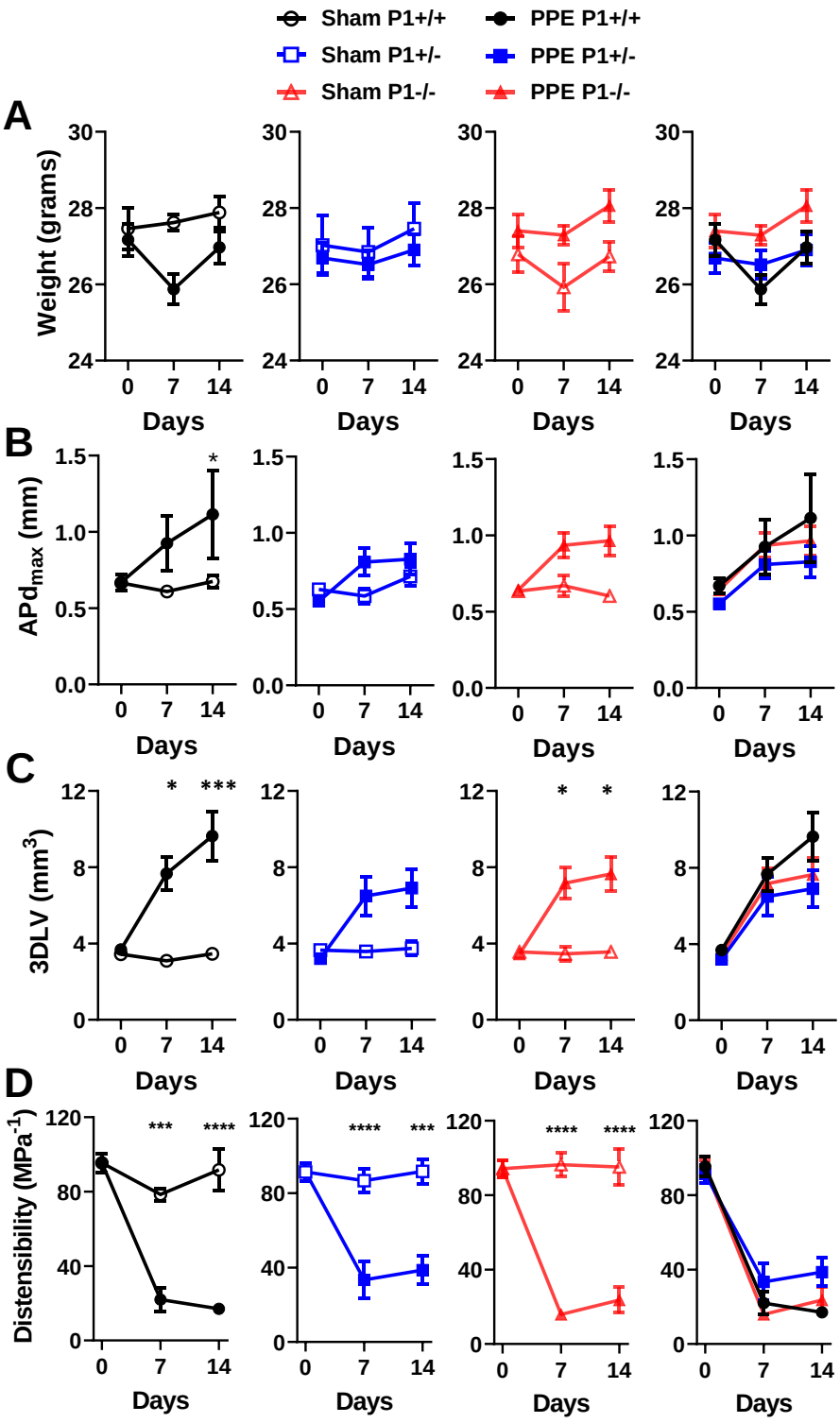

Figure 58. Interval plots illustrating differences and changes in weight (A), APd_{max} (B), 3DLV (C), and vessel distensibility (D) by genotype and surgical procedure.

Sham group= open shape. PPE group= closed shape. $P1^{+/+}$= black circle, $P1^{+/-}$= blue square, $P1^{-/-}$= red triangle. Error bar represents mean ±SEM. *= $p<0.05$, ***= $p<0.001$, ****= $p<0.0001$.

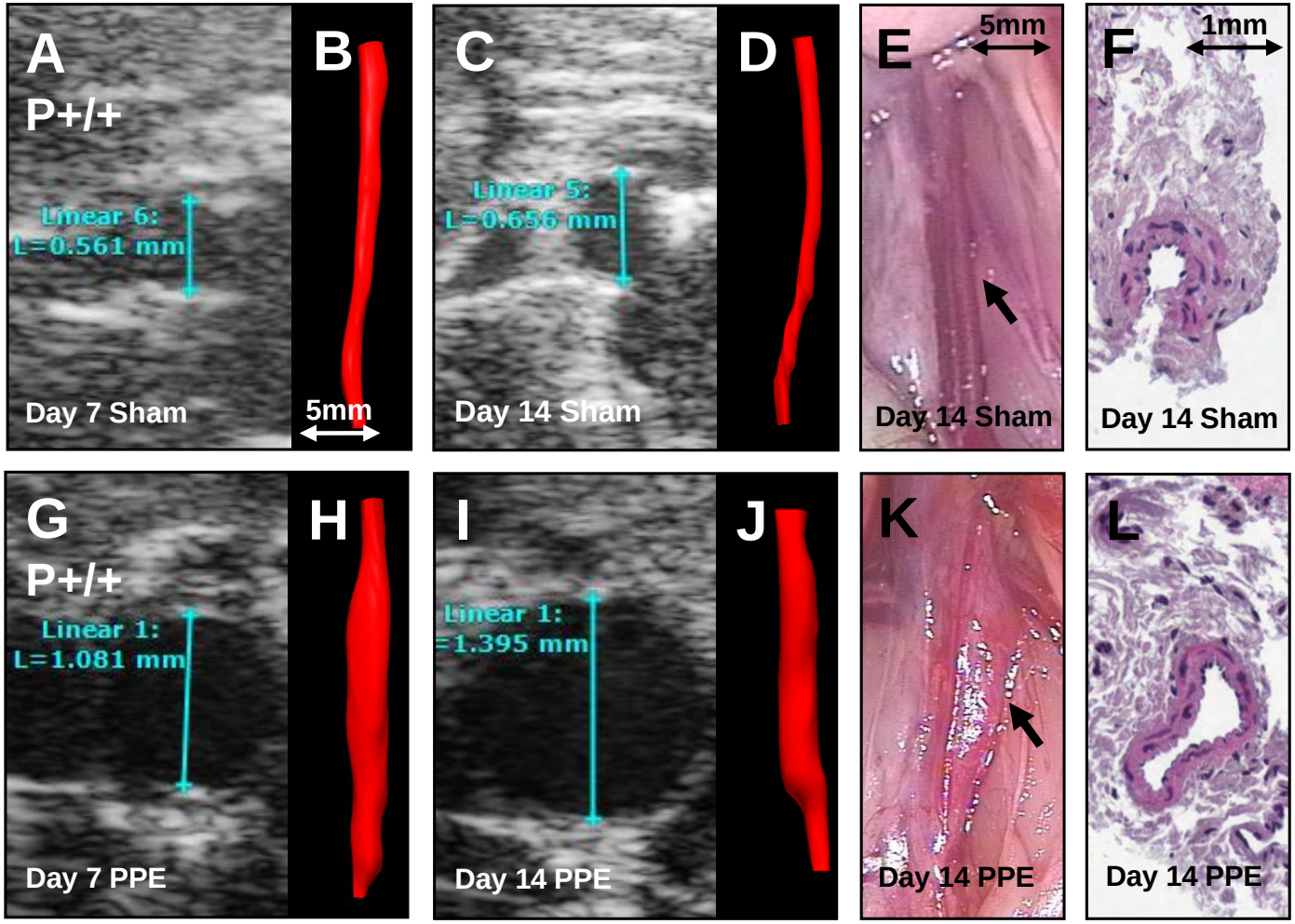

Figure 59. Representative examples of sequential ultrasound images, photograph and histological cross-section of the infra-renal aorta following sham (top) and PPE (bottom) surgery in $P1^{+/+}$ mice.

A&G; Day 7 Apd_{max}. B&H; Day 7 3DLV (sham 3.78mm^3 and PPE 10.48mm^3), C&I; Day 14 APd_{max}. D&J; Day 14 3DLV (sham 3.02mm^3 and PPE 15.15mm^3), E&K; in-situ photo of the aorta under physiological blood pressure at day 14 following sham and PPE surgery. Arrow points to infra-abdominal aortic region. F&L; Representative histological cross-section of the aorta at day 14 following sham and PPE surgery.

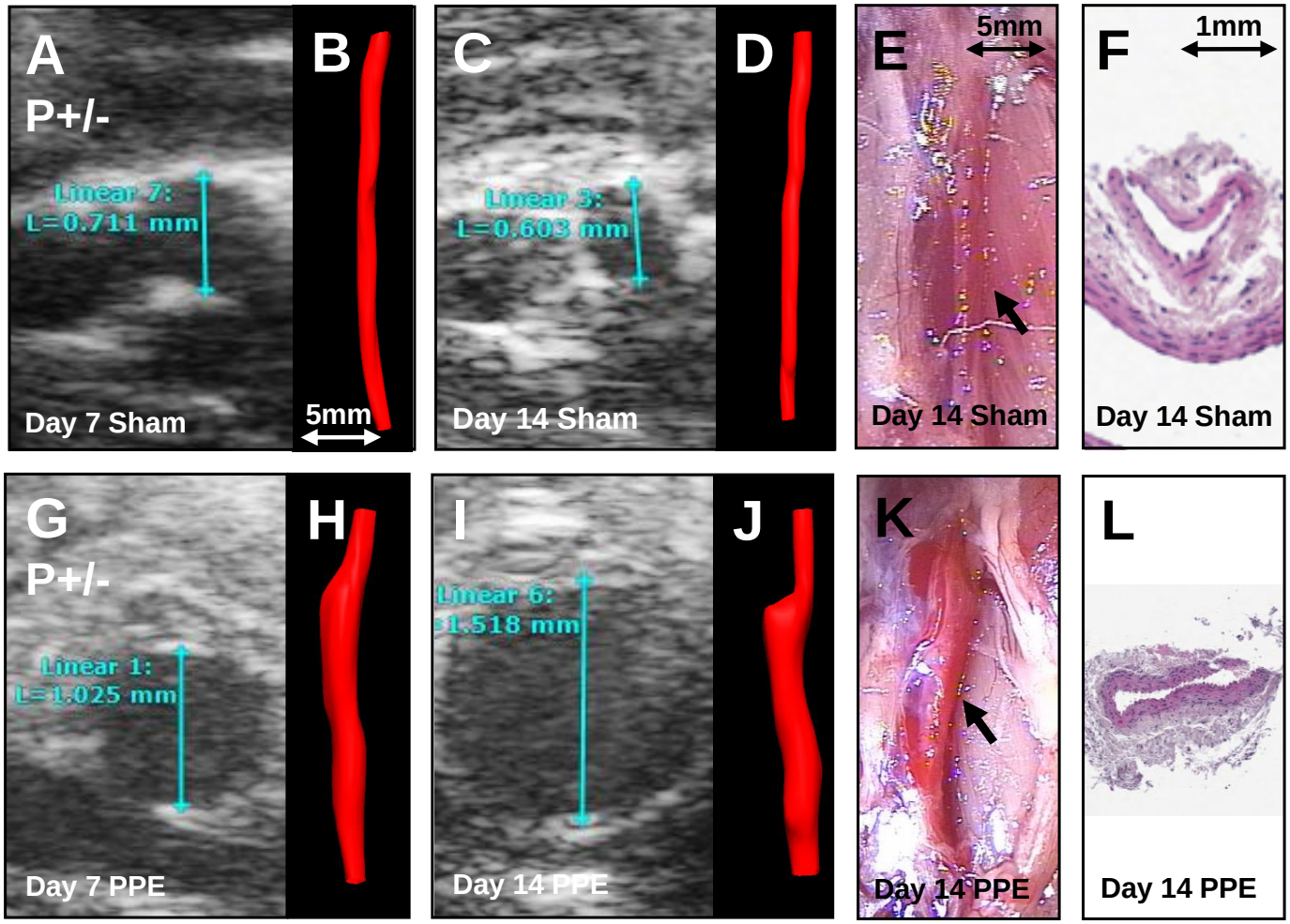

Figure 60. Representative examples of sequential ultrasound images, photograph and histological cross-section of the infra-renal aorta following sham (top) and PPE (bottom) surgery in $P1^{+/-}$ mice.

A&G; Day 7 Apd_{max}. B&H; Day 7 3DLV ($3.74mm^3$ and PPE $10.15mm^3$), C&I; Day 14 APd_{max}. D&J; Day 14 3DLV (sham $2.85mm^3$ and PPE $15.32mm^3$), E&K; In-situ photo of the aorta under physiological blood pressure at day 14 following sham and PPE surgery. F&L; Representative histological cross-section of the aorta at day 14 following sham and PPE surgery.

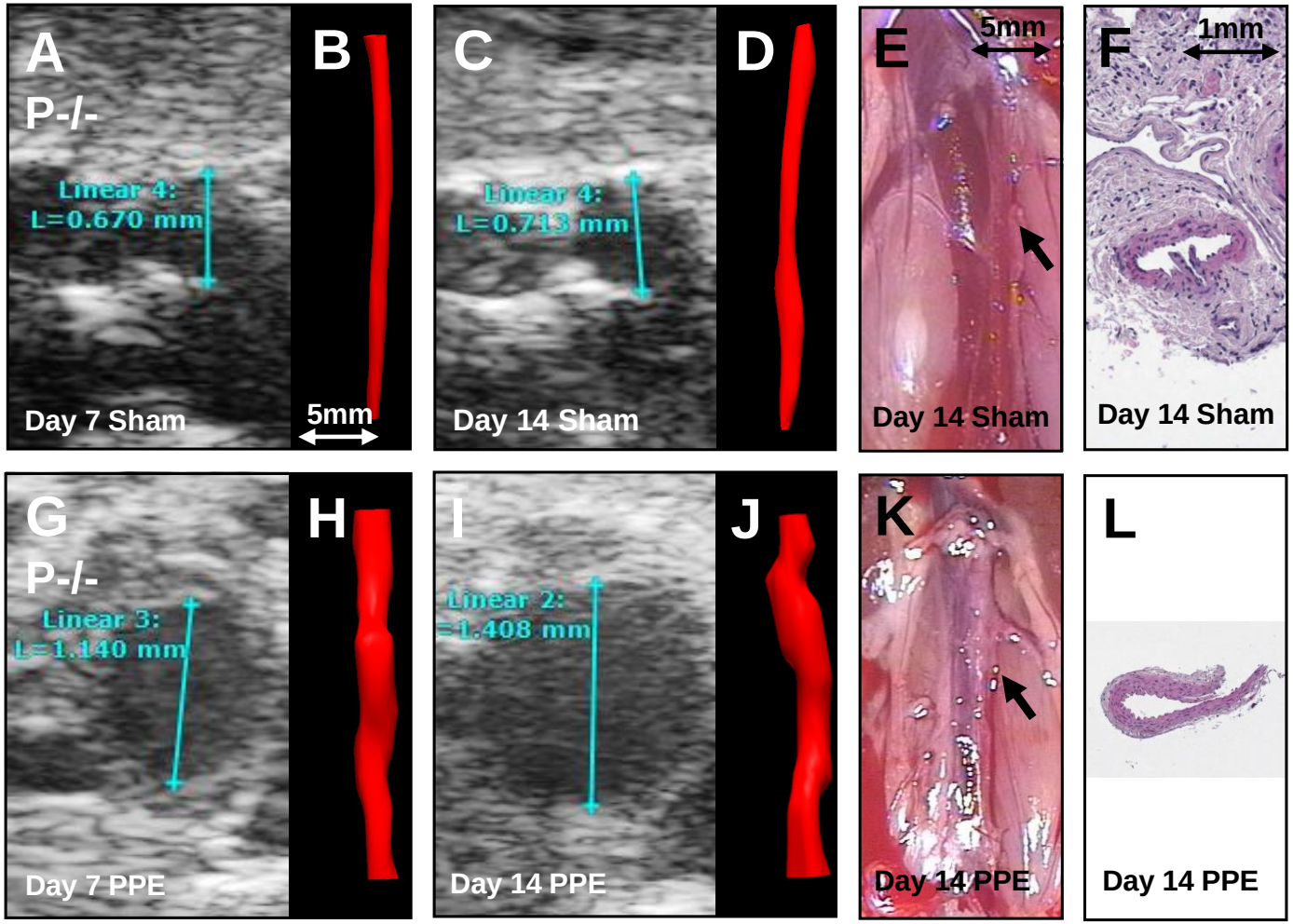

Figure 61. Representative examples of sequential ultrasound images, photograph and histological cross-section of the infra-renal aorta following sham (top) and PPE (bottom) surgery in P1$^{-/-}$ mice.

A&G; Day 7 Apd_{max}. B&H; Day 7 3DLV (sham 3.82mm^3 and PPE 11.97mm^3), C&I; Day 14 APd_{max}. D&J; Day 14 3DLV (sham 3.47mm^3 and PPE 13.84mm^3), E&K; in-situ photo of the aorta under physiological blood pressure at day 14 following sham and PPE surgery. F&L; Representative histological cross-section at day 14 following sham and PPE surgery.

4.4.2. Expression of PIEZO-1, PIEZO-2, KLF-2, KLF-4 and TG-2 in Transgenic mice

It was important to identify any difference in PIEZO, KLF-2, KLF-4 and TG2 mRNA expression to validate the relationships observed. The aorta of the transgenic mice were harvested on day 14.

There were no significant changes to PIEZO-1 mRNA expression following sham and PPE surgery across the three genotypes, Figure 62A. However, there was a trend towards increased PIEZO-1 expression in the PPE groups compared to the sham control groups (mean difference [sham vs PPE] in PIEZO-1 expression; $P1^{+/+}$ -9.3, 95% CI-25.0 to 6.7, p=0.52; $P1^{+/-}$ -4.5, 95% CI -18.8 to 9.7, p=0.93; $P1^{-/-}$ -7.6, 95% CI -22.0 to 6.9, p=0.63). Furthermore, a comparison of the PPE groups in isolation by genotype showed no significant differences in PIEZO-1 expression. Similarly, there were no significant differences in gene expression of PIEZO-2 in aorta on day 14 following sham and PPE surgery by genotype or when comparing PPE groups in isolation by genotype, Figure 62B. Again, there was a non-significant trend towards increased expression of PIEZO-2 in mouse aorta following PPE surgery in all genotypes (mean difference [sham vs PPE] in PIEZO-2 expression; $P1^{+/+}$ -3.5, 95% CI -10.0 to 3.1, p=0.62; $P1^{+/-}$ -2.3, 95% CI -8.2 to 3.7, p=0.86; $P1^{-/-}$ -4.6, 95% CI -11.0 to 1.5, p=0.23).

In $P1^{+/-}$ mice, there was a significantly reduced expression of KLF-2 in the PPE group compared to the sham group (mean difference 161.8, 95% CI 41.7 to 281.9, p<0.001). No other significant differences were evident in relation to the expression of KLF-2, Figure 62C. No significant differences in the expression of KLF-4 were evident, Figure 62D. Similar to KLF-2, the expression of TG2 on day 14 was significantly lower following PPE surgery compared with sham surgery in $P1^{+/-}$ mice aorta (mean difference 75.3, 95% CI 9.4 to 141.2, p=0.017). No other significant differences were evident in relation to the expression of TG2, Figure 62E.

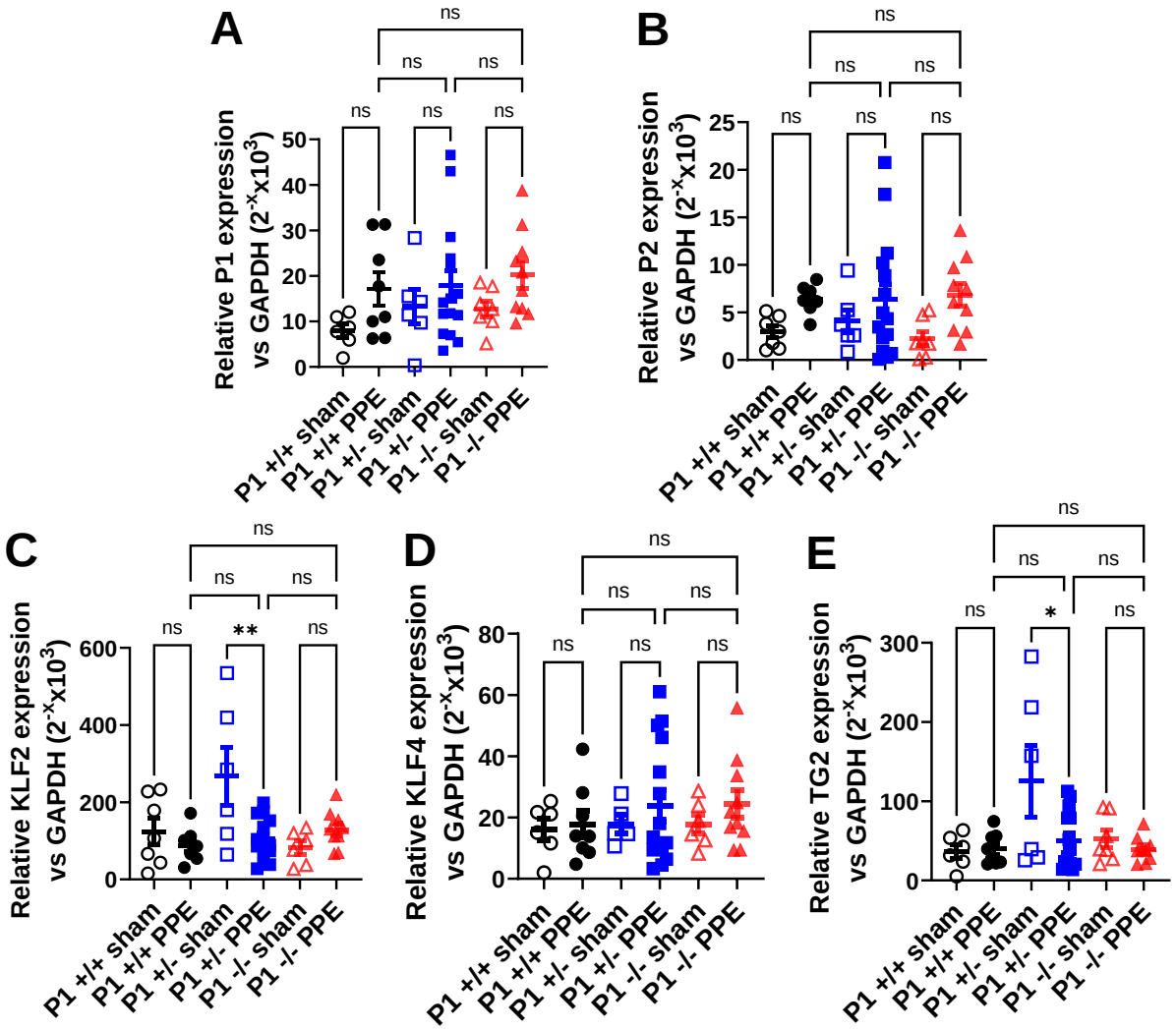

Figure 62. Relative (to GAPDH) gene expression of PIEZO-1 [A], PIEZO-2 [B], KLF-2 [C], KLF-4 [D] and TG2 [E] by genotype following sham and PPE surgery at day 14.

Sham group= open shape. PPE group= closed shape. $P1^{+/+}$= black circle, $P1^{+/-}$= blue square, $P1^{-/-}$= red triangle. Error bars represent mean ±SEM. *=p<0.05, **=p<0.01, ns = no significant differences.

4.4.3. Functional effects of aortic VSMC PIEZO-1 knockout on Wire Myography

Wire myography of the transgenic $P1^{+/+}Tam^{+}$ and $P1^{-/-}Tam^{+}$ mice aorta was performed to assess for any physiological differences in vessel contraction associated with conditional VSMC PIEZO-1 knockout. Functional responses to vasoactive stimuli (i.e. Phenylephrine [PE]), Yoda-1 and KC289 (another synthetic agonist of PIEZO-1) were recorded. No significant differences in vasomotor function between aorta from $P1^{-/-}tam^{+}$ and $P1^{+/+}tam^{+}$ mice were observed with any of the vasoactive stimuli, Figure 63.

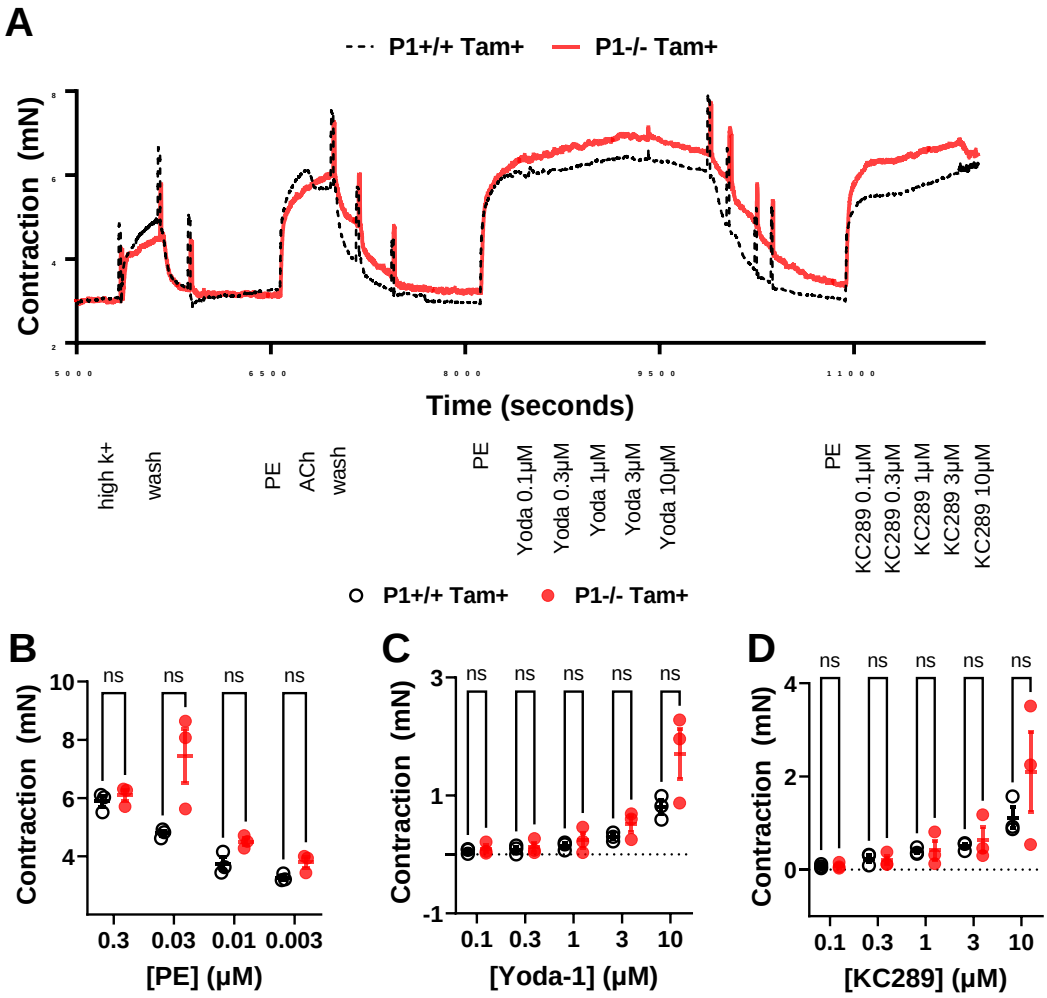

Figure 63. Representative example trace of wire myography of aorta from $P1^{+/+}$ and $P1^{-/-}$ mice (A) with scatter graphs comparing responses with PE (B), Yoda-1 (C) and KC289 (D).

$P1^{+/+}Tam^{+}$= open black circle, $P1^{-/-}Tam^{+}$= closed red circle. Error bars represent mean ±SEM. ns = no significant difference. N/n = 2/6.

4.5. Comparison of Aneurysm Morphology of C57BL6/J and Transgenic Mice

Comparisons were made in the aneurysm morphology between C57BL6/J and SMMHCCreERT2. Piezo1 mice were compared to identify any differences between the knockout mice and the genetic background from which they were derived. There were no significant differences between the APd_{max} and 3DLV when comparing mice on days 7 or 14, Figure 64. However, vessel distensibility was significantly higher in P1+/- mice compared to C57BL6/J mice on days 7 and 14.

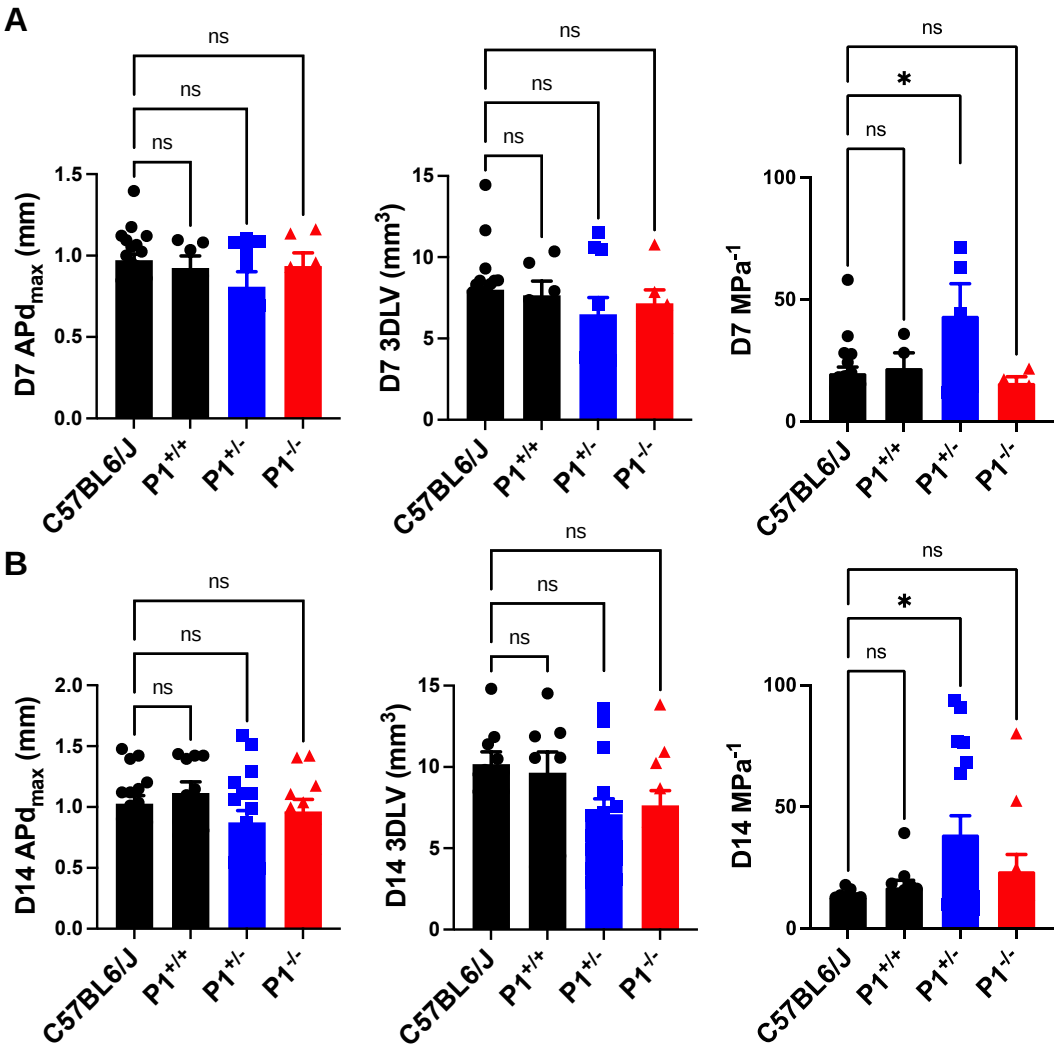

Figure 64. Comparison of the APd$_{max}$, 3DLV and vessel distensibility between C57BL6/J and SMMHCCreERT2.Piezo1 mice at day 14 following PPE surgery.

C57BL6/J= black circle, P1$^{+/+}$= black circle, P1$^{+/-}$= blue square, P1$^{-/-}$= red triangle. Error bars represent mean ±SEM. *=p<0.05, ns = no significant differences.

4.6. Summary of In-Vivo Experiments

AAAs were evident in C57BL6/J mouse aortas from day 7 onwards following PPE surgery. There was an inverse relationship between aortic size and aortic distensibility. On day 7 post-op, there was a higher expression of PIEZO-1, PIEZO-2, KLF-4 and TG2 mRNA in aneurysmal aorta compared to sham control. However, by day 14 only PIEZO-2 mRNA remained elevated and KLF-2 mRNA expression was higher in the aorta following PPE surgery compared with sham surgery. Furthermore, there was a significant relationship between aortic size and PIEZO-2 mRNA expression.

There were no obvious differences in the baseline characteristics of the transgenic mice ($P1^{+/+}$, $P1^{+/-}$ and $P1^{-/-}$). The Cre knockout system was functional. PIEZO-1 knockout was evident on PCR performed on aortic tissue following tamoxifen induction. However, following PPE surgery, there were no differences in aortic size over time between the different genotypes. Furthermore, no significant differences in the expression of PIEZO-1, PIEZO-2, KLF-2, KLF-4, or TG2 mRNA were evident between wild-type mice ($P1^{+/+}$) and knockout mice ($P1^{-/-}$). No functional differences in wire myography were evident.

Chapter 5: Discussion

5.1. Summary of Key Findings

5.1.1. Summary of Key Findings in relation to the PIEZO Mechanosensors

In Vitro experiments

- PIEZO-1 mRNA was expressed in NAVSMCs and AAAVSMCs at baseline and could be functionally activated with the PIEZO-1 agonist Yoda-1. PIEZO-2 mRNA was also expressed in NAVSMCs and AAAVSMCs, but was negligible compared with PIEZO-1.
- Reciprocal expression of PIEZO-1 and PIEZO-2 mRNA was observed when comparing NAVSMCs and AAAVSMCs.
- Higher PIEZO-1 dependent intracellular calcium movement were observed in NAVSMCs at lower passages compared to those at higher passages, however no significant differences in PIEZO-1 and PIEZO-2 mRNA expression was evident between cells of different passages.
- Stimulation of NAVSMCs with Yoda-1 resulted in the increased expression of PIEZO-1 mRNA and a reciprocal changes in PIEZO-2 expression.
- The application of constant oscillatory shear force to NAVSMCs resulted in increased mRNA expression of both PIEZO-1 and PIEZO-2 as well as increased PIEZO-1 dependent intracellular calcium entry.
- Cell culture of NAVSMCs in serum deprived culture media resulted in the increased mRNA expression of both PIEZO-1 and PIEZO-2.
- siRNA knockdown of PIEZO-1 in NAVSMCs resulted in a compensatory increase in PIEZO-2 mRNA expression, however, did not translate to a functional knockdown of PIEZO-1.

In Vivo experiments

- PIEZO-1 mRNA expression was evident in C57BL6/J mice aortas at

baseline. PIEZO-2 mRNA was also expressed, however it was again negligible compared with PIEZO-1.

- Both PIEZO-1 and PIEZO-2 mRNA expression was significantly higher in wild-type mice aorta following aneurysm induction surgery compared with the sham surgery on day 7. However, by day 14 only PIEZO-2 mRNA expression remained significantly elevated in aneurysmal mice aorta.
- A significant positive correlation was observed between PIEZO-2 mRNA expression and AAA size, which was not evident for PIEZO-1.
- No significant differences in PIEZO-1 mRNA expression were evident between the transgenic mice on day 14 following surgery.
- There were no significant differences in the aneurysmal aortic sizes between the transgenic mice following aneurysm induction surgery.

5.1.2. Summary of Key Findings in relation to VSMC Cell Proliferation

In Vitro experiments

- KLF-4 mRNA expression was significantly lower in NAVSMCs of the highest passage.
- A significantly higher cell proliferation was identified in NAVSMCs treated with the PIEZO-1 agonist Yoda-1 and an increased mRNA expression of KLF-2 and KLF-4 was observed.
- The application of constant oscillatory shear force to NAVSMCs resulted in increased mRNA expression of both KLF-2 and KLF-4.
- siRNA knockdown of PIEZO-1 mRNA in NAVSMCs resulted in increased mRNA expression of KLF-2 and KLF-4.

In Vivo experiments

- All mice developed significantly larger aorta following PPE induction surgery, with the bulk of the vessel wall being formed of VSMCs.

- In wild-type mice, mRNA expression of KLF-4 was significantly higher on day 7 following aneurysm induction surgery, however this difference was no longer evident on day 14. Conversely no significant difference in KLF-2 mRNA expression was observed on day 7, however a significantly higher expression of KLF-2 on day 14.
- No significant differences in KLF-2 and KLF-4 expression was observed between transgenic mice.

5.1.3. Summary of Key Findings concerning Cell and Matrix Stiffness

In Vitro experiments

- TG2 mRNA expression was lower in AAAVSMCs compared to NAVSMCs.
- While matrix stiffness was significant in NAVSMC survival, there was no association between matrix stiffness and PIEZO mechanosensors.
- Treatment of NAVSMCs with Yoda-1 resulted in reduced mRNA expression of TG2.
- Application of oscillatory shear force to NAVSMCs resulted in increased mRNA expression of TG2.
- Higher cell passages were associated with a reduction in mRNA expression of TG2.
- siRNA knockdown of PIEZO-1 in NAVSMCs resulted in increased mRNA expression of TG2.

In Vivo experiments

- In wild-type mice, mRNA expression of TG2 was significantly higher following aneurysm induction surgery on days 7 and 14.
- No significant differences in TG2 mRNA expression were in the aorta from the different transgenic mice.
- There were no significant differences in aortic stiffness between transgenic

mice following aneurysm induction surgery.

	Pathological stage of AAA		
	Early	**Intermediate**	**Late**
PIEZO-1	Elevated	Elevated	Reduced
PIEZO-2	Reduced	Elevated	Elevated
KLF-2	Elevated	Elevated	Unequivocal
KLF-4	Elevated	Elevated	Unequivocal
TG2	Reduced	Reduced	Elevated

Table 7. Revised mechanistic summary of hypothesis describing changes in the PIEZO mechanosensors and markers of proliferation.

5.2. General Discussion

Research on the potential role of the PIEZO mechanosensors has increased exponentially, with a recent high impact publication describing its potential role in AAA disease (Qian et al., 2022). The hypothesis that activation of PIEZO-1 mechanosensor in aortic VSMCs by stressors (i.e. mechanical and physiological) drives vascular remodelling (i.e. cell proliferation and stiffness) was assessed using in vitro and in vevo models. The identification of potentially novel pharmacological target(s) in the early stages of the pathological vascular remodelling seen in the aneurysmal aorta would be indispensable in medically treating this life-threatening condition in an elderly multi-morbid population of patients.

In this thesis, the PIEZO mechanosensors were shown to be evident in VSMCs and could detect and adapt to common mechanical stimuli and stressors likely to be experienced in the AAA microenvironment. PIEZO-1 mRNA was shown to be elevated in aortic VSMCs following; treatment with the PIEZO-1 agonist Yoda-1, the application of constant oscillatory shear stress, and cell culture with serum-deprived media. Reciprocal and compensatory changes in the expression of PIEZO-2 were observed. Proliferation was significantly slower following prolonged stimulation with PIEZO-1. Although there was no physiological evidence linking vessel distensibility and PIEZO-1, there was some suggestion that PIEZO-1 influences the expression of TG2. Overall, the findings of the in vitro experiments were supported by those of in vivo experiments. Unfortunately, physiological knockdown of PIEZO-1 could not be achieved and there is uncertainty regarding the knockdown of VSMC PIEZO-1 in transgenic mice. While the focus of this thesis is on the PIEZO-1 mechanosensor the finding within the thesis point to PIEZO-2 being an equally important if not more important in the AAA disease process. Without question, additional validation and research is required to confirm these findings and further interrogate the mechanistic role of the PIEZO mechanosensors in AAA disease.

5.3. PIEZO-1, Aortic VSMCs and Mechanical Stressors

Until recently, the study of PIEZO-1 in relation to VSMC pathophysiology in AAA disease was non-existent (Qian et al., 2022). This thesis demonstrates that PIEZO-1 mRNA is expressed and functionally present on calcium imaging in both non-diseased NAVSMCs and diseased AAAVSMCs. However, a comparative assessment of PIEZO-1 mRNA expression and PIEZO-1 mediated intracellular calcium entry in AAAVSMCs and NAVSMCs did not highlight there to be any significant differences. This raises the question of whether VSMC PIEZO-1 has a role in this disease, as previously described (Qian et al., 2022). Qian and colleagues describe how VSMCs adopt a solid-like state through cytoskeletal cross-linking in the presence of Netrin-1, which results in increased PIEZO-1 activity. They reported the inhibition of the PIEZO-1 mechanosensor to prevent any pathological vascular remodelling typically seen in AAA in mice models. The content of this thesis attempted to verify these recent findings through PIEZO-1 modulation in both in vitro and in-vevo models.

The absence of any genomic and physiological differences between pre-operative and non-disease human VSMCs in this thesis does not necessarily imply that PIEZO-1 to be obsolete in the AAA disease process. However, the role of VSMC PIEZO-1 could be transient and change as the disease develops and anatomical and physiological microenvironment changes. Mechanical stressors such as axial stretch, oscillatory force and matrix stiffness, mimicking those likely to be experienced by VSMCs in the new pathological environment, were applied over time to non-diseased NAVSMCs. This was to ascertain any dynamic changes in PIEZO-1 mRNA expression and physiological behaviour at fixed time points (i.e. on days 7 and 14).

Changes in the character of the blood flow within the aortic lumen, from an uninterrupted, uniform and laminar flow to a disrupted, turbulent and multi-dimensional flow, have been previously described to drive the changes in VSMC physiology (Amirbekian et al., 2009). In this thesis, the application of constant uni-axial stretch to NAVSMCs did not result in any changes in

PIEZO-1 mRNA expression. This finding was reassuring as the forces experienced within the aneurysm macro-environment are dynamic, as opposed to static and one dimensional, as was the case in this experiment. However, the application of constant uninterrupted oscillatory shear force resulted in a significantly higher expression of PIEZO-1 mRNA and a functional increase in intracellular calcium entry observed in NAVSMCs through PIEZO-1. Furthermore, sustained application of the potent PIEZO-1 agonist Yoda-1 to NAVSMCs, resulted in the increased expression of PIEZO-1 mRNA as anticipated. This translated to a significantly lower rate of cell proliferation in NAVSMCs, like that typically observed in AAAVSMCs during cell culture.

Additionally, NAVSMCs were cultured in serum-deprived media to mimic a hostile nutrient deplete micro-environment experienced by cells due to the intra-luminal wall being sealed off by intra-luminal thrombi (Hinnen et al., 2005). NAVSMC cultured in serum-deprived media had a significantly higher expression of PIEZO-1 mRNA, compared with those cultured in standard culture media. However, this only translated to a non-significant trend towards increased intracellular calcium entry through the PIEZO-1 mechanosensor. It is likely that the combination of these factors, i.e., constant oscillatory shear stress and a hostile micro-environment all play a compounding role in the AAA disease process in the activation of PIEZO-1.

The human aortic wall is predominantly composed of VSMCs and can react and adapt to accommodate changes in the intra-luminal flow. The absence of continued VSMC proliferation reduces the ability of the aorta to compensate through remodelling. The combination of constant turbulent blood flow, nutrient-deprived micro-environment, prolonged activation of PIEZO-1 and the resulting reduction in cell proliferation may be one possible mechanistic explanation of the role of PIEZO-1 in this disease process. Consequently, this may impede the ability of the vessel to dilate, morphologically change, and evolve. This may be relevant in the latter pre-rupture stages of the AAA remodelling process, where altered sac curvature and reduced vessel

thickness have been shown to predispose the aneurysmal sac to rupture (Giannoglou et al., 2006). Importantly, sustained activation of the PIEZO-1 mechanosensor with Yoda-1 did not appear to impact cell survival and viability.

To validate these observations, PIEZO-1 was knocked down from NAVSMCs to re-evaluate the effects of prolonged PIEZO-1 activation on cell proliferation. However, we only managed to successfully knockdown PIEZO-1 mRNA in NAVSMCs, which failed to translate to a functional knockdown of the PIEZO-1 membrane protein. PIEZO-1-dependent intracellular calcium entry was still evident when Yoda-1 was applied to cells following successful PIEZO-1 mRNA knockdown. Even with prolonged transfection, we failed to observe any functional differences in intracellular calcium entry. Therefore, we found it futile and financially unfeasible to conduct physiological studies on NAVSMCs with various stressors with only mRNA knockdown evident in cells. Consequently, investigations were focused on the application of extrinsic forces and stressors along with mice models to gain further mechanistic insights. Nevertheless, based on the findings described above, it may be reasonable to suggest that PIEZO-1 plays a role in the AAA disease process.

5.4. PIEZO-1 and AAA in Mice Models

All C57BL6/J mice developed an AAA on day 7 following PPE induction surgery. Interestingly, at this time point, there was a significantly higher expression of PIEZO-1 mRNA in the aneurysmal aorta compared to the sham aorta; alluding to a potential relationship between aneurysm formation and the PIEZO-1 mechanosensor. The aneurysm sac continued to grow until day 14, however, the rate of AAA growth appeared to slow down after day 7. By day 14, no significant differences were in PIEZO-1 mRNA expression between PPE and sham mice aorta. This further supports the notion that PIEZO-1 may play a transient role in the AAA disease process. These findings support the observations seen in the in vitro experiments that the application of oscillatory

shear stress, similar to that encountered in the dilated murine aneurysmal sac, was associated with an initial increase in PIEZO-1 mRNA expression. The regression in the rate of growth of the aneurysm sac, observed between days 7-14, could have been due to the over-stimulation of PIEZO-1 resulting in a reduction in VSMC proliferation, as observed in the latter half of the in-vitro experiments. The transient relationship between PIEZO-1 and aneurysmal growth is further supported by the absence of any correlation between the size of the aneurysmal aorta and the mRNA expression of the PIEZO-1 mechanosensor.

Similar to that observed in C57BL6/J mice, the aorta of the transgenic mice, regardless of the genotype (i.e. $P1^{+/+}$, $P1^{+/-}$ and $P1^{-/-}$), all developed an AAA by day 7 following PPE induction surgery. Therefore, it may be reasonable to deduce that AAAs using the PPE mouse model are established by day 7 and studies investigating AAA initial growth should focus within this time frame. The rate of aneurysm growth was the greatest up to day 7 and then declined between days 7 to 14. There were no significant differences in the aortic sizes on day 7 or day 14 when the 3 different genotypes were compared. Furthermore, there were also no significant differences in the aortic sizes when comparing measurements recorded on day 7 to those recorded on day 14, irrespective of the mouse genotype. This was different to the observations seen in the C57BL6/J mice aorta where the aorta continued to increase in size between days 7 and 14. Unfortunately, histological sample sizes were too small to perform any meaningful quantitative comparisons by genotype. However, functional assessment of vessel contraction on wire myography using the PIEZO-1 agonists Yoda-1 and KC289 did not highlight any significant differences in vessel contraction in VSMC PIEZO-1 knockout mice aorta. These findings further suggest that PIEZO-1 is potentially insignificant in the AAA disease process.

The absence of any differences in the AAA morphology seen in transgenic mice contradicts the observations in wild-type mice. However it develops the hypothesis that overstimulation of the PIEZO-1 mechanosensor results in

increased VSMC proliferation, thereby, increasing AAA sac enlargement. If this hypothesis were to be true, $P1^{-/-}$ transgenic mice should have developed the smallest aortic aneurysms as VSMC PIEZO-1 could not be stimulated compared with $P1^{+/+}$ mice who should have developed the largest aortic aneurysms due to overstimulation of VSMC PIEZO-1. Furthermore, subjectively it initially appeared as though the rate of growth of the AAA may have been slower in the $P1^{+/-}$ and $P1^{-/-}$ mice, however, on ROC analysis, this did not appear to be the case. Nevertheless, the findings of these experiments suggest that there to be no difference, casting doubt over the role of PIEZO-1 in this disease process.

There is some evidence that there was successful knockdown of VSMC PIEZO-1 in the transgenic mice utilised in this thesis. The TAT-Cre system appeared to be working as anticipated, which translated to a functional knockdown of PIEZO-1 on calcium imaging in cardiac fibroblasts obtained from the transgenic mice. Tamoxifen injections were given to all transgenic mice, which should have induced VSMC PIEZO-1 knockout in $P1^{-/-}$ mice, before baseline assessment of PIEZO-1 knockout in the mouse aorta. Successful knockdown of PIEZO-1 mRNA was evident in aortae harvested from mice in each of the 3 difference genotypes (i.e. $P1^{+/+}$, $P1^{+/-}$ and $P1^{-/-}$). As a result, there was relative confidence that VSMC PIEZO-1 was knocked out to have occurred in the transgenic mice. It was unexpected, that PIEZO-1 mRNA expression was no different between the 3 different mice genotypes on day 14 post-surgery. It was anticipated that the mRNA expression of PIEZO-1 would be the lowest in $P1^{-/-}$ mice aorta and highest in the $P1^{+/+}$ mice aorta.

The reasons behind the absence in PIEZO-1 knockout observed in the transgenic mice line must be considered and several plausible explanations have been outlined below. Firstly, VSMC PIEZO-1 knockout in the transgenic mice may have been unsuccessful. Alternative methods for validating PIEZO-1 knockout in aortic VSMCs should have been conducted as described in section 5.9.2. Secondly the mice aorta harvested were often contaminated

with peri-adventitial tissue, other cell types from the vessel was such as endothelial cells and even blood cells, despite efforts to clean and prepare the aorta during the harvesting process. Tissue contamination may therefore explain why no differences in PIEZO-1 mRNA expression were observed during qPCR. Thirdly, even with the successful knockout of PIEZO-1 in VSMCs, there may have been compensatory increases in PIEZO-2 activity that may explain the absence of any morphological differences observed. Finally, effect size of VSMC PIEZO-1 in aneurysmal vascular remodelling may be so small that despite using a relatively large cohort of transgenic mice, it was undetectable on ultrasound. This raises further questions regarding the clinical significance of any potential statistical differences (if any). Using a larger sample size would not have been ethically justifiable and contravened the 3 R's principle.

5.5. Relationship between PIEZO-1 and PIEZO-2

Both PIEZO-1 and PIEZO-2 are mechanosensitive calcium-permeable membrane channels. The mechanistic role of PIEZO-1 has been extensively described in vascular biology and PIEZO-2 in sensory neurobiology (Li et al., 2014; Woo et al., 2014). However, PIEZO-2 has also been suggested to play an important role in blood pressure management by regulating arterial baroreceptor activity and function in mice carotid sinus (Zeng et al,. 2018). Furthermore, a synergistic compensatory relationship has been previously described, where one channel may substitute for the other to maintain cellular homeostasis (Lee et al,. 2014). Therefore the disruption of one of the PIEZO mechanosensors may fail to demonstrate any functional disruption.

In this thesis, the expression of both PIEZO-1 and PIEZO-2 were observed in all tissue types utilised, which included NAVSMCs, AAAVSMCs, sham and PPE-treated aorta, from C57BL6/J mice and transgenic mice. The expression of PIEZO-2 mRNA was negligible compared to PIEZO-1 in baseline specimens as anticipated. However, there was an insignificant decrease in

the mRNA expression of PIEZO-1 and a significantly higher mRNA expression of PIEZO-2 in AAAVSMCs, compared with NAVSMCs. Similarly, when PIEZO-1 mRNA was successfully knocked down in NAVSMCs, using siRNA, a significant increase in PIEZO-2 mRNA expression was observed. These findings support a compensatory relationship between PIEZO-1 and PIEZO-2 as suggested by Lee et al,.2014. Whether there is a functional increase in the PIEZO-2 membrane protein could not be assessed as there was no known PIEZO-2 agonist, at the time of conducting the experiments, which could have been used to perform calcium imaging. A similar inverse relationship between PIEZO-1 and PIEZO-2 was observed in this thesis following prolonged activation of the PIEZO-1 mechanosensors in NAVSMCs with the PIEZO-1 agonist Yoda-1. In this experiment, PIEZO-1 mRNA expression was significantly elevated in NAVSMCs treated with Yoda-1 and PIEZO-2 mRNA expression was significantly reduced. This finding again supports the fact that there may be a reciprocal compensatory relationship between PIEZO-1 and PIEZO-2 in VSMC biology. To the best of my knowledge, this is the first time a co-dependent compensatory relationship like this between the PIEZO mechanosensors has been demonstrated in VSMCs.

The application of constant oscillatory shear stress on NAVSMCs, however, resulted in significant increases in both PIEZO-1 and PIEZO-2 mRNA expression and a functional increase in PIEZO-1-dependent intracellular calcium entry. Similarly, when NAVSMCs were cultured in serum-deprived media to mimic a hostile micro-environment, there was a significantly higher expression of PIEZO-1 and PIEZO-2 mRNA in NAVSMCs cultured in serum-deprived media compared to the standard culture media. These findings imply that both PIEZO-1 and PIEZO-2 may also function in unison supportively when the stressors applied to VASCs require them to do so. Additional alterations to the composition of the culture media were not attempted as the culture media came as a preformulated solution, which only required the addition of FBS and antibiotics. Furthermore, the constituents of the culture media were kept the same to minimise bias when comparing results from different experiments.

The observations from in vivo experiments also support the findings of the in vitro experiments. Following PPE induction surgery, wild-type mouse aorta had significantly increased expression of both PIEZO-1 and PIEZO-2 mRNA on day 7 compared with wild-type mice aorta following sham surgery. However, by day 14, the expression of PIEZO-1 mRNA was no longer elevated in aneurysmal aorta but the expression of PIEZO-2 remained significantly elevated. These findings suggest that although the mRNA expression of PIEZO-1 and PIEZO-2 may be initially concomitantly elevated, there is a gradual transition from PIEZO-1 to PIEZO-2 as the dominant mechanosensory apparatus in chronic disease processes. The increase in PIEZO-2 mRNA expression, from baseline, following AAA induction surgery was surprisingly comparable to the expression of PIEZO-1 mRNA. Furthermore, there was a significant strong positive correlation between the expression of PIEZO-2 mRNA and the aneurysmal aortic size in wild-type mice, which was not observed with PIEZO-1. Therefore, PIEZO-2 may in fact be central in the AAA disease process, contrary to the hypothesis. In the transgenic PIEZO-1 knockout mice, there was no evidence to suggest any compensatory changes to PIEZO-2 on day 14 following surgery. However, as previously discussed, the knockout of VSMC PIEZO-1 cannot be fully guaranteed based on the experiments conducted in this thesis. Furthermore, I would have wanted to perform additional experiments to harvest aorta on day 7 following surgery to quantify if there were any dynamic relationships between PIEZO-1 and PIEZO-2. However, as doubt over the knockout of VSMC PIEZO-1 in the transgenic mice was suspected, these additional experiments were not conducted.

The PIEZO-1 mechanosensor has been extensively described to play a mechanistic role in a variety of vascular pathologies and physiological processes in isolation (Kang et al., 2019; Shadrina et al., 2019; Retailleau et al., 2015). However, based on the findings in this thesis, it is evident that PIEZO-1 and PIEZO-2 may potentially play a shared role in these complex processes. They appear to support one another in either a synergistic or

compensatory manner dictated by the physiological demands of the environment. Unexpectedly, it was evident that PIEZO-2 may play an important role in the AAA disease process and this could have been evaluated further as described below in section 4.9.2. However, the findings of this thesis support the original hypothesis describing an anticipated participation of the PIEZO mechanosensors in response to mechanical stimuli. It is likely that PIEZO-1 acts as the predominant mechanosensory in VSMCs, however, when exhausted through chronic activation, PIEZO-2 may increase in a compensatory manner.

5.6. PIEZO-1 and VSMC Proliferation

It has previously been demonstrated by Riches et al, that end-stage AAAVSMCs have reduced cell proliferation capacity (39% reduction) compared to age-matched SVVSMCs (Riches et al., 2013). These findings were comparable to their assessment of VSMCs from the porcine AAA model (47% reduction) and controls (Riches et al., 2013). However, in this thesis when comparing the mRNA expression of KLF2 and KLF4, which are commonly associated with cell proliferation, the mRNA expression of KLF2 was significantly increased in AAAVSMCs compared with NAVSMCs and there was a trend towards a reduced expression of KLF4. It is difficult to explain the increase in KLF-2 mRNA expression in AAAVSMCs, as these cells have been traditionally shown to have reduced cell proliferation. Potential factors influencing these findings include the size of the AAA, indications for operative intervention and the patient co-morbidities such as diabetes.

Current UK guidelines recommend open aortic repair when the aortic sac size is equal to or more than 5.5 cm or where the annual sac expansion is greater than 0.5 cm. AAAs of various sizes are prevalent in the population due to the asymptomatic nature of the disease, especially in patients before the advent of the screening programme. VSMCs obtained from larger AAAs may have had longer exposure to mechanical stressors, therefore, influencing the

mRNA expression the PIEZO mechanosensors and proliferative markers being assessed. Furthermore, patients with diabetes have potentially high serum glucose levels and would be expected to have a higher VSMC proliferation rate (Faries et al., 2001; Wang, K. et al., 2017). These potential confounders may also help explain the variability in calcium movement observed in calcium imaging and qPCR experiments using AAAVSMCs.

Furthermore, in this thesis, normal aortic vascular smooth muscle cells were compared to AAAVSMCs, whereas in the study by Riches et al. (2013) AAAVSMCs were compared to SVVSMCs. It may be argued that VSMCs obtained from saphenous veins may have different properties to those from the aorta. Nevertheless, the exact origin of the aortic VSMCs was not specified by the supplier or manufacturer of the NAVSMCs utilised in this thesis, therefore, it is difficult to ascertain whether control VSMCs were from the infra-renal aorta. The region of the aorta the VSMCs were derived from is important as they have different embryological origins, which determines their phenotypical characteristics as previously described. Therefore, both control VSMC specimens from the saphenous veins and locations other than the infra-renal abdominal aorta could be a suboptimal comparison, resulting in inconclusive results.

It is well-established that during the formation of the abdominal aortic aneurysm sac, aortic VSMCs initially proliferate, allowing the vessel to remodel, dilate and expand (Lu, H. et al., 2021). In this thesis, NAVSMCs were encouraged to proliferate through controlled multiple cell passages to mimic this initial process. There were no significant differences between cell passage and KLF-2 mRNA expression. However, KLF-4 expression was lower in NAVSMCs at the higher cell passages, most likely due to physiological fatigue. No significant differences were observed in the expression of PIEZO-1 mRNA between cell passages. This was expected as PIEZO-1 is a mechanical flow sensor, therefore, in the absence of any flow application during the cell culture process, changes in PIEZO-1 mRNA expression would be unexpected. However, higher PIEZO-1 dependent intracellular calcium

entry was observed in NAVSMCs of lower cell culture passage. This may have been due to the PIEZO-1 membrane protein potentially becoming dysfunctional with each passage.

The application of constant oscillatory shear force to NAVSMCs for a sustained period resulted in the increased expression of both KLF-2 and KLF-4 mRNA. This suggests that the application of oscillatory force drives the increased proliferation seen in the initial phase of aneurysmal development. Similarly, prolonged treatment of NAVSMCs with Yoda-1 resulted in increased mRNA expression of both KLF-2 and KLF-4. Evidence of an initial increase in NAVSMC proliferation was observed in proliferation assays using Yoda-1. However, this was short-lived as cell proliferation plateaued and declined with continued stimulation. Overall, NAVSMC proliferation was significantly higher in cells treated with Yoda-1 compared to the control group and, subjectively, NAVSMCs behaved in a senescent manner like AAAVSMCs in later stages. This was potentially due to chronic stimulation and burnout of the PIEZO-1 mechanosensor, as previously described. This is further supported as a similar trend in mRNA expression of KLF-2 and KLF-4 was observed with PIEZO-1 siRNA knockdown.

The mice aorta following AAA induction surgery had larger aortas with a thickening of the tunica intima. The mRNA expression of KLF-4 was also significantly higher in C57BL6/J mice aorta on day 7 following aneurysm induction surgery, however this difference was no longer evident on day 14. This correlates with the morphological changes observed in the mice aorta where rapid dilatation occurs up to day 7 post-surgery followed by a period of slowed growth. This also supports the findings of the in vitro experiments, where an initial increase in KLF-2 and KLF-4 is demonstrated after the stimulation with PIEZO-1. The knockout of VSMC PIEZO-1 in transgenic mice did not result in any significant changes in aortic aneurysmal morphology or expression of mRNA markers of interest between genotypes. In addition to the explanations already described, it has been to be considered whether the activation of endothelial PIEZO-1 could influence VSMC physiology and

passing the need for VSMC PIEZO-1 modulation. The signalling pathways involving endothelial activation of PIEZO-1 and vascular remodelling are well established, therefore, must be considered (Retailleau et al., 2015; Qian et al., 2022).

5.7. PIEZO-1, TG2 and Stiffness

It has recently been demonstrated that cytoskeletal stiffening and subsequent activation of PIEZO-1 are mechanistically significant in the AAA disease process. Transglutaminases serve as scaffolds to maintain membrane integrity and adhesion. They also function in signal transduction (Eckert et al., 2014). TG2 is a marker of matrix stiffness, which has also been demonstrated to play a potential role in the AAA disease process. The results of this thesis suggest no association between the PIEZO mechanosensors and matrix stiffness as no significant differences in PIEZO-1 and PIEZO-2 mRNA expression were observed in NAVSMCs cultured in low and high matrix stiffnesses. Similarly, no significant differences in PIEZO-1-dependent intracellular calcium entry were observed between NAVSMCs cultured on different matrix stiffnesses. Surprisingly, the expression of TG2 was also significantly lower in AAAVSMCs than in NAVSMCs contrary to that previously described (Griffin et al., 2021). This may be explained due to PIEZO-1 is a sensor of shear stress and not stiffness, therefore, these results are not completely unexpected. However, matrix stiffness was found to be essential for cell survival and growth as a significant proportion of cells died when cultured on the plates with low matrix stiffness.

The mRNA expression of TG2 was found to be significantly higher in NAVSMCs with each passage during cell culture. This may be due to the increasing membrane stiffness observed with the cellular ageing process. Furthermore, the application of constant oscillatory force resulted in increased TG2 mRNA expression. This may be a reflection of cellular adaptation to maintain cell adhesion with the vessel base in the presence of the oscillatory

force. However, when treated with Yoda-1, there was reduced mRNA expression of TG2. Conversely, the siRNA knockdown of PIEZO-1 increased mRNA expression of TG2. The mechanisms to explain the latter finding is unclear, as one would have anticipated TG2 mRNA expression to increase to overcome cellular contraction initiated by the activation of PIEZO-1.

Aortic distensibility in mouse models was significantly reduced by day 7 compared to baseline assessment. No further deterioration in vessel distensibility was observed on day 14. There was a strong negative correlation between aortic size and aortic distensibility up to day 7. This trend was evident in both C57BL6/J and transgenic mice utilised in this thesis. These findings suggest that most of the anatomical and physiological remodelling involved in the AAA disease process are established by day 7 in mice models. Importantly, there was no relationship between aortic distensibility and PIEZO-1 mRNA expression. However, the expression of TG2 was significantly higher in C57BL6/J mice aorta with an aneurysm. This would be consistent with the increase in vessel distensibility observed as TG2 has been shown to be implicated in vessel stiffness.

5.8. Limitations of the Thesis

Before conducting the work described in this thesis, the wider laboratory group predominantly studied PIEZO-1 in endothelial cells, human embryonic kidney cells and adipocytes. This was the first time that someone in the group had studied PIEZO-1 in VSMCs. However, members of the team were experienced in studying calcium channels in VSMCs. Validation studies were required to adapt existing protocols, all of which could not be completed. This was primarily due to the universal restriction as a direct result of the COVID-19 pandemic and the immediate aftermath. It is also important to mention that this was the first time I had personally conducted laboratory-based research, and there was an anticipated learning curve in developing laboratory specific technical skills, which made technical validation of techniques pertinent to the

success of this thesis. The combination of these factors unfortunately impacted my ability to conduct certain experiments and validate the results obtained from some experiments.

Other than the logistical issues described, the content of this thesis was limited by the heterogeneity in results obtained from AAAVSMC experiments. PCR findings and PIEZO-1 dependent intracellular movement appeared to be more variable in AAAVSMCs compared to NAVSMCs, the reasons behind which is uncertain. Ideally AAAVSMCs should have utilised from a single homogenous sample to minimise any technical bias. However, these cells were very slow to replicate, which made it impractical and time consuming to only expand a single colony for experimentation. Multiple independent AAAVSMC samples were therefore used to ensure an adequate supply of experimental AAAVSMCs. This potentially introduced endogenous bias as patient co-morbidities and aortic characteristics from which the AAAVSMCs were unknow. Ideally, many of these variables should have been matched to minimise bias. The size of the human AAA the VSMCs were derived from may be a confounder, as VSMCs from larger AAA may be phenotypically different from those obtained from smaller aneurysms. Similarly, patient co-morbidities such as diabetes could impact cell proliferation and matrix stiffness (Faries et al., 2001; Sowers, 2013). Alternatively, a larger number of AAAVSMC samples could have been used to minimise the impact of potential unknown confounders. Furthermore, AAAVSMCs in experimental wells also often remained sparsely distributed despite time allowances to encourage them to form a confluent monolayer. This may have also impacted calcium imaging performed as a confluent uniform monolayer of cells is required. Additionally, NAVSMC were immunohistochemically stained for α-SMA, which alone does not confirm the cells utilised to be VSMCs as other cells such as myofibroblasts also express α-SMA. Other markers such as SM-MHC have been shown to be more specific (Wang, G. et al., 2015). Finally, the inability to functionally knockdown PIEZO-1 in NAVSMCs and questions regarding the knockdown of VSMC PIEZO-1 in-vevo significantly hindered the mechanistic interrogation of the hypothesis and validation of results obtained.

Despite these limitations, the thesis boasts many positive aspects. The influence of mechanical forces in relation to PIEZO-1 was investigated in a single homogeneous sample of NAVSMCs, which negated any baseline confounders. It is also reassuring that results obtained from in vitro experiments were supported by the findings of in vivo experiments. Furthermore, all experiments were conducted by a single researcher, negating any observer and technical bias. Experiments were also performed following a period of robust training delivered by experienced (i.e. more than 5 years post-doctoral) researchers. All experiments were initially performed under close inspection and guidance of the trainer before being performed independently by myself. However, it could be argued that a second observer may have been useful in detecting any technical errors in experiments conducted. Additionally, existing protocols, such as three-dimensional aortic ultrasound imaging, which was routinely utilised by the group were successfully validated and published. Finally, both in vitro and in vivo experiments were conducted in parallel. This allowed for well-powered interrogation of the hypothesis using a modest sample size of transgenic mice, as breeding the colony was started right at the beginning.

5.9. Further Work

Additional in vitro and in vivo experiments to support the findings in this thesis are much needed.

5.9.1. Further In-Vitro Experiments

Firstly, the inability to functionally knockdown PIEZO-1 in VSMCs in vitro requires troubleshooting to validate the findings observed with the application of chemical, mechanical and physiological stressors evaluated. Patch clamping of VSMCs following successful transfection and mRNA knockdown may help definitively assess and confirm physiological knockdown. Transfection with lipophectamine with siRNA PIEZO-1 sequences described

could be attempted as mRNA knockdown was also evident using this inexpensive method compared to Accell transfection. If successful functional knockdown of PIEZO-1 cannot be achieved, PIEZO-1 inhibition studies utilising either Ruthenium Red or GsMTx4 should be considered as it is important to validate these results (Bae et al., 2011). Secondly, as described above, the application of rhythmic dynamic axial force should also be considered. Unfortunately, I did not have the relevant apparatus in our laboratory to apply dynamic axial forces (i.e. stretch and relaxation phases to mimic arterial distension and relaxation). Our group was in the process of applying for funding and researching the feasibility of purchasing an apparatus that would have allowed these experiments to be performed. However, the time scale was out with the timeframe of this thesis. Finally, calcium imaging targeting the activation of the PIEZO-2 mechanosensor would be important in the future, if possible. There were indications of PIEZO-2 being potentially involved in the AAA disease process. Unfortunately, at the time of conducting the work in this thesis, there was no known PIEZO-2 agonist.

5.9.2. Further In Vivo Experiments

Firstly, the knockout of VSMC PIEZO-1 in the transgenic mice utilised needs to be conclusively validated. For example, VSMCs could have been isolated from the aorta of each of the 3 genotypes of transgenic mice and cultured, then treated with TAT-Cre before calcium imaging. This would specifically help demonstrate the functional knockdown of VSMC PIEZO-1. Alternatively, patch clamping could have been performed on individual VSMCs, pressure applied to activate the PIEZO-1 membrane protein and PIEZO-1-dependent calcium movement compared. Significantly less or no calcium movement would be expected in VSMCs from $P1^{-/-}$ mice aorta due to the absence of the channel and normal calcium movement would be expected in VSMCs obtained from the aortae of $P1^{+/+}$ transgenic mice. Additionally, the VSMC PIEZO-1 knockout mice could have been cross-bred with the mice line with HLA-tagged PIEZO-1 membrane proteins our laboratory processes. This would have allowed for immunohistochemical validation of successful knockout and quantification of

membrane proteins using western blotting. Our laboratory had prior experience in all three validation methods described, but due to the restrictions imposed by the COVID-19 pandemic and the consequences of the immediate aftermath limiting access to facilities, it was not possible to perform these experiments. Alternatively, VSMC PIEZO-1 knockout mice could have been purchased from pre-validated stocks of commercial suppliers.

If conclusive evidence of VSMC PIEZO-1 cannot be demonstrated, then Yoda-1 infusion or of an equivalent analogue should be considered into mice AAA models. Aortic tissue from transgenic mice or an equivalent model would need to be assessed on day 7 to evaluate any dynamic changes as demonstrated in this thesis. Unfortunately, histological assessment with H&E staining of mice aorta obtained from wild-type and transgenic mice was incomplete. Therefore, statistical assessment of the constituent vessel layers could not be performed. Additional histological staining with Masson trichrome stain could also have been used to specifically stain VSMCs that would have made it more easily quantifiable. Finally, there is strong evidence to suggest that PIEZO-2 plays a role in the AAA disease process, therefore, PIEZO-2 knockout mice should be considered to evaluate the relationships identified further.

5.10. Conclusions

The role of PEIZO-1 in the aneurysm disease process may be transient and potentially of little clinical significance. Constant oscillatory shear force and cell culture in serum-deprived media resulted in increased P1 activity. Activation of P1 was associated with reduced proliferation. Increased P1 expression was observed in the aneurysmal aorta initially and later lost. The results of this thesis unfortunately could not be validated due to the inability to attain functional knockdown of P1 in VSMCs and uncertainty regarding VSMC P1 knockdown in transgenic mice. Further investigation is required to ascertain the findings within this thesis and draw valid mechanistic conclusions describing the relationship between PIEZIO-1 and AAA disease.

References

Amirbekian, S., Long Jr, R.C., Consolini, M.A., Suo, J., Willett, N.J., Fielden, S.W., Giddens, D.P., Taylor, W.R. and Oshinski, J.N. 2009. In vivo assessment of blood flow patterns in abdominal aorta of mice with MRI: implications for AAA localization. *American Journal of Physiology-Heart and Circulatory Physiology.* **297**(4), pp.H1290-H1295.

Anidjar, S., Salzmann, J.-L., Gentric, D., Lagneau, P., Camilleri, J.-P. and Michel, J.-B. 1990. Elastase-induced experimental aneurysms in rats. *Circulation.* **82**(3), pp.973-981.

Anwar, M., Shalhoub, J., Lim, C., Gohel, M. and Davies, A. 2012. The effect of pressure-induced mechanical stretch on vascular wall differential gene expression. *Journal of vascular research.* **49**(6), pp.463-478.

Armstrong Filho, D.M., Sikka, G., Armstrong, A.d.C., Saad, K.R., Freitas, W.R.d., Berkowitz, D.E., Fagundes, D.J., Santhanam, L. and Taha, M.O. 2018. Knockdown of transglutaminase-2 prevents early age-induced vascular changes in mice. *Acta Cirúrgica Brasileira.* **33**, pp.991-999.

Bacakova, L., Travnickova, M., Filova, E., Matějka, R., Stepanovska, J., Musilkova, J., Zarubova, J. and Molitor, M. 2018. The role of vascular smooth muscle cells in the physiology and pathophysiology of blood vessels. *Muscle Cell and Tissue-Current Status of Research Field.* **1**, p13.

Bae, C., Sachs, F. and Gottlieb, P.A. 2011. The mechanosensitive ion channel Piezo1 is inhibited by the peptide GsMTx4. *Biochemistry.* **50**(29), pp.6295-6300.

Bahia, S.S., Vidal-Diez, A., Seshasai, S.R., Shpitser, I., Brownrigg, J.R., Patterson, B.O., Ray, K.K., Holt, P.J., Thompson, M.M. and Karthikesalingam, A. 2016. Cardiovascular risk prevention and all-cause mortality in primary care patients with an abdominal aortic aneurysm. *Journal of British Surgery.* **103**(12), pp.1626-1633.

Bailey, M.A., Baxter, P.D., Jiang, T., Charnell, A.M., Griffin, K.J., Johnson, A.B., Bridge, K.I., Sohrabi, S. and Scott, D.J.A. 2013. Modeling the growth of infrarenal abdominal aortic aneurysms. *Aorta.* **1**(06), pp.268-273.

Bakker, E.N., Buus, C.L., Spaan, J.A., Perree, J., Ganga, A., Rolf, T.M., Sorop, O., Bramsen, L.H., Mulvany, M.J. and VanBavel, E. 2005. Small artery remodeling depends on tissue-type transglutaminase. *Circulation research.* **96**(1), pp.119-126.

Bappoo, N., Syed, M., Khinsoe, G., Kelsey, L., Forsythe, R., Powell, J., Conlisk, N., Hoskins, P., McBride, O. and Shah, A. 2022. Low Shear Stress at Baseline is Associated with Aortic Expansion and Aneurysm Related Events in Patients with Abdominal Aortic Aneurysms. *European Journal of Vascular and Endovascular Surgery.* **63**(2), pe28.

Beech, D.J. 2018. Endothelial Piezo1 channels as sensors of exercise. *The Journal of Physiology.* **596**(6), pp.979-984.

Beech, D.J. and Kalli, A.C. 2019. Force sensing by piezo channels in cardiovascular health and disease. *Arteriosclerosis, thrombosis, and vascular biology.* **39**(11), pp.2228-2239.

Bennett, M.R., Sinha, S. and Owens, G.K. 2016. Vascular smooth muscle cells in atherosclerosis. *Circulation Research.* **118**(4), pp.692-702.

Bhamidipati, C.M., Mehta, G.S., Lu, G., Moehle, C.W., Barbery, C., DiMusto, P.D., Laser, A., Kron, I.L., Upchurch Jr, G.R. and Ailawadi, G. 2012. Development of a novel murine model of aortic aneurysms using peri-adventitial elastase. *Surgery.* **152**(2), pp.238-246.

Bhatnagar, P., Wickramasinghe, K., Wilkins, E. and Townsend, N. 2016. Trends in the epidemiology of cardiovascular disease in the UK. *Heart.* **102**(24), pp.1945-1952.

Boucher, P., Gotthardt, M., Li, W.-P., Anderson, R.G. and Herz, J. 2003. LRP: role in vascular wall integrity and protection from atherosclerosis. *Science.* **300**(5617), pp.329-332.

Boussel, L., Rayz, V., McCulloch, C., Martin, A., Acevedo-Bolton, G., Lawton, M., Higashida, R., Smith, W.S., Young, W.L. and Saloner, D. 2008. Aneurysm growth occurs at region of low wall shear stress: patient-specific correlation of hemodynamics and growth in a longitudinal study. *Stroke.* **39**(11), pp.2997-3002.

Bown, M.J., Jones, G.T., Harrison, S.C., Wright, B.J., Bumpstead, S., Baas, A.F., Gretarsdottir, S., Badger, S.A., Bradley, D.T. and Burnand, K. 2011. Abdominal aortic aneurysm is associated with a variant in low-density

lipoprotein receptor-related protein 1. *The American Journal of Human Genetics.* **89**(5), pp.619-627.

Brayden, J.E., Earley, S., Nelson, M.T. and Reading, S. 2008. Transient receptor potential (TRP) channels, vascular tone and autoregulation of cerebral blood flow. *Clinical and Experimental Pharmacology and Physiology.* **35**(9), pp.1116-1120.

Brohawn, S.G. 2015. How ion channels sense mechanical force: insights from mechanosensitive K2P channels TRAAK, TREK1, and TREK2. *Annals of the New York Academy of Sciences.* **1352**(1), pp.20-32.

Bulley, S., Fernández-Peña, C., Hasan, R., Leo, M.D., Muralidharan, P., Mackay, C.E., Evanson, K.W., Moreira-Junior, L., Mata-Daboin, A. and Burris, S.K. 2018. Arterial smooth muscle cell PKD2 (TRPP1) channels regulate systemic blood pressure. *Elife.* **7**, pe42628.

Burg, E., Remillard, C. and Yuan, J.J. 2008. Potassium channels in the regulation of pulmonary artery smooth muscle cell proliferation and apoptosis: pharmacotherapeutic implications. *British journal of pharmacology.* **153**(S1), pp.S99-S111.

Busch, A., Bleichert, S., Ibrahim, N., Wortmann, M., Eckstein, H.-H., Brostjan, C., Wagenhäuser, M.U., Goergen, C.J. and Maegdefessel, L. 2021. Translating mouse models of abdominal aortic aneurysm to the translational needs of vascular surgery. *JVS: Vascular Science.* **2**, pp.219-234.

Busch, A., Chernogubova, E., Jin, H., Meurer, F., Eckstein, H.-H., Kim, M. and Maegdefessel, L. 2018. Four surgical modifications to the classic elastase perfusion aneurysm model enable haemodynamic alterations and extended elastase perfusion. *European Journal of Vascular and Endovascular Surgery.* **56**(1), pp.102-109.

Butlin, M. and Avolio, A.P. 2015. Age-related changes in the mechanical properties of large arteries. *Mechanical properties of aging soft tissues.* Springer, pp.37-74.

Chen, Y., Ju, L., Rushdi, M., Ge, C. and Zhu, C. 2017. Receptor-mediated cell mechanosensing. *Molecular biology of the cell.* **28**(23), pp.3134-3155.

Chiou, A.C., Chiu, B. and Pearce, W.H. 2001. Murine aortic aneurysm produced by periarterial application of calcium chloride. *Journal of Surgical Research.* **99**(2), pp.371-376.

Choi, D., Park, E., Jung, E., Cha, B., Lee, S., Yu, J., Kim, P.M., Lee, S., Hong, Y.J. and Koh, C.J. 2019. Piezo1 incorporates mechanical force signals into the genetic program that governs lymphatic valve development and maintenance. *JCI insight.* **4**(5).

Coselli, J.S. and Green, S.Y. 2013. A brief history of aortic surgery: Insight into distal aortic repair. *The Journal of thoracic and cardiovascular surgery.* **145**(3), pp.S123-S125.

Coste, B., Mathur, J., Schmidt, M., Earley, T.J., Ranade, S., Petrus, M.J., Dubin, A.E. and Patapoutian, A. 2010. Piezo1 and Piezo2 are essential components of distinct mechanically activated cation channels. *Science.* **330**(6000), pp.55-60.

Coughlin, P., Jackson, D., White, A., Bailey, M., Farrow, C., Scott, D. and Howell, S. 2013. Meta-analysis of prospective trials determining the short-and mid-term effect of elective open and endovascular repair of abdominal aortic aneurysms on quality of life. *British Journal of Surgery.* **100**(4), pp.448-455.

Crow, M. 1996. Atherosclerosis and the vascular biology of aging. *Aging clinical and experimental research.* **8**(4), pp.221-234.

Dalton, M.L., Gadson Jr, P.F., Wrenn, R.W. and Rosenquist, T.H. 1997. Homocysteine signal cascade: production of phospholipids, activation of protein kinase C, and the induction of c-fos and c-myb in smooth muscle cells. *The FASEB journal.* **11**(8), pp.703-711.

Daugherty, A. and Cassis, L.A. 2004. Mouse models of abdominal aortic aneurysms. *Arteriosclerosis, thrombosis, and vascular biology.* **24**(3), pp.429-434.

De Bruin, J.L., Baas, A.F., Buth, J., Prinssen, M., Verhoeven, E.L., Cuypers, P.W., van Sambeek, M.R., Balm, R., Grobbee, D.E. and Blankensteijn, J.D. 2010. Long-term outcome of open or endovascular repair of abdominal aortic aneurysm. *New England Journal of Medicine.* **362**(20), pp.1881-1889.

De Ceniga, M.V., Gomez, R., Estallo, L., Rodriguez, L., Baquer, M. and Barba, A. 2006. Growth rate and associated factors in small abdominal aortic aneurysms. *European Journal of Vascular Endovascular Surgery.* **31**(3), pp.231-236.

Desjardins, P. and Conklin, D. 2010. NanoDrop microvolume quantitation of nucleic acids. *JoVE.* (45), pe2565.

Dietrich, A., Mederos y Schnitzler, M., Gollasch, M., Gross, V., Storch, U., Dubrovska, G., Obst, M., Yildirim, E., Salanova, B. and Kalwa, H. 2005. Increased vascular smooth muscle contractility in TRPC6−/− mice. *Molecular and cellular biology.* **25**(16), pp.6980-6989.

Doevendans, P.A., J. Daemen, M., de Muinck, E.D. and Smits, J.F. 1998. Cardiovascular phenotyping in mice. *Cardiovascular research.* **39**(1), pp.34-49.

Douguet, D., Patel, A., Xu, A., Vanhoutte, P.M. and Honoré, E. 2019. Piezo ion channels in cardiovascular mechanobiology. *Trends in pharmacological sciences.* **40**(12), pp.956-970.

Doyle, B.J., Callanan, A., Burke, P.E., Grace, P.A., Walsh, M.T., Vorp, D.A. and McGloughlin, T.M. 2009. Vessel asymmetry as an additional diagnostic tool in the assessment of abdominal aortic aneurysms. *Journal of Vascular Surgery.* **49**(2), pp.443-454.

Drummond, H.A., Grifoni, S.C. and Jernigan, N.L. 2008. A new trick for an old dogma: ENaC proteins as mechanotransducers in vascular smooth muscle. *Physiology.* **23**(1), pp.23-31.

Duchemin, A.-L., Vignes, H. and Vermot, J. 2019. Mechanically activated piezo channels modulate outflow tract valve development through the Yap1 and Klf2-Notch signaling axis. *Elife.* **8**, pe44706.

Earley, S. and Brayden, J.E. 2015. Transient receptor potential channels in the vasculature. *Physiological reviews.* **95**(2), pp.645-690.

Eckert, R.L., Kaartinen, M.T., Nurminskaya, M., Belkin, A.M., Colak, G., Johnson, G.V. and Mehta, K. 2014. Transglutaminase regulation of cell function. *Physiological reviews.* **94**(2), pp.383-417.

Evans, E.L., Cuthbertson, K., Endesh, N., Rode, B., Blythe, N.M., Hyman, A.J., Hall, S.J., Gaunt, H.J., Ludlow, M.J. and Foster, R. 2018. Yoda1 analogue (D ooku1) which antagonizes Y oda1-evoked activation of P iezo1 and aortic relaxation. *British journal of pharmacology.* **175**(10), pp.1744-1759.

EVAR Trial Investigators. 2010. Endovascular repair of aortic aneurysm in patients physically ineligible for open repair. *New England Journal of Medicine.* **362**(20), pp.1872-1880.

Fang, Y., Wu, D. and Birukov, K.G. 2019. Mechanosensing and Mechanoregulation of Endothelial Cell Functions. *Comprehensive Physiology.* **9**, pp.873-904.

Faries, P.L., Rohan, D.I., Takahara, H., Wyers, M.C., Contreras, M.A., Quist, W.C., King, G.L. and LoGerfo, F.W. 2001. Human vascular smooth muscle cells of diabetic origin exhibit increased proliferation, adhesion, and migration. *Journal of vascular surgery.* **33**(3), pp.601-607.

Filardo, G., Powell, J.T., Martinez, M.A.M. and Ballard, D.J. 2015. Surgery for small asymptomatic abdominal aortic aneurysms. *Cochrane Database of Systematic Reviews.* (2).

Fillinger, M.F., Marra, S.P., Raghavan, M.L. and Kennedy, F.E. 2003. Prediction of rupture risk in abdominal aortic aneurysm during observation: wall stress versus diameter. *Journal of vascular surgery.* **37**(4), pp.724-732.

Fillinger, M.F., Raghavan, M.L., Marra, S.P., Cronenwett, J.L. and Kennedy, F.E. 2002. In vivo analysis of mechanical wall stress and abdominal aortic aneurysm rupture risk. *Journal of vascular surgery.* **36**(3), pp.589-597.

Fitzgibbon, G.M., Kafka, H.P., Leach, A.J., Keon, W.J., Hooper, G.D. and Burton, J.R. 1996. Coronary bypass graft fate and patient outcome: angiographic follow-up of 5,065 grafts related to survival and reoperation in 1,388 patients during 25 years. *Journal of the American College of Cardiology.* **28**(3), pp.616-626.

Folkow, B. 1964. Description of the myogenic hypothesis. *Circ Res.* **15**(1), pp.279-287.

Franck, G., Dai, J., Fifre, A., Ngo, S., Justine, C., Michineau, S., Allaire, E. and Gervais, M. 2013. Reestablishment of the endothelial lining by endothelial cell therapy stabilizes experimental abdominal aortic aneurysms. *Circulation.* **127**(18), pp.1877-1887.

Frutkin, A.D., Shi, H., Otsuka, G. and Dichek, D.A. 2007. Targeted rearrangement of floxed alleles in smooth muscle cells in vivo. *Circulation Research.* **101**(12), pp.e124-e125.

Fukaya, E., Flores, A.M., Lindholm, D., Gustafsson, S., Zanetti, D., Ingelsson, E. and Leeper, N.J. 2018. Clinical and genetic determinants of varicose veins: prospective, community-based study of≈ 500 000 individuals. *Circulation.* **138**(25), pp.2869-2880.

Giannoglou, G., Giannakoulas, G., Soulis, J., Chatzizisis, Y., Perdikides, T., Melas, N., Parcharidis, G. and Louridas, G. 2006. Predicting the risk of rupture of abdominal aortic aneurysms by utilizing various geometrical parameters: revisiting the diameter criterion. *Angiology.* **57**(4), pp.487-494.

Gnanasambandam, R., Ghatak, C., Yasmann, A., Nishizawa, K., Sachs, F., Ladokhin, A.S., Sukharev, S.I. and Suchyna, T.M. 2017. GsMTx4: mechanism of inhibiting mechanosensitive ion channels. *Biophysical journal.* **112**(1), pp.31-45.

Goergen, C.J., Johnson, B.L., Greve, J.M., Taylor, C.A. and Zarins, C.K. 2007. Increased anterior abdominal aortic wall motion: possible role in aneurysm pathogenesis and design of endovascular devices. *Journal of Endovascular Therapy.* **14**(4), pp.574-584.

Goldenberg, N.M., Wang, L., Ranke, H., Liedtke, W., Tabuchi, A. and Kuebler, W.M. 2015. TRPV4 is required for hypoxic pulmonary vasoconstriction. *Anesthesiology.* **122**(6), pp.1338-1348.

Golledge, J., Moxon, J., Pinchbeck, J., Anderson, G., Rowbotham, S., Jenkins, J., Bourke, M., Bourke, B., Dear, A. and Buckenham, T. 2017. Association between metformin prescription and growth rates of abdominal aortic aneurysms. *Journal of British Surgery.* **104**(11), pp.1486-1493.

Gomez, D. and Owens, G.K. 2012. Smooth muscle cell phenotypic switching in atherosclerosis. *Cardiovascular research.* **95**(2), pp.156-164.

Greenhalgh, R. 2004. Comparison of endovascular aneurysm repair with open repair in patients with abdominal aortic aneurysm (EVAR trial 1), 30-day operative mortality results: randomised controlled trial. *The Lancet.* **364**(9437), pp.843-848.

Greenhalgh, R., Brown, L., Epstein, D., Kwong, G., Powell, J. and Sculpher, M. 2005. Endovascular aneurysm repair and outcome in patients unfit for open repair of abdominal aortic aneurysm (EVAR trial 2): randomised controlled trial. *The Lancet.* **365**(9478), pp.2187-2192.

Greenwald, S. 2007. Ageing of the conduit arteries. *The Journal of Pathology: A Journal of the Pathological Society of Great Britain and Ireland.* **211**(2), pp.157-172.

Griffin, K.J., Simpson, K.R., Beckers, C.M., Newell, L.M., Cheah, L.T., Yuldasheva, N.Y., Iismaa, S., Jackson, C.L., Scott, J.D. and Pease, R.J. 2021.

Transglutaminase 2 moderates the expansion of mouse abdominal aortic aneurysms. *JVS: Vascular Science.* **2**, pp.95-109.

Grishagin, I.V. 2015. Automatic cell counting with ImageJ. *Analytical biochemistry.* **473**, pp.63-65.

Gurney, A. and Manoury, B. 2009. Two-pore potassium channels in the cardiovascular system. *European Biophysics Journal.* **38**(3), pp.305-318.

Hellström, M., Kalén, M. and Lindahl, P. 1999. Abramsson, a & Betsholtz, C. Role of PDGF-B and PDGFR-beta in recruitment of vascular smooth muscle cells and pericytes during embryonic blood vessel formation in the mouse. *Development.* **126**(14), pp.3047-3055.

Hernesniemi, J.A., Vänni, V. and Hakala, T. 2015. The prevalence of abdominal aortic aneurysm is consistently high among patients with coronary artery disease. *Journal of vascular surgery.* **62**(1), pp.232-240. e233.

Hill-Eubanks, D.C., Werner, M.E., Heppner, T.J. and Nelson, M.T. 2011. Calcium signaling in smooth muscle. *Cold Spring Harbor perspectives in biology.* **3**(9), pa004549.

Hinchliffe, R. and Earnshaw, J. 2020. Endovascular treatment of abdominal aortic aneurysm: a NICE U-turn. *Journal of British Surgery.* **107**(8), pp.940-942.

Hinnen, J.-W., Koning, O.H., Visser, M.J. and Van Bockel, H.J. 2005. Effect of intraluminal thrombus on pressure transmission in the abdominal aortic aneurysm. *Journal of vascular surgery.* **42**(6), pp.1176-1182.

Humphrey, J.D. and Holzapfel, G.A. 2012. Mechanics, mechanobiology, and modeling of human abdominal aorta and aneurysms. *Journal of biomechanics.* **45**(5), pp.805-814.

Humphrey, J.D., Schwartz, M.A., Tellides, G. and Milewicz, D.M. 2015. Role of mechanotransduction in vascular biology: focus on thoracic aortic aneurysms and dissections. *Circulation Research.* **116**(8), pp.1448-1461.

Iismaa, S.E., Mearns, B.M., Lorand, L. and Graham, R.M. 2009. Transglutaminases and disease: lessons from genetically engineered mouse models and inherited disorders. *Physiological reviews.* **89**(3), pp.991-1023.

Ilkan, Z., Wright, J.R., Goodall, A.H., Gibbins, J.M., Jones, C.I. and Mahaut-Smith, M.P. 2017. Evidence for shear-mediated Ca2+ entry through

mechanosensitive cation channels in human platelets and a megakaryocytic cell line. *Journal of Biological Chemistry.* **292**(22), pp.9204-9217.

Investigators, I.T. 2014. Endovascular or open repair strategy for ruptured abdominal aortic aneurysm: 30 day outcomes from IMPROVE randomised trial. *BMJ.* **348**, pf7661.

Jacomelli, J., Summers, L., Stevenson, A., Lees, T. and Earnshaw, J. 2016. Impact of the first 5 years of a national abdominal aortic aneurysm screening programme. *British Journal of Surgery.* **103**(9), pp.1125-1131.

Johnston, K.W., Rutherford, R.B., Tilson, M.D., Shah, D.M., Hollier, L. and Stanley, J.C. 1991. Suggested standards for reporting on arterial aneurysms. *Journal of vascular surgery.* **13**(3), pp.452-458.

Jones, G.T., Tromp, G., Kuivaniemi, H., Gretarsdottir, S., Baas, A.F., Giusti, B., Strauss, E., van 't Hof, F.N., Webb, T.R. and Erdman, R. 2017. Meta-analysis of genome-wide association studies for abdominal aortic aneurysm identifies four new disease-specific risk loci. *Circulation Research.* **120**(2), pp.341-353.

Jongkind, V., Yeung, K.K., Akkersdijk, G.J., Heidsieck, D., Reitsma, J.B., Tangelder, G.J. and Wisselink, W. 2010. Juxtarenal aortic aneurysm repair. *Journal of vascular surgery.* **52**(3), pp.760-767.

Kaess, B.M., Rong, J., Larson, M.G., Hamburg, N.M., Vita, J.A., Levy, D., Benjamin, E.J., Vasan, R.S. and Mitchell, G.F. 2012. Aortic stiffness, blood pressure progression, and incident hypertension. *Jama.* **308**(9), pp.875-881.

Kang, H., Hong, Z., Zhong, M., Klomp, J., Bayless, K.J., Mehta, D., Karginov, A.V., Hu, G. and Malik, A.B. 2019. Piezo1 mediates angiogenesis through activation of MT1-MMP signaling. *American Journal of Physiology-Cell Physiology.* **316**(1), pp.C92-C103.

Kazmers, A., Perkins, A.J. and Jacobs, L.A. 1998. Outcomes after abdominal aortic aneurysm repair in those≥ 80 years of age: recent Veterans Affairs experience. *Annals of vascular surgery.* **12**(2), pp.106-112.

Kent, K.C., Zwolak, R.M., Egorova, N.N., Riles, T.S., Manganaro, A., Moskowitz, A.J., Gelijns, A.C. and Greco, G. 2010. Analysis of risk factors for abdominal aortic aneurysm in a cohort of more than 3 million individuals. *Journal of vascular surgery.* **52**(3), pp.539-548.

Khosla, S., Morris, D., Moxon, J., Walker, P.J., Gasser, T. and Golledge, J. 2014. Meta-analysis of peak wall stress in ruptured, symptomatic and intact abdominal aortic aneurysms. *J British Journal of Surgery.* **101**(11), pp.1350-1357.

Korneva, A. and Humphrey, J.D. 2019. Maladaptive aortic remodeling in hypertension associates with dysfunctional smooth muscle contractility. *American Journal of Physiology-Heart and Circulatory Physiology.* **316**(2), pp.H265-H278.

Kuivaniemi, H., Ryer, E.J., Elmore, J.R. and Tromp, G. 2015. Understanding the pathogenesis of abdominal aortic aneurysms. *Expert review of cardiovascular therapy.* **13**(9), pp.975-987.

Kuo, C.T., Veselits, M.L., Barton, K.P., Lu, M.M., Clendenin, C. and Leiden, J.M. 1997. The LKLF transcription factor is required for normal tunica media formation and blood vessel stabilization during murine embryogenesis. *Genes & development.* **11**(22), pp.2996-3006.

Lacroix, J.J., Botello-Smith, W.M. and Luo, Y. 2018. Probing the gating mechanism of the mechanosensitive channel Piezo1 with the small molecule Yoda1. *Nature Communications.* **9**(1), p2029.

Lederle, F. 2012. *The strange relationship between diabetes and abdominal aortic aneurysm*. Elsevier. 43. pp.254-256.

Lederle, F.A. 2013. Abdominal aortic aneurysm: still no pill. *Annals of Internal Medicine.* **159**(12), pp.852-853.

Lederle, F.A., Freischlag, J.A., Kyriakides, T.C., Matsumura, J.S., Padberg Jr, F.T., Kohler, T.R., Kougias, P., Jean-Claude, J.M., Cikrit, D.F. and Swanson, K.M. 2012. Long-term comparison of endovascular and open repair of abdominal aortic aneurysm. *N Engl J Med.* **367**, pp.1988-1997.

Lederle, F.A., Freischlag, J.A., Kyriakides, T.C., Padberg, F.T., Matsumura, J.S., Kohler, T.R., Lin, P.H., Jean-Claude, J.M., Cikrit, D.F. and Swanson, K.M. 2009. Outcomes following endovascular vs open repair of abdominal aortic aneurysm: a randomized trial. *Jama.* **302**(14), pp.1535-1542.

Lederle, F.A., Johnson, G.R., Wilson, S.E., Acher, C.W., Ballard, D.J., Littooy, F.N., Messina, L.M. and Study, M.V.A.C. 2003a. Quality of life, impotence, and activity level in a randomized trial of immediate repair versus surveillance

of small abdominal aortic aneurysm. *Journal of vascular surgery.* **38**(4), pp.745-752.

Lederle, F.A., Johnson, G.R., Wilson, S.E., Ballard, D.J., Jordan Jr, W.D., Blebea, J., Littooy, F.N., Freischlag, J.A., Bandyk, D. and Rapp, J.H. 2002. Rupture rate of large abdominal aortic aneurysms in patients refusing or unfit for elective repair. *Jama.* **287**(22), pp.2968-2972.

Lederle, F.A., Kyriakides, T.C., Stroupe, K.T., Freischlag, J.A., Padberg Jr, F.T., Matsumura, J.S., Huo, Z. and Johnson, G.R. 2019. Open versus endovascular repair of abdominal aortic aneurysm. *New England Journal of Medicine.* **380**(22), pp.2126-2135.

Lederle, F.A., Nelson, D.B. and Joseph, A.M. 2003b. Smokers' relative risk for aortic aneurysm compared with other smoking-related diseases: a systematic review. *Journal of vascular surgery.* **38**(2), pp.329-334.

Lee, J.S., Yu, Q., Shin, J.T., Sebzda, E., Bertozzi, C., Chen, M., Mericko, P., Stadtfeld, M., Zhou, D. and Cheng, L. 2006. Klf2 is an essential regulator of vascular hemodynamic forces in vivo. *Developmental cell.* **11**(6), pp.845-857.

Lee, W., Leddy, H.A., Chen, Y., Lee, S.H., Zelenski, N.A., McNulty, A.L., Wu, J., Beicker, K.N., Coles, J. and Zauscher, S. 2014. Synergy between Piezo1 and Piezo2 channels confers high-strain mechanosensitivity to articular cartilage. *Proceedings of the National Academy of Sciences.* **111**(47), pp.E5114-E5122.

Li, J., Hou, B., Tumova, S., Muraki, K., Bruns, A., Ludlow, M.J., Sedo, A., Hyman, A.J., McKeown, L. and Young, R.S. 2014. Piezo1 integration of vascular architecture with physiological force. *Nature.* **515**(7526), p279.

Lipsitz, L.A. 1989. Orthostatic hypotension in the elderly. *New England Journal of Medicine.* **321**(14), pp.952-957.

Louis, K.S. and Siegel, A.C. 2011. Cell viability analysis using trypan blue: manual and automated methods. *Mammalian cell viability.* Springer, pp.7-12.

Lu, G., Su, G., Davis, J.P., Schaheen, B., Downs, E., Roy, R.J., Ailawadi, G. and Upchurch Jr, G.R. 2017. A novel chronic advanced stage abdominal aortic aneurysm murine model. *Journal of vascular surgery.* **66**(1), pp.232-242. e234.

Lu, H., Du, W., Ren, L., Hamblin, M.H., Becker, R.C., Chen, Y.E. and Fan, Y. 2021. Vascular smooth muscle cells in aortic aneurysm: from genetics to mechanisms. *Journal of the American Heart Association.* **10**(24), pe023601.

Lucitti, J.L., Jones, E.A., Huang, C., Chen, J., Fraser, S.E. and Dickinson, M.E. 2007. Vascular remodeling of the mouse yolk sac requires hemodynamic force.

Ma, L., Roman-Campos, D., Austin, E.D., Eyries, M., Sampson, K.S., Soubrier, F., Germain, M., Trégouët, D.-A., Borczuk, A. and Rosenzweig, E.B. 2013. A novel channelopathy in pulmonary arterial hypertension. *N Engl J Med.* **369**, pp.351-361.

Majesky, M.W., Lindner, V., Twardzik, D.R., Schwartz, S.M. and Reidy, M.A. 1991. Production of transforming growth factor beta 1 during repair of arterial injury. *The Journal of clinical investigation.* **88**(3), pp.904-910.

Martín-Bórnez, M., Galeano-Otero, I., Del Toro, R. and Smani, T. 2020. TRPC and TRPV channels' role in vascular remodeling and disease. *International Journal of Molecular Sciences.* **21**(17), p6125.

Massagué, J. 2012. TGFβ signalling in context. *Nature reviews Molecular cell biology.* **13**(10), pp.616-630.

Mathie, A. and Veale, E.L. 2007. Therapeutic potential of neuronal two-pore domain potassium-channel modulators. *Current opinion in investigational drugs (London, England: 2000).* **8**(7), pp.555-562.

McDonald, D. 1968. Regional pulse-wave velocity in the arterial tree. *Journal of Applied Physiology.* **24**(1), pp.73-78.

Meijer, C.A., Stijnen, T., Wasser, M., Hamming, J.F., van Bockel, J.H. and Lindeman, J. 2013. Doxycycline for stablization of abdominal aortic aneurysms. *Ann Intern Med.* **159**, pp.815-823.

Merali, F.S. and Anand, S.S. 2002. Immediate repair compared with surveillance of small abdominal aortic aneurysms. *Vascular medicine (London, England).* **7**(3), pp.249-250.

Milewicz, D.M., Trybus, K.M., Guo, D.-c., Sweeney, H.L., Regalado, E., Kamm, K. and Stull, J.T. 2017. Altered smooth muscle cell force generation as a driver of thoracic aortic aneurysms and dissections. *Arteriosclerosis, thrombosis, and vascular biology.* **37**(1), pp.26-34.

Moehle, C.W. and Owens, G.K. 2009. Krüppel-like Factors KLF2, KLF4, and KLF5: Central Regulators of Smooth Muscle Function. *The Biology of Krüppel-like Factors.* pp.185-204.

Mohanta, S., Yin, C., Weber, C., Hu, D. and Habenicht, A.J. 2016. Aorta atherosclerosis lesion analysis in hyperlipidemic mice. *Bio-protocol.* **6**(11).

Moll, F.L., Powell, J.T., Fraedrich, G., Verzini, F., Haulon, S., Waltham, M., van Herwaarden, J.A., Holt, P.J., van Keulen, J.W. and Rantner, B. 2011a. Management of abdominal aortic aneurysms clinical practice guidelines of the European society for vascular surgery. *European Journal of Vascular Endovascular Surgery.* **41**, pp.S1-S58.

Moll, F.L., Powell, J.T., Fraedrich, G., Verzini, F., Haulon, S., Waltham, M., van Herwaarden, J.A., Holt, P.J., van Keulen, J.W. and Rantner, B. 2011b. Management of abdominal aortic aneurysms clinical practice guidelines of the European society for vascular surgery. *European journal of vascular and endovascular surgery.* **41**, pp.S1-S58.

Munezane, T., Hasegawa, T., Tanaka, A., Okada, K. and Okita, Y. 2010. Activation of transglutaminase type 2 for aortic wall protection in a rat abdominal aortic aneurysm formation. *Journal of vascular surgery.* **52**(4), pp.967-974.

Murthy, S.E., Dubin, A.E. and Patapoutian, A. 2017. Piezos thrive under pressure: mechanically activated ion channels in health and disease. *Nature reviews Molecular cell biology.* **18**(12), pp.771-783.

Mutchler, S.M., Kirabo, A. and Kleyman, T.R. 2021. Epithelial sodium channel and salt-sensitive hypertension. *Hypertension.* **77**(3), pp.759-767.

Nakata, Y., Shionoya, S. and Kamiya, K. 1968. Pathogenesis of mycotic aneurysm. *Angiology.* **19**(10), pp.593-601.

Nam, H.Y., Murali, M.R., Ahmad, R.E., Pingguan-Murphy, B., Raghavendran, H.R.B. and Kamarul, T. 2020. Mechanical strain-mediated tenogenic differentiation of mesenchymal stromal cells is regulated through epithelial sodium channels. *Stem cells international.* **2020**.

Nemeth, Z., Hildebrandt, E., Ryan, M.J., Granger, J.P. and Drummond, H.A. 2020. Pressure-induced constriction of the middle cerebral artery is abolished in TrpC6 knockout mice. *American Journal of Physiology-Heart and Circulatory Physiology.* **319**(7), pp.H42-H50.

Nicholls, S.C., Gardner, J.B., Meissner, M.H. and Johansen, K.H. 1998. Rupture in small abdominal aortic aneurysms. *Journal of vascular surgery.* **28**(5), pp.884-888.

Nonomura, K., Lukacs, V., Sweet, D.T., Goddard, L.M., Kanie, A., Whitwam, T., Ranade, S.S., Fujimori, T., Kahn, M.L. and Patapoutian, A. 2018. Mechanically activated ion channel PIEZO1 is required for lymphatic valve formation. *Proceedings of the National Academy of Sciences.* **115**(50), pp.12817-12822.

Nordon, I., Karthikesalingam, A., Hinchliffe, R., Holt, P., Loftus, I. and Thompson, M. 2010. Secondary interventions following endovascular aneurysm repair (EVAR) and the enduring value of graft surveillance. *European Journal of Vascular Endovascular Surgery.* **39**(5), pp.547-554.

O'Leary, S.A., Healey, D.A., Kavanagh, E.G., Walsh, M.T., McGloughlin, T.M. and Doyle, B.J. 2014. The biaxial biomechanical behavior of abdominal aortic aneurysm tissue. *Annals of Biomedical Engineering.* **42**(12), pp.2440-2450.

Oliver-Williams, C., Sweeting, M.J., Jacomelli, J., Summers, L., Stevenson, A., Lees, T. and Earnshaw, J.J. 2019. Safety of men with small and medium abdominal aortic aneurysms under surveillance in the NAAASP. *Circulation.* **139**(11), pp.1371-1380.

Opie, L.H. and Paterson, D.J. 2004. Blood pressure and peripheral circulation. *Opie L. Heart physiology: from cell to circulation. 4th ed. Philadelphia, USA: Lippincott Williams & Wilkins. p.* pp.431-454.

Owens, G.K. 1995. Regulation of differentiation of vascular smooth muscle cells. *Physiological Reviews.* **75**(3), pp.487-517.

Owens, G.K. 1996. Role of mechanical strain in regulation of differentiation of vascular smooth muscle cells. *Circulation research.* **79**(5), pp.1054-1055.

Owens, G.K., Geisterfer, A., Yang, Y.W.-H. and Komoriya, A. 1988. Transforming growth factor-beta-induced growth inhibition and cellular hypertrophy in cultured vascular smooth muscle cells. *The Journal of cell biology.* **107**(2), pp.771-780.

Owens, G.K., Kumar, M.S. and Wamhoff, B.R. 2004. Molecular regulation of vascular smooth muscle cell differentiation in development and disease. *Physiological reviews.* **84**(3), pp.767-801.

Pancheri, F.Q., Peattie, R.A., Reddy, N.D., Ahamed, T., Lin, W., Ouellette, T.D., Iafrati, M.D. and Dorfmann, A.L. 2017. Histology and biaxial mechanical behavior of abdominal aortic aneurysm tissue samples. *Journal of Biomechanical Engineering.* **139**(3), p031002.

Papadimitriou, D., Xanthos, T., Dontas, I., Lelovas, P. and Perrea, D. 2008. The use of mice and rats as animal models for cardiopulmonary resuscitation research. *Laboratory animals.* **42**(3), pp.265-276.

Passman, J.N., Dong, X.R., Wu, S.-P., Maguire, C.T., Hogan, K.A., Bautch, V.L. and Majesky, M.W. 2008. A sonic hedgehog signaling domain in the arterial adventitia supports resident Sca1+ smooth muscle progenitor cells. *Proceedings of the National Academy of Sciences.* **105**(27), pp.9349-9354.

Patel, A.J., Honoré, E., Maingret, F., Lesage, F., Fink, M., Duprat, F. and Lazdunski, M. 1998. A mammalian two pore domain mechano-gated S-like K+ channel. *The EMBO journal.* **17**(15), pp.4283-4290.

Patel, R., Sweeting, M.J., Powell, J.T., Greenhalgh, R.M. and Investigators, E.T. 2016. Endovascular versus open repair of abdominal aortic aneurysm in 15-years' follow-up of the UK endovascular aneurysm repair trial 1 (EVAR trial 1): a randomised controlled trial. *The Lancet.* **388**(10058), pp.2366-2374.

Penumatsa, K.C., Toksoz, D., Warburton, R.R., Hilmer, A.J., Liu, T., Khosla, C., Comhair, S.A. and Fanburg, B.L. 2014. Role of hypoxia-induced transglutaminase 2 in pulmonary artery smooth muscle cell proliferation. *American Journal of Physiology-Lung Cellular and Molecular Physiology.* **307**(7), pp.L576-L585.

Porter, K.E., Naik, J., Turner, N.A., Dickinson, T., Thompson, M.M. and London, N.J. 2002. Simvastatin inhibits human saphenous vein neointima formation via inhibition of smooth muscle cell proliferation and migration. *Journal of Vascular Surgery.* **36**(1), pp.150-157.

Powell, J. 2007. Final 12-year follow-up of Surgery versus Surveillance in the UK Small Aneurysm Trial: UK Small Aneurysm Trial participants. *British Journal of Surgery: Incorporating European Journal of Surgery.* **94**(6), pp.702-708.

Powell, J.T., Sweeting, M.J., Ulug, P., Blankensteijn, J.D., Lederle, F., Becquemin, J.P., Greenhalgh, R., EVAR-1, D., OVER, Trialists, A., Greenhalgh, R. and Beard, J. 2017. Meta-analysis of individual-patient data

from EVAR-1, DREAM, OVER and ACE trials comparing outcomes of endovascular or open repair for abdominal aortic aneurysm over 5 years. *British Journal of Surgery.* **104**(3), pp.166-178.

Prinssen, M., Verhoeven, E.L., Buth, J., Cuypers, P.W., Van Sambeek, M.R., Balm, R., Buskens, E., Grobbee, D.E. and Blankensteijn, J.D. 2004. A randomized trial comparing conventional and endovascular repair of abdominal aortic aneurysms. *New England Journal of Medicine.* **351**(16), pp.1607-1618.

Psaltis, P.J., Harbuzariu, A., Delacroix, S., Witt, T.A., Holroyd, E.W., Spoon, D.B., Hoffman, S.J., Pan, S., Kleppe, L.S. and Mueske, C.S. 2012. Identification of a monocyte-predisposed hierarchy of hematopoietic progenitor cells in the adventitia of postnatal murine aorta. *Circulation.* **125**(4), pp.592-603.

Qian, W., Hadi, T., Silvestro, M., Ma, X., Rivera, C.F., Bajpai, A., Li, R., Zhang, Z., Qu, H. and Tellaoui, R.S. 2022. Microskeletal stiffness promotes aortic aneurysm by sustaining pathological vascular smooth muscle cell mechanosensation via Piezo1. *Nature communications.* **13**(1), pp.1-19.

Raines, E.W. 2004. PDGF and cardiovascular disease. *Cytokine & growth factor reviews.* **15**(4), pp.237-254.

RESCAN Collaborators, Bown, M., Sweeting, M., Brown, L., Powell, J. and Thompson, S. 2013. Surveillance intervals for small abdominal aortic aneurysms. *Jama.* **309**(8), pp.806-813.

Retailleau, K., Duprat, F., Arhatte, M., Ranade, S.S., Peyronnet, R., Martins, J.R., Jodar, M., Moro, C., Offermanns, S. and Feng, Y. 2015. Piezo1 in smooth muscle cells is involved in hypertension-dependent arterial remodeling. *Cell reports.* **13**(6), pp.1161-1171.

Riches, K., Angelini, T.G., Mudhar, G.S., Kaye, J., Clark, E., Bailey, M.A., Sohrabi, S., Korossis, S., Walker, P.G. and Scott, D.J.A. 2013. Exploring smooth muscle phenotype and function in a bioreactor model of abdominal aortic aneurysm. *Journal of Translational Medicine.* **11**(1), p208.

Rode, B., Shi, J., Endesh, N., Drinkhill, M.J., Webster, P.J., Lotteau, S.J., Bailey, M.A., Yuldasheva, N.Y., Ludlow, M.J. and Cubbon, R.M. 2017. Piezo1 channels sense whole body physical activity to reset cardiovascular homeostasis and enhance performance. *Nature Communications.* **8**(1), p350.

Rodríguez, J.F., Ruiz, C., Doblaré, M. and Holzapfel, G.A. 2008. Mechanical stresses in abdominal aortic aneurysms: influence of diameter, asymmetry, and material anisotropy. *Journal of Biomechanical Engineering.* **130**(2), p021023.

Rogers, I.S., Massaro, J.M., Truong, Q.A., Mahabadi, A.A., Kriegel, M.F., Fox, C.S., Thanassoulis, G., Isselbacher, E.M., Hoffmann, U. and O'Donnell, C.J. 2013. Distribution, determinants, and normal reference values of thoracic and abdominal aortic diameters by computed tomography (from the Framingham Heart Study). *The American journal of cardiology.* **111**(10), pp.1510-1516.

Ross, R. and Glomset, J.A. 1973. Atherosclerosis and the arterial smooth muscle cell: Proliferation of smooth muscle is a key event in the genesis of the lesions of atherosclerosis. *Science.* **180**(4093), pp.1332-1339.

Rudijanto, A. 2007. The role of vascular smooth muscle cells on the pathogenesis of atherosclerosis. *Acta Med Indones.* **39**(2), pp.86-93.

Sakalihasan, N., Limet, R. and Defawe, O.D. 2005. Abdominal aortic aneurysm. *The Lancet.* **365**(9470), pp.1577-1589.

Salata, K., Syed, M., Hussain, M.A., de Mestral, C., Greco, E., Mamdani, M., Tu, J.V., Forbes, T.L., Bhatt, D.L. and Verma, S. 2018. Statins reduce abdominal aortic aneurysm growth, rupture, and perioperative mortality: a systematic review and meta-analysis. *Journal of the American Heart Association.* **7**(19), pe008657.

Salmon, M., Johnston, W.F., Woo, A., Pope, N.H., Su, G., Upchurch Jr, G.R., Owens, G.K. and Ailawadi, G. 2013. KLF4 regulates abdominal aortic aneurysm morphology and deletion attenuates aneurysm formation. *Circulation.* **128**(11_suppl_1), pp.S163-S174.

Salomonsson, M., Brasen, J.C. and Sorensen, C.M. 2017. Role of renal vascular potassium channels in physiology and pathophysiology. *Acta physiologica.* **221**(1), pp.14-31.

Sampson, U.K., Norman, P.E., Fowkes, F.G.R., Aboyans, V., Song, Y., Harrell Jr, F.E., Forouzanfar, M.H., Naghavi, M., Denenberg, J.O. and McDermott, M.M. 2014. Estimation of global and regional incidence and prevalence of abdominal aortic aneurysms 1990 to 2010. *Global heart.* **9**(1), pp.159-170.

Saotome, K., Murthy, S.E., Kefauver, J.M., Whitwam, T., Patapoutian, A. and Ward, A.B. 2018. Structure of the mechanically activated ion channel Piezo1. *Nature.* **554**(7693), pp.481-486.

Saraff, K., Babamusta, F., Cassis, L.A. and Daugherty, A. 2003. Aortic dissection precedes formation of aneurysms and atherosclerosis in angiotensin II-infused, apolipoprotein E-deficient mice. *Arteriosclerosis, thrombosis, and vascular biology.* **23**(9), pp.1621-1626.

Schild, L. 1996. The ENaC channel as the primary determinant of two human diseases: Liddle syndrome and pseudohypoaldosteronism. *Nephrologie.* **17**(7), pp.395-400.

Scott, R. and Group, M.A.S.S. 2002. The Multicentre Aneurysm Screening Study (MASS) into the effect of abdominal aortic aneurysm screening on mortality in men: a randomised controlled trial. *The Lancet.* **360**(9345), pp.1531-1539.

Shadrina, A.S., Sharapov, S.Z., Shashkova, T.I. and Tsepilov, Y.A. 2019. Varicose veins of lower extremities: Insights from the first large-scale genetic study. *PLoS genetics.* **15**(4), pe1008110.

Shantikumar, S., Ajjan, R., Porter, K. and Scott, D. 2010. Diabetes and the abdominal aortic aneurysm. *European Journal of Vascular Endovascular Surgery.* **39**(2), pp.200-207.

Sharif-Naeini, R., Folgering, J.H., Bichet, D., Duprat, F., Lauritzen, I., Arhatte, M., Jodar, M., Dedman, A., Chatelain, F.C. and Schulte, U. 2009. Polycystin-1 and-2 dosage regulates pressure sensing. *Cell.* **139**(3), pp.587-596.

Sheinberg, D.L., McCarthy, D.J., Elwardany, O., Bryant, J.-P., Luther, E., Chen, S.H., Thompson, J.W. and Starke, R.M. 2019. Endothelial dysfunction in cerebral aneurysms. *Neurosurgical focus.* **47**(1), pE3.

Sillesen, H., Eldrup, N., Hultgren, R., Lindeman, J., Bredahl, K., Thompson, M., Wanhainen, A., Wingren, U., Swedenborg, J. and Investigators, A.T. 2015. Randomized clinical trial of mast cell inhibition in patients with a medium-sized abdominal aortic aneurysm. *British Journal of Surgery.* **102**(8), pp.894-901.

Smith, S.A., Travers, R.J. and Morrissey, J.H. 2015. How it all starts: Initiation of the clotting cascade. *Critical reviews in biochemistry and molecular biology.* **50**(4), pp.326-336.

Sonesson, B., Sandgren, T. and Länne, T. 1999. Abdominal aortic aneurysm wall mechanics and their relation to risk of rupture. *European Journal of Vascular and Endovascular Surgery.* **18**(6), pp.487-493.

Sowers, J.R. 2013. Diabetes mellitus and vascular disease. *Hypertension.* **61**(5), pp.943-947.

Stegemann, J.P., Hong, H. and Nerem, R.M. 2005. Mechanical, biochemical, and extracellular matrix effects on vascular smooth muscle cell phenotype. *Journal of applied physiology.* **98**(6), pp.2321-2327.

Sughimoto, K., Shimamura, Y., Tezuka, C., Tsubota, K.i., Liu, H., Okumura, K., Masuda, Y., Haneishi, H. and vessels. 2016. Effects of arterial blood flow on walls of the abdominal aorta: distributions of wall shear stress and oscillatory shear index determined by phase-contrast magnetic resonance imaging. *Heart.* **31**(7), pp.1168-1175.

Sweeting, M., Thompson, S., Brown, L. and Powell, J. 2012a. Meta-analysis of individual patient data to examine factors affecting growth and rupture of small abdominal aortic aneurysms. *Journal of British Surgery.* **99**(5), pp.655-665.

Sweeting, M., Thompson, S., Brown, L., Powell, J. and collaborators, R. 2012b. Meta-analysis of individual patient data to examine factors affecting growth and rupture of small abdominal aortic aneurysms. *British Journal of Surgery.* **99**(5), pp.655-665.

Sweeting, M.J., Patel, R., Powell, J.T., Greenhalgh, R.M. and Investigators, E.T. 2017. Endovascular repair of abdominal aortic aneurysm in patients physically ineligible for open repair: very long-term follow-up in the EVAR-2 randomized controlled trial. *Annals of surgery.* **266**(5), pp.713-719.

Syeda, R., Xu, J., Dubin, A.E., Coste, B., Mathur, J., Huynh, T., Matzen, J., Lao, J., Tully, D.C. and Engels, I.H. 2015. Chemical activation of the mechanotransduction channel Piezo1. *Elife.* **4**, pe07369.

Takahashi, K., Tanabe, K., Ohnuki, M., Narita, M., Ichisaka, T., Tomoda, K. and Yamanaka, S. 2007. Induction of pluripotent stem cells from adult human fibroblasts by defined factors. *cell.* **131**(5), pp.861-872.

Takahashi, K. and Yamanaka, S. 2006. Induction of pluripotent stem cells from mouse embryonic and adult fibroblast cultures by defined factors. *cell.* **126**(4), pp.663-676.

Tang, W., Yao, L., Roetker, N.S., Alonso, A., Lutsey, P.L., Steenson, C.C., Lederle, F.A., Hunter, D.W., Bengtson, L.G. and Guan, W. 2016. Lifetime risk and risk factors for abdominal aortic aneurysm in a 24-year prospective study: the ARIC study (atherosclerosis risk in communities). *Arteriosclerosis, thrombosis, and vascular biology.* **36**(12), pp.2468-2477.

The UK Small Aneurysm Trial Participants. 1998. Mortality results for randomised controlled trial of early elective surgery or ultrasonographic surveillance for small abdominal aortic aneurysms. *The Lancet.* **352**(9141), pp.1649-1655.

Thijssen, D.H., Carter, S.E. and Green, D.J. 2016. Arterial structure and function in vascular ageing: are you as old as your arteries? *The Journal of physiology.* **594**(8), pp.2275-2284.

Thompson, A., Cooper, J., Ashton, H. and Hafez, H. 2010. Growth rates of small abdominal aortic aneurysms correlate with clinical events. *Journal of British Surgery.* **97**(1), pp.37-44.

Thompson, J.E. 1998. Early history of aortic surgery. *Journal of vascular surgery.* **28**(4), pp.746-752.

Tromp, G., Kuivaniemi, H., Hinterseher, I. and Carey, D.J. 2010. Novel genetic mechanisms for aortic aneurysms. *Current atherosclerosis reports.* **12**(4), pp.259-266.

Tucker, W.D., Arora, Y. and Mahajan, K. 2017. Anatomy, blood vessels.

van Schaik, T.G., Yeung, K.K., Verhagen, H.J., de Bruin, J.L., van Sambeek, M.R., Balm, R., Zeebregts, C.J., van Herwaarden, J.A., Blankensteijn, J.D. and Grobbee, D. 2017. Long-term survival and secondary procedures after open or endovascular repair of abdominal aortic aneurysms. *Journal of vascular surgery.* **66**(5), pp.1379-1389.

Venkatasubramaniam, A., Fagan, M., Mehta, T., Mylankal, K., Ray, B., Kuhan, G., Chetter, I. and McCollum, P. 2004. A comparative study of aortic wall stress using finite element analysis for ruptured and non-ruptured abdominal aortic aneurysms. *European Journal of Vascular and Endovascular Surgery.* **28**(2), pp.168-176.

Villard, C. and Hultgren, R. 2018. Abdominal aortic aneurysm: Sex differences. *Maturitas.* **109**, pp.63-69.

Wang, G., Jacquet, L., Karamariti, E. and Xu, Q. 2015. Origin and differentiation of vascular smooth muscle cells. *The Journal of physiology.* **593**(14), pp.3013-3030.

Wang, J., Zohar, R. and McCulloch, C.A. 2006. Multiple roles of α-smooth muscle actin in mechanotransduction. *Experimental cell research.* **312**(3), pp.205-214.

Wang, K., Deng, X., Shen, Z., Jia, Y., Ding, R., Li, R., Liao, X., Wang, S., Ha, Y. and Kong, Y. 2017. High glucose promotes vascular smooth muscle cell proliferation by upregulating proto-oncogene serine/threonine-protein kinase Pim-1 expression. *Oncotarget.* **8**(51), p88320.

Wang, L., Zhou, H., Zhang, M., Liu, W., Deng, T., Zhao, Q., Li, Y., Lei, J., Li, X. and Xiao, B. 2019. Structure and mechanogating of the mammalian tactile channel PIEZO2. *Nature.* **573**(7773), pp.225-229.

Wang, S., Chennupati, R., Kaur, H., Iring, A., Wettschureck, N. and Offermanns, S. 2016. Endothelial cation channel PIEZO1 controls blood pressure by mediating flow-induced ATP release. *The Journal of clinical investigation.* **126**(12), pp.4527-4536.

Webb, R.C. 2003. Smooth muscle contraction and relaxation. *Advances in physiology education.* **27**(4), pp.201-206.

Wirth, A., Benyó, Z., Lukasova, M., Leutgeb, B., Wettschureck, N., Gorbey, S., Örsy, P., Horváth, B., Maser-Gluth, C. and Greiner, E. 2008. G12-G13–LARG–mediated signaling in vascular smooth muscle is required for salt-induced hypertension. *Nature medicine.* **14**(1), pp.64-68.

Woo, S.-H., Ranade, S., Weyer, A.D., Dubin, A.E., Baba, Y., Qiu, Z., Petrus, M., Miyamoto, T., Reddy, K. and Lumpkin, E.A. 2014. Piezo2 is required for Merkel-cell mechanotransduction. *Nature.* **509**(7502), pp.622-626.

Wu, J., Bohanan, C.S., Neumann, J.C. and Lingrel, J.B. 2008. KLF2 transcription factor modulates blood vessel maturation through smooth muscle cell migration. *Journal of Biological Chemistry.* **283**(7), pp.3942-3950.

Wu, J., Lewis, A.H. and Grandl, J. 2017. Touch, tension, and transduction–the function and regulation of Piezo ion channels. *Trends in biochemical sciences.* **42**(1), pp.57-71.

Xie, X., Lu, H., Moorleghen, J.J., Howatt, D.A., Rateri, D.L., Cassis, L.A. and Daugherty, A. 2012. Doxycycline does not influence established abdominal aortic aneurysms in angiotensin II-infused mice.

Yamaguchi, O. 2004. Response of bladder smooth muscle cells to obstruction: signal transduction and the role of mechanosensors. *Urology.* **63**(3), pp.11-16.

Yang, H., Liu, C., Zhou, R.-M., Yao, J., Li, X.-M., Shen, Y., Cheng, H., Yuan, J., Yan, B. and Jiang, Q. 2016. Piezo2 protein: A novel regulator of tumor angiogenesis and hyperpermeability. *Oncotarget.* **7**(28), p44630.

Ye, G.J., Nesmith, A.P. and Parker, K.K. 2014. The role of mechanotransduction on vascular smooth muscle myocytes cytoskeleton and contractile function. *The Anatomical Record.* **297**(9), pp.1758-1769.

Yoshida, T., Kaestner, K.H. and Owens, G.K. 2008. Conditional deletion of Kruppel-like factor 4 delays downregulation of smooth muscle cell differentiation markers but accelerates neointimal formation following vascular injury. *Circulation research.* **102**(12), pp.1548-1557.

Zaragoza, C., Márquez, S. and Saura, M. 2012. Endothelial mechanosensors of shear stress as regulators of atherogenesis. *Current Opinion in Lipidology.* **23**(5), pp.446-452.

Zeng, W.-Z., Marshall, K.L., Min, S., Daou, I., Chapleau, M.W., Abboud, F.M., Liberles, S.D. and Patapoutian, A. 2018. PIEZOs mediate neuronal sensing of blood pressure and the baroreceptor reflex. *Science.* **362**(6413), pp.464-467.

Zhao, Q., Zhou, H., Chi, S., Wang, Y., Wang, J., Geng, J., Wu, K., Liu, W., Zhang, T. and Dong, M.-Q. 2018. Structure and mechanogating mechanism of the Piezo1 channel. *Nature.* **554**(7693), pp.487-492.

Appendices

Appendix A: RNA-seq Gene Expression in Human Tissue

PIEZO-1

https://genome.ucsc.edu/cgi-bin/hgGene?hgg_gene=ENST00000301015.14&hgg_prot=ENST00000301015.14&hgg_chrom=chr16&hgg_start=88715337&hgg_end=88785220&hgg_type=knownGene&db=hg38&hgsid=764650383_AhxDBhKRA4a1U4mAotnriPa0dPLU

PIEZO-2

https://genome.ucsc.edu/cgi-bin/hgGene?hgg_gene=ENST00000503781.7&hgg_prot=ENST00000503781.7&hgg_chrom=chr18&hgg_start=10671526&hgg_end=11148588&hgg_type=knownGene&db=hg38&hgsid=764650383_AhxDBhKRA4a1U4mAotnriPa0dPLU

KLF2

https://genome.ucsc.edu/cgi-bin/hgGene?hgg_gene=ENST00000248071.5&hgg_prot=ENST00000248071.5&hgg_chrom=chr19&hgg_start=16324816&hgg_end=16327874&hgg_type=knownGene&db=hg38&hgsid=764650383_AhxDBhKRA4a1U4mAotnriPa0dPLU

KLF4

https://genome.ucsc.edu/cgi-bin/hgGene?hgg_gene=ENST00000374672.4&hgg_prot=ENST00000374672.4&hgg_chrom=chr9&hgg_start=107484851&hgg_end=107489646&hgg_type=knownGene&db=hg38&hgsid=764650383_AhxDBhKRA4a1U4mAotnriPa0dPLU

TGM2

https://genome.ucsc.edu/cgi-bin/hgGene?hgg_gene=ENST00000361475.6&hgg_prot=ENST00000361475.6&hgg_chrom=chr20&hgg_start=38127386&hgg_end=38165372&hgg_type=knownGene&db=hg38&hgsid=764650383_AhxDBhKRA4a1U4mAotnriPa0dPLU

Appendix B: Targets of PIEZO-1 siRNA SMART POOL Sequences on PIEZO-1 mRNA and PIEZO-2 mRNA

Black and blue represent different exons.

PIEZO-1

GGGAGCCGCCGTCCGGCCCAGCTCGGCCCCAGTGAGCCGAGCGCTG
CGCTCCGCCGAGGGGCAGGGCGGTCGCCTGAGCGAGCGCGGGCCCG
GGACGTCGGCACCGGCGGGGCGGCCGAAGGAGAAGGAGGAAGAGGA
GAAGGCGGCGCGCGGGTCCCCGCGGGTCAGCCATGGCGCGCCGGCC
CCGGGGCCCCCGCACCGCCCCATAGCGCCGCGGCGTCCGCTCGGTC
TGGGCCGGGCCCTGGGCCCTCCAGCCATGGAGCCGCACGTGCTCGG
CGCGGTCCTGTACTGGCTGCTGCTGCCCTGCGCGCTGCTGGCTGCCT
GCCTGCTCCGCTTCAGCGGACTCTCGCTGGTCTACCTGCTCTTCCTGC
TGCTGCTGCCCTGGTTCCCCGGCCCCACCCGATGCGGCCTCCAAGGT
CACACAGGCCGCCTCCTGCGGGCATTGCTGGGCCTCAGCCTGCTCTT
CCTGGTGGCCCATCTCGCCCTCCAGATCTGCCTGCATATTGTGCCCCG
CCTGGACCAGCTCCTGGGACCCAGCTGCAGCCGCTGGGAGACCCTCT
CGCGACACATAGGGGTCACAAGGCTGGACCTGAAGGACATCCCCAAC
GCCATCCGGCTGGTGGCCCCTGACCTGGGCATCTTGGTGGTCTCCTCT
GTCTGCCTCGGCATCTGCGGGCGCCTTGCAAGGAACACCCGGCAGAG
CCCACATCCACGGGAGCTGGATGATGATGAGAGGGATGTGGATGCCA
GCCCGACGGCAGGGCTGCAGGAAGCAGCAACGCTGGCCCCTACACG
GAGGTCACGGCTGGCCGCTCGTTTCCGAGTCACGGCCCACTGGCTGC
TGGTGGCGGCTGGGCGGGTCCTGGCCGTAACACTGCTTGCACTGGCA
GGCATCGCCCACCCCTCGGCCCTCTCCAGTGTCTACCTGCTGCTCTTC
CTGGCCCTCTGCACCTGGTGGGCCTGCCACTTTCCCATCAGCACTCGG
GGCTTCAGCAGACTCTGCGTCGCGGTGGGGTGCTTCGGCGCCGGCCA
TCTCATCTGCCTCTACTGCTACCAGATGCCCTTGGCACAGGCTCTGCTC
CCGCCTGCCGGCATCTGGGCTAGGGTGCTGGGTCTCAAGGACTTCGT
GGGTCCCACCAACTGCTCCAGCCCCCACGCGCTGGTCCTCAACACCG
GCCTGGACTGGCCTGTGTATGCCAGCCCCGGCGTCCTCCTGCTGCTG
TGCTACGCCACGGCCTCTCTGCGCAAGCTCCGCGCGTACCGCCCCTC
CGGCCAGAGGAAGGAGGCGGCAAAGGGGTATGAGGCTCGGGAGCTG

GAGCTAGCAGAGCTGGACCAGTGGCCCCAGGAACGGGAGTCTGACCA
GCACGTGGTGCCCACAGCACCCGACACCGAGGCTGATAACTGCATCG
TGCACGAGCTGACCGGCCAGAGCTCCGTCCTGCGGCGGCCTGTGCGG
CCCAAGCGGGCTGAGCCCAGGGAGGCGTCTCCGCTCCACAGCCTGGG
CCACCTCATCATGGACCAGAGCTATGTGTGCGCGCTCATTGCCATGAT
GGTATGGAGCATCACCTACCACAGCTGGCTGACCTTCGTACTGCTGCT
CTGGGCCTGCCTCATCTGGACGGTGCGCAGCCGCCACCAACTGGCCA
TGCTGTGCTCGCCCTGCATCCTGCTGTATGGGATGACGCTGTGCTGCC
TACGCTACGTGTGGGCCATGGACCTGCGCCCTGAGCTGCCCACCACC
CTGGGCCCCGTCAGCCTGCGCCAGCTGGGGCTGGAGCACACCCGCTA
CCCCTGTCTGGACCTTGGTGCCATGTTGCTCTACACCCTGACCTTCTG
GCTCCTGCTGCGCCAGTTTGTGAAAGAGAAGCTGCTGAAGTGGGCAGA
GTCTCCAGCTGCGCTGACGGAGGTCACCGTGGCAGACACAGAGCCCA
CGCGGACGCAGACGCTGTTGCAGAGCCTGGGGGAGCTGGTGAAGGG
CGTGTACGCCAAGTACTGGATCTATGTGTGTGCTGGCATGTTCATCGT
GGTCAGCTTCGCCGGCCGCCTCGTGGTCTACAAGATTGTCTACATGTT
CCTCTTCCTGCTCTGCCTCACCCTCTTCCAGGTCTACTACAGCCTGTGG
CGGAAGCTGCTCAAGGCCTTCTGGTGGCTCGTGGTGGCCTACACCATG
CTGGTCCTCATCGCCGTCTACACCTTCCAGTTCCAGGACTTCCCTGCCT
ACTGGCGCAACCTCACTGGCTTCACCGACGAGCAGCTGGGGGACCTG
GGCCTGGAGCAGTTCAGCGTGTCCGAGCTCTTCTCCAGCATCCTGGTG
CCCGGCTTCTTCCTCCTGGCCTGCATCCTGCAGCTGCACTACTTCCAC
AGGCCCTTCATGCAGCTCACCGACATGGAGCACGTGTCCCTGCCTGGC
ACGCGCCTCCCGCGCTGGGCTCACAGGCAGGATGCAGTGAGTGGGAC
CCCACTGCTGCGGGAGGAGCAGCAGGAGCATCAGCAGCAGCAGCAGG
AGGAGGAGGAGGAGGAGGAGGACTCCAGGGACGAGGGGCTGGGCGT
GGCCACTCCCCACCAGGCCACGCAGGTGCCTGAAGGGGCAGCCAAGT
GGGGCCTGGTGGCTGAGCGGCTGCTGGAGCTGGCAGCCGGCTTCTC
GGACGTCCTCTCACGCGTGCAGGTGTTCCTGCGGCGGCTGCTGGAGC
TTCACGTTTTCAAGCTGGTGGCCCTGTACACCGTCTGGGTGGCCCTGA
AGGAGGTGTCC[Accel siRNA Seq3]TGGTGGTGCTGTGGGCCTTC
GCCCTGCCCTACCCACGCTTCCGGCCCATGGCCTCCTGCCTGTCCACC
GTGTGGACCTGCGTCATCATCGTGTGTAAGATGCTGTACCAGCTCAAG
GTTGTCAACCCCCAGGAGTATTCCAGCAACTGCACCGAGCCCTTCCCC

AACAGCACCAACTTGCTGCCCACGGAGATCAGCCAGTCCCTGCTGTAC
CGGGGGCCCGTGGACCCTGCCAACTGGTTTGGGGTGCGGAAAGGGTT
CCCCAACCTGGGCTACATCCAGAACCACCTGCAAGTGCTGCTGCTGCT
GGTATTCGAGGCCATCGTGTACCGGCGCCAGGAGCACTACCGCCGGC
AGCACCAGCTGGCCCCGCTGCCTGCCCAGGCCGTGTTTGCCAGCGGC
ACCCGCCAGCAGCTGGACCAGGATCTGCTCGGCTGCCTCAAGTACTTC
ATCAACTTCTTCTTCTACAAATTCGGGCTGGAGATCTGCTTCCTGATGG
CCGTGAACGTGATCGGGCAGCGCATGAACTTTCTGGTGACCCTGCACG
GTTGCTGGCTGGTGGCCATCCTCACCCGCAGGCACCGCCAGGCCATT
GCCCGCCTCTGGCCCAACTACTGCCTCTTCCTGGCGCTGTTCCTGCTG
TACCAGTACCTGCTGTGCCTGGGGATGCCCCCGGCCCTGTGCATTGAT
TATCCCTGGCGCTGGAGCCGGGCCGTCCCCA
AAGTGGCTGTACCTGCCTGATTTCTTCCGGGC
CTCATCAGCGACTTTCTCCTGCTGCTGTGCGCCTCCCAGCAGTGGCAG
GTGTTCTCAGCTGAGCGCACAGAGGAGTGGCAGCGCATGGCTGGCGT
CAACACCGACCGCCTGGAGCCGCTGCGGGGGGAGCCCAACCCCGTG
CCCAACTTTATCCACTGCAGGTCCTACCTTGACATGCTGAAGGTGGCC
GTCTTCCGATACCTGTTCTGGCTGGTGCTGGTGGTGGTGTTTGTCACG
GGGGCCACCCGCATCAGCATCTTCGGGCTGGGCTACCTGCTGGCCTG
CTTCTACCTGCTGCTCTTCGGCACGGCCCTGCTGCAGAGGGACACACG
GGCCCGCCTCGTGCTGTGGGACTGCCTCATTCTGTACAACGTCACCGT
CATCATCTCCAAGAACATGCTGTCGCTCCTGGCCTGCGTCTTCGTGGA
GCAGATGCAGACCGGCTTCTGCTGGGTCATCCAGCTCTTCAGCCTTGT
ATGCACCGTCAAGGGCTACTATGACCCCAAGGAGATGATGGACAGAGA
CCAGGACTGCCTGCTGCCTGTGGAGGAGGCTGGCATCATCTGGGACA
GCGTCTGCTTCTTCTTCCTGCTGCTGCAGCGCCGCGTCTTCCTTAGCC
ATTACTACCTGCACGTCAGGGCCGACCTCCAGGCCACCGCCCTGCTAG
CCTCCAGGGGCTTCGCCCTCTACAACGCTGCCAACCTCAAGAGCATTG
ACTTTCACCGCAGGATAGAGGAGAAGTCCCTGGCCCAGCTGAAAAGAC
AGATGGAGCGTATCCGTGCCAAGCAGGAGAAGCACAGGCAGGGCCGG
GTGGACCGCAGTCGCCCCCAGGACACCCTGGGCCCCAAGGACCCCG
GCCTGGAGCCAGGGCCCGACAGTCCAGGGGGCTCCTCCCCGCCACG
GAGGCAGTGGTGGCGGCCCTGGCTGGACCACGCCACAGTCATCCACT
CCGGGGACTACTTCCTGTTTGAGTCCGACAGTGAGGAAGAGGAGGAG

Accel siRNA Seq1

GCTGTTCCTGAAGACCCGAGGCCGTCGGCACAGAGTGCCTTCCAGCT
GGCGTACCAGGCATGGGTGACCAACGCCCAGGCGGTGCTGAGGCGG
CGGCAGCAGGAGCAGGAGCAGGCAAGGCAGGAACAGGCAGGACAGC
TACCCACAGGAGGTGGTCCCAGCCAGGAGGTGGAGCCAGCAGAGGGC
CCCGAGGAGGCAGCGGCAGGCCGGAGCCATGTGGTGCAGAGGGTGC
TGAGCACGGCGCAGTTCCTGTGGATGCTGGGGCAGGCGCTAGTGGAT
GAGCTGACACGCTGGCTGCAGGAGTTCACCCGGCACCACGGCACCAT
GAGCGACGTGCTGCGGGCAGAGCGCTACCTCCTCACACAGGAGCTCC
TGCAGGGCGGCGAAGTGCACAGGGGCGTGCTGGATCAGCTGTACACA
AGCCAGGCCGAGGCCACGCTGCCAGGCCCCACCGAGGCCCCCAATG
CCCCAAGCACCGTGTCCAGTGGGCTGGGCGCGGAGGAGCCACTCAGC
AGCATGACAGACGACATGGGCAGCCCCCTGAGCACCGGCTACCACAC
GCGCAGTGGCAGTGAGGAGGCAGTCACCGACCCCGGGGAGCGTGAG
GCTGGTGCCTCTCTGTACCAGGGACTGATGCGGACGGCCAGCGAGCT
GCTCCTGGACAGGCGCCTGCGCATCCCAGAGCTGGAGGAGGCAGAGC
TGTTTGCGGAGGGGCAGGGCCGGGCGCTGCGGCTGCTGCGGGCCGT
GTACCAGTGTGTGGCCGCCCACTCGGAGCTGCTCTGCTACTTCATCAT
CATCCTCAACCACATGGTCACGGCCTCCGCCGGCTCGCTGGTGCTGC
CCGTGCTCGTCTTCCTGTGGGCCATGCTGTCGATCCCGAGGCCCAGCA
AGCGCTTCTGGATGACGGCCATCGTCTTCACCGAGATCGCGGTGGTCG
TCAAGTACCTGTTCCAGTTTGGGTTCTTCCCCTGGAACAGCCACGTGGT
GCTGCGGCGCTACGAGAACAAGCCCTACTTCCCGCCCCGCATCCTGG
GCCTGGAGAAGACTGACGGCTACATCAAGTACGACCTGGTGCAGCTCA
TGGCCCTTTTCTTCCACCGCTCCCAGCTGCTGTGCTATGGCCTCTGGG
ACCATGAGGAGGACTCACCATCCAAGGAGCATGACAAGAGCGGCGAG
GAGGAGCAGGGAGCCGAGGAGGGGCCAGGGGTGCCTGCGGCCACCA
GTGGAAGCCAGGGTCGGACCCACGGACGGG
GGAGCTCAGGCCCCGTGATACGAGGCGCAT
CAGTCTACGTTTTAGAAGAAGGAAGAAGGAGGGCCCAGCACGGAAAG
GAGCGGCAGCCATCGAAGCTGAGGACAGGGAGGAAGAAGAGGGGGA
GGAAGAGAAAGAGGCCCCCACGGGGAGAGAGAAGAGGCCAAGCCGC
TCTGGAGGAAGAGTAAGGGCGGCCGGGCGGCGGCTGCAGGGCTTCT
GCCTGTCCCTGGCCCAGGGCACATATCGGCCGCTACGGCGCTTCTTC
CACGACATCCTGCACACCAAGTACCGCGCAGCCACCGACGTCTATGCC

Accel siRNA Seq4

CTCATGTTCCTGGCTGATGTTGTCGACTTCATCATCATCATTTTTGGCTT
CTGGGCCTTTGGGAAGCACTCGGCGGCCACAGACATCACGTCCTCCCT
ATCAGACGACCAGGTACCCGAGGCTTTCCTGGTCATGCTGCTGATCCA
GTTCAGTACCATGGTGGTTGACCGCGCCCTCTACCTGCGCAAGACCGT
GCTGGGCAAGCTGGCCTTCCAGGTGGCGCTGGTGCTGGCCATCCACC
TATGGATGTTCTTCATCCTGCCCGCCGTCACTGAGAGGATGTTCAACCA
GAATGTGGTGGCCCAGCTCTGGTACTTCGTGAAGTGCATCTACTTCGC
CCTGTCCGCCTACCAGATCCGCTGCGGCTACCCCACCCGCATCCTCG
GCAACTTCCTCACCAAGAAGTACAATCATCTCAACCTCTTCCTCTTCCA
GGGGTTCCGGCTGGTGCCGTTCCTGGTGGAGCTGCGGGCAGTGATGG
ACTGGGTGTGGACGGACACCACGCTGTCCCTGTCCAGCTGGATGTGT
GTGGAGGACATCTATGCCAACATCTTCATCATCAAATGCAGCCGAGAG
ACAGAGAAGAAATACCCGCAGCCCAAAGGGCAGAAGAAGAAGAAGATC
GTCAAGTACGGCATGGGTGGCCTCATCATCCTCTTCCTCATCGCCATC
ATCTGGTTCCCACTGCTCTTCATGTCGCTGGTGCGCTCCGTGGTTGGG
GTTGTCAACCAGCCCATCGATGTCACCGTCACCCTGAAGCTGGGCGGC
TATGAGCCGCTGTTCACCATGAGCGCCCAGCAGCCGTCCATCATCCCC
TTCACGGCCCAGGCCTATGAGGAGCTGTCCCGGCAGTTTGACCCCCA
GCCGCTGGCCATGCAGTTCATCAGCCAGTACAGCCCTGAGGACATCGT
CACGGCGCAGATTGAGGGCAGCTCCGGGGCGCTGTGGCGCATCAGTC
CCCCCAGCCGTGCCCAGATGAAGCGGGAGCTCTACAACGGCACGGCC
GACATCACCCTGCGCTTCACCTGGAACTTCCAGAGGGACCTGGCGAAG
GGAGGCACTGTGGAGTATGCCAACGAGAAGCACATGCTGGCCCTGGC
CCCCAACAGCACTGCACGGCGGCAGCTGGCCAGCCTGCTCGAGGGCA
CCTCGGACCAGTCTGTGGTCATCCCTAATCTCTTCCCCAAGTACATCCG
TGCCCCCAACGGGCCCGAAGCCAACCCTGTGAAGCAGCTGCAGCCCA
ATGAGGAGGCCGACTACCTCGGCGTGCGTATCCAGCTGCGGAGGGAG
CAGGGTGCGGGGGCCACCGGCTTCCTCGAATGGTGGGTCATCGAGCT
GCAGGAGTGC[illegible]TGCTGCCCATGGTCATTTTCAG
TGACAAGGTC[illegible]CTTC
TCATGGGGCT[illegible]
GCGGATTCTTCAGCGAGATCTCGCACTCCATTATGTTCGAGGAGCTGC
CGTGCGTGGACCGCATCCTCAAGCTCTGCCAGGACATCTTCCTGGTGC
GGGAGACTCGGGAGCTGGAGCTGGAGGAGGAGTTGTACGCCAAGCTC

Beech forward

PIEZO-1 primer

Accel siRNA Seq2

ATCTTCCTCTACCGCTCACCGGAGACCATGATCAAGTCGACTCCTGAG
AAGGACTAGGAGCTGCTGCTGGCGCCCG[illegible]CC
TGCTGGGCAGCGTGGCCACAAGGGGCGC[illegible]GG
AGCCACTGCCCCGTCCAAGGCCGCCAGC[illegible]GC
CTGCCTGAGCCCTGATGCTGCTGTCAGAGAAGGACACTGCGTCCCCAC
GGCCTGCGTGGCGCTGCCGTCCCCCACGTGTACTGTAGAGTTTTTTTT
TTAATTAAAAAATGTTTTATTTATACAAATGGACAATCAGA

Beech reverse
PIEZO-1 primer

PIEZO-2

ATGGCCTCAGAAGTGGTGTGCGGGCTCATCTTCAGGCTGCTGCTGCCC
ATCTGCCTGG[illegible]CGATACAATGGGCTCTCCTTTG
TCTACCTTAT[illegible]TCTGTTCTCAGAACCAACAAAA
ACGACGATGCAAG[illegible]GTTATTAAAGTCTCTGTGCTTC
ATCAGTCTTTCCTTCCTGTTGCTGCACATCATTTTCCACATCACGTTGGT
GAGCCTTGAAGCTCAACATCGTATTGCACCTGGCTACAACTGCTCAACA
TGGGAAAAGACATTCCGGCAGATCGGCTTTGAAAGCTTAAAGGGAGCT
GATGCTGGCAATGGGATCAGAGTGTTTGTACCTGACATCGGGATGTTC
ATTGCTAGTCTGACCATCTGGCTCCTCTGTAGAAACATTGTTCAGAAAC
CT[illegible]ACAGAGTAACCCGGAGTTTGAAAATGAAG
AA[illegible]AATTGATTCAGAAGAGGCACTGATCTATGA
AG[illegible]GATGGTGTTGAAGGCGAGTTGGAAGAAAG
CACGAAGTTAAAAATGTTCCGCAGGCTTGCCTCTGTGGCCTCTAAGCTC
AAGGAGTTCATTGGCAACATGATCACCACTGCTGGGAAAGTCGTTGTTA
CCATCTTACTGGGCTCCTCGGGCATGATGTTGCCGTCTTTGACATCATC
TGTGTATTTTTTTGTATTTTTGGGTCTGTGCACCTGGTGGTCCTGGTGC
CGGACGTTCGACCCATTGCTGTTCAGCTGTCTCTGTGTTCTGCTGGCTA
TTTTCACTGCTGGACATTTGATTGGACTTTATTTATACCAGTTCCAATTC
TTTCAAGAGGCAGTTCCACCCAATGACTACTATGCAAGGTTGTTTGGTA
TCAAGTCAGTAATTCAAACGGACTGTTCAAGTACTTGGAAGATCATAGT
GAACCCGGACCTGTCGTGGTACCACCACGCCAACCCTATCCTCCTGCT
GGTGATGTACTACACTCTGGCCACTCTGATCCGCATCTGGCTGCAAGA
GCCCCTTGTGCAGGATGAGGGGACCAAAGAAGAGGACAAAGCCCTGG

Beech forward
PIEZO-2 primer

Beech reverse
PIEZO-2 primer

CTTGTAGCCCCATCCAAATAACAGCGGGGAGGAGGCGGAGCCTGTGG
TACGCAACCCATTACCCCACTGATGAGAGAAAACTTTTATCCATGACCC
AGGATGACTACAAACCATCTGATGGCCTGCTGGTGACTGTGAACGGCA
ACCCCGTGGATTACCACACCATCCACCCAAGCCTGCCCATGGAGAACG
GCCCTGGCAAAGCCGACCTCTACTCCACCCCTCAGTACCGGTGGGAG
CCCTCTGATGAATCCTCAGAAAAGCGAGAGGAGGAAGAGGAAGAGAAA
GAAGAATTTGAAGAAGAAAGGAGCCGTGAGGAAAAAAGAAGTATCAAA
GTTCATGCCATGGTCTCCGTATTCCAATTTATTATGAAACAAAGTTACAT
CTGTGCCCTCATAGCTATGATGGCCTGGAGCATCACCTATCACAGCTG
GCTGACCTTCGTGCTGCTGATCTGGTCGTGCACTCTTTGGATGATTCG
CAACAGAAGAAAATATGCCATGATCAGCTCTCCCTTCATGGTGGTTTAT
GGAAACCTATTGTTGATATTACAGTATATATGGAGTTTTGAACTTCCTGA
AATTAAAAAAGTTCCAGGATTTTTAGAAAAGAAAGAGCCAGGAGAACTT
GCTTCCAAAATCCTTTTCACCATTACTTTTTGGCTACTGCTGAGGCAGC
ACCTCACAGAGCAAAAAGCTCTGCAAGAAAAGGAAGCTCTTTTATCGGA
AGTCAAAATTGGCAGTCAGGAAAATGAAGAAAAAGATGAGGAACTTCAA
GATATACAAGTGGAAGGAGAGCCCAAAGAGGAGGAAGAAGAGGAAGC
GAAGGAAGAGAAGCAAGAGAGAAAGAAGGTAGAGCAAGAGGAAGCTG
AAGAAGAAGATGAGCAGGACATCATGAAAGTCCTGGGCAATCTGGTGG
TGGCCATGTTCATCAAGTACTGGATCTACGTCTGCGGAGGCATGTTCTT
CTTCGTCAGCTTCGAGGGTAAAATCGTAATGTACAAAATCATCTACATG
GTGCTGTTCCTGTTCTGTGTGGCCCTATACCAGGTGCACTATGAATGGT
GGAGGAAAATTCTAAAATATTTTTGGATGTCAGTGGTTATTTACACTATG
CTGGTGCTTATCTTTATATACACATATCAGTTTGAGAACTTCCCAGGCCT
GTGGCAAAATATGACTGGACTGAAAAAAGAAAAGCTTGAGGATCTTGG
CTTAAAGCAGTTTACTGTGGCTGAACTATTCACTCGCATATTCATCCCAA
CCTCCTTTCTGCTGGTGTGCATTTTACACCTGCACTACTTCCATGACCG
GTTCCTTGAACTCACAGACCTCAAGTCCATTCCCAGCAAAGAAGACAAC
ACCATCTACAGACTGGCCCACCCGGAAGGAAGCCTCCCGGACCTCAC
CATGATGCATCTGACTGCCAGCCTGGAGAAGCCGGAGGTGAGGAAGTT
GGCTGAGCCTGGGGAGGAGAAGCTTGAGGGCTACTCTGAAAAAGCCC
AGAAGGGTGATCTTGGGAAAGACAGCGAGGAGTCAGAGGAGGACGGA
GAGGAAGAGGAGGAATCCGAGGAGGAGGAAGAAACATCAGACTTAAG
GAACAAATGGCACCTGGTGATTGACCGCCTCACTGTGCTCTTCTTAAAA

TTCCTGGAGTATTTTCACAAGCTGCAGGTGTTCATGTGGTGGATTTTGG
AGTTGCACATCATCAAAATCGTTTCCTCTTACATTATCTGGGTTTCTGTG
AAAGAGGTGTCTCTGTTCAACTATGTATTTTTGATTTCTTGGGCTTTTGC
TCTGCCGTACGCCAAGCTGCGCCGTCTGGCTTCAAGTGTCTGCACAGT
CTGGACGTGTGTGATCATCGTCTGCAAAATGTTGTACCAGCTCCAAACC
ATTAAGCCTGAGAACTTCTCTGTTAACTGTTCCTTGCCAAATGAAAATCA
AACAAACATCCCCTTTAATGAGTTGAACAAGTCTCTGCTCTACAGCGCT
CCTATCGATCCTACAGAGTGGGTCGGCCTGCGGAAGTCTTCGCCTCTG
CTAGTCTACCTGAGGAATAACCTCCTGATGCTGGCTATCCTGGCCTTTG
AAGTCACCATTTACCGCCATCAGGAATACTATCGAGGTCGAAATAACCT
GACGGCCCCTGTGTCTAGAACTATCTTTCATGACATTACAAGACTACAT
CTAGATGATGGACTTATTAATTGTGCCAAATATTTCATTAATTACTTCTTT
TACAAGTTTGGTCTGGAGACCTGTTTCCTAATGTCAGTTAACGTCATTG
GCCAGCGAATGGATTTCTATGCCATGATCCACGCCTGCTGGCTGATCG
CTGTCTTATATAGACGCAGAAGGAAAGCCATCGCAGAGATCTGGCCCA
AGTACTGCTGCTTCCTGGCATGCATCATCACCTTCCAGTATTTCATCTG
CATTGGCATCCCACCTGCTCCTTGCCGAGATTACCCGTGGAGATTCAA
GGGTGCCAGCTTCAATGACAACATCATAAAGTGGCTGTACTTCCCAGAT
TTCATTGTGCGGCCCAACCCTGTGTTTCTCGTCTATGACTTCATGCTGC
TTCTGTGTGCCTCCTTACAACGGCAGATTTTTGAGGATGAGAACAAGGC
TGCAGTGCGAATCATGGCAGGTGACAATGTCGAGATCTGCATGAACCT
TGATGCGGCCTCCTTCAGCCAACATAACCCTGTGCCAGATTTTATTCAC
TGCAGATCTTACTTAGACATGTCCAAAGTGATCATCTTCAGCTACCTCTT
CTGGTTTGTGCTCACCATCATCTTCATCACTGGGACCACCAGGATCAGC
ATCTTTTGCATGGGGTACCTGGTGGCCTGTTTCTACTTCCTGCTCTTTG
GGGGCGATTTGCTGTTGAAACCCATCAAGAGCATCCTGCGCTACTGGG
ACTGGCTGATCGCATACAACGTTTTTGTGATTACGATGAAAAATATCCT
GTCAATAGGAGCATGTGGATACATTGGAACATTGGTGCACAATAGTTGT
TGGTTGATCCAGGCTTTCAGCCTGGCCTGCACAGTCAAAGGCTATCAA
ATGCCTGCTGCTAATTCACCCTGTACACTTCCCAGTGGGGAAGCAGGA
ATCATTTGGGACAGCATATGTTTTGCCTTCCTCCTGCTGCAAAGAAGAG
TTTTCATGAGTTATTATTTTCTACATGTTGTGGCTGATATAAAAGCTTCC
CAGATTCTGGCATCAAGAGGAGCTGAACTTTTCCAGGCCACAATTGTAA
AAGCTGTAAAGGCAAGAATTGAGGAAGAGAAGAAGTCCATGGACCAGC

TGAAGCGACAGATGGATCGCATCAAGGCCAGGCAACAGAAATATAAAA
AGGGTAAGGAGAGGATGCTGAGCTTGACCCAGGAGCCAGGGGAAGGC
CAGGACATGCAAAAACTCTCTGAAGAGGATGATGAAAGAGAAGCAGAC
AAACAGAAAGCCAAGGGCAAAAAAAAGCAGTGGTGGCGGCCTTGGGTT
GATCATGCTTCCATGGTCAGGAGTGGAGATTATTATTTGTTTGAAACGG
ATAGTGAAGAGGAGGAAGAGGAAGAATTAAAGAAGGAAGATGAAGAAC
CTCCACGAAGGTCAGCATTCCAGTTTGTTTATCAAGCCTGGATTACTGA
TCCTAAAACAGCACTCCGACAAAGACACAAAGAGAAAAAAAGGTCTGCA
AGAGAAGAACGGAAACGAAGGCGGAAAGGATCCAAGGAGGGTCCTGT
GGAATGGGAAGACCGGGAGGATGAACCAATCAAAAAGAAATCCGATGG
ACCAGATAATATCATCAAGAGGATATTTAATATTTTGAAATTTACCTGGG
TCCTATTTCTGGCAACAGTGGACAGTTTCACTACTTGGCTTAACTCCATT
TCAAGGGAGCATATTGATATATCTACAGTTCTGAGAATTGAACGATGCA
TGCTGACCAGAGAAATTAAGAAGGGCAATGTTCCAACTCGGGAGAGCA
TCCACATGTACTATCAGAACCACATCATGAACCTTTCCAGAGAGTCGGG
ACTGGACACCATTGACGAGCATCCCGGAGCTGCTTCAGGTGCACAGAC
AGCCCACAGGATGGATAGTTTAGATTCACATGACAGTATCTCCAGCGA
GCCCACGCAGTGTACCATGCTGTACTCACGCCAGGGGACCACTGAGA
CCATCGAGGAGGTGGAGGCTGAGCAGGAGGAGGAGGCAGGGAGCAC
GGCGCCTGAGCCCAGGGAGGCCAAGGAGTACGAGGCCACTGGGTAC
GATGTGGGAGCCATGGGTGCCGAGGAGGCCAGCCTCACCCCAGAGGA
AGAGCTGACACAGTTCTCCACCTTGGACGGGGATGTGGAGGCCCCAC
CCTCCTACAGCAAGGCTGTGAGCTTCGAGCATCTGTCCTTCGGCTCGC
AGGACGACTCTGCAGGCAAGAACCGTATGGCAGTCAGCCCGGACGAC
AGCCGCACCGACAAGCTGGGGTCCAGCATCTTACCTCCCCTGACCCAT
GAGCTGACGGCCAGCGAGCTGCTGCTGAAAAAGATGTTTCACGACGAT
GAGCTTGAAGAGTCAGAGAAATTCTACGTGGGGCAGCCCCGATTTCTG
CTGCTCTTCTATGCCATGTACAATACCCTGGTGGCCCGCTCGGAGATG
GTGTGCTACTTCGTGATCATCCTCAACCACATGGTCTCTGCCTCCATGA
TCACGCTCCTGCTTCCCATCCTCATCTTCCTCTGGGCCATGTTGTCCGT
CCCCAGGCCCAGCCGCCGGTTCTGGATGATGGCCATCGTCTATACTGA
GGTGGCAATTGTAGTCAAGTATTTCTTCCAATTTGGGTTCTTTCCCTGG
AATAAGAATGTGGAGGTGAACAAAGATAAACCGTATCACCCCCCAAACA
TCATAGGAGTGGAAAAGAAGGAAGGTTATGTTCTCTATGACCTCATCCA

GCTCCTGGCTCTGTTCTTTCATCGATCAATTTTGAAGTGCCATGGCTTA
TGGGATGAAGATGACATGACTGAAAGTGGCATGGCCAGGGAGGAATCA
GATGATGAGCTCTCCCTCGGTCATGGCAGGAGGGACTCCTCCGATTCT
CTCAAGTCCATCAACCTGGCCGCGTCTGTGGAGTCAGTGCATGTGACC
TTCCCGGAGCAGCAGACAGCTGTCCGGAGGAAGCGCTCCGGCAGCAG
CTCCGAGCCATCCCAGAGATCCAGCTTTTCTTCAAACAGATCCCAAAGA
GGCAGCACAAGCACCCGAAACAGCAGTCAAAAAGGAAGCAGTGTTTTG
AGTATTAAGCAAAAAGGCAAAAGGGAACTTTATATGGAAAAGCTTCAAG
AACATTTAATCAAAGCAAAAGCCTTTACCATAAAGAAGACGCTGGAGAT
CTATGTGCCCATCAAACAGTTCTTTTACAACCTCATCCACCCGGAGTAT
AGCGCCGTGACTGACGTGTATGTACTCATGTTCCTGGCTGACACTGTG
GACTTCATCATCATTGTCTTCGGCTTTTGGGCCTTTGGGAAACACTCAG
CAGCTGCAGACATCACCTCTTCACTGTCAGAGGACCAGGTCCCGGGGC
CGTTTTTGGTGATGGTCCTCATTCAGTTTGGAACCATGGTGGTGGACC
GAGCCCTCTACCTCAGGAAGACTGTACTGGGAAAGGTCATCTTCCAGG
TCATTCTTGTGTTCGGAATTCACTTCTGGATGTTCTTCATCTTACCTGGT
GTGACTGAGAGGAAATTCAGCCAGAACCTGGTTGCCCAGCTTTGGTAC
TTTGTGAAATGTGTTTACTTCGGGTTGTCTGCTTACCAGATCCGTTGTG
GCTACCCAACGCGAGTCCTGGGGAACTTCCTCACCAAGAGCTACAATT
ACGTCAACCTCTTCTTATTCCAAGGGTTTCGCCTCGTGCCCTTTTTGAC
TGAGCTGAGGGCAGTGATGGACTGGGTGTGGACGGACACAACTTTGA
GCCTGTCCAGCTGGATCTGTGTGGAGGACATCTATGCTCACATATTCAT
CCTGAAGTGTTGGCGGGAGTCGGAGAAGAGATACCCTCAGCCACGGG
GCCAGAAGAAGAAGAAAGTGGTGAAGTATGGCATGGGAGGAATGATCA
TCGTCCTGCTCATCTGCATTGTCTGGTTTCCTCTTCTCTTCATGTCTTTG
ATCAAATCTGTGGCTGGGGTCATCAACCAGCCCCTGGACGTCTCCGTC
ACAATTACCCTGGGAGGGTATCAGCCTATTTTCACAATGAGTGCCCAAC
AAAGCCAGTTGAAAGTTATGGACCAGCAGAGCTTTAACAAATTTATACA
AGCTTTTTCTAGGGACACCGGTGCTATGCAATTTCTGGAAAATTATGAA
AAAGAAGACATAACAGTAGCAGAACTGGAAGGAAACTCAAATTCTTTGT
GGACCATCAGCCCACCCAGTAAGCAGAAAATGATACACGAACTCCTGG
ACCCCAATAGTAGCTTCTCTGTTGTTTTTTCATGGAGTATTCAGAGAAAC
TTAAGTCTGGGTGCAAAATCGGAAATAGCAACAGATAAGCTTTCTTTTC
CTCTTAAAAATATTACTCGAAAGAATATCGCTAAAATGATAGCAGGCAAC

AGCACAGAAAGTTCAAAAACACCAGTGACCATAGAAAAGATTTATCCAT
ATTATGTGAAAGCACCTAGTGATTCTAACTCAAAACCTATAAAGCAACTT
TTATCTGAAAATAATTTCATGGATATTACCATCATTTTGTCCAGAGACAA
TACAACTAAATATAACAGTGAGTGGTGGGTTCTCAACCTGACTGGAAAC
AGAATATACAATCCGAACTCTCAGGCCCTGGAACTGGTGGTCTTCAATG
ACAAAGTCAGTCCCCCAAGTCTGGGGTTCCTGGCTGGCTATGGTATTA
TGGGATTATATGCTTCAGTTGTCCTTGTGATTGGGAAATTTGTCCGTGA
ATTCTTCAGTGGGATTTCTCACTCCATCATGTTTGAAGAGCTTCCAAATG
TGGATCGAATTTTGAAGTTGTGCACAGATATTTTTTTAGTTCGAGAGACA
GGAGAACTGGAGCTAGAAGAAGATCTCTATGCCAAATTAATATTCCTAT
ATCGCTCACCAGAGACAATGATCAAATGGACTAGAGAAAAAACAAATTG
A

Appendix C: Standardisation of Aortic Size to Weight

Table 8. Comparison of C57BL6/J mice aortic morphology standardised to weight at day 14 following sham and PPE surgery.

Characteristic	Sham N= 5	PPE N= 10	P-value
Age (weeks)	13.9 (± 0.64)	14.25 (± 0.31)	0.375
Pre-op Weight (grams)	27.76 (±1.51)	28.00 (± 1.76)	0.804
Termination weight (grams)	27.4 (± 1.57)	27.87(± 1.48)	0.646
Percent weight change (%)	1.1 (± 3.2)	0.37 (± 3.89)	0.717
Day 14 APd_{max} (mm)	0.72 (± 0.14)	0.69 (± 0.07)	0.747
Day 14 3DLV (mm^3)	4.74 (± 1.99)	5.89 (± 3.53)	0.492
APd_{max} / weight (mm/g)	0.02 (± 0.00)	0.02 (± 0.00)	0.674
3DLV / weight (mm^3/g)	0.17 (± 0.06)	0.21 (± 0.12)	0.489